RICE UNIVERSITY

# Bioactive Poly(ethylene glycol)-based Hydrogels for Characterization of Matrix Influences on a Lung Cancer Metastasis Model

by

**Bartley Joseph Gill**

A THESIS SUBMITTED
IN PARTIAL FULFILLMENT OF THE
REQUIREMENTS FOR THE DEGREE

**Doctor of Philosophy**

APPROVED, THESIS COMMITTEE

Jennifer L. West, Professor, Committee Chair
Bioengineering

Jeffrey G. Jacot
Assistant Professor, Bioengineering

M. Cindy Farach-Carson
Professor, Biochemistry and Cell Biology

HOUSTON, TEXAS
JANUARY 2013

# ABSTRACT

## Bioactive Poly(ethylene glycol)-based Hydrogels for Characterization of Matrix Influences on a Lung Cancer Metastasis Model

by

Bartley Joseph Gill

Pathological changes to tumor extracellular matrix (ECM) composition, mechanics, and architecture promote cancer progression and metastasis. Exploration of tumor-ECM interactions using *in vitro* matrix-mimetic culture systems has largely been restricted to naturally-derived matrix materials that permit limited experimental control. Such study of a novel lung adenocarcinoma model in Matrigel™ (MG) has suggested key matrix cues that mediate epithelial-mesenchymal transition (EMT) and metastasis. In this thesis work, synthetic hydrogel scaffolds based on poly(ethylene glycol) (PEG) featuring high experimental control and modular bioactivity were used to study matrix influences on the EMT-prone model line 344SQ.

Encapsulation of 344SQ cells in PEG hydrogels modified for cell adhesivity and cell-mediated enzymatic degradability induced formation of lumenized, polarized spheres mimicking the epithelial phenotype observed in three-dimensional MG. Tuning matrix stiffness, adhesive ligand concentration, and ligand spatial presentation altered epithelial morphogenesis. Exploration of the EMT phenotype of PEG-encapsulated 344SQ cells revealed TGFβ-initiated changes in morphology, polarity, expression levels of EMT marker genes and their epigenetic controller, and the organization of cell-secreted ECM. Notably, a potent role for adhesive ligand was illuminated as matrices with low PEG-

RGDS concentration even in the absence of TGFβ induced formation of spheres with a post-EMT phenotype by several of these measures. A matrix-invasive phenotype was also revealed by altering matrix structural parameters and tuned with incorporation of an alternative protease-cleavable sequence. Finally, the influence of cell-cell contacts was explored by covalent incorporation of cadherin proteins into the matrix. Matrix-tethered E- and -N-cadherin affected 344SQ sphere development in otherwise non-cell-adhesive matrices and modulated polarity and the degree of TGFβ response. Further, in 344SQ with a knockdown of the essential polarity-determining protein Scribble, matrix-tethered cadherin influenced the formation of a phenotype with partially normalized epithelial polarity with corresponding differences in membrane localization of cell-expressed E-cadherin.

Overall, this thesis demonstrates the utility of the more experimentally controllable PEG system in studying ECM influences on cancer progression with findings providing greater insight into stromal biomechanical, biochemical, and cell-cell factors that mediate lung adenocarcinoma epithelial morphogenesis and EMT. These contributions help advance the state of the field towards a goal of developing new metastasis-targeting cancer therapeutics.

# Acknowledgements

A huge thank you first to Dr. Jennifer West for your mentorship and support throughout my graduate studies. Your guidance and kindness have been sincerely appreciated. Also thank you to my other committee members Dr. Jeff Jacot and Dr. Cindy Farach-Carson for their assistance and advice.

Big thanks also go to Dr. Jonathan Kurie and Dr. Don Gibbons for enabling this research collaboration and whose helpful discussions and advice have made this work possible. And a thank you to the advisers and staff of the Baylor College of Medicine MD/PhD Program for their continued support and assistance.

Thank you to my West Lab colleagues past and present who have provided invaluable time, assistance, and advice to my efforts, both professional and personal. In particular, thanks to Andrew Coughlin and Drs. Joseph Hoffmann, Stephanie Nemir, Melissa McHale, Maude and Michael Cuchiara, John Slater, Anita Shukla, LaShan Simpson, and Christy Franco as well as Zain Rizvi and Dr. Jonathon Roybal from the Gibbons Lab. Special recognition is due to Dr. Jennifer Saik for starting this work with me and Laila Roudsari for her research assistance and continuation of this project.

Finally, thank you to my family, Bart, Helen, Brandi, and Mew Gill for your encouragement and support. And special thanks to Michael for his love, care, and support through the years.

This research was supported by grants from the National Institutes of Health, including a Biotechnology Training Grant, and the Cancer Prevention Research Institute of Texas.

# CONTENTS

# List of Figures

# List of Tables

# List of Abbreviations

344SQ.scrib.....344SQ scribble knock-down

393P.scrib ..... 393P scribble knock-down

aPKC..... Atypical protein kinase C

BM .....Basement membrane

c(RGDfk) ..... Cyclic RGD

DIPEA..... N, N-Diisopropylethylamine

DMF..... Dimethylformamide

E-score ..... Epithelial score

ECM. .....Extracellular matrix

EMT. ..... Epithelial-mesenchymal transition

GFP ..... Green fluorescent protein

GPC..... Gel permeation chromatography

HA..... Hyaluronic acid/Hyaluronan

HBP .....Hhuman brain pericytes

HBS..... HEPES buffered saline

HGF ..... Hepatocyte growth factor

HUVEC..... Human umbilical vein endothelial cells

IFP.....Interstitial fluid pressure

JNK..... c-Jun N-terminal kinase

LOX .....Lysyl oxidase

MG .....Matrigel™

MET. .....Mesenchymal-epithelial transition

miR ..... microRNA

MMP. ..... Matrix metalloproteinase

MSM ..... VPMSMRGG

NSCLC..... Non-small cell lung cancer

NVP ..... N-vinylpyrrolidone

PA ..... Polyacrylamide

PEG .....Poly(ethylene glycol)

PEG-PQ ..... PEG-PQ-PEG

PEG-MSM ..... PEG-MSM-PEG

PEG-SCM ..... Poly(ethylene glycol)-succinimidyl carboxymethyl

PEG-SVA..... PEG-succinimidyl valerate

PLG.....Poly(lactic-co-glycolic acid)

PQ ..... GGGPQGIWGQGK

scrib..... Scribble

Scrib/Dlg/Lgl ..... Scribble/Discs large/Lethal giant larvae complex

TAF. ..... Tumor-associated fibroblast

TEOA.....Ttriethanolamine

TGFβ..... Transforming growth factor-β

ZO-1..... Zonula occludens-1

# 1. Introduction and Background

Excluding surgery-curative non-melanoma skin cancer, there are over 1.6 million new cancer diagnoses each year in the United States with an individual lifetime incidence of at least one form of cancer approximately 40% for men and women[1]. With more than 1500 Americans dying per day, cancer is ultimately implicated in 1 in 4 deaths. Lung cancer specifically is the second most common cancer in men and women and is the leading cause of cancer-related mortality, responsible for over 25% of cancer deaths. While lung cancer mortality rates have been slowly declining, this decline is mostly attributable to long-term trends in smoking cessation, and the rate still remains high due to the limited availability of lung cancer detection and treatment options, particularly for patients with metastatic disease[1].

While cancer development and progression was traditionally thought to result solely from sequential accumulation of mutations in proto- or anti-oncogenes and related proteins, mounting research over the past few decades has illuminated a much more complex picture, wherein tumorigenesis is regulated by networks of genetic, epigenetic, protein, and other molecular interactions[2]. These networks are dynamic and both positively and negatively regulated, preventing or promoting the switching of epithelial cells between phenotypic states of differing malignant potential. One such prominent influence outside of the traditionally studied cell-intrinsic genetic dysregulation is the extracellular matrix (ECM), which may prove important not just to a more complete understanding of tumor formation, but as central to the understanding of how tumors invade and metastasize, the primary cause of cancer-related death[3].

This chapter first provides an overview of the myriad ECM properties that influence the behavior of ECM-resident cells and examines important pathological changes to these properties that contribute to cancer development and progression. In particular, the changes to ECM composition, organization, stiffness, and both solid and fluid tumor pressures as well as the role of pathological stromal support cells will be reviewed. Then, current *in vitro* approaches to modeling and studying these influences on 2D culture substrates and in naturally derived 3D matrices are discussed. Following this foundational overview, a synthetic poly(ethylene glycol)-based hydrogel system that avoids key limitations of these other culture systems will be proposed as a tool to further study matrix cues on epithelial-mesenchymal transition and metastasis of a newly characterized lung adenocarcinoma model. This dissertation will first deploy the PEG system to recapitulate important phenotypic behaviors derived from 3D culture and study new matrix biochemical and biomechanical factors that influence the epithelial morphogenesis of a model metastasis-prone line. It will then examine the phenotypic response of the lung cancer model and its matrix interaction in the face of metastasis-inducing soluble signals and probe for the role of cadherin cell contacts in modulating polarity and morphogenesis. Overall, this thesis establishes a new, versatile matrix-mimetic tool with which ECM influences on cancer pathogenesis can be studied with high experimental control and contributes to a greater understanding of how matrix cues work to promote or inhibit cancer metastasis.

## 1.1 The ECM in Health and Cancer

The ECM is the 3D environment that provides structural support for cells and tissues, facilitating attachment of cells and providing substrates for migration. Beyond

this structural support, the ECM, in concert with other stromal support cells, performs a number of vital roles, controlling diffusion of nutrients and waste, mediating growth factor, hormone and other cell signaling effectors, and affecting a wide variety of cell behaviors, including growth, proliferation, differentiation, and apoptosis. The ECM is composed of a large variety of molecules whose combination, organization, and modifications regulate these processes and help define the structure and function of different tissues[4].

Principal ECM constituents include the collagen family, a group of over 20 molecules with specialized functions and tissue locations. Collagen molecules provide a wealth of cell-interactive binding sites to facilitate matrix bioactivity and some organize to form fibrils and networks of larger fibers to provide major tissue mechanical support[5]. Other major ECM proteins and their notable functions include laminin, a key basement membrane constituent and a key mediator of matrix interactivity for epithelial cells[6]; elastin, arranged into elastic fibers to facilitate tissue recoil mechanics[4]; and fibronectin, a glycoprotein vital for cell adhesion that distinctively interacts with several other ECM components[7]. In addition to these components, the polysaccharide-based glycosaminoglycans are covalently linked to protein backbones to form proteoglycans that provide for further structural support, cell interactivity, growth factor sequestration, and organization of other ECM constituents, amongst other diverse functions[8].

Along with other adhesive or structural glycoproteins, ECM-associated growth factors, and stromal support cells, these major ECM components come together to form a stroma that is vital in both the development and maintenance of healthy tissue. The stroma also plays a key role in disease processes, including cancer. The stroma-tumor

relationship is an area of increasingly important focus in cancer research as investigators strive to further understand its role in the tumorigenic regulatory network and metastasis, and explore it as a target of new cancer therapeutics[2].

### 1.1.1 ECM Properties Influence Cell Behavior: Overview

The ECM features both important biochemical and physical properties that influence cells as well as the ability for cells to remodel these properties (Fig. 1-1). The ECM sequesters growth factors, acting as a reservoir for growth factor-related signaling in resident cells, controlling their diffusive range, and altering binding affinity by enhancing or limiting assessable binding sites[9–12]. This ability can create a concentration

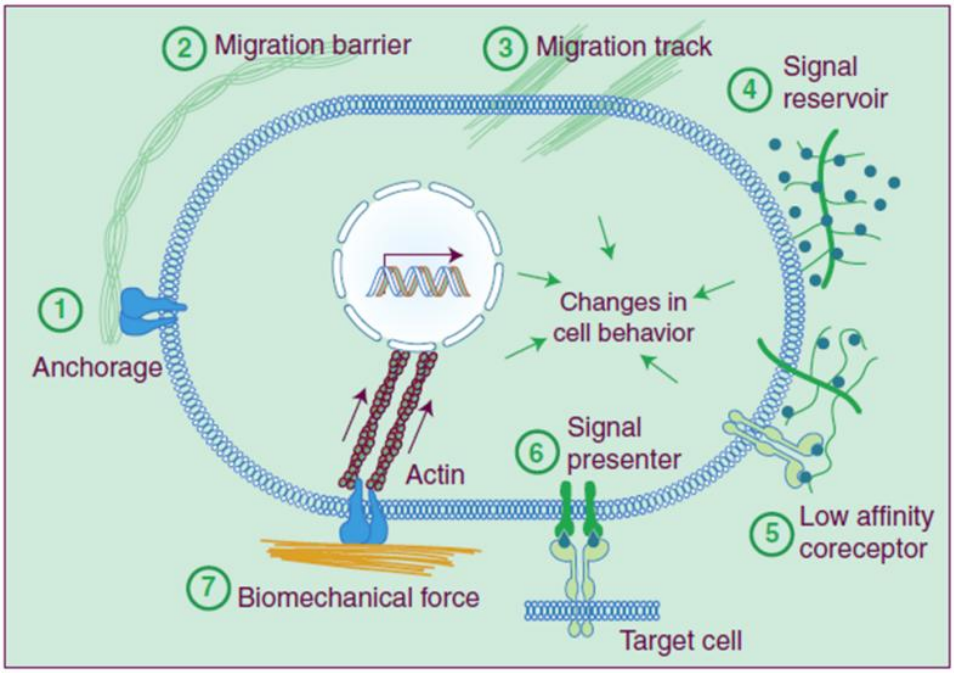


**Figure 1-1: Physical and biochemical properties of the ECM influence cell behavior.** These influences include anchorage to the basement membrane (BM) and other ECM proteins (1) and BM action as a migration barrier (2). Physical and architectural ECM cues can facilitate migration (3). The ECM sequesters growth factors (GFs, 4), in part to modulate a concentration gradient, and selectively binds certain GFs to assist cell binding as co-receptors (5) or presenters (6). ECM molecules themselves also may have GF-like domains. Finally, cells sense the biomechanical forces of the ECM (7) to exert a wide variety of gene expression and behavioral changes. Adapted from Lu, *et al*.[44]

gradient to tune cell behaviors like migration or polarity, or can help modulate dosage of particularly potent growth factors whose small concentration changes elicit drastic phenotypic changes, as in cell differentiation, for example[13]. The ECM also assists in maturation of ligands, storing factors in inactivated forms or activating secreted inactive precursors. TGF-β, for example, is often secreted in an inactive form and activated in the ECM by MMP-related proteolysis or other mechanisms[14].

Beyond modulation of non-ECM proteins, the structural ECM proteins themselves play a role in biochemical influence of cells through several mechanisms. Fragments of ECM proteins can function as precursors for biologically active signaling ligands that exert effects upon proteolytic processing[15–18]. Many ECM proteins, such as laminin, tenascin and thrombospondin, also feature growth-factor-like domains that may exert signaling effects with or without proteolysis[19,20]. Finally, integrins and other adhesion-related receptors that bind ECM proteins are themselves signal transduction receptors, activating the Rho/ROCK and MAPK signaling pathways amongst many others to yield a wide-variety of intracellular consequences[9].

The physical properties of the ECM, including its porosity, topography and rigidity, also play a key role in cell behaviors. In modulating cell migration, it can act as a barrier or a facilitator. For example, the densely structured basement membrane, predominantly composed of components laminin and collagen IV, notably acts as a key migration barrier both in development and in inflammatory, fibrotic and neoplastic disease processes[21]. Topographic cues like alignment of collagen fibers can enhance directional migration through growth factor signaling- or mechanics-related effects[22,23].

In addition, a plethora of evidence indicates that cells sense matrix architecture and rigidity with these physical cues initiating both direct and indirect responses.

Cells sense underlying matrix rigidity through mechanotransduction of ECM-bound integrins. Tension from focal adhesions formed at the site of integrin binding is transmitted across integrin receptors to intracellular cytoskeletal components and the nucleus, activating several different intracellular signaling pathways (Rho/ROCK, ERK, MAP, etc.)[24]. The tension-related changes that result are first made evident by changes in easily observable cell behaviors like cell spreading and migration; investigators have demonstrated that stiffer matrices generally lead to increased cell spreading with more organized and mature cytoskeletal elements[25,26] and modulated lamellapodia activity and cell motility[27,28]. Substrate elasticity can have profound effects on other cell functions essential to overall function of tissues. In cardiomyocytes, for example, an intermediate matrix stiffness promotes myotube elongation and striation[29] and peak contractile functionality[30]. Further, matrix stiffness plays a key role in stem cell differentiation, with osteogenic precursors[31], neurogenic precursors[32], and multipotent mesenchymal stem cells[33], amongst many others demonstrating altered differentiation on substrates of varying elasticities, with peak lineage specificity often occurring on substrates whose elasticities closely match that of the tissue where cells of that lineage typically reside *in vivo* (Fig 1-2)[34]. Studies have implicated ECM architectural control over cell shape in regulation of similar cell processes. Size and geometric restrictions on cell shape alter growth and apoptosis[35], cytoskeletal arrangement[36], gene expression and protein synthesis[37], and stem cell differentiation[38,39], acting primarily through RhoA GTPase and its effector ROCK. In addition to this physical influence on differentiation, cues from

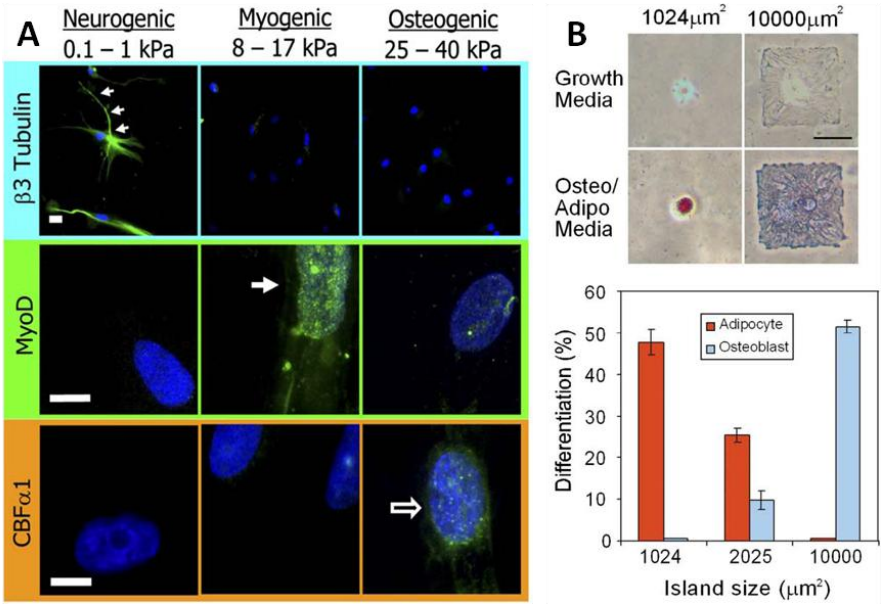


**Figure 1-2: Cells sense and respond to physical features of their environment: Differentiation**. (A) Mesenchymal stem cells (MSCs) cultured on polyacrylamide gels of varying stiffnesses demonstrate different matrix elasticity-related neurogenic, myogenic, and osteogenic lineage-specificity as shown by lineage-specific immunostaining (arrows). Scale bar = 5 μm. Adapted from Engler, *et al.*[33] (B) MSCs also show cell shape-related osteogenic or adipogenic differentiation on differently sized microcontact printed adhesive patterns. Oil red O (red stain), alkaline phosphatase (purple), scale bar = 50 μm. Adapted from McBeath, *et al.*[38]

certain ECM molecules have proven essential for the maintenance of stemness in the stem cell "niche;" laminin in the subventricular zone of the brain, for example, engages $\alpha_6\beta_1$ integrin on neural stem cells to maintain their adherence and self-renewal[40].

Cells can remodel the ECM to alter these biochemical and physical properties by producing different amounts of the ECM structural proteins themselves, secreting molecules that alter the structure or function of ECM proteins already present, or releasing proteases that degrade matrix components. Secreted matrix metalloproteinases (MMPs), for example, target a variety of large structural proteins like fibronectin, laminin and the collagens in addition to certain proteoglycans[41]. They also exhibit key roles in cleaving growth factor precursor proteins and the pro-forms of other MMPs[42]. Beyond secretion and degradation of ECM molecules, cells can also alter their organization and

topography; the posttranslational cross-linking of collagen in the ECM is mediated by action of lysyl oxidase (LOX) and lysyl hydroxylase, altering tissue mechanics and collagen fiber orientation[43]. Regulation of ECM remodeling is controlled at multiple levels, both transcriptionally and post-translationally, to yield not only a specific remodeling response and one that is controlled temporally, but also one specialized at certain subcellular locations[44]. For instance, MMPs localize specifically to invadopodia to facilitate movement through the matrix by the migrating cell[45]. Remodeling can be further regulated by secretion of proteases that degrade other ECM-targeting proteases or secretion of inhibitors, like the TIMPs family of proteins that block MMP action[44].

Given that ECM biochemical and physical properties exert potent influence over such a wide variety of cell functions and that cells are able to remodel the matrix and these resulting matrix-derived influences in myriad regulated ways, it is easy to see how a dynamic cell-ECM interaction can be vital to tissue and organism function, development, and disease. Among developmental processes, cell-ECM dynamics are essential to processes such as epithelial branching where local concentrations of ECM molecules and ECM degradation determines epithelial branch location, bifurcation, and overall direction[42,46,47]. In multiple disease processes, ECM properties are altered in pathologic ways as either a cause or result of the disease pathogenesis. For example, it has been long-recognized that diseased tissues are often stiffer and fibrotic, more concentrated in ECM components relative to their healthy counterparts[48]. ECM in aging tissue is stiffer as well, but also inappropriately organized and mechanically compromised, contributing to tissue dysfunction in age-related diseases[49]. Increased stiffness of the ECM arterial wall contributes to arterial disease and is a strong and sensitive early marker of

atherosclerosis[50]. Finally, increasing research has focused on changes to ECM physical properties, architecture, and composition in tumors. These pathologic ECM changes and how they work in concert with abnormal stromal cell activity and the genomic instability of tumor cells themselves to promote cancer progression will now be reviewed.

### 1.1.2 ECM in Cancer Initiation and Progression

Mounting evidence indicates that the stroma is essential to cancer development and progression. Tumor cells and their microenvironment surroundings act together as an "organ-like tissue" with constituents that display different characteristics than normal tissue, but also necessarily change with time to permit progression and metastasis (Fig. 1-3A)[3,51]. *In vivo* transplantation experiments in mice have soundly demonstrated this essential role for a healthy or diseased stroma in epithelial cancer development. In the chemical carcinogen N-nitrosomethylurea model, fat-pad transplantation of mammary epithelial cells not exposed to the carcinogen prior to implantation neoplastically transform when placed into carcinogen-exposed stroma[52]. Similar results were seen in a prostate model, where an activated stroma promoted the transformation of a non-tumorigenic prostate line[53]. The converse situation has also been studied; when carcinogen-exposed cells are transplanted into healthy, unexposed stroma, they do not always form tumors and are readily able to form ducts with normal growth patterns despite their neoplastic transformation[52,54,55].

In addition, experiments have shown that the 3D architecture of epithelial tissue is heavily influenced by the underlying mesenchyme. Studies decades ago demonstrated that isolated mammary epithelial cells maintain milk protein secretion, but display a salivary

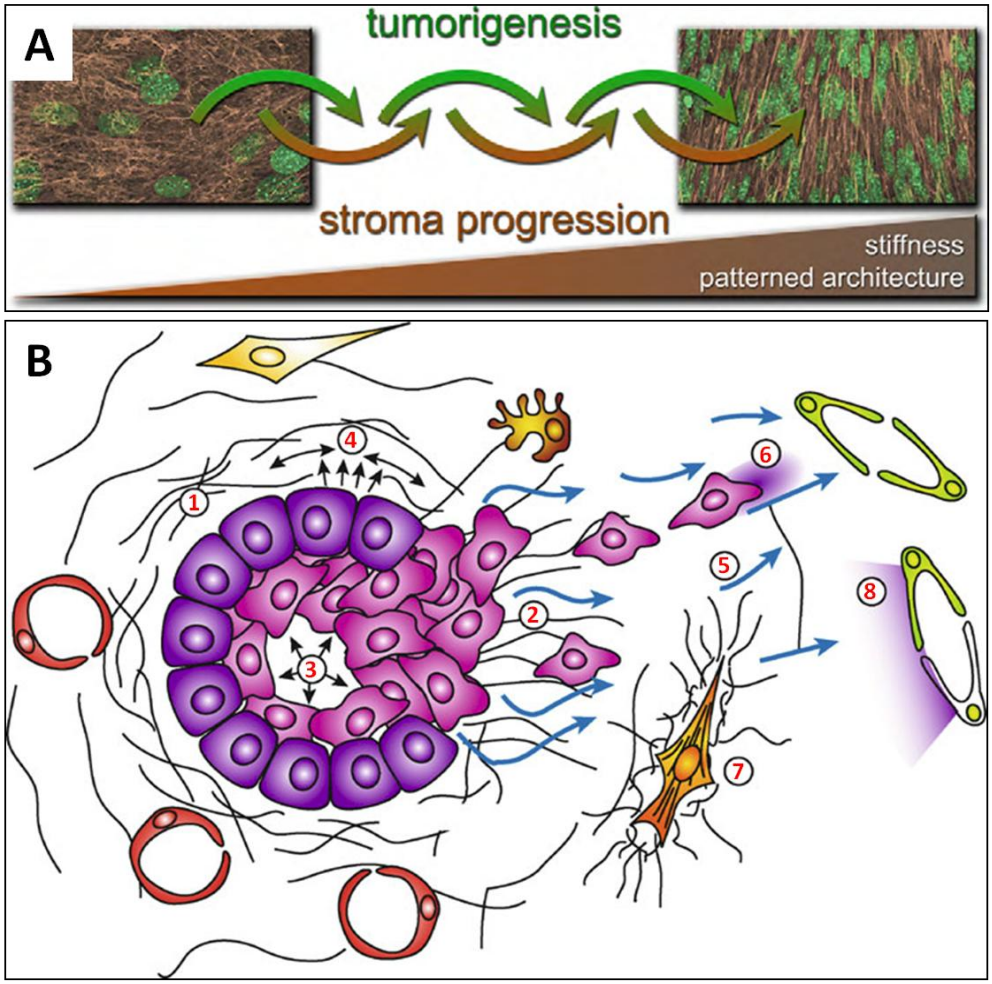


**Figure 1-3: The ECM in cancer**. (A) Tumorigenesis proceeds in concert with pathological changes to the stroma with prominent changes in ECM concentration and architecture. Fibroblast-derived ECM (brown), cell nuclei (green), from Cukierman and Bassi[3]. (B) In addition to these changes in ECM protein concentration/stiffness (1) and organization (2), growing tumors themselves generate solid stresses (3), generating radial and compressive forces (4). Interstitial fluid pressure increases due to pathological tumor-associated angiogenesis, resulting in a directional fluid flux (5) that tumors can exploit by producing chemokine concentration gradients to facilitate directional migration (6). Finally, there is also enhanced matrix stress-induce myofibroblast differentiation (7) and lymphatic chemokine secretion (8). Adapted from Shieh[90].

gland-like morphology when recombined with isolate salivary gland mesenchyme[56]. In normal development, epithelial tissue growth and architecture is in large part dictated by the remodeling of underlying mesenchyme, specifically the basement membrane (BM), and the dynamics between its focal degradation or secretion[57,58]. The BM has also long been recognized as a vital player in cancer progression. Ultrastructural changes occur in

the BM in early tumorigenesis prior to formation of sizable tumors with areas of altered BM thickening, altered relationship to other ECM components, and the appearance of gap regions[59–61]. BM breach and these resulting discontinuities are a long-recognized hallmark of transition from carcinoma *in situ* to invasive carcinoma and metastasis[21], but these breaks are not a universal sign of neoplastic advancement of the epithelial compartment. For example, different tumors from the same metastatic murine mammary cancer model differ in the number and size of BM breaks[62], and intact BMs are sometimes found surrounding metastatic tumors at the site of implantation or even in some heavily malignant primary tumors despite significant transformation of these tumor cells[60,63,64]. Thus, these BM changes may be the result of other more complex microenvironmental interactions in addition to tumor-guided remodeling.

The BM as an ECM-related barrier is only one part of the broader role that the ECM plays in migration and invasion. 3D migration of tumor cells through ECM, for example, is a complex and coordinated process that requires cell-ECM interactions that are both identity-specific and spatially controlled. Cells form invadopodia at their leading edge that require relatively stiff ECM with a high density of integrin-binding sequences at distant ends for attachment[65]. These invadopodia express proteases like membrane-type 1 MMP at intensely localized foci at the lateral-posterior areas of pseudopodia to degrade sufficiently wide tracks through the matrix for movement of the cell body bulk[66]. Meanwhile, more diffuse proteolytic activity also occurs in areas posterior to invadopodia near the cell body and generates fragments of collagen, laminin and fibronectin, which help compete for integrin binding sites with still-incorporated ECM, facilitating cell detachment and further migration [66–68]. This matrix proteolysis

also helps release sequestered growth and chemotactic factors. Finally, ECM remodeling during rear retraction of the cell body leaves collagen fibers aligned and oriented in the direction of migration, creating collagen tracts that decrease resistance to favor additional migration[69].

Beyond factors directly related to cancer cell migration, tumor ECM composition and structure are dramatically different than normal ECM and can influence this invasion process and many other behaviors[70]. Even before they were widely studied *in vitro*, excess ECM production or abnormal remodeling in cancer was noted in patients, revealed clinically by enhanced radiographic tumor density measurements[71,72]. In breast cancer, for example, enhanced mammanographic measurement of breast tissue reflect elevated collagen and proteoglycan levels and has been demonstrated as a prognostic indicator of disease severity and treatment response[48,73]. A variety of ECM components have been shown to be present in tumor ECM at higher concentrations than in normal tissue including collagens I, II, III, V and IX[74–77]. ECM remodeling enzymes are also upregulated or dysregulated in tumor ECMs, with reports finding overexpression of haparanases and many MMPs in various cancers[42,78]. Beyond ECM protein concentrations, architecture is also altered. Likely owing to increased concentration of LOX[79,80], collagen I in tumor ECM is highly linearized compared to its healthy counterparts and is oriented in specific patterns adjacent to the tumor epithelium or projecting perpendicularly into the tissue[23,81,82]. This increased collagen density and/or its altered organization has been found to promote tumor metastasis or recurrence following tumor excision[83,84].

These changes in non-soluble ECM dynamics are accompanied by changes in tumor stromal fluid flow (Fig. 1-3B). Increased interstitial fluid pressure (IFP) is found in tumors primarily due to higher concentrations of new, poorly functioning and leaky vasculature derived from enhanced tumor angiogenic signaling[85]. Higher IFP may have a direct effect on the tumor itself, increasing cell proliferation or promoting the section of additional angiogenic factors[86,87], but also works in concert with increased lympangiogenesis to enhance overall fluid flux through the tumor stroma[88]. Increased flow around tumors acts to increase fluid shear stress, realigning fibroblasts around tumors and promoting their differentiation into tumor-associated myofibroblasts[89,90]. Critically, it also acts to promote the formation of chemokine and growth factor concentration gradients, with the flow of chemokines from the high pressure pericellular environment to lower pressure lymphatics providing a potential metastasis guidance cue[91,92]. In addition to the stress generated by the high IFP, the growing tumors themselves generate a great deal of solid stress, upwards of 10 kPa in some *in vitro* models[93]. This tumor stress may also work to enhance myofibroblast differentiation and activity and thereby promote a positive feedback loop to further enhance environmental stresses through myofibroblast-mediated ECM protein secretion or cell contraction[90,94].

These tumor stresses, working in concert with altered ECM secretion, cross-linking and remodeling, leave the tumor stroma substantially stiffer than normal ECM, and most studies find that this stiffness potentiates malignant events[90,95]. Normal breast tissue, for example, has a Young's Modulus of ~0.15 kPa, increasing several fold to around 4 kPa in advanced malignancy[96], and women with mammographically dense breasts are several times likelier to develop breast cancer[71]. Altered matrix elasticity may

in part explain the results of *in vivo* transplantation studies; lack of pathologic stiffening in normal host mesenchyme likely contributed to the reversion of neoplastically transformed implanted cells to normal epithelial organization[52,54,55]. Initial *in vitro* exploration decades ago using natural matrices suggested a potent role for matrix stiffness in cancer behavior as mammary epithelial cells on softer, floating collagen gels respond to lactogenic hormones to form differentiated, polarized acini, but those on glass or plastic surfaces or stiffer, tethered collagen gels form proliferating colonies with compromised polarity[97,98]. In a more recent report by Paszek, *et al*., mammary epithelial cells formed small, growth-arrested, polarized lumenized acini in soft BM-based matrices, but when stiffness was increased with cross-linked collagen, this organization was lost, lumen formation was inhibited, and adherens junctions were destabilized (Fig. 1-4)[99]. This process was found to be associated with increased integrin clustering with observed changes mediated by enhanced ERK and ROCK activation. The clarity of conclusions drawn from this and similar systems are uncertain, however, due to poor control of biochemistry with the alteration of matrix stiffness and other problems, discussed at length in later sections of this thesis. Beyond direct effects on the cells, a stiffer ECM may also influence other metastasis-relevant ECM constituents; for example, when a silicone membrane culture system with cultured myofibroblasts was stiffened and stretched, latent TGFβ became exposed and activated, potentiated by enhanced myofibroblast contraction[100].

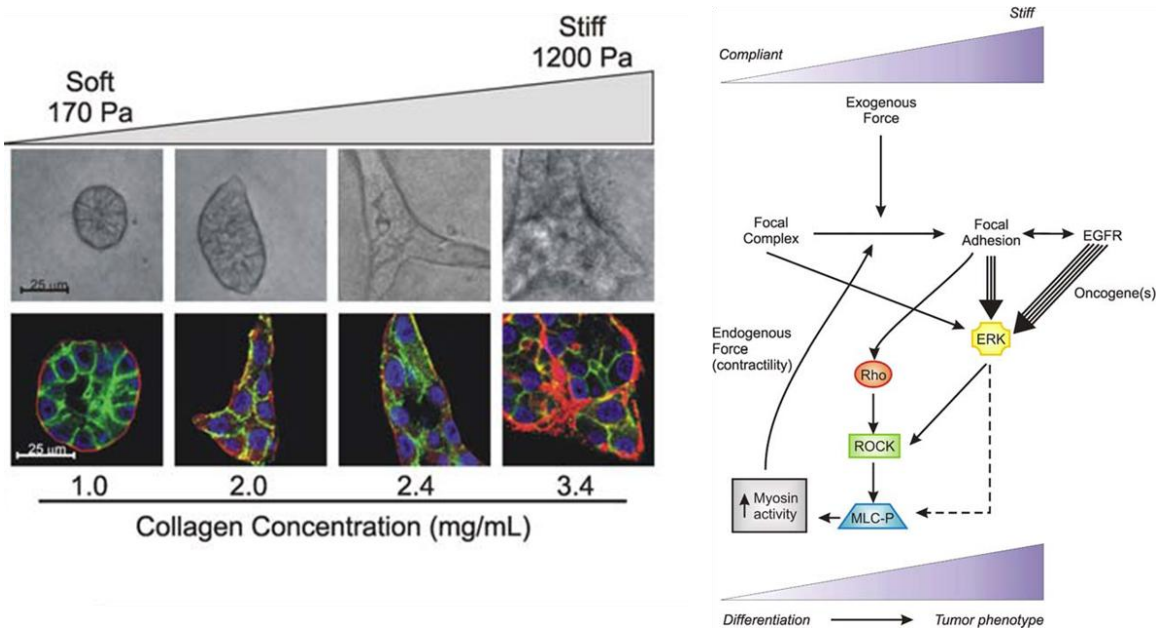


**Figure 1-4: Matrix rigidity regulates growth and morphogenesis in a MG breast cancer model**. (*Left*) MCF10A cells in MG stiffened with increasing collagen concentrations showed enhanced growth, loss of lumenized morphology, and disruption of polarity at higher matrix elasticities with (*Right*) matrix rigidity postulated to induce Rho-generated cytoskeletal tension to promote focal adhesion assembly and increase growth factor-dependent ERK activation. $\alpha_6\beta_4$ integrin (red), β-catenin (green), DAPI (blue). Adapted from Paszek *et al*.[99]

### 1.1.3 Extrinsic Cellular Influences on Cancer Progression

Other cells in the tumor stroma, which signal through ECM proteins, by paracrine mechanisms, or via cell-cell contacts, have a profound influence on the inhibition of tumor formation and progression. Beyond being primarily responsible for secreting the BMs that constrain epithelial cells to tissue boundaries[101], they may play a more direct role in other ways. In normal breast tissue, for example, myoepithelial cells secrete a relatively higher concentration of proteinase inhibitors like TIMPs and angiogenic inhibitors that help prevent breast cancer invasion and angiogenesis promotion[102]. Normal fibroblasts also act to limit the growth rate of tumor cells when present at sufficient ratios[103] and help to normalize duct structure and polarity[104], both directly through paracrine signaling and more indirectly through mediation of ECM constituents

to alter epithelial cell integrin-ECM interaction. This anti-neoplastic control in part explains the protective effect that normal stroma can exert over grafted neoplastic cells to prevent tumor at graft sites[52,55].

In cancerous stroma, however, not only are protective measures eroded, but tumor-associated fibroblasts (TAFs) actively contribute to tumor growth and spread. Genes for a number of secreted proteins are differentially expressed in TAFs including ECM proteins, cytokines, growth factors, proteases, and cell surface receptors[105], and they work to enhance the growth and oncogenic potential of neighboring epithelia via activation of myriad growth factor signaling pathways (Table 1-1)[106–109]. Notably, TAFs

**Table 1-1: Growth factors and signaling proteins differentially expressed by stromal cells in tumorigenesis.** Adapted from Bhowmick, *et al.*[109]

| Soluble factors | Cells expressed | Responding cells | Possible role |
|---|---|---|---|
| HGF and MSP | Fibroblasts | Epithelia | + Proliferation<br>+ Transformation<br>+ Morphogenic |
| IGF-1, IGF-2 | Fibroblasts | Epithelia (breast) | - Apoptosis<br>+ Proliferation |
| EGF and TGF-α | Epithelia and fibroblasts | Epithelia | + Proliferation<br>+ Morphogenic |
| TGF-β1, -β2, -β3 | Epithelia and fibroblasts | Epithelia and fibroblasts | - Proliferation<br>+/- Apoptosis<br>+ Morphogenic |
| FGF7 / KGF | Fibroblasts | Epithelia | + Proliferation<br>+ Transformation |
| IL6, LIF, oncostatin M | Fibroblasts | Epithelia (colonic) | + Proliferation<br>+ Transformation |
| FGF2 | Fibroblasts | Epithelia | + Proliferation<br>+ Transformation |
| FGF10 | Fibroblasts | Epithelia | + Proliferation |
| NGF | Fibroblasts | Epithelia | + Transformation |
| SDF-1α (CXCL12) | Fibroblasts | Epithelia (glioblastoma) | + Proliferation<br>+ Transformation |
| Wnt1, Wnt3 | Fibroblasts | Epithelia | + Proliferation<br>+ Transformation |
| MMP-1, MMP-7 | Fibroblasts | ECM and growth-factor activation in the stroma affect epithelia | +/- Proliferation<br>+/- Apoptosis<br>+ Morphogenic |

IL6, interleukin 6; LIF, leukemia inhibitory factor; NGF, nerve growth factor; SDF-1α, stromal cell-derived factor 1α

also express higher levels of fibroblast activation protein, which has been shown to induce tumor growth[110] and secrete high levels of tenascin-C, a marker of desmoplastic stroma with anti-adhesive, fibronectin-blocking properties[111]. TAFs also enhance tumor angiogenesis by secreting elevated amounts of VEGF and bFGF[112,113]. Finally, TAFs overproduce several ECM components including collagens I, VI and XV and hyaluronan, amongst others[107,114–116], promoting to tumorogenesis, but show limited production of laminin-1, contributing to BM breakdown[117]. All of these changes together significantly alter the behavior of adjacent epithelium. For example, mammary epithelial cells overlayed on disrupted myoepithelial cell layers show altered expression of proliferation and tumor progression marker genes, microsatellite instability, increased invasion into the stroma, and enhanced angiogenesis[118,119]. TAFs may also play a role in metastatic disease; bone-marrow-derived cells have been found to colonize sites of metastasis prior to the arrival of tumor cells, potentially working to establish a "pre-metastatic niche" in new stroma that is more permissive to metastases implantation and growth[120,121].

Of additional importance in the cellular component of tumor stroma is the role of cell-cell contacts on tumor progression. Within epithelial tumor cells themselves, a loss of cell-cell adhesion permits disaggregation of tumor cells to facilitate matrix invasion and metastasis. Cadherins, acting with their cytosolic effectors α-, β- and γ-catenin, are one of the main cell-cell adhesion molecules that is altered in tumors[122]. *In vitro* evaluation of a number of model lines for different epithelial cancers showed a correlation between E-cadherin expression and invasiveness, with constitutive expression of E-cadherin in the more malignant lines abrogating their invasive ability and restoring epithelial phenotype[123,124]. Similar observations have been reported *in vivo* for breast[125],

nasopharyngeal[126], prostate[127], and lung cancers[128], amongst others, with decreased levels of E-cadherin found in tumors and a lack of stable E-cadherin expression generally correlating with metastatic phenotype and poor patient prognosis[129]. In human patients, aberrant E-cadherin expression or the combination of aberrant E-cadherin and catenin expression has been shown in some studies to be an independent prognostic marker for the presence of occult lymph node or distant metastases in patients initially classified as having no metastatic involvement and, to a lesser extent, overall survival[130–134]. In contrast to E-cadherin, N-cadherin expression correlates to more malignant and invasive tumors, acting to increase invasion and metastasis in part through enhanced sensitivity to FGF-induced MMP-9 secretion and promotion of adhesion to endothelial cells to facilitate metastasis[135].

Beyond a more apparent role in promoting cell aggregation to hinder tumor cell invasion and metastasis, the E-cadherin/catenin complex may play more signaling-related roles in cancer progression (Fig. 1-5). Much evidence exists for a mitotic role of E-cadherin's intracellular binding partner β-catenin. The importance of β-catenin is mostly related to its role in the Wnt signaling pathway, with its disrupted function in cancer commonly altering its cytosolic sequestration and breakdown[136–138]. When left free in the cytosol at high concentrations, β-catenin translocates to the nucleus where it binds to transcription factors LEF and TCF to exert a pro-mitotic effect, activating genes that inhibit apoptosis and promoting cell proliferation- and migration-related genes including c-myc and cyclinD1[122,139,140]. While the complete role of E-cadherin in free β-catenin TCF/LEF-related action is still unclear, the growth inhibitory effects of undisrupted E-cadherin binding show a clear correlation with a reduction in β-catenin/TCF activity, and

it likely does interfere to some degree with this Wnt-related signaling by decreasing the available β-catenin nuclear pool[141–143]. E-cadherin binding may also inhibit cell proliferation through cell arrest resulting from activation of the cyclin-dependent kinase inhibitor p27[144] or may interfere with EGF receptor-mediated growth signaling in a separate β-catenin-dependent mechanism unrelated to TCF/LEF action[145].

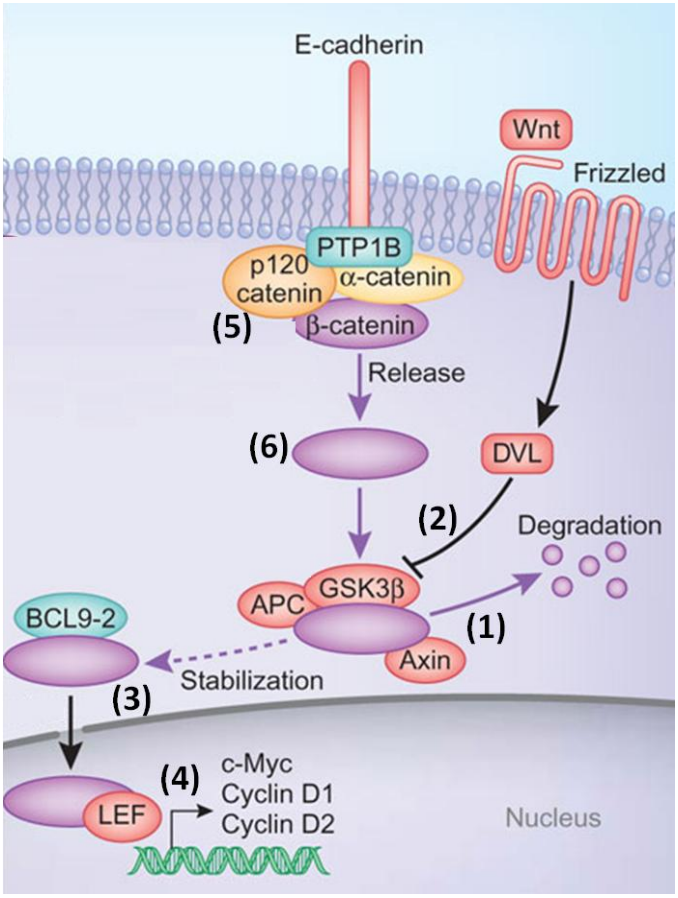


**Figure 1-5: E-cadherin mediates Wnt-related β-catenin action**. Free β-catenin is typically maintained at low levels in the cytosol due to degradation by the GSK3β-APC-Axin complex (1). When degradation is inhibited by activated Wnt signaling (2), free β-catenin translocates into the nucleus (3) and in conjunction with LEF/TCF transcription factors promotes the transcription of several pro-mitotic genes (4). β-catenin also forms a complex with the cytosolic portion of E-cadherin and other catenins (5) such that when E-cadherin binding is disrupted, it is released (6), increasing its available nuclear pool. Adapted from McVicar and Trinchieri.[138]

## 1.2 Tissue Engineering Approaches to Modeling Tumor ECM

Some initial understanding of the physical, chemical, and stromal cellular factors that promote tumorigenesis can be gleaned by the study of extracted tumor tissue and use of *in vivo* transplantation models, but a more complete understanding is obtained through the use of *in vitro* culture platforms that model tumor ECM[146]. Ideally such platforms would permit study of specific ECM cues of interest, enabling the discovery of specific causal relationships between matrix factors and notable cancer cell phenotypes and facilitating the screening of potential new therapeutic agents that target these relationships. 2D culture substrates like tissue culture polystyrene, glass, and similar surfaces with or without cell-adhesive protein coatings have been used to further some research into environmental tumor cues, but they suffer several important drawbacks that limit the scope of study and the extent to which conclusions can be appropriately translated to actual *in vivo* processes.

This section will first review the many limitations of 2D culture in studying cell behavior in general and in cancer pathogenesis in particular. It will then provide an overview of naturally derived biomaterials that support the three-dimensional culture that more accurately models physiologic tissue architecture and certain cell-matrix processes, but also presents experimental problems related to their natural source. Finally, it will describe synthetic systems that have been used to model cancer ECM and propose the use of a bioactive hydrogel system based on poly(ethylene glycol). These hydrogels improve on other synthetic systems and enable versatile study of matrix influences on cancer progression with high experimental control.

### 1.2.1 Key Differences in 2D vs. 3D in Modeling Tumor ECM

In modeling important biochemical, structural, and stromal cell-derived influences of the tumor ECM environment, there are several important limitations of 2D culture platforms related to key differences in cell behavior resulting from a spatial environment that is different from the 3D tissue matrix (Fig. 1-6). Most obviously, differences in the spatial organization of cell-ECM binding resulting from lack of adhesive ECM surrounding cells on all sides lead to major changes in cell structure and shape with concomitant changes in cell metabolism and gene expression[147–150]. Expression, composition, and clustering of integrins and other cell surface receptors is heavily influenced by the proximity of culture nutrients, growth factors and other ligands, presenting a potential problem with 2D culture where these influences are strongest on the culture media side of the cell, away from the underlying adhesive surface where they need to act to exert their effects[151,152]. Due to these issues, and because only a small proportion of the cell in 2D culture is able to bind to ECM and other cells, cell

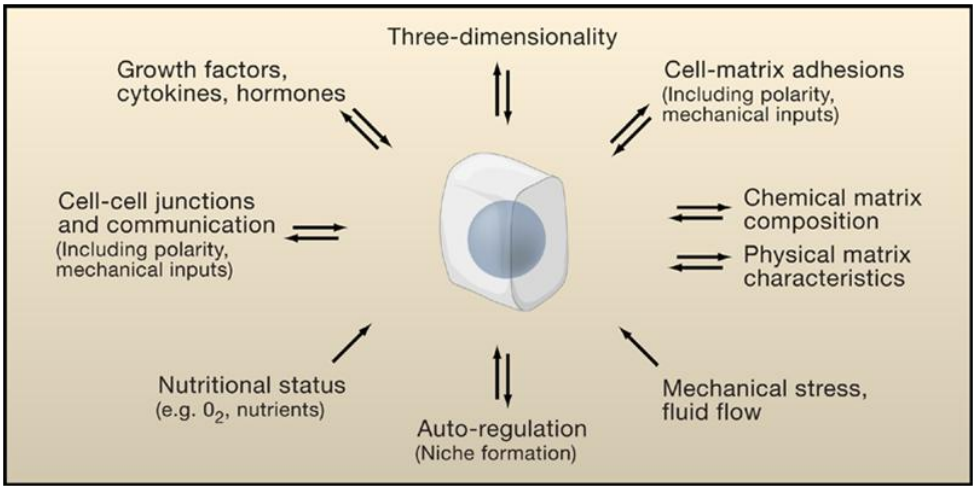


**Figure 1-6: Microenvironmental factors differently affect cell behavior in 2D vs. 3D culture**. Multiple aspects of a cell's interaction with its microenvironment are more physiologically appropriate in a 3D context including cell shape (with loss of polarity in 2D), gene expression, growth, morphogenesis (notably, vessel sprouting and gland branching), motility (single vs. collective cell motility patterns), and differentiation. From Yamada and Cukierman.[150]

polarization is non-physiological. Polarity is a critical feature to model effectively in the culture of epithelial cancer cells. Abnormal polarized integrin binding and the resultant abnormal mechanotransduction dramatically influences intracellular signaling, gene expression, and phenotypic fate[146,153].

Two additional key differences between 2D and 3D culture regard molecular gradients and migration. Gradients of growth factors and nutrients are impossible to establish in a physiologically appropriate way in conventional 2D cultures, but are essential to cell proliferation, migration, and differentiation, and other cellular processes that are vital to model appropriately in cancer[154]. With migration in particular, not only are the chemotactic influences altered in 2D, but the frank physical nature is completely different; migrating 2D cells encounter little matrix-derived resistance to migration and exhibit dramatic temporal and spatial differences in integrin expression, focal contact formation and breakage, and secretion of proteases and other ECM molecules during remodeling[66,152]. These migration and remodeling differences found in single cells have ever greater implications when attempting to model migration over larger organizational scales and longer time scales like that in cancer metastasis.

These and other differences have contributed to the finding of differences in key phenotypic behavior between 2D or 3D culture of cancer models. For example, metabolism of a hepatoma model was found altered in 3D culture compared to 2D monolayer with enhanced glycolysis and production of lactic acid in 3D[147]. Expression of important angiogenesis genes like VEGF or HIF-2 and important chemokines like IL-8 are upregulated in 3D culture in a melanoma model compared to 2D levels and are more comparable to observed in *in vivo* human tumors[148]. Finally, cancer models in 3D show

key differences in susceptibility to cancer therapy with tumor cells exhibiting altered apoptosis due to death receptor ligand therapy[155] and radiotherapy[156] and altered sensitivity to interferons or other chemotherapeutic agents[157]. For example, scaffold-less spheroid culture of a breast cancer model, absent of any potential scaffold-related diffusion barriers, showed a higher IC50 of cisplatin compared to 2D monolayer culture due to differences in TGFβ production and the upregulation of drug resistance responses[158].

Perhaps most critically, 2D cultures largely lack a stromal component, which proves essential to modeling cancer as the majority of tissues that give rise to epithelial tumors are composed of non-epithelial stroma (80% by volume in the breast, for example). All of these stromal effects are unaccounted for in traditional 2D culture methods[159]. In addition to lacking ECM structural and growth factor components, 2D culture of cancer cells largely prevents modeling of the cellular heterogeneity found in the tumor environment. 3D culture enables modeling of mixed cell populations found in different compartments (epithelial vs. stromal) or of epithelial tumor cells with different phenotypes (proliferating, apoptotic, necrotic, etc.) that result from the more physiologic 3D mass transport and biochemical gradients[159]. Because of this and all of the above reasons, study in 3D cell culture systems provides much more biologically relevant information and offer far better hope for the discovery and characterization of key matrix-tumor interactions that are of true significance for cancer patients. Such natural and synthetic 3D systems will now be reviewed.

### 1.2.2 Natural Biomaterials for Tumor Microenvironment Engineering

Natural materials such as collagen, fibrin, and MG have been widely used as scaffolds in tissue engineering applications as they are derived from or are themselves components of the natural ECM and as such offer a cell-friendly 3D environment, providing for ample cell adhesion and proliferation[160,161]. In general, they can be modified and degraded by most cell types to permit migration with cells replacing their surroundings with cell-secreted matrix. Further, these matrices facilitate substantial cellular interaction by offering a wealth of sites for integrin binding and a reservoir of growth factors that may help provide the complex biochemical cues endemic to native ECM. Finally, the mechanical properties of collagen gels and MG can be altered with the addition of collagen or non-integrative crosslinkers during formation for studies examining cellular response to matrix elasticity[99,162].

As 3D substrates for the study of ECM influences on cancer models specifically, MG with and without collagen crosslinking has been widely used and has resulted in important findings. Matrices like MG, derived from reconstituted BM from the Engelbreth-Holm-Swarm tumor, were used decades ago in early 3D studies from the Bissell group and others to illuminate important morphological and functional behaviors (Fig. 1-7). In these studies, first done using harvested non-transformed mammary epithelial cells and then using transformed breast lines, MG-cultured cells form functional hollow spheres with distinct polar compartments and feature BM formation and vectorial secretion of milk proteins[163,164]. Gels composed of collagen I were also early tools to study epithelial morphogenesis and important 3D structural characteristics with mammary cells embedded within or under collagen forming similar functional duct-

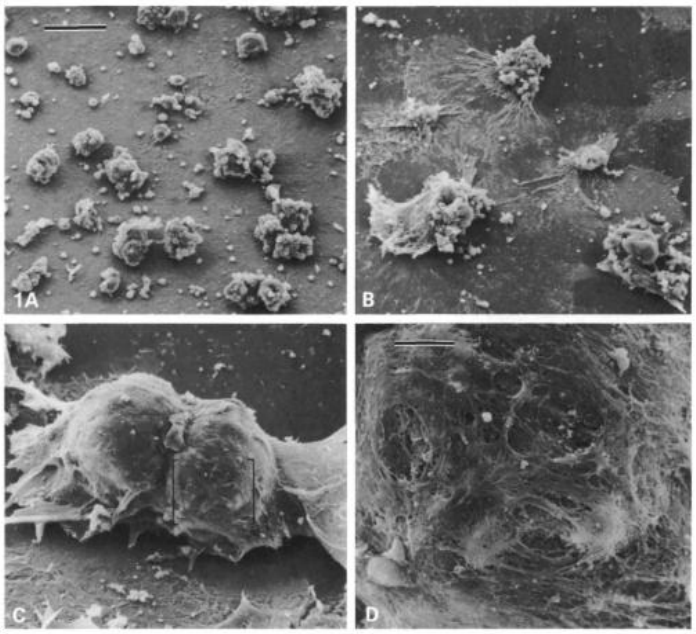


**Figure 1-7: Mammary cells form lumen-containing structures when cultured on a 3D BM-based matrix.** Primary mammary cells cultured in the presence of lactogenic hormones and imaged by SEM rapidly adhered at 3h (A), and organized together to form large clumps with large regions of the culture area cleared by 24h (B). By 4-6 days, cells formed lumenized spheroids (C) completely surrounded by a fibrillar matrix (D, close-up of C). Scale bar = 100 μm (A-C), 25 μm (D). Modified from Barcellos-Hoff, *et al.*[164]

like structures depending on cell type and culture arrangement[97,165,166]. Collagen is the most abundant ECM protein, rich in cell-interactive ligands with a fibular nature providing key architectural cues. As such, reconstituted collagen matrices have been used extensively *in vitro* to evaluate a variety of other cancer model behaviors, notably migration and invasion[167].

In the past several years, use of these matrices has facilitated several important discoveries regarding tumor-ECM interactions. Investigators have further probed the unique morphologic changes that epithelial cells adopt when embedded in MG or collagen, studying the differences in structure and BM secretion due to different degrees of malignancy[168], the combination of localized apoptosis and inter-cellular cavitation that occurs to form lumenized structures[169,170], and the nature of migration and invasion into

the matrix under certain cellular or matrix conditions[135,171–173]. The Weaver and Bissell groups, amongst others, have used these matrices to identify key ECM molecules related to tumor formation and progression; for example, the important role for integrins $\beta_1$ and $\beta_4$ in maintenance of epithelial polarity or reversion of a malignant phenotype[174–177] and the interaction of these integrins and others with extracellular laminin to regulate this process[117,175,178,179]. BM-based matrices have helped elucidate the importance of various growth factors in impacting cancer model organization and progression, such as hepatocyte growth factor (HGF) in MDCK cells and EGF in breast tumor lines[180,181], and key regulatory genes involved in 3D cancer cell growth and invasion[182,183]. Further, the unique structure that cancer cells adopt in these matrices and their resultant integrin organization have illuminated mechanisms of chemotherapeutic resistance. For example, NFkB activation from integrin $\beta_4$ ligation in 3D polarized mammary structures yields resistance to apoptosis-inducing agents regardless of malignant potential of the cells (Fig. 1-8)[176]. Finally, primarily using breast model lines, *in vitro* exploration into the influence of matrix stiffness on tumor progression was pioneered in collagen or MG/collagen mixtures stiffened with increased collagen concentration or crosslinking. These stiffer natural matrices perturbed epithelial polarity and lumen formation and led to enhanced cell growth, focal adhesion formation, and integrin clustering with increased matrix invasiveness, all regulated by Rho-ROCK and FAK-ERK signaling pathways[43,99,184].

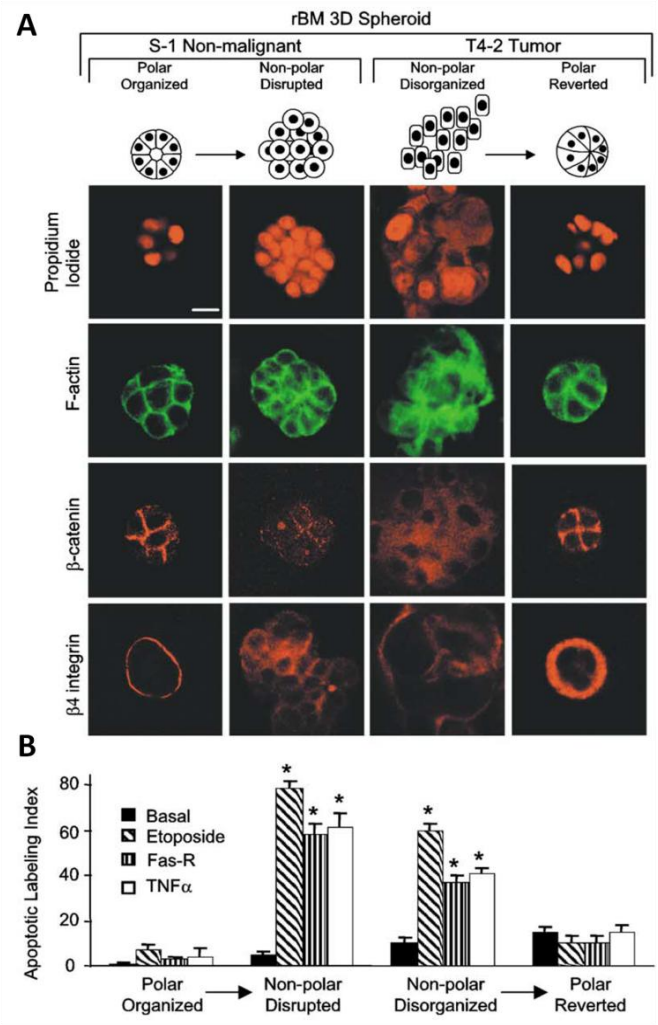


**Figure 1-8: Polarized mammary epithelial cells (MECs) in 3D BM matrices resist apoptosis-inducing agents.** Non-malignant S-1 MECs and malignant T4-2 MECs were examined under different polarized conditions (A) for a polarity influence in response to several apoptosis-inducing chemotherapeutics (B). Markers of polarity show that readily polarizing S-1 cells lose their polarity upon exposure to an E-cadherin blocking antibody (*left*) and non-polarizing T4-2 exhibit polar reversion upon exposure to a β1 integrin blocking antibody (*right*). (B) In both cases, cells display a resistance to apoptotic agents when in the organized, polarized state as indicated by apoptotic labeling. Scale bar = 10 μm. Adapted from Weaver, *et al.*[176]

### 1.2.3 Synthetic Biomaterials for Tumor Microenvironment Engineering

While the ease of use, ready availability, and high bioactivity of the naturally-derived matrices facilitated this work, complex proteinaceous natural matrices suffer important limitations. The ease of degradation of natural matrices permits study of cell migration and matrix invasion, but may be a liability for longer-term studies that require

the matrix to remain intact. MG batch-to-batch variability and growth factor contamination and the variability in collagen gel properties based on minor changes preparation methods can make comparisons between studies difficult[162,185–187]. Additionally, MG and collagen matrices exhibit weak mechanical strength (E = 0.1 - 10 kPa), limiting their relevance in the study of higher range elasticities that may be more typical of cancerous soft tissue (E = 1 - 100 kPa) or stiffer sites of common metastasis like bone (E >> 100 kPa)[188,189]. Further, this fragility may present handling difficulties when transitioning to more involved experimental manipulations; for example, more complex methods used to pattern bioactivity. In addition, while complex proteinaceous natural matrices are highly bioactive, there is limited experimental control over this bioactivity with variable bioactivity between different natural matrices resulting in differences in adhesion, cytoskeletal arrangement, and migration in the same pool of cells[190]. Finally, they feature a critical flaw in that the adjustment of matrix mechanics almost always alters matrix biochemistry, presenting a significant confounder, particularly in studies that strive to parse out the relative importance of ECM ligand and stiffness influences[189,191,192].

Tissue engineers have sought to avoid these problems by pioneering the development of scaffolds composed of synthetic materials, typically polymers, with some of these scaffolds permitting more precise experimental control over mechanical properties, degradation, and cell-matrix interactions. Polymers in the polyester group like poly(lactic acid) or its copolymer with poly(glycolic acid), poly(lactic-co-glycolic acid) (PLG), have been widely used in the field in part because of their predictable and tunable degradation and the ability to tune their modulus by altering the amount of copolymer

used[193,194]. Other traditionally used synthetic scaffolds include those based on the polyurethanes or polydimethoxysiloxane, given their biocompatibility, versatility, and partial control over mechanical properties[195]. Synthetic matrices made of polyacrylamide (PA) have been used extensively in two-dimensional studies examining substrate stiffness-related effects on cell behavior and differentiation primarily because they offer precise control of elastic modulus over a wide range[27,33].

3D culture of cancer models already has begun to transition to the realm of synthetic scaffolds. For example, an oral squamous cell carcinoma model cultured in a porous PLG scaffold formed *in vivo*-like tumors with high angiogenic capacity and chemotherapy resistance[196]. Scaffolds composed of PLG or other polyesters have been used to study growth, morphology, and chemotherapy response in many other cancer models, including other breast lines[197], osteosarcoma[198], glioblastoma multiforme[199], and leukemia[200]. PA gels, meanwhile, have been widely used in two-dimensional cancer models to further the study of cancer response to matrix rigidity or illuminate new cancer migration findings[201–203].

In general these traditional synthetic materials suffer from more limited bioactivity compared to natural biomaterials. Any bioactivity present, such as cell adhesion, typically relies on nonspecific adsorption of proteins from the media. This nonspecific adsorption can make the engineering and study of specific ECM growth factors or other matrix constituents a challenge. Further, the traditional polyester scaffolds and similar materials often require an additional and potentially unphysiological porogen processing step to create a porous matrix amenable to 3D cell seeding and 3D culture[204]. With other synthetic materials, notably PA, harsh crosslinking conditions or

monomer toxicity endanger cell viability in 3D experiments, limiting their use to two-dimensions[205]. Further, while polymer degradation with traditional synthetic scaffolds is often engineered with more predictability than natural matrices, cell-mediated degradation may be lacking. This cell-directed reorganization of the matrix is a vital feature when studying drastic switches in cancer behavior like those that occur in EMT and metastasis. In the study of cancer-microenvironment interactions, the use of synthetic matrices that feature the combination of high 3D biocompatibility, tunable mechanics, and the capability to model the full range of bioactivity that the ECM affords is in its infancy, with poly(ethylene glycol)-based hydrogel matrices an exciting option to explore in this effort.

### 1.2.4 Poly(ethylene glycol)-based Hydrogel Matrices

Poly(ethylene glycol) or PEG is an FDA-approved hydrophilic polymer widely studied in both *in vitro* and *in vivo* tissue engineering applications and is well-suited as an ECM mimic in studies probing cancer-matrix interactions[187,206–208]. PEG molecules with bi-terminal acrylate groups can be combined with a chemical photoinitiator and exposed to an activating light source to form a cross-linked hydrogel matrix, with appropriately mild cross-linking conditions permitting cell encapsulation into the hydrogel bulk with high viability, thus facilitating three-dimensional study [209,210]. Fully hydrated, PEG matrices are mostly composed of water and closely mimic soft tissues with physiologic diffusional and mechanical properties[189,211]. Furthermore, in their unmodified state, PEG hydrogels resist nonspecific protein adsorption and subsequent cell adhesion and interaction [212–214]. This characteristic offers a “blank slate” biomaterial for which one can

be confident that any biologic response observed is the result of an intentionally engineered modification.

Bioactivity can be incorporated into PEG hydrogels by the inclusion of a variety of ligands, from oligopeptides to whole protein growth factors (Fig. 1-9). Making use of well-characterized chemistry, a free amine or terminal carboxyl group in proteins or peptide sequences is attached to a bifunctional PEG chain forming an acryloyl-PEG-ligand molecule that can then be incorporated into the bulk of the hydrogel matrix during formation[215]. For example, the fibronectin-derived RGD peptide sequence can be added to the PEG hydrogels to enable basic cell adhesion and promote cell migration[216,217]. Other ECM-mimetic peptides, like the laminin-derived YIGSR and IKVAV and the elastin-derived VAPG have been incorporated into PEG hydrogels as an analogue to their respective ECM proteins to explore a variety of cell responses[218,219]. Further, because this conjugation chemistry can be performed in aqueous solution, whole proteins can be incorporated without compromising protein structure and function[215,220]. Growth factors

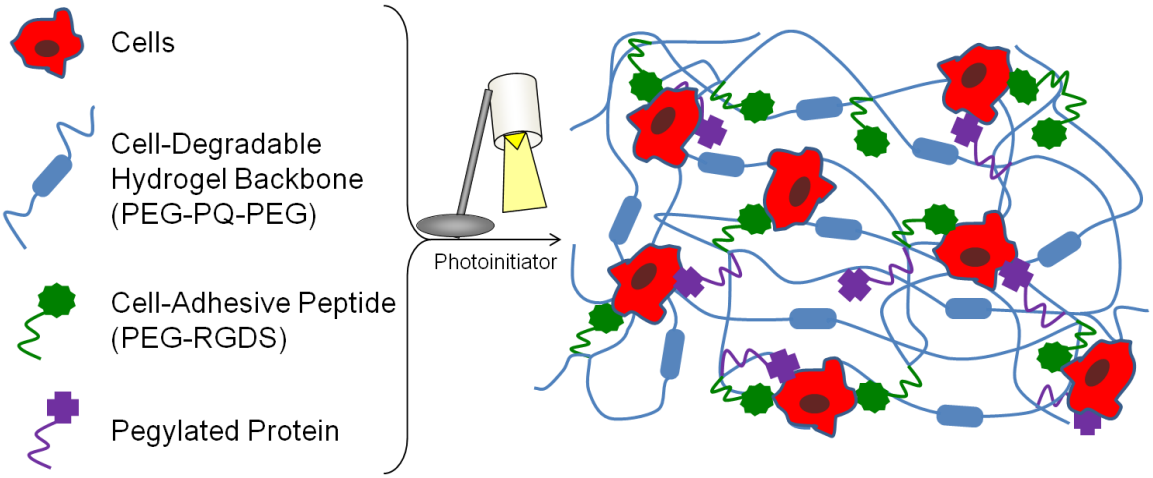


**Figure 1-9: Bioactive PEG-based hydrogels.** In the presence of a photoinitiator and activating light, cells can be encapsulated into PEG-based hydrogels with high viability. Bioactive molecules can be incorporated into the matrix, like PEG-RGDS to permit cell adhesion, a degradable sequence in the PEG-PQ-PEG backbone to permit cell-mediated degradation, and pegylated proteins to exert matrix-derived biochemical effects.

like vascular endothelial growth factor, bone morphogenetic protein-2, ephrinA1, TGFβ-1, and many others have been incorporated into PEG hydrogels to exert matrix-derived biochemical signaling (Fig. 1-10)[207,210,221–223]. The PEG conjugation reaction can be carefully controlled to prevent over-modification of proteins that require structure maintenance to signal with more complex tertiary signaling, like FGF[210]. The covalent tethering of growth factors to the scaffold via PEG may make the proteins resistant to proteolytic degradation and endocytosis by cells and prevent loss by diffusion thus allowing prolonged growth factor delivery[220,224].

For 3D studies examining cancer-matrix interactions and metastasis, the scaffold used would ideally be degradable to permit cell and tumor spheroid reorganization and migration. Chemistry similar to that discussed above can be used to bind protease-sensitive sequences to flanking acrylate-PEG chains, and the resulting molecule can be polymerized to form PEG-based hydrogels capable of cell-mediated degradation[225,226]. Such a system has been well-studied in vascular tissue engineering applications where, for example, MMP-sensitive hydrogels permit self-organization of an angiogenic co-culture into a vascular network with characteristics similar to native tissues[207]. The degradable sequence can be tailored to permit different degrees of reactivity with a variety of individual proteases, like other MMP species or plasmin, with specifically engineered reaction kinetics[225–227].

In addition to designed bioactivity, PEG hydrogels also exhibit tunable mechanical properties. Matrix elasticity can be tuned by altering the concentration of PEG used in the prepolymer solution or by changing the molecular weight of the PEG polymer chain[228]. High molecular weight PEG yields matrices with lower crosslink

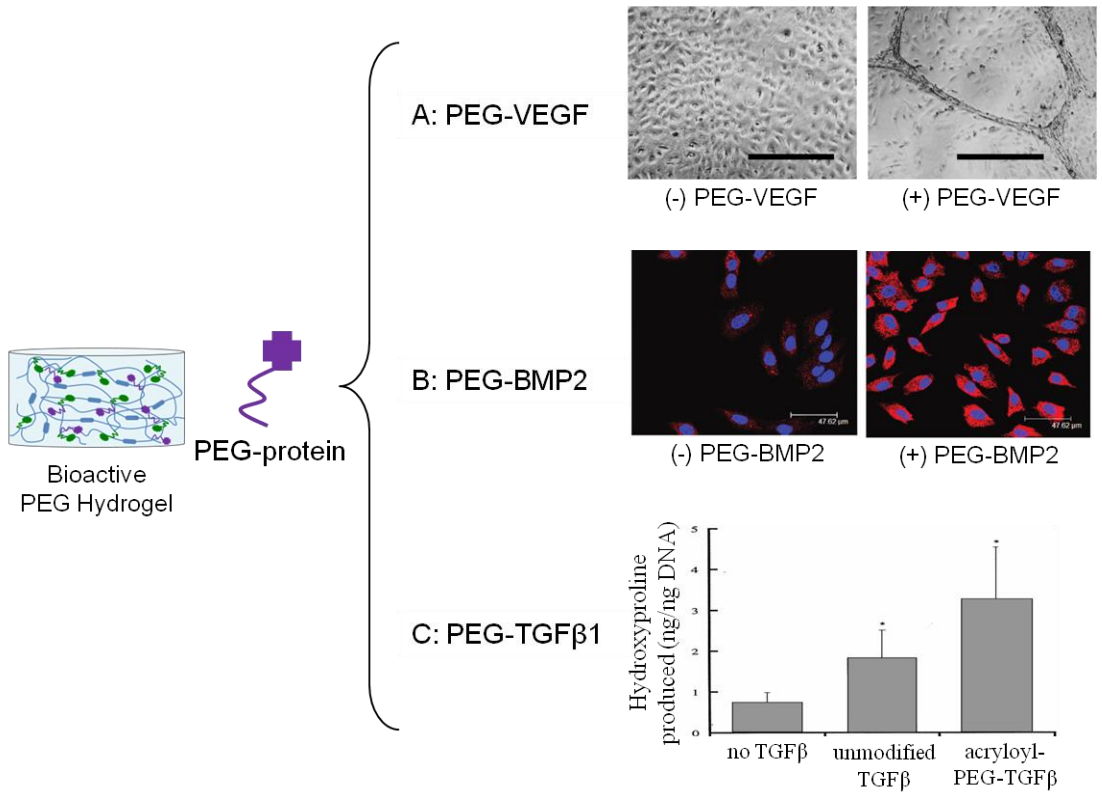


**Figure 1-10: PEG-proteins can exert diverse biological effects.** For example, (*A*) matrix-tethered PEG-VEGF promotes endothelial cell tubule formation. Scale bar is 500 μm. Adapted from Leslie-Barbick, *et al.*[221] (*B*) PEG-BMP2 promotes expression of osteocalcin (red) of cultured osteoblasts. DAPI (blue). Modified from Liu, *et al.*[223] (C) Matrix-tethered PEG-TGFβ improved smooth muscle cell ECM secretion compared to soluble, unmodified TGFβ. Adapted from Mann, *et al.*[222]

densities and higher water content to produce a softer substrate. Altering these factors together enables relatively precise tunability of the stiffness over a broad physiologic range. Further, because the system is photo-controlled, hydrogels with more complex arrangements of matrix elasticity can be presented to cells. For example, hydrogels with a gradient of elasticity varying linearly from 2-100 kPa down the length of the gel can be formed through controlled mixing of two different prepolymer solutions of low and high molecular weight PEG during polymerization[228]. In addition, a photomask can be deployed during polymerization or in subsequent manipulations to yield hydrogels with distinct areas of patterned stiffness, or if used in concert with separate pegylated bioactive species, designed areas of patterned bioactivity (Fig. 1-11)[228,229]. Further, in place of a

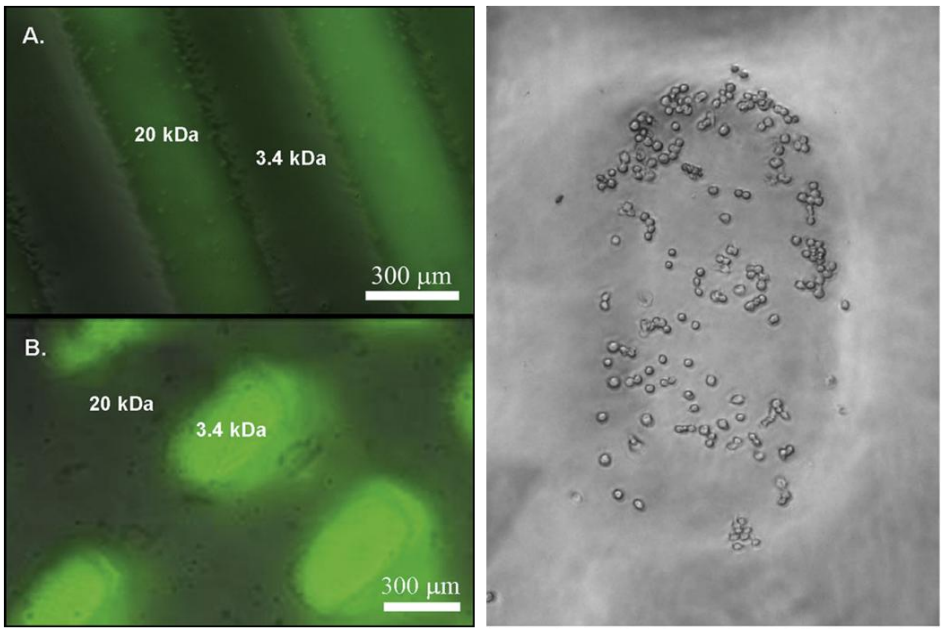


**Figure 1-11: Patterned elasticity on PEG hydrogels.** (*Left*) PEGDA hydrogels with photomask-patterned elasticity with (A) dextran-fluorescein soaking into softer 20 kDa regions after patterning or (B) acrylated fluorescein incorporated into stiff 3.4 kDa regions during patterning. (*Right*) RAW 264.7 macrophages preferentially adhere to stiff regions after 48 hours. Modified from Nemir *et al*.[228]

lamp light source, a confocal laser scanning microscope can be used to incorporate additional patterned bioactivity like micron-scale vascular-mimetic geometries of angiogenic growth factors or, through use of two-photon excitation, complex and precise three-dimensional patterned bioactivity[230,231].

Finally, because cells are incapable of interacting with the PEG itself, changing hydrogel stiffness by altering the concentration or molecular weight of PEG chains does not alter the bioactivity of the matrix. This offers an important advantage for the PEG-based system over natural matrices and many other synthetic materials. The mechanics of the overall matrix are determined by the crosslinking properties of the base PEG chains while bioactivity is incorporated distinct from this process, and as such, any response seen in cells cultured on the matrix is the result of known changes to mechanics or biochemistry with little danger of unknown interaction between the two factors.

Furthermore, the versatility in incorporation of bioactive peptides and proteins permits exploration of a wide variety of ECM factors that may play a role in tumor growth and metastasis with a similar high degree of experimental control. This control, coupled with high biocompatibility and potential in more advanced experimental manipulations, makes PEG-based hydrogels an excellent matrix-mimetic platform with which to study matrix-derived influences on cancer behavior and metastasis.

## 1.3 Summary and Overview of Thesis

The stromal environment plays an essential role in a variety of cellular behaviors in health and disease. Investigation into the stromal role in cancer has demonstrated that disruptions in tumor ECM composition, architecture, and mechanics in concert with pathological stromal cells are essential to cancer progression and metastasis. Researchers have begun to further explore these interactions using *in vitro* ECM-mimetic matrix systems, illuminating key findings on the ECM's role in morphogenesis, epithelial-mesenchymal transition (EMT) and metastasis, but study has been hindered by the limitations in control and versatility of naturally-derived matrices.

In this thesis work, a bioactive, ezymatically degradable PEG-based hydrogel system is used study a newly characterized lung cancer model that is highly responsive to ECM-derived cues. First, the PEG system is deployed to recapitulate key MG findings related to epithelial morphogenesis of an EMT-prone lung adenocarcinoma model line and further understanding of this process by examining the influence of matrix bioactivity and mechanics. Next, the response of cells in the PEG system to TGFβ is investigated, examining the influence of matrix parameters and a protease-sensitive sequence in degree of matrix invasion. Furthermore, the EMT-related remodeling of cell-secreted ECM and

its modulation by matrix parameters is investigated. Finally, the PEG system is deployed to examine the role of cell-cell contacts in epithelial morphogenesis and EMT. Specifically, matrix-tethered E- and N-cadherin are used to modulate the behavior of both the representative metastatic model line, 344SQ, and a mutant line that is incompetent in morphogenesis in the absence of intercellular interactions due to a mutant polarity gene. Overall, this thesis advances the state of the field of ECM influences on cancer progression, demonstrating how the PEG system can be used to robustly study such extrinsic cues and deploying it to describe key matrix parameters that are important in guiding EMT-related morphogenetic and metastatic processes.

# 2. PEG Hydrogels for Investigation of Matrix-derived Influences on Lung Adenocarcinoma Epithelial Morphogenesis

A significant portion of this chapter is from BJ Gill, DL Gibbons, LC Roudsari, JE Saik, ZH Rizvi, JD Roybal, JM Kurie, and JL West (2012). *Cancer Research*, 72, 6013-23.

## 2.1 Introduction

Non-small cell lung cancer (NSCLC) is the leading cause of cancer-related death with most patients diagnosed at an advanced stage. Of the remaining patients who undergo curative surgery, upwards of 50% will have a disease recurrence with metastatic cancer at non-lung sites[232]. One model of metastasis purposes that a subset of cells in primary epithelial tumors undergoes EMT characterized by loss of apical-basal epithelial polarity, loss of intercellular adhesions, the acquisition of mesenchymal differentiation properties, and subsequent migratory potential and matrix invasion[233]. Similarly, it is postulated that once they reach new sites of metastatic implantation, metastatic cells undergo mesenchymal-epithelial transition (MET) characterized by loss of mesenchymal characteristics and motility, formation of extensive cell-cell contacts, and reacquisition of epithelial polarity[234]. Researchers have sought to develop cell lines and matrix systems that effectively model EMT and MET processes in the hope that a more complete understanding of the matrix's role in EMT/MET might illuminate new therapeutic targets.

### 2.1.1 A Novel Lung Cancer Model with ECM-mediated EMT

Research into EMT and metastasis in lung cancer has been hampered by lack of good models to study these behaviors in animals or in *in vitro* systems. Most of the

previous models have used human cells derived from immunodeficient animal xenograft studies to yield important findings regarding cell-intrinsic genetic and epigenetic changes, but they provide little information about the role a supportive ECM may play in tumor development or progression[232,235]. To circumvent issues with these xenograft models, a few groups have developed genetic mouse models based on mice with mutant K-ras alleles in which spontaneous lung adenocarcinomas develop, but all of these models lack metastatic disease, the central feature of interest to study for patients with NSCLC. Unsurprisingly, given the overall lack of reliable NSCLC models suitable for any type of study, little examination of matrix-derived influences on NSCLC behavior and metastasis has been done, with most studies of this kind using a group of the same commonly studied breast cancer model lines. This limitation potentially risks the inappropriate generalization of cell line- or cancer type-specific findings to cancer more broadly.

A new panel of lung adenocarcinoma model lines has been developed to model metastatic lung cancer and probe for ECM-related influences on lung cancer invasion and metastasis (Fig. 2-1). These tumor cell lines were derived by examining mice that were heterozygous for a somatically activated $KRas^{G12D}$ allele, a germline $p53^{R172H\Delta G}$ allele, or both[235]. Mutant K-ras was found necessary for the development of high-frequency primary lung adenocarcinomas, and while the presence of the mutant p53 allele did not affect primary tumor development, the mutation did have a dramatic effect on the rate of metastases from the primary site (37% vs. 4.5%). Metastases in $KRas^{G12D}/p53^{R172H\Delta G}$ mice were found at sites frequently observed in human NSCLC patients, and displayed a

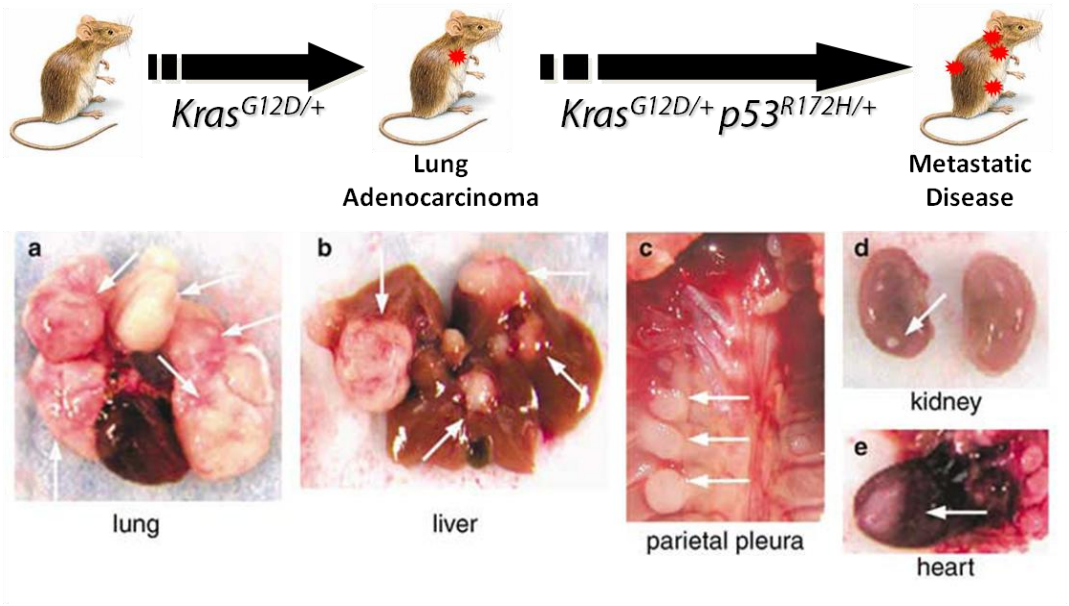


**Figure 2-1: A genetic mouse model for metastatic lung adenocarcinoma.** (*Top*) Mice with somatically activated K-ras formed primary lung adenocarcinomas with no metastatic disease. When mated with mice with a p53 mutation, the heterozygous mutations induced formation of lung adenocarcinoma with widespread metastatic disease, (*Bottom*) featuring high tumor burden in the lung (a), and metastases to the liver (b), parietal pleura (c), kidney(d), and heart (e). Modified from Zheng, *et al.*[235]

gene expression signature similar to that of tumors in these patients, with a stronger correlation to patients with particularly poor prognosis [236].

In additional findings, several cell lines developed from primary or metastatic tumor sites were re-injected into healthy syngeneic mice and were found to differ in their ability to cause new metastatic disease (vs. subcutaneous tumors) despite identical initial genetic abnormalities[232]. When further studied *in vitro* in 3D MG assays, one representative metastatic cell line from this model, 344SQ, transitioned from a mesenchymal to epithelial phenotype, forming highly polarized, growth-arrested, lumenized spheres reminiscent of a lung acinus (Fig. 2-2). Upon TGFβ exposure, these

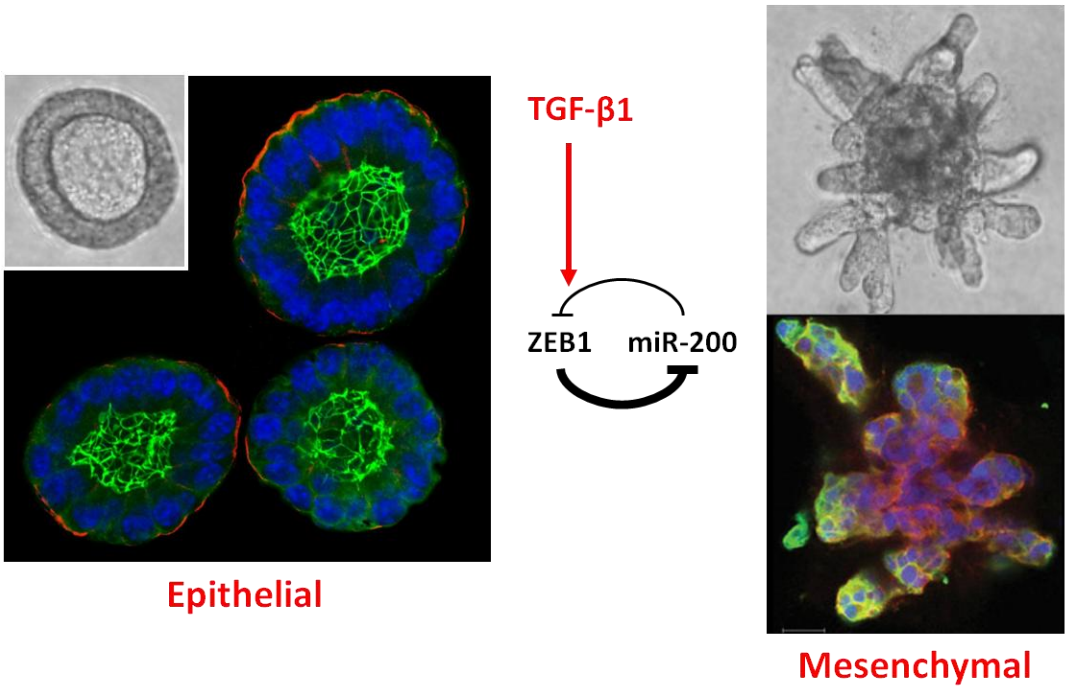


**Figure 2-2: Contextual ECM cues regulate EMT of the 344SQ NSCLC model.** 344SQ forms growth-arrested, lumenized spheres in 3D MG culture with localized expression of epithelial polarity markers. Upon TGF-β1 exposure, cells proliferate, lumenization and polarity are lost, and matrix-invasive outgrowths are formed. This process is mediated by a double-negative feedback loop between miR-200 and the pro-EMT transcription factor Zeb1. α6-integrin (red), ZO-1 (green), Torpro-3 (blue). Adapted from Gibbons, *et al.*[232]

epithelial 344SQ structures progressed through EMT, becoming larger, losing apical-basal polarity, and forming invasive outgrowths, coincident with alteration in expression of several EMT-related genes. Meanwhile, a nonmetastatic $KRas^{G12D}/p53^{R172H\Delta G}$ line, 393P, was resistant to TGFβ, requiring much longer time of exposure to cause morphologic changes and preserving expression of some epithelial markers. This EMT response was found to be regulated by the microRNA (miR)-200 family, with miR-200 levels much higher in 393P vs. 344SQ and falling in 344SQ upon TGFβ exposure. The change occurred in concert with a rise in Zeb1, a master EMT transcription factor that modulates several pro-EMT proteins and forms a double negative feedback loop with miR-200[233,237]. Constitutive expression of miR-200 in 344SQ prevented an increase in

Zeb1, blocked EMT-related gene expression and morphological changes induced by TGFβ exposure, and prevented metastatic disease seen with syngeneic reinjection[232].

To summarize important findings, the KRas$^{G12D}$/p53$^{R172H\Delta G}$ 393P and 344SQ lines showed dramatically different metastatic potential despite a common genotype, and the representative metastatic line (344SQ) exhibited a markedly different phenotypic response *in vitro* depending on to extracellular context (3D vs. 2D, +/- TGFβ). These findings were expounded upon by a recent report that demonstrated that cells that differ in their metastatic capacity and miR-200 expression also differentially express a wealth and wide variety of cell surface and ECM matrix proteins that no-doubt play a role in their different matrix-related phenotypes (Fig. 2-3)[238]. Notably, differentially expressed

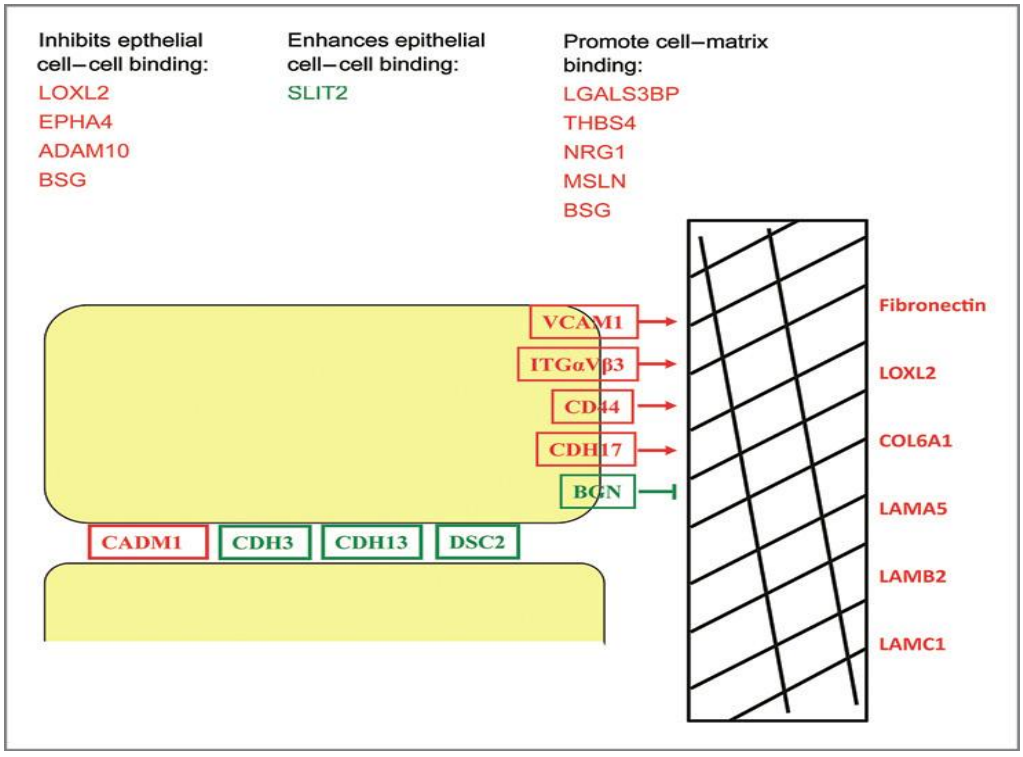


**Figure 2-3: Differential expression of ECM-related proteins in 344SQ.** A global liquid chromatography -tandem mass spectrometry analysis found notable proteins upregulated (red) or downregulated (green) in metastatic 344SQ compared to non-metastatic 393P. In general, expression demonstrated increased secreted ECM, enhanced binding to ECM, and decreased cell-cell adhesion. Modified from Schliekelman, *et al.*[238]

proteins included integrins $\alpha_v$ and $\beta_3$, the important adhesion protein CD44, the ECM-crosslinker LOXL2, and a variety of ECM proteins themselves including fibronectin, collagen VI, and several laminin subunits. An additional study suggested that alterations in cell-cell contacts, specifically the Notch-Jagged signaling system, may also play a role[239]. Interaction with the surrounding microenvironment of cells at the leading edge of *in vivo* 344SQ-derived tumors was found to drive a Jagged2-dependent development of a metastatic subpopulation.

Taken together, these findings suggest that the EMT and metastatic capacity of NSCLC is not solely dependent on cell-intrinsic chromosomal changes or somatic mutations, but is likely heavily influenced by physical and soluble factors of the surrounding ECM environment, potentially mediated through effects on miR-200. Further, they suggest that it may be possible to convert metastasis-prone tumor cells to a metastasis-incompetent state by manipulating these stromal interactions[2,232]. This idea provides an exciting potential avenue for new therapeutic interventions, but requires much more experimental investigation into the nature of these key interactions. The use of the PEG system in place of MG in the service of this investigation should circumvent issues with purity and the confounding of bioactivity and mechanics while providing robust experimental flexibility and control in probing potentially important cell-matrix and cell-cell interactions.

### 2.1.2 Matrix Tools to Study Lung Adenocarcinoma Epithelial Morphogenesis and EMT

As reviewed in Chapter 1, the tumor ECM is central to growth, gene expression, migration and a number of other processes important to cancer pathophysiology and

progression. Much research focus has been directed toward the use of *in vitro* matrix-mimetic materials that can facilitate the study of features of this tumor-ECM interaction and matrix factors that guide tumor behavior. Some of this work has been done using two-dimensional culture systems, namely polyacrylamide (PA) gels engineered with stiffness that is more physiological than traditional 2D culture surfaces, to provide glimpses on the influence of matrix stiffness on narrowly-focused facets of behavior of single cultured cells. For example, an early report from Wang, *et al*., used PA gels to study differences in matrix stiffness-influenced cell proliferation and apoptosis between normal and neoplastically transformed cells[240]. Other reports have sought to deploy 2D PA systems to study cancer cell spreading, motility, and invadopodia formation to suggest insight into tumor growth and migration[203,241]. However, as described previously, these characteristics and many others are dramatically different in cells in 2D culture compared to their more physiological 3D environment. This is of even greater importance in cancer as the dramatic differences in 3D matrix invasion, growth factor response, and intercellular organization leave conclusions based on 2D culture wanting and incomplete.

To facilitate this 3D culture, naturally-derived materials such as collagen and MG have been largely used due to their ready availability, biocompatibility, and rich presentation of cell adhesive ligands to facilitate cell culture and growth. 3D culture of different cancer lines in these materials has enabled modeling and study of crucial physiologically relevant behaviors impossible to observe in 2D culture, like formation of organized, multi-cellular tumor spheroids by epithelial tumors and their disruption in malignant progression[104,168,174,176,181]. These matrices have also enabled more relevant

exploration of matrix-derived biochemical and mechanical influences on cancer progression, EMT, and invasion. For example, increased collagen density and organization in collagen-based matrices promote tumor progression[22,23,83], and increased collagen crosslinking leads to EMT and invasion[43]. Stiffening of MG and collagen matrices perturbs epithelial morphogenesis of the MCF10A mammary cell line and promotes an invasive phenotype through alteration of integrin clustering and regulation of Rho activity and the FAK-ERK pathway[99,184]. While most of the study has been focused on breast models, work by the Gibbons and Kurie groups using natural matrices has shown important matrix-related influences on lung adenocarcinoma, with model lines in MG showing important morphogenic responses in a 3D environment[232], influenced by surrounding growth factors[238] and binding of the Jagged-notch cell-cell signaling system[239].

As described in Chapter 1, the use of naturally-derived material in these matrices presents obstacles in the reliable engineering of the matrix environment related to growth factor contamination, batch-to-batch variability, and key limitations in matrix mechanics whereby only a relatively low maximum stiffness can be achieved and the tuning of mechanics frequently leads to concordant changes in biochemistry. In addition, the baseline level of high cell interactivity that these matrices afford makes the study of specific matrix-derived influences difficult. To examine the specific influence of particular integrins or other cell surface receptors in these matrices, for example, one typically has to rely on blocking antibodies or knockdowns as a potentially inaccurate surrogates to actual changes to the ECM[99,174,176,239]. In this one-sided, cell-centered approach, cancer cells are altered to modulate their reactivity to the ECM and the

response typically recorded by measuring changes to these altered cells. This approach may be less physiologically relevant than one that seeks to introduce cell-extrinsic changes to the ECM to probe the matrix-induced response of otherwise unaltered tumor cells.

The use of synthetic matrices that attempt to avoid the pitfalls of natural matrices while providing a modular platform to independently probe 3D matrix cues like matrix stiffness or specific biochemical ligands for influence on cancer behavior is of increasing research focus. One report has deployed Michael-type crosslinked hyaluronic acid-based (HA) hydrogels with tunable mechanical properties conjugated to a RGD-based adhesion peptide to influence glioma cell adhesion and behavior in 2D and 3D in an attempt to parse the separate effects of matrix mechanics and biochemistry[191]. Bilayered, bioactive HA matrices have also been used to illuminate the unique morphologic and growth factor secretion changes of a prostate cancer model line resulting from 3D culture[242]. The study of cancer models in systems with decoupled mechanics and bioactivity has been attempted in other systems including glioma and liver cells in collagen gels respectively stiffened with non-bioactive agarose[243] and PEG[244] and in breast cells in a self-assembling peptide matrix[192]. However, in the former cases, the bulk matrix components are still themselves bioactive, and in the latter, bioactivity is mediated by passive protein adsorption, rather than tuned with specific engineered control.

With high resistance to protein adsorption and non-specific cell interactions, PEG hydrogels offer a baseline non-interactive, but still biocompatible material with which to introduce and study the effect of matrix-derived influences on cancer behavior. Because the system is modular, and the mechanical component is distinct from the bioactive

component, these matrices feature independently tunable mechanics and biochemistry with each factor available for testing of an independent biologic effect with high experimental control. In this chapter, PEG hydrogels were used to study matrix influences on the behavior of lung cancer cell lines from the $KRas^{G12D}/p53^{R172H\Delta G}$ model with focus on the representative metastatic line 344SQ. First, a PEG system featuring biospecific cell adhesion and cell-mediated proteolytic degradation was used to recapitulate this MET morphogenesis previously observed in the MG system. Matrix stiffness and the concentration of cell-adhesive ligand were altered and found to significantly influence epithelial morphogenesis. This influence was manifest by differences in the extent of lumenization, in patterns of intrasphere apoptosis and proliferation, and in expression of epithelial polarity markers. Finally, a cyclic form of RGD was introduced in place of the linear form to further alter this matrix bioactivity-mediated response.

## 2.2 Materials and Methods

### 2.2.1 Cell Culture

The 344SQ, 393P, and 344P cell lines were derived from $KRas^{G12D}/p53^{R172H\Delta G}$ mice as described previously in Gibbons, *et al*. and Zheng, *et al*.[232,235]. The 344SQ_429 cells are derived from 344SQ parental cells and contain a constitutive expression vector encoding the miR-200b_a_429 locus). Cells and cell-laden hydrogels were cultured in a humidified atmosphere at 37˚C and 5% $CO_2$ in RPMI 1640 (Mediatech, Manassas, VA) with 10% fetal bovine serum (Atlanta Biologicals, Lawrenceville, GA), 10 μg/ml gentamicin and 0.25 μg/ml amphotericin B (Invitrogen, Carlsbad, CA).

### 2.2.2 Synthesis and Purification of PEG-RGDS and PEG-PQ-PEG

Bioactive hydrogel constituents were first synthesized (Fig. 2-4). Monoacrylate-poly(ethylene glycol)-succinimidyl carboxymethyl (PEG-SCM; Laysan Bio, Arab, AL) and Arg-Gly-Asp-Ser peptide (RGDS; American Peptide, Sunnyvale, CA) were dissolved separately in dimethyl sulfoxide (DMSO; Cambridge Isotope Laboratories, Andover, MA), and then the PEG-SCM solution was slowly added to the RGDS solution at a molar ratio of 1:1.2 (PEG-SCM:RGDS). A small volume of N, N-Diisopropylethylamine (DIPEA; Sigma, St. Louis, MO) was added to that mixture at a molar ratio 1:2 PEG-SCM: DIPEA. The resulting solution was mixed, reacted overnight on a rocker, and dialyzed against deionized water in a 3500 MWCO regenerated cellulose membrane (Spectrum Laboratories, Rancho Dominguez, CA) to remove unreacted products and organic solvents. In a separate reaction, the same process was used to conjugate a cyclic form of RGD (c(RGDfk), Creative Peptide, Shirley, NY) to synthesize

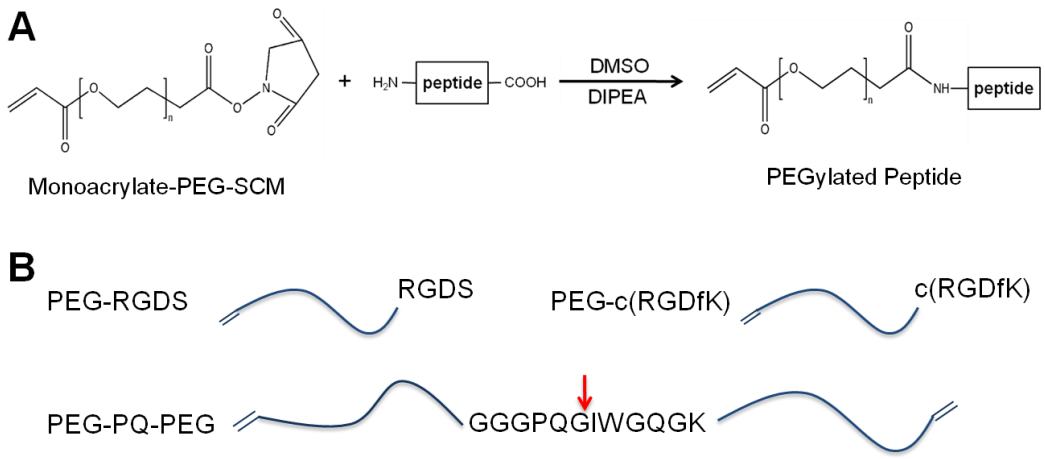


**Figure 2-4: Bioactivity of PEG matrix**. *A*, bioactive peptides are reacted with monoacrylate-PEG-succinimidyl carboxymethyl (SCM) to form *B*, pegylated peptides: linear and cyclic forms of PEG-RGDS to permit cell adhesion and PEG-PQ-PEG that serves as a matrix backbone susceptible to cell-mediated degradation via cleavage by MMP-2 and -9 (cleavage cite at red arrow).

the PEG-c(RGDfK) molecule.

The MMP-sensitive peptide GGGPQGIWGQGK (PQ) was similarly reacted to form PEG-PQ-PEG ("PEG-PQ"); PEG-PQ was synthesized to make the backbone of the hydrogel network susceptible to cleavage by secreted MMP-2 and -9, enabling cell-mediated matrix degradation and remodeling[207,245]. First, the PQ peptide was synthesized via standard Fmoc chemistry on an APEX 396 solid phase peptide synthesizer (Aapptec, Louisville, KY) and characterized with MALDI-TOF. The PQ peptide was then conjugated to PEG-SCM following a similar procedure as PEG-RGDS, but with a 2.1:1 molar ratio PEG-SCM:PQ. Following lyophilization, conjugation of PEG-peptide products were confirmed using gel permeation chromatography (GPC; Varian, Inc., Palo Alto, CA) with PEG-peptides dissolved in dimethylformamide (DMF) with 0.1% (w/v) ammonium acetate and compared to PEG-SCM standards.

### 2.2.3 Cell Encapsulation in Hydrogels

Polymer mixtures were prepared with PEG-PQ and PEG-RGDS in 10 mM HEPES buffered saline (HBS; pH 8.5) with 1.5% v/v triethanolamine (TEOA, Fluka BioChemika, St. Louis, MO), 3.5 µl /ml N-vinylpyrrolidone (NVP, Sigma) and 10 µM eosin Y photoinitiator (Sigma), and the solutions were sterilely filtered. For initial experiments recapitulating 3D morphogenesis, PEG-PQ was mixed at 10% (w/v) and linear PEG-RGDS added at 3.5 mM. 344SQ cells were pelleted by centrifugation at 500 x g for 4 min and then resuspended in the polymer solution at 1500 cell/µl (1.5 M cell/ml) unless otherwise noted.

For easy handling, hydrogels were formed attached to a methacrylated coverglass base. Methacrylated coverglass was made by etching a glass coverslip with piranha

solution (30% v/v 9 M $H_2O_2$ and 70% v/v 37.5 N $H_2SO_4$) and reacting with 85 mM 3-(Trimethoxysilyl)propyl methacrylate (Fluka) in 95% ethanol (pH 4.5) overnight. Under sterile conditions, hydrogel disks were fabricated by sandwiching a 5 µl droplet of polymer solution containing cells between a glass slide and a methacrylated glass coverslip separated by two 380 µm thick polydimethylsiloxane spacers (Fig. 2-5). The set-up was then immediately exposed to high intensity white light for 30 s (Fiber-Lite Series 180, 150 W halogen, Dolan Jenner), leading to hydrogel polymerization and covalent linkage to the methacrylated coverglass base. High cell viability was confirmed 24 h after encapsulation (2 µM calcein AM and 4 µM ethidium homodimer, Live/Dead Kit, Invitrogen).

### 2.2.4 Mechanical Testing

For material compressive properties, acellular hydrogel disks were formed as above using 5, 10 or 15 % (w/v) PEG-PQ solutions. For comparison, MG samples were

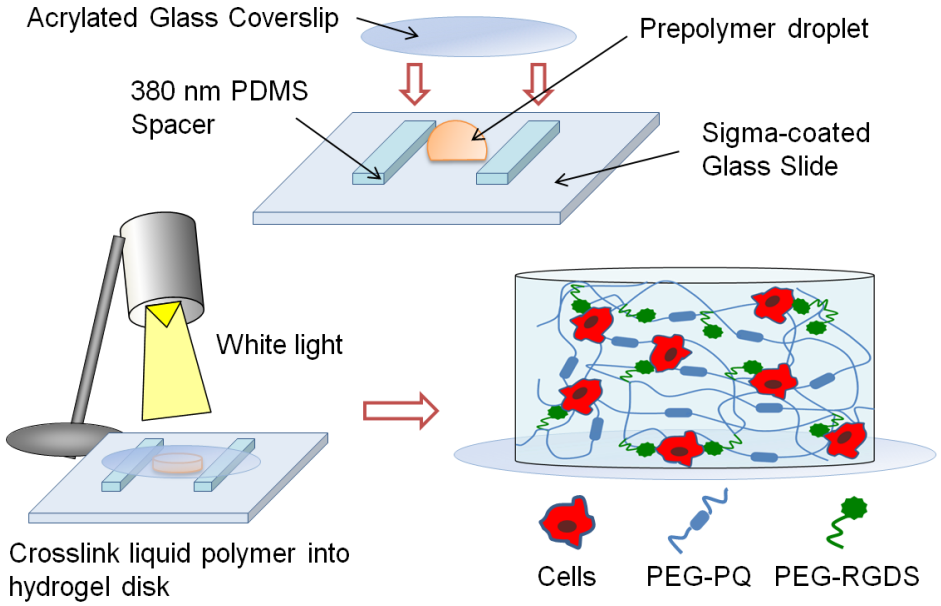


**Figure 2-5: Hydrogel fabrication schematic.** Matrix components are mixed with cells and eosin Y photoinitiator and polymerized under white light to form a PEG hydrogel attached to a coverslip for handling. Encapsulated cells interact with bioactive hydrogel components.

prepared as in Gibbons, *et al.* using a chamber plate with removable walls[232]. Sample dimensions were obtained using digital calipers prior to subjecting samples (n = 4 per formulation) to compressive testing using an Instron Model 3340 mounted with a 10 N load cell. Instron Series IX/s software was used for testing control and data acquisition as uniaxial compressive strain was applied at 0.5 mm/min. Force-elongation data was converted to stress-strain data with corrected cross-sectional area and plotted to derive the elastic modulus from the slope of the linear portion of the curve.

### 2.2.5 344SQ Sphere Lumenization and Size

344SQ cells were encapsulated in hydrogels with varied PEG-PQ concentration (5, 10, or 15 % (w/v)) and fixed 3.5 mM linear PEG-RGDS or with fixed 5% PEG-PQ concentration and varied PEG-RGDS concentration (1, 3.5 or 7 mM) to assess for matrix-related influences on the size and degree of lumenization of cell spheres. Hydrogel samples (n = 5 per formulation) were imaged every 2 days on an Axiovert 135 inverted fluorescent microscope (Zeiss, Oberkochen, Germany) and sphere diameter was measured using Image J (NIH). Lumenization scoring was done blinded to grouping and, for initial experiments with linear PEG-RGDS, quantified as the number of spheres exhibiting central clearing on brightfield images over total spheres formed. Both size and lumenization data were expressed as means for all spheres in a given hydrogel sample. Further, size data from spheres across all hydrogel samples of a particular formulation were pooled and organized into histograms to better visualize matrix formulation-related variation in sphere organization.

### 2.2.6 Immunohistochemistry

Hydrogels with encapsulated cells were fixed in 3.7% paraformaldehyde (EMS, Hatfield, PA) for 45 min, permeabilized with 0.25% (v/v) Triton X-100 (Sigma) for 10 min and blocked overnight at 4˚C with 5% (v/v) donkey serum (Sigma). Samples were then incubated with the following primary antibodies overnight at 4˚C: for polarity staining - mouse anti-β-catenin (BD Biosciences, San Jose, CA), mouse α6-integrin (Chemicon/EMD Millipore, Billerica, MA) and rabbit anti-ZO-1 (Invitrogen); for apoptosis and proliferation staining - rabbit anti-cleaved caspase-3 (Cell Signaling, Danvers, MA) and goat anti-ki-67 (Santa Cruz, Dallas, TX). Following an 8 h rinse in PBS + 0.01% (v/v) Tween (Sigma), samples were incubated overnight at 4 ˚C with either an Alexafluor 488 or 555 tagged donkey anti-rabbit, -mouse or –goat secondary antibody (Invitrogen). Samples were counterstained overnight with a 2 μM DAPI solution to visualize cell nuclei and 0.11 μM Alexafluor 647 phalloidin (Invitrogen) to visualize actin organization and then imaged using a Zeiss 5Live confocal microscope.

### 2.2.7 Epithelial Morphogenesis of 344SQ in Matrices with Cyclic PEG-RGDS

As above, 344SQ were encapsulated in hydrogels with fixed 5% PEG-PQ concentration, but with varied PEG-c(RGDfK) concentrations (1, 3.5 or 7 mM). 5% PEG-PQ gels with the same concentrations of linear PEG-RGDS were also used as controls. Hydrogel samples (n = 3 per formulation) were cultured for 12 days, stained as above for polarity markers, and imaged on a Zeiss 5Live confocal microscope to assess for differences in sphere size and epithelial morphogenesis. Mean sphere size was measured using ImageJ, evaluated as sphere diameter across maximum cross-section on the phalloidin channel (~80-100 spheres per gel sample), and expressed as means for all

spheres in a given hydrogel sample. To better characterize subtle morphologic differences in samples of these mixed sphere populations, a different lumenization scoring method was deployed using the finer nuclear and polarity marker spatial information afforded by confocal imaging (epithelial score or E-score method). E-score criteria and example images are summarized in Table 2-1. Lumenization percentages were expressed as a mean for all spheres in a given hydrogel sample and evaluated as the sum of percentage of spheres with E-score = 3, 4, or 5 over total sphere number. Size and lumenization data were evaluated for significance by ANOVA with Tukey's HSD post-hoc test.

**Table 2-1: E-score Criteria.**

| E-score | Features | |
|---|---|---|
| 1 | • No nuclear organization<br>• No polarity marker organization | 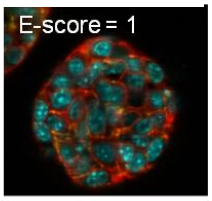 |
| 2 | • Some radial organization<br>• Some segregation of polar markers | |
| 3 | • Some sort of lumen present<br>• Some polar organization | 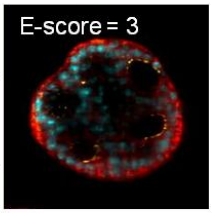 |
| 4 | • Significant lumenal clearing<br>• Clear polar organization<br>• No peripheral nuclear ring | |
| 5 | • Cleared lumen with ~single peripheral nuclear ring and clear polarity | 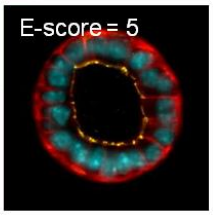 |

## 2.3 Results and Discussion

### 2.3.1 Material Characterization

Reaction of PEG-SCM with RGDS and PQ peptides created pegylated peptides that could be incorporated to render hydrogels bioactive. The efficiency of these conjugation reactions was determined by GPC which separates species by size and outputs signal from an evaporative light scattering detector (Fig. 2-6). Demonstrating a left-shifted peak of pegylated products compared to unconjugated PEG-SCM, GPC plots of PEG-RGDS and PEG-PQ showed conjugation efficiencies of greater than 90%, consistent with previous work in the laboratory.

### 2.3.2 Mechanical Testing

Because of the potential for scaffold physical properties to influence cancer cell behavior, a series of hydrogels with increasing PEG-PQ concentration were subjected to uniaxial compressive mechanical testing to determine the elastic moduli, a measure of material stiffness (Fig. 2-7). PEG-PQ matrices (5%, 10% and 15%) had compressive moduli of 21 ± 6, 42 ± 8 and 55 ± 11 kPa, respectively. To provide context with previous

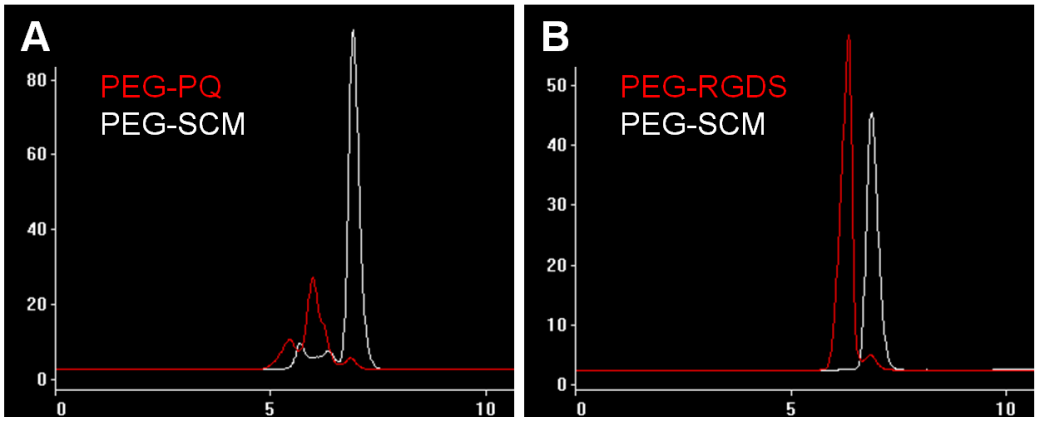


**Figure 2-6: GPC analysis of PEG-peptide conjugates.** Trace of conjugated PEG-peptide products (red) for (A) PEG-PQ and (B) PEG-RGDS with overlayed trace of unmodified acryl-PEG-SCM (white) shows near 100% conjugation efficiency for reactions.

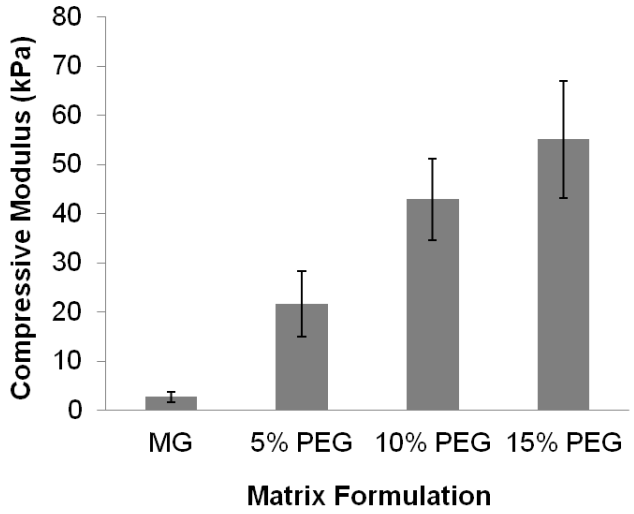


**Figure 2-7: PEG matrix mechanical properties.** Elastic moduli derived from uniaxial compressive testing demonstrate matrix stiffness can be tuned by altering weight percent PEG incorporated in the polymer mixture. All PEG matrices are stiffer than MG ($p<0.01$).

work, MG samples were also tested and found to be much softer than these PEG formulations with a compressive modulus of ~2.5 kPa. Encapsulation of cells did not significantly change the difference in elastic moduli between hydrogels of different PEG-PQ concentrations (Fig. 2-8).

### 2.3.3 3D Culture in Bioactive PEG Hydrogels Recapitulates MG Morphology of $KRas^{G12D}$ / $p53^{R172H\Delta G}$ Model Cell Lines

Cell adhesion in the PEG hydrogel was facilitated by incorporation of the RGD peptide as a scaffold pendant group. The RGD sequence is a motif found in fibronectin and other ECM molecules that is well-characterized in use in synthetic matrices to promote baseline adhesive bioactivity via ligation of a number of integrin pairs including $\alpha_v\beta_3$, $\alpha_v\beta_5$, and $\alpha_5\beta_1$ [246]. Meanwhile, cell-mediated proteolytic degradation of the hydrogel was permitted by incorporation of the MMP-2- and -9-degradable PQ sequence into the hydrogel backbone PEG chains. Parental 344SQ lung adenocarcinoma cells

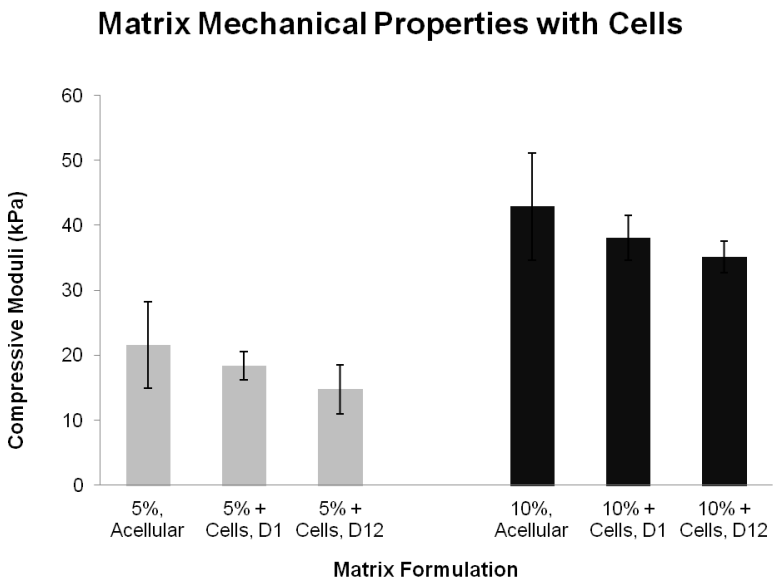


**Figure 2-8: Difference in matrix mechanical properties unchanged with incorporation of cells.** Elastic moduli derived from uniaxial compressive testing of 5% (gray bars) and 10% (black bars) PEG-PQ hydrogels without cells, with cells at day 1 in culture, and with cells at day 12 in culture shows that the difference in mechanical properties between bulk hydrogels of different PEG-PQ weight percent is unchanged with encapsulation of cells. Differences between 5% and 10% acellular and (+) cell groups are not statistically significant.

were encapsulated in PEG-based hydrogel matrices by mixing them with the PEG-PQ and PEG-RGDS components in buffer in the presence of the photoinitiator eosin Y.

The mild crosslinking resulting from exposure to white light enabled high cell viability and, over several days in culture, cells proliferated and began to form multicellular spheres. After 7-10 days in culture, the cell clusters in PEG hydrogels (10% PEG-PQ/3.5 mM linear PEG-RGDS) showed central clearing and formation of a lumen surrounded by an organized layer of single cells reminiscent of the lung acinus (Fig. 2-9). The morphology of these lumenized spheres closely mirrored that of 344SQ cells in MG. Cells encapsulated in the PEG-based matrix formulation generally formed smaller spheres (~40 μm) than those in MG (~80 μm) and took longer to lumenize (7-10 days vs. 6-8 days, not shown) [232]. To assess the extent of epithelial morphogenesis, structures were stained for epithelial polarity markers: α6-integrin marking the basal surface and

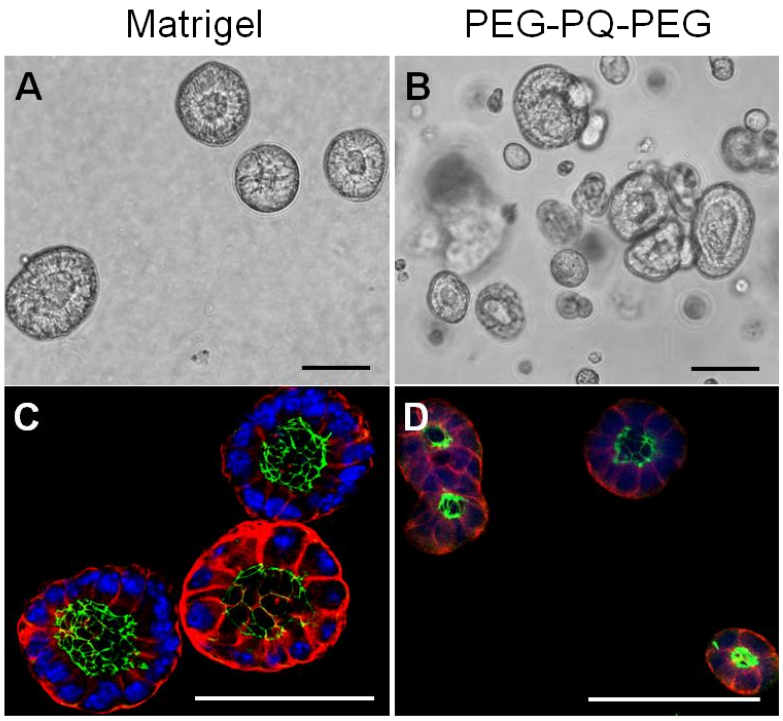


**Figure 2-9: 344SQ culture in PEG matrix recapitulates 3D culture in Matrigel (MG).** *A and B*, brightfield images of 344SQ cells encapsulated in MG (*A*) or a 10% PEG-PQ/3.5 mM PEG-RGDS matrix (*B*) after 10 days in culture show sphere lumenization. *C and D*, staining for basolateral marker α6-integrin (red) and apical marker ZO-1 (green) in 344SQ cells encapsulated in MG (*C*) and PEG (*D*) indicate that spheres have adopted organized epithelial polarity. DAPI (blue) staining used for visualization of cell nuclei. Scale bar = 50 μm.

zonula occludens-1 (ZO-1) for apical tight junctions. Lumenized PEG-encapsulated spheres showed distinct separation of polarity markers, demonstrating clear formation of apical-basal polarity (Fig. 2-9*C-D*). This staining pattern was comparable to that seen for MG-encapsulated structures and suggested a MET with extensive cell-cell contact reformation and polarity restoration.

To demonstrate the PEG system as a reliable 3D culture platform across cancer models, other adenocarcinoma lines previously studied in MG were encapsulated and stained for epithelial polarity markers β-catenin (lateral) and ZO-1 (Fig. 2-10). The cell lines tested include 393P, a $KRas^{G12D}/p53^{R172H\Delta G}$ line that does not widely metastasize when reintroduced into syngeneic mice and expresses lower levels of EMT markers.

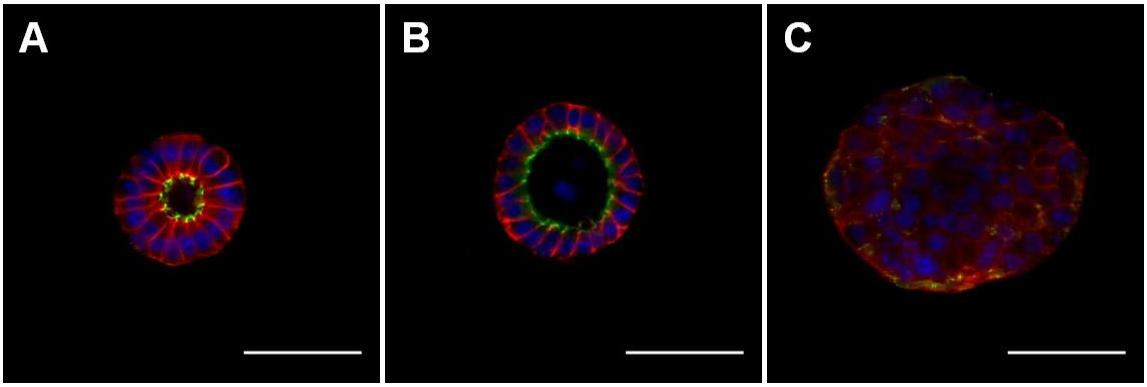


**Figure 2-10: Other lung adenocarcinoma lines in PEG matrices**. Staining for polarity markers β-catenin (red) and ZO-1 (green) of 344P (*A*), 429 (*B*) and 393P (*C*) cells encapsulated in PEG-PQ matrices recapitulate morphology and polarity seen in 3D MG culture (Gibbons, *et al.*). DAPI (blue). Scale bar = 50 μm.

Also tested was another metastatic line derived from a primary tumor of $KRas^{G12D}/p53^{R172H\Delta G}$ mice (344P) and a transfectant based on the 344SQ line (344SQ.429) that constitutively expresses the miR200b_a_429 locus to prevent EMT and metastatic changes with TGFβ treatment. In the PEG hydrogel system (10% PEG-PQ/3.5 mM linear PEG-RGDS), both the 344P and 344SQ.429 lines formed lumenized spheres and expressed markers of epithelial polarity in appropriate patterns, mimicking their response in 3D MG. Meanwhile, cells from the metastasis-incompetent 393P cell line generally formed large, disorganized cell aggregates with no clear epithelial organization, typical of its behavior in MG.

We have confirmed that a PEG-based system, with simple bioactivity incorporated through the use of cell-adhesive PEG-RGDS and enzyme-degradable PEG-PQ backbone was able to recapitulate interesting morphological phenomenon observed with 3D culture of the $KRas^{G12D}/p53^{R172H\Delta G}$ model lines. Notably, encapsulation in the PEG system induced MET in 344SQ cells to form lumenized, polarized spheres similar to that observed in MG. This observation was important as it suggests that this distinctive behavior is not dependent on excess bioactivity from residual growth factors or the

presence of highly bioactive ECM components like laminin found in high concentrations in MG, but is simply a result of the innate differentiation capacity of these cells in a three-dimensional environment. This observation also established the PEG system as a reliable platform to study matrix-derived influences on the cancer cell behavior.

### 2.3.4 Matrix Stiffness Influences Epithelial Morphogenesis

Having established that a PEG-based system was capable of recapitulating epithelialization behavior exhibited by 344SQ in 3D MG culture, we sought to examine the influence of key matrix parameters on this behavior. One such parameter, matrix stiffness, has been widely studied in 3D cancer models in naturally-derived matrices[83,99] with some initial study in synthetic matrices with better controlled mechanics and biochemistry[191,192,244]. Examination of 344SQ in MG suggests that it is highly susceptible to extrinsic matrix cues like elasticity[232], but the role of stiffness has yet to be specifically studied due to limitations in altering MG stiffness in a biochemically neutral fashion.

To probe for these influences in the PEG system, the concentration of PEG-PQ, which forms the bulk of the material, was varied at 5%, 10% or 15% while maintaining the cell-adhesive PEG-RGDS at a fixed 3.5 mM. Utilizing higher polymer concentrations increased crosslink density and decreased mesh size, leading to a stiffer matrix. Multicellular spheres formed in all matrix formulations, but spheres showed important differences in morphology and epithelialization behavior (Fig. 2-11*A*-*C*), with larger spheres and a lower percentage of lumenized structures forming in the softer, 5% PEG-PQ matrices. By monitoring sphere diameter with time (Fig. 2-11*D*), it is evident that the structures underwent rapid growth in the first few days of culture regardless of

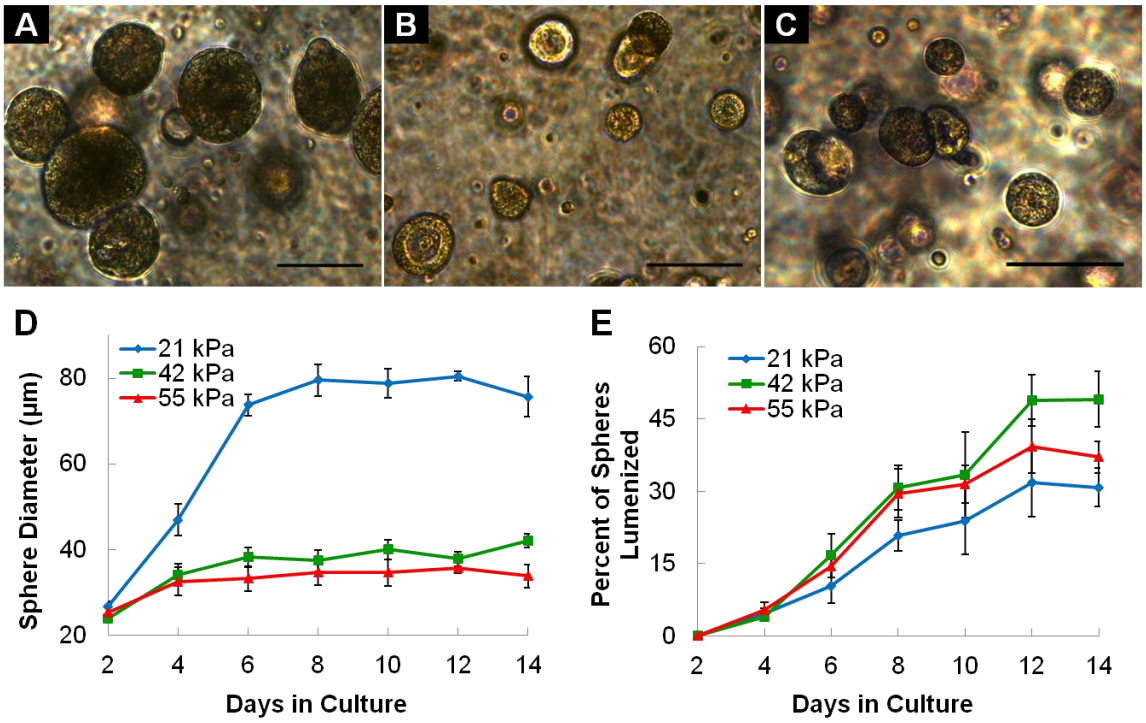


**Figure 2-11: Matrix stiffness influences epithelial morphogenesis.** *A-C*, brightfield images of spheres at 12 days in culture in 5% PEG-PQ (*A*, 21 kPa), 10% PEG-PQ (*B*, 42 kPa) and 15% PEG-PQ (*C*, 55 kPa) matrices with 3.5 mM PEG-RGDS show differences in sphere size and lumenization. *D*, significantly larger spheres form in the softer hydrogel (Day 12, 21 kPa vs. others, $p<0.01$) while *E*, a higher degree of lumenization occurred in stiffer matrices (Day 12, 42 kPa compared to 21 kPa, $p<0.05$). Scale bar = 100 µm.

matrix stiffness, but growth persisted through day 8 only in the softer matrix (21 kPa), eventually yielding spheres that were significantly larger relative to the other formulations (~80 µm in 21 kPa hydrogels vs. ~35 µm in the other formulations). Quantifying the percentage of spheres that showed cells arranged around a completely cleared central lumen, an inverse relationship between stiffness and sphere lumenization was found (Fig. 2-11*E*); while all matrices exhibited increasing sphere lumenization throughout the culture period, fewer encapsulated spheres were lumenized in the 21 kPa matrix (35%) compared to the 42 kPa matrix (50%). It was also observed that spheres in the 21 kPa matrix tended to be more heterogeneous in regards to size and morphology relative to the stiffer matrix formulations; this observation was reflected when diameter

data was pooled and plotted in a histogram showing much greater variation in structure size in the softer 21 kPa, 5% gel relative to stiffer formulations (Fig. 2-12).

Although the matrices examined in this study ranged from 21 to 55 kPa, the PEG system can be tailored in future studies for either softer or stiffer matrices by varying the concentration of PEG base component or employing a PEG chain with a different number of monomer repeats and molecular weight[228,247]. Although all of the hydrogels tested were stiffer than MG-based matrices, all were capable of supporting 344SQ culture and lumenized structure formation, suggesting that the comparatively softer environment of MG is not required for epithelial morphogenesis. Any alteration in cell behavior related to this softer environment may be compensated for by the excessive bioactivity afforded by the ligand-rich MG.

Observed sphere size differences were explored further under confocal microscopy in samples stained with DAPI and phalloidin, respectively used to identify nuclei for cell counts and to stain membrane-associated actin for cell area measurements (Fig. 2-13). Images taken at central sphere cross-sections indicated that the cells that compose spheres in 21 kPa matrices were slightly larger than those in 42 kPa matrices ($87.5 \pm 22.7$ μm$^2$ vs. $63.6 \pm 8$ μm$^2$, not significant). More notably, the number of cells in

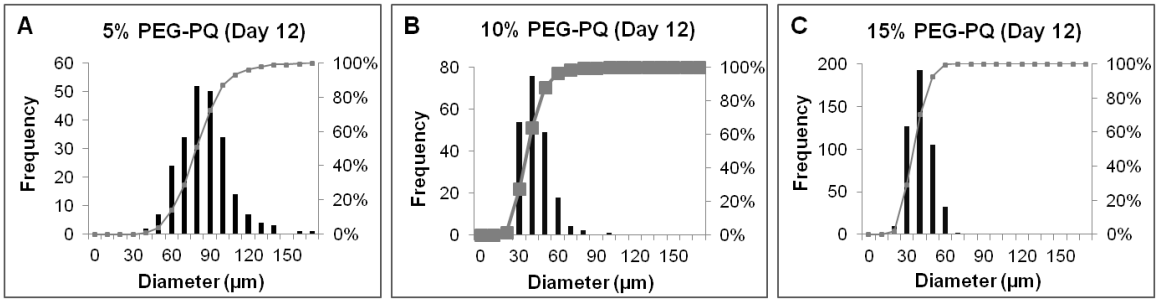


**Figure 2-12: Spheres in stiffer matrices form a more homogeneous population.** Histograms of pooled size data for all spheres in all hydrogel samples show much greater heterogeneity in sphere development in softer, 5% hydrogels (*A*) compared to stiffer formulations (*B-C*).

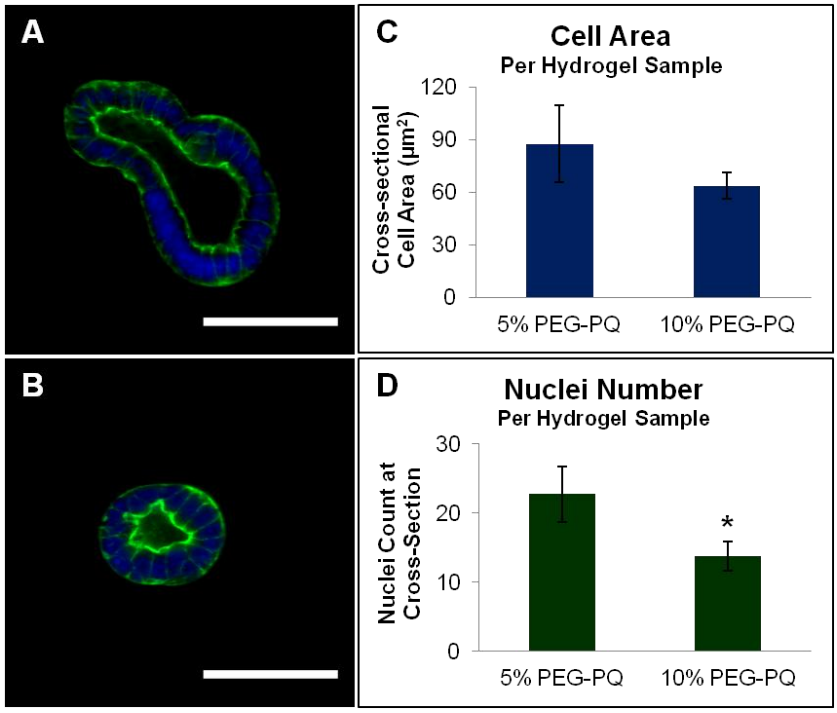


**Figure 2-13: Cell area and cell number contribute to sphere size differences observed between 5% and 10% hydrogels.** *A-B,* DAPI (blue) and phalloidin (green) stained spheres in 5% (*A*) and 10% (*B*) hydrogels taken at maximum sphere cross-section show (*C*) a trend in smaller cell area derived from the phalloidin data and (*D*) significantly fewer number of nuclei derived from DAPI count in the 10% matrix compared to the 5% matrix (*p<0.05). Scale bar = 50 μm.

21 kPa matrix spheres was significantly greater than that in 42 kPa matrix spheres (22 ± 4 vs. 13 ± 2, $p < 0.05$). Both of these factors contributed to overall differences observed in sphere diameter. This sphere size difference may also be reflective of a difference in epithelial organization; work in other systems suggests that a transition to larger, less uniform structure indicates loss of epithelialization [99].

Samples of spheres grown in the hydrogel matrices were stained for markers of proliferation and apoptosis as well as polarity markers to more closely assess matrix stiffness-related influences in sphere development and extent of epithelialization (Fig. 2-14). Ki-67 staining revealed diffuse proliferation throughout spheres encapsulated in soft matrices at day 4 (Fig. 2-14*A*), while spheres in stiffer matrices exhibited a more localized peripheral staining pattern (Fig. 2-14*B*). Proliferation persisted though day 6 in

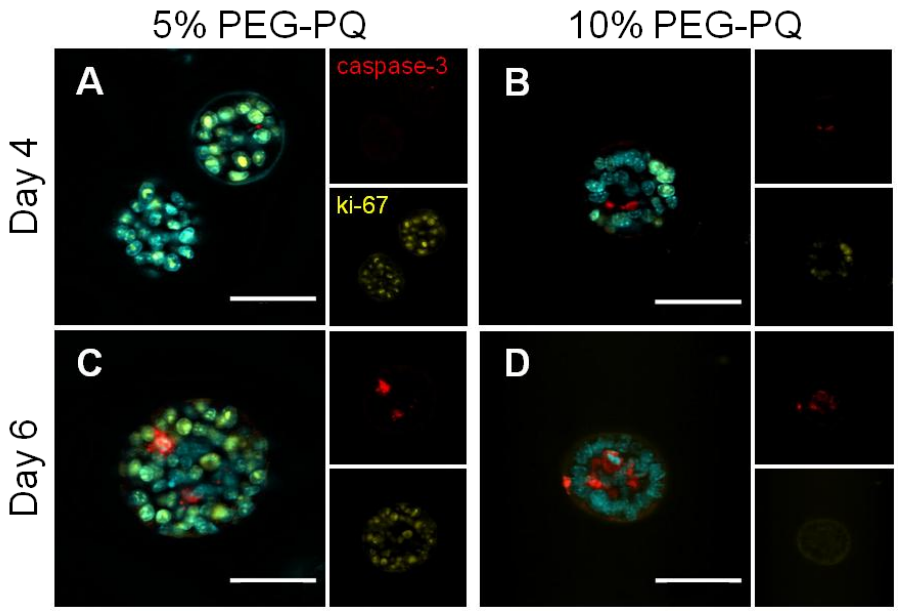


**Figure 2-14: Matrix stiffness influences apoptosis and proliferation in developing spheres.** *A-D*, staining for cleaved caspsase-3 (red) and ki-67 (yellow) at day 4 (*A and B*) and day 6 (*C and D*) in 5% (*A and C*) and 10% (*B and D*) hydrogels show earlier localization of proliferation at sphere periphery (*B*) in the stiffer hydrogel and high core apoptosis activity to induce more rapid lumenization (*D*) compared to diffuse proliferation activity (*A*) and unlocalized apoptosis (*C*) in softer hydrogels. DAPI (cyan), scale bar = 50 μm.

21 kPa matrices (Fig. 2-14*C*), but decreased in stiffer matrices as spheres became more completely lumenized (Fig. 2-14*D*). These patterns may have contributed to the significant cell number differences between spheres in differently stiff gels. Proliferation observations correlated with differences in apoptosis as spheres in softer matrices showed unlocalized caspase-3 activity (Fig. 2-14*C*), whereas spheres in stiffer matrices showed strong core caspase activity (Fig. 2-14*D*).

After several days in culture, spheres in soft and stiff matrices showed differences in epithelial polarity (Fig. 2-15). At day 6 the epithelial markers β-catenin (lateral) and ZO-1 (apical) remained disorganized in softer matrices (Fig. 2-15*A*), whereas spheres in stiffer matrices (Fig. 2-15*B*) showed peripheral nuclear alignment and polar organization, albeit incomplete as β-catenin persisted on the apical edge. By day 12, however, lumenized spheres were found in both soft (Fig. 2-15*C*) and stiff (Fig. 2-15*D*) matrices,

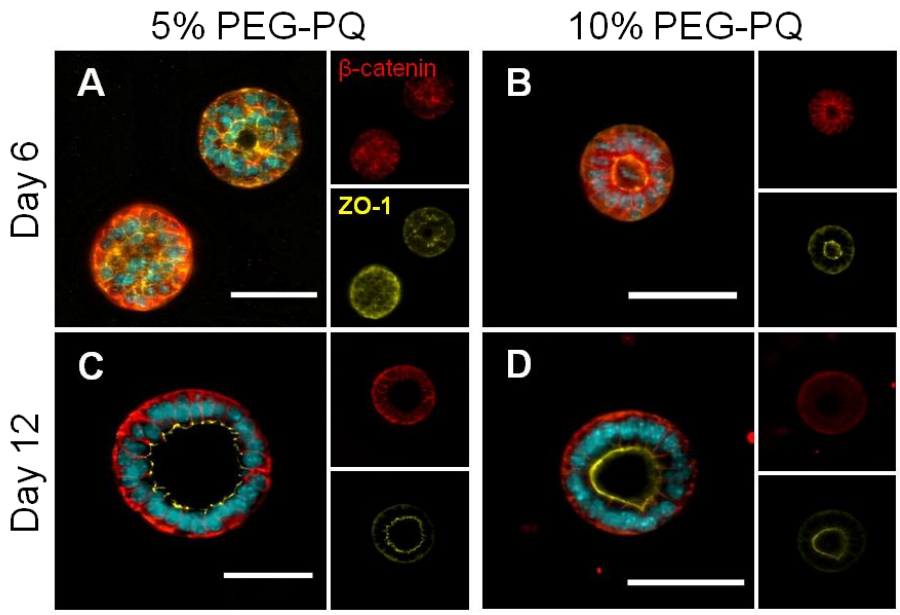


**Figure 2-15: Matrix stiffness influences degree of epithelial polarity.** *A-D*, staining for polarity markers β-catenin (red) and ZO-1 (yellow) at day 6 (*A and B*) and day 12 (*C and D*) in 5% (*A and C*) and 10% (*B and D*) PEG-PQ hydrogels shows polar organization in spheres in only stiff hydrogels (*B*) at early timepoints compared to disorganization in softer hydrogels (*A*) while at later timepoints lumenized spheres in both softer and stiffer matrices show a high degree of organized polarity (*C and D*) with a notable absence of basolateral β-catenin on the apical edge. DAPI (cyan), scale bar = 50 μm

with lumenized spheres exhibiting a high degree of epithelial organization and clear segregation of polar markers.

Given this data on differences between 21 kPa and 42 kPa matrices on the rate and extent of lumenization and differences in sphere development and polar organization, our data on balance suggests that 344SQ epithelial structures were more organized in stiffer matrices. This result runs counter to much of the work in the field that suggests high matrix stiffness favors less tumor organization and enhanced progression[43,99,184]. The disparity may simply highlight the unpredictability of natural matrix biochemistry. Despite best efforts to incorporate similar bioactivity or mechanics, other investigators have demonstrated that the same cells behave differently when cultured on MG or other materials including collagen[172], naturally derived materials like small intestinal

submucosa[248], and PA[249], suggesting it is very difficult to control for bioactivity in complex proteinaceous natural matrices like MG.

Our work was also motivated by a desire to disentangle mechanics from bioactivity, a difficult task with natural matrices in which mechanics and ligand density often change concordantly. Discerning the independent contribution of these factors is important given that collagen density, organization and crosslinking are thought to promote tumor progression[23,43,83]. Indeed, when investigators have deployed synthetic systems like PA with better control over biochemistry and biomechanics, in some cases certain cancer cells actually adopt a more benign, differentiated state on the stiffer substrate tested or display peak tumorogenic activity in matrices of intermediate stiffness[241,250,251]. A few reports have transitioned this effort into 3D, finding a diminished invasive phenotype in the stiffer formulation of a HA- based gel and enhanced epithelialization in stiffer collagen gels crosslinked with bioinert PEG[191,244]. However, the 2D PA studies are restricted to two dimensions, and may offer limited insight into the more physiologic behaviors seen in 3D environments. The 3D systems used previously are also imperfect as, despite attempts to control ligand concentration[191] and use bioinert crosslinkers[244], both of the bulk matrix components used are still themselves bioactive, inevitably leading to biochemical changes with increased crosslinking and stiffening. Unlike PA, our PEG system is a biocompatible 3D culture system, and it avoids the limitations of these other 3D systems as it can be stiffened in a purely biochemically independent fashion.

In addition, while the bulk of work in the field has been done using a collection of the same commonly studied breast cancer model lines, when other cell lines have been

examined, the matrix stiffness-related behavior observed is often highly dependent on the identity of the cell line tested or the nature and extent of its malignant transformation[201,250–254]. Our KRas$^{G12D}$/p53$^{R172H\Delta G}$ lines may exhibit either a different response to matrix stiffness or a higher degree of rigidity-independence than the commonly used breast lines[201]. Further, because very little work in the field has been done using cell lines that specifically and reliably model human lung adenocarcinoma, our work may highlight unique influences of matrix stiffness on metastatic properties of lung adenocarcinoma.

### 2.3.5 Adhesive Ligand Concentration Influences Epithelial Morphogenesis

The influence of biochemically active matrix components on cancer model behavior has been demonstrated in many different systems[83,175,176,191]. To probe for similar influence in our system, we next evaluated if the concentration of cell adhesive ligand PEG-RGDS would influence epithelial morphogenesis in the absence of changes to matrix stiffness. By encapsulating 344SQ cells in matrices with a fixed 5% PEG-PQ concentration (21 kPa) and linear PEG-RGDS at 1 mM (Fig. 2-16*A*), 3.5 mM (Fig. 2-16*B*) or 7 mM (Fig. 2-16*C*), we first examined adhesive ligand-related changes in sphere size and lumenization behavior. Although spheres initially grew rapidly in all matrices, average sphere diameters (Fig. 2-16*D*) in the matrices with higher concentrations of adhesive ligand increased to only around 60 μm through day 6. Spheres in matrices with lower concentrations of adhesive ligand grew more rapidly and persistently up to 80-90 μm in diameter. The percentages of spheres lumenizing (Fig. 2-16*E*) showed a strong relationship with adhesive ligand concentration; spheres rapidly and more completely lumenized in soft matrices with 7 mM PEG-RGDS, whereas a very low percentage of

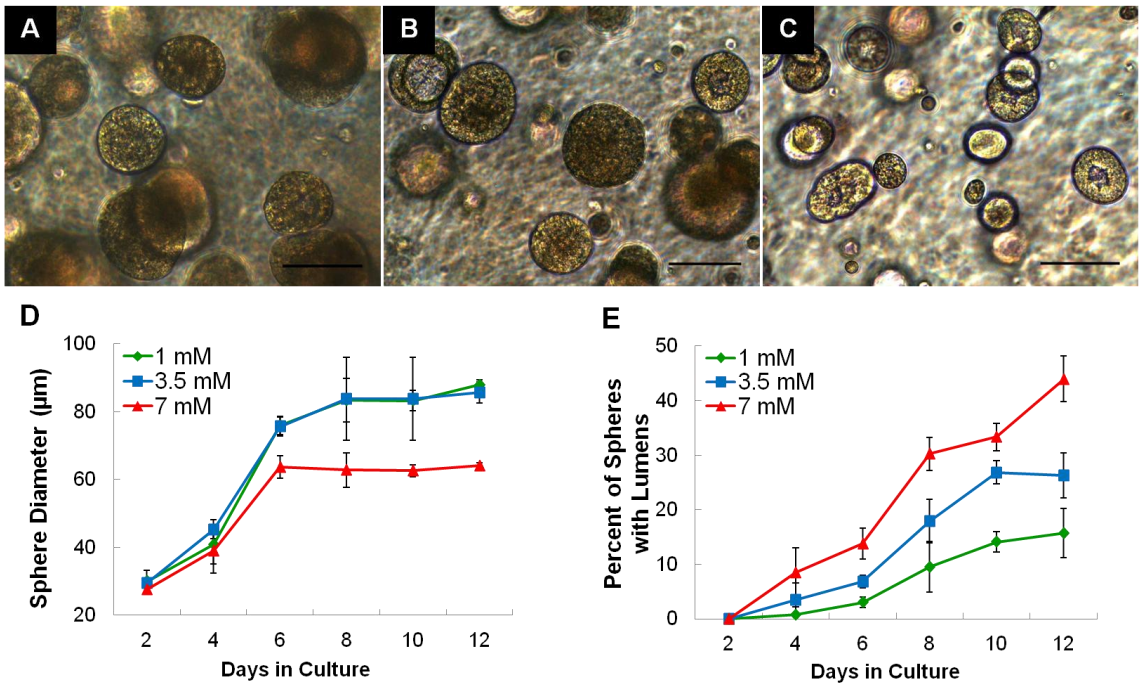


**Figure 2-16. Adhesive ligand concentration influences epithelial morphogenesis.** *A-C*, brightfield images of spheres at 12 days in culture in 5% PEG-PQ gels with linear PEG-RGDS at a concentration of 1 mM (*A*), 3.5 mM (*B*) or 7 mM (*C*) show differences in sphere size and lumenization. *D*, smaller spheres formed in matrices with a high PEG-RGDS concentration (7 mM vs. others, $p<0.01$ at Day 12) while *E*, lumenization occurred more rapidly and completely in spheres encapsulated in matrices with higher PEG-RGDS concentrations (Day 12, 7 mM vs. others, $p< 0.01$, 3.5 mM vs. 1 mM, $p< 0.05$). Scale bar = 100 μm.

spheres (15%) lumenized in soft matrices with low adhesive ligand concentration even after 12 days in culture. It was also observed that matrices with low PEG-RGDS concentration induced formation of a much more heterogeneous population of spheres, while incorporation of high concentrations of adhesive ligand into matrices induced formation of a much more homogenous sphere population (Fig. 2-17). Supporting our interpretation that these changes are ligand-dependent, incorporation of varying amounts of PEG-RGDS did not result in changes to hydrogel mechanical properties (1 mM 18.5 ± 4.6 kPa vs. 7 mM 19.2 ± 3.8 kPa, not statistically significant).

To further assess the influence of adhesive ligand concentration on epithelial morphogenesis, spheres in 21 kPa matrices with either 1 mM or 7 mM linear PEG-RGDS

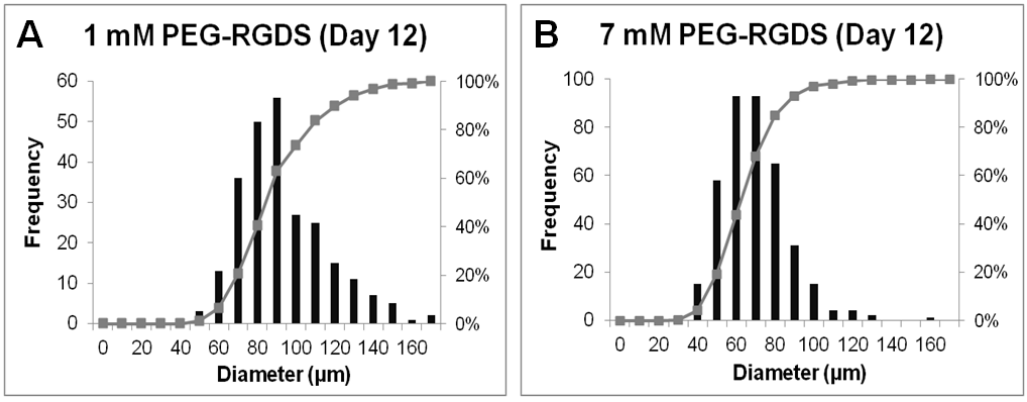


**Figure 2-17: Spheres in high linear PEG-RGDS matrices form a more homogeneous sphere population.** Histograms of pooled size data demonstrate greater heterogeneity in sphere development in hydrogels with little adhesive ligand (*A*) compared to those with high concentrations of adhesive ligand (*B*).

were stained for markers of proliferation, apoptosis, and epithelial polarity (Fig. 2-18). While proliferation was extensive at day 4 in matrices with low PEG-RGDS concentration (Fig. 2-18*A*), it exhibited no localization pattern, whereas matrices with high PEG-RGDS induced more complete epithelial development with structures already exhibiting proliferation at the sphere periphery and central caspase-3 activity (Fig. 2-18*B*). At day 6, both sphere proliferation and apoptosis activity was scattered and diffuse in 1 mM PEG-RGDS matrices (Fig. 2-18*C*). Meanwhile, structure in matrices with high PEG-RGDS developed into well-lumenized spheres by day 6 featuring negligible proliferative activity, lingering core caspase activity, and well-organized peripheral nuclei (Fig. 2-18*D*).

These observed differences in sphere development led to changes in epithelial organization (Fig. 2-19); spheres in matrices with low PEG-RGDS concentration adopted disorganized morphologies by day 6 with spotty and unorganized expression of the lateral and apical markers, β-catenin and ZO-1, respectively (Fig. 2-19*A*), whereas spheres in matrices with high PEG-RGDS concentrations formed lumens and developed appropriate apical-basal polarity (Fig 2-19*B*). Well-organized spheres with clearly

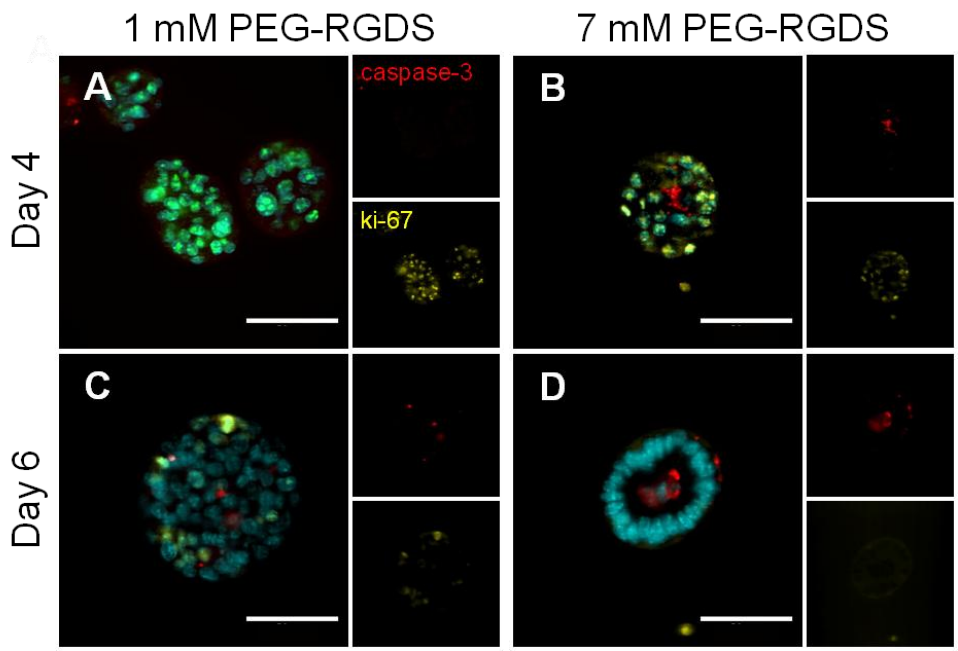


**Figure 2-18: Adhesive ligand concentration influences apoptosis and proliferation in developing spheres.** *A-D*, representative images stained for cleaved caspsase-3 (red) and ki-67 (yellow) at day 4 (*A and B*) and day 6 (*C and D*) in 5% PEG-PQ hydrogels with 1 mM (*A and C*) or 7 mM (*B and D*) PEG-RGDS. Early peripheral proliferation and central apoptosis localization is evident with higher adhesive ligand concentrations (*B*) followed by rapid and organized lumenization (*D*), while spheres in matrices with low adhesive ligand concentration show a high degree of proliferation (*A*) and unlocalized apoptotic activity (*C*). DAPI (cyan), scale bar = 50 μm.

segregated polar edges were widely prevalent by 12 days in 7 mM PEG-RGDS matrices (Fig. 2-19*D*). Although some spheres did lumenize in matrices with low concentrations of adhesive ligand, polarity markers remained disordered and morphology irregular with nuclei failing to arrange neatly around a clear central lumen (Fig. 2-19*C*).

As a whole, we observed a pro-organizational effect of higher concentrations of adhesive ligand in experiments altering PEG-RGDS concentration at a fixed matrix stiffness. This result is interesting in the context of results from the bulk of the field showing that a higher ligand concentration, usually collagen, leads to a more aggressive tumors[43,83]. This disparity suggests that the identity of ECM ligand and the integrins subsequently bound are crucial to understanding the effect of ECM biochemistry on

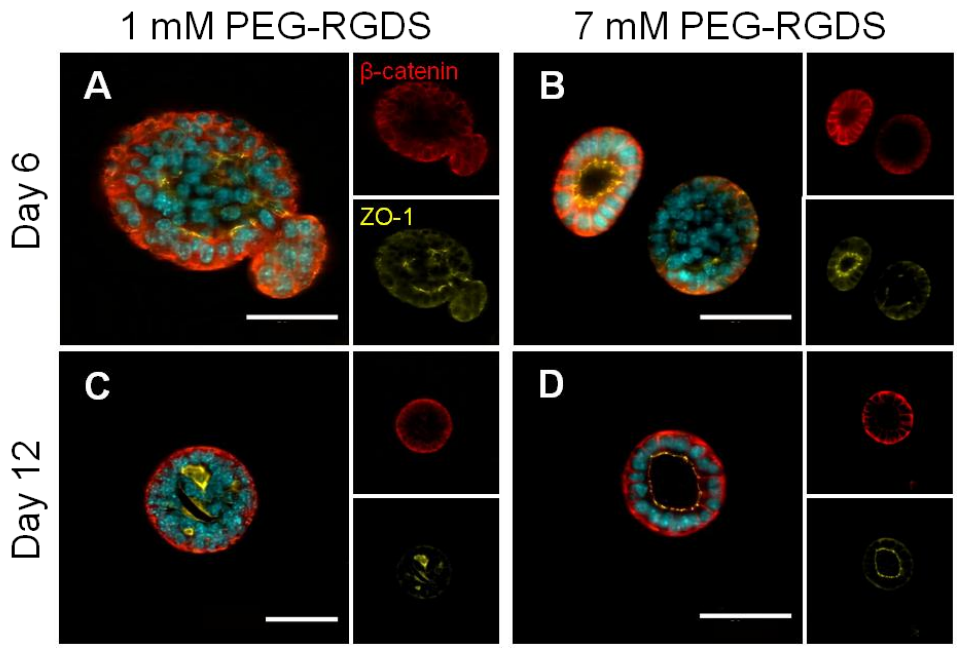


**Figure 2-19: Adhesive ligand concentration influences degree of epithelial polarity.** *A-D*, representative images stained for polarity markers β-catenin (red) and ZO-1 (yellow) at day 6 (*A and B*) and day 12 (*C and D*) in 5% matrices with PEG-RGDS at 1 mM (*A and C*) or 7 mM *(B and D*), show the appearance of spheres with polar organization at early timepoints in matrices with high adhesive ligand concentration (*B*) with completely polar structures widespread at later timepoints (D). Spheres in hydrogels with low adhesive ligand concentration do not show organized polarity at early timepoints (*A*), and at later timepoints, spheres that do display lumenization and polarity (*C*) have adopted less organized, more irregular morphologies. DAPI (cyan), scale bar = 50 μm.

tumor progression. While little work in this regard has been done with fibronectin, from which RGDS is derived, this point is driven home by the many studies showing that, in contrast to collagen, increased laminin concentration promotes epithelial morphogenesis[172,178,249]. This difference is likely related to features of the contextual environment of epithelial cells *in vivo*, where they are often found associated with a laminin-rich ECM [178]. The PEG system has a unique advantage in that specific peptide sequences or domains from these large ECM molecules may be incorporated with high control and examined for a specific effect whereas, in other matrices, incorporation of a whole molecule with its multiple integrin binding sites may make the system too

convoluted, leaving some matrix-derived signaling and gene expression events intractable.

### 2.3.6 Adhesive Ligand Spatial Presentation Influences Epithelial Morphogenesis

The above results suggest that enhanced engagement of integrins at higher PEG-RGDS concentrations promotes organization and epithelial morphogenesis of our EMT model line. Work from the literature suggests that the RGD sequence presented in a cyclic form is far more effective at cell binding than when presented as a linear sequence (Fig. 2-20).

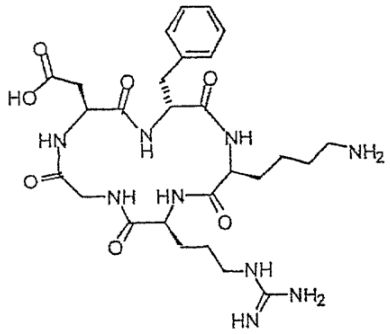

**Figure 2-20: Cyclic RGD (c(RGDfK))**

When presented in solution prior to cell adhesion, free cyclic RGD-containing peptides are upwards of 100 times more effective at inhibiting cell adhesion through binding and blocking of integrins than their linear counterparts[255,256]. Both cyclic and linear forms bind integrins $\alpha_v\beta_3$ and $\alpha_5\beta_1$, but the cyclic form may have higher relative specificity for $\alpha_v\beta_3$ in addition to an overall enhanced non-integrin-specific binding[257,258]. Because these integrins are highly upregulated in cancer, with possible role in facilitating tumor cell migration or angiogenesis of tumor-activated endothelial cells, cyclic RGD peptides have been explored clinically to aide in cancer imaging and therapy[259–261]. Action of cyclic RGD may be of particular interest in our lung adenocarcinoma model as protein expression analysis revealed upregulation of both integrin $\alpha_v$ and $\beta_3$ protein subunits in metastatic $KRas^{G12D}/p53^{R172H\Delta G}$ cells compared to their non-metastatic counterparts.

The influence of cyclic RGD on 344SQ morphogenesis in 3D culture was examined in 5% PEG-PQ hydrogels at varied PEG-c(RGDfK) concentrations (1 mM, 3.5 mM, 7 mM) and compared to control cells in matrices with linear PEG-RGDS at the same concentration. Staining for polarity markers β-catenin and ZO-1 after 12 days in culture showed that spheres in matrices with 1 mM PEG-c(RGDfK) did not display the same morphogenesis abnormalities previously observed in matrices with comparable low levels of linear PEG-RGDS (Fig. 2-21). Well-lumenized spheres with segregated polarity markers and a single cell layer around a central lumen were widespread in all matrices with cyclic PEG-RGD regardless of concentration. Similarly, there were not as readily obvious differences in sphere size between matrices with different PEG-c(RGDfK) concentrations as was found in matrices with linear PEG-RGDS.

To reveal potential subtle differences in morphogenesis between cells in matrices

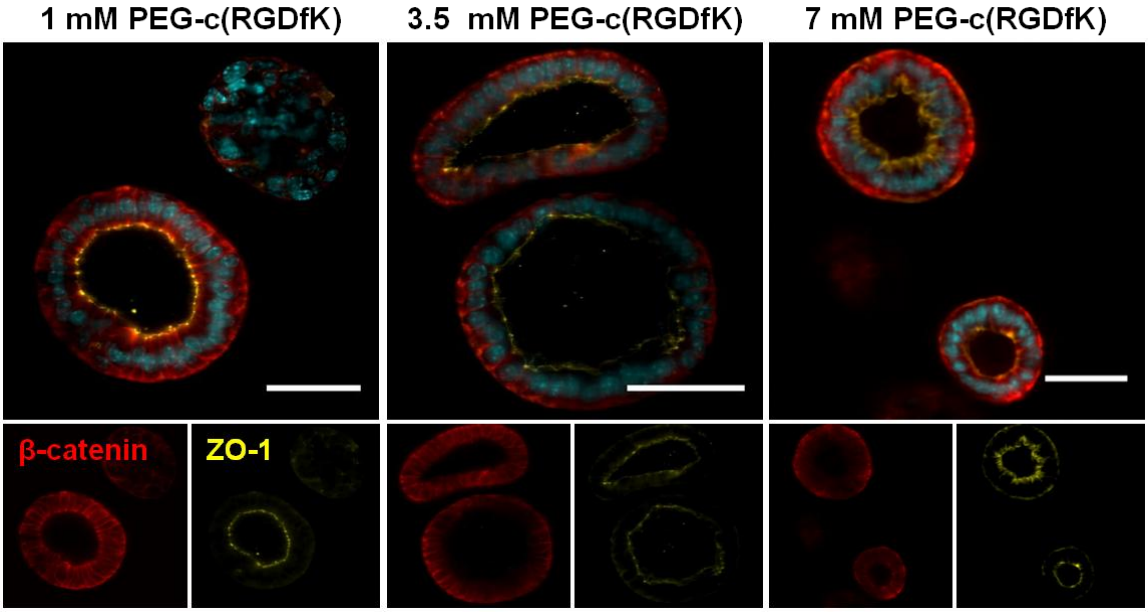


**Figure 2-21: 344SQ in matrices with cyclic PEG-RGDS**. Representative images stained for polarity markers β-catenin (red) and ZO-1 (yellow) at day 12 in 5% matrices with PEG-c(RGDfK) at 1 mM, 3.5 mM, or 7 mM show that spheres with well-organized polarity are widespread in all matrices. Spheres with irregular morphologies were relatively uncommon with 1 mM cyclic RGD compared to 1 mM linear RGD matrices. DAPI (cyan), scale bar = 50 μm.

with cyclic or linear forms, confocal images of spheres stained with these polarity markers were evaluated to quantify size and lumenization (Fig. 2-22). This analysis is potentially more robust than that of brightfield images as it facilitates the more accurate measurement of size at maximum sphere cross-sections and the scoring of lumenization in spheres that may not exhibit an obviously apparent completely cleared lumen. In gels with cyclic RGD, sphere sizes were not significantly different between high and low concentrations ranging from 106 ± 15 μm in 1 mM PEG-c(RGDfK) to 89 ± 2 μm in 7 mM PEG-c(RGDfK) matrices ($p = 0.55$). This compared to much more dramatic size differences seen in matrices with different concentrations of linear PEG-RGDS (136 ± 21 μm in 1 mM and 84 ± 3 μm in 7 mM, $p<0.05$).

Analysis using the E-score method showed substantial lumenization with cyclic RGD even at a low concentration (Fig. 2-23). There was a slightly decreased

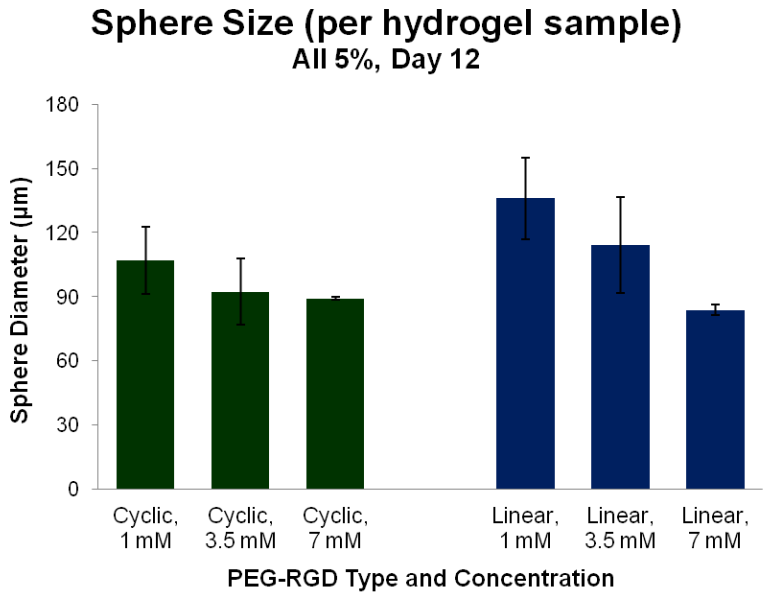


**Figure 2-22: Sphere size is not dependent on RGD concentration with cyclic spatial presentation.** The significant difference in sphere sizes seen between high and low concentrations of RGDS with linear formulation (1 mM vs. 7 mM, $p< 0.05$) are not found with cyclic formulation (1 mM vs. 7 mM, not statistically different), suggesting more uniform epithelial morphogenesis with the cyclic formulation even at low concentrations (other significant differences present).

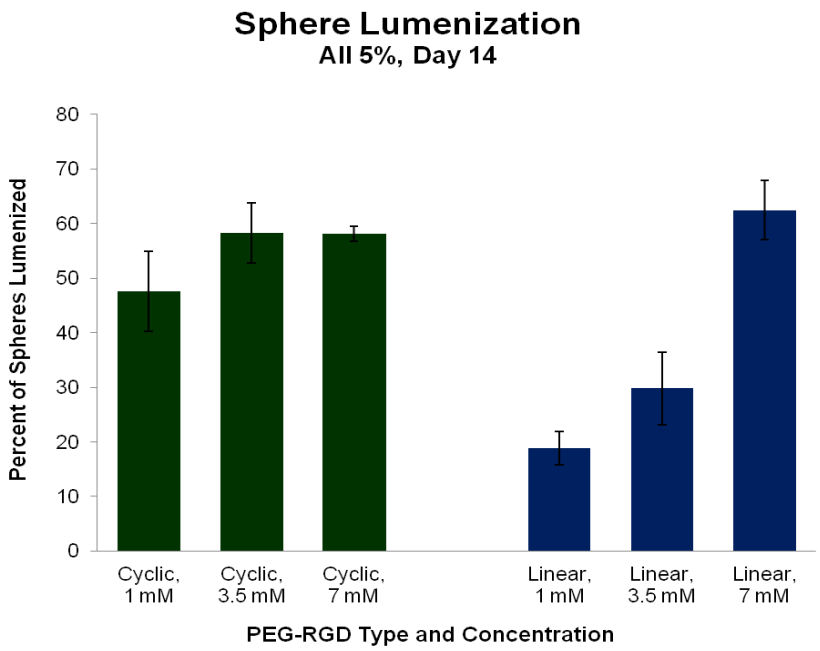


**Figure 2-23: Cyclic spatial presentation of RGD induces greater lumenization than linear RGD at low concentrations.** The significantly diminished degree of lumenization at lower concentrations of linear PEG-RGDS is not observed in matrices with cyclic RGD (cyclic vs. linear 1 mM and 3.5 mM, $p < 0.05$; cyclic 1 mM vs. other cyclic concentrations, not statistically different). High concentrations of linear RGD yielded comparable lumenization as cyclic RGD (linear 7 mM vs. all cyclic formulations). Other significant differences present.

lumenization rate with 1 mM PEG-c(RGDfK) compared to higher-concentration amounts although this difference was not significant (48 ± 7% with 1 mM vs. 58 ± 2% with 7 mM). In 1 mM and 3.5 mM groups, lumenization was significantly enhanced in matrices with cyclic RGDS compared to same-concentration linear RGD ($p<0.01$). Notably, the 1 mM cyclic RGD group even showed greater lumenization than the 3.5 mM linear RGD group ($p<0.05$). Small standard deviations in both size and lumenization levels in both 7 mM groups suggested highly uniform sphere populations in these matrices. A comparable high degree of lumenization found between these groups also suggested that there is a limit to the pro-organizational benefit of the cyclic spatial presentation with potential differences overcome by increasing linear PEG-RGDS concentrations.

**Overall this data indicates that morphogenesis is enhanced with the presentation of adhesive ligand in cyclic form with very little required in the matrix to facilitate widespread organization and little difference in morphogenesis with higher concentrations.** The more potent pro-organizational effect of cyclic RGD compared to linear may reflect overall enhanced integrin binding to facilitate organization or a more specific effect resulting from enhanced $\alpha_v\beta_3$ selectivity. This question may be worthy of further investigation especially given the upregulation of both $\alpha_v$ and $\beta_3$ subunits in 344SQ compared to non-metastatic $KRas^{G12D}/p53^{R172H\Delta G}$ cells [238]. In either case, modulation of morphogenesis with altered spatial presentation of adhesive peptide suggests an additional matrix-derived factor influencing 344SQ MET and demonstrates an additional facet of the PEG system's versatility that can be deployed to study matrix-related metastasis cues.

## 2.4 Conclusion

The study of cancer models in *in vitro* 3D culture systems capable of mimicking the wealth of physical and biochemical cues of the tumor ECM is of critical importance in understanding cancer progression and metastasis. This work presents the development of a PEG-based hydrogel system to support 3D culture of a lung adenocarcinoma model and permit the study of these matrix-derived cues. Protease-degradable PEG hydrogels modified to permit biospecific cell adhesion facilitated morphogenesis of several lung adenocarcinoma cell lines with comparable morphology and patterns of epithelial polarity seen in the MG system. Using this system, matrix stiffness and biochemistry were independently altered to influence morphogenesis of the representative metastatic line 344SQ. Critical features related to 344SQ epithelial morphogenesis were altered

including size, organization of epithelial polarity, and coordinated patterns of proliferation and apoptosis that contribute to differences in lumenization. Further, an altered spatial presentation of adhesive ligand was studied and found to exert strong influence on morphogenesis even at relatively low concentrations. Through these studies, the more experimentally controllable synthetic hydrogel system was demonstrated as a useful tool for the cancer biologist to examine matrix-derived influences on tumor development and an important improvement over the standard of the field.

Moving forward, because the PEG matrix is a completely bioinert material in its unmodified form, this system will enable much more robust study of additional ECM ligands and biochemical cues that modulate EMT and invasion. The system also can be used to present bioactive proteins covalently tethered to the PEG matrix in a more physiologic fashion than soluble media supplementation, offering the potential to study the effect of matrix-tethered TGFβ or the modulation of EMT with cell-cell contact ligands like E-cadherin, N-cadherin, or Jagged, as will be demonstrated in later chapters. In the chapter immediately following, the response to soluble TGFβ in 344SQ encapsulated in the PEG system will be studied, with the degree of EMT, cell-secreted ECM remodeling, and matrix invasion examined and controlled by tuning matrix parameters. Finally, given the tunability of the system demonstrated with these studies, future studies may seek to use patterning techniques already deployed in tissue engineering applications with PEG hydrogels to study three-dimensional spatial relationships between tumors and pro-metastatic ECM cues in an entirely new area of investigation[230,262].

# 3. Investigation of TGFβ-induced EMT and Matrix Invasion in PEG-encapsulated 344SQ

## 3.1 Introduction

The transforming growth factor-β (TGFβ) superfamily of cytokines consists of over 30 members including both TGFβ isoforms, the bone morphogenetic proteins, and other differentiation factors that regulate a number of processes in development, normal homeostasis and disease[263,264] (Fig. 3-1). For example, TGFβ1 is the key player in many diseases of chronic inflammation and fibrosis, acting directly to increase cell secretion of fibrotic ECM and acting indirectly to promote the conversion of epithelial cells to pro-fibrotic myofibroblasts[265]. TGFβ is important in cancer pathogenesis as well, serving two opposing roles in the progression of primary tumors and in EMT and metastasis (Fig. 3-2).

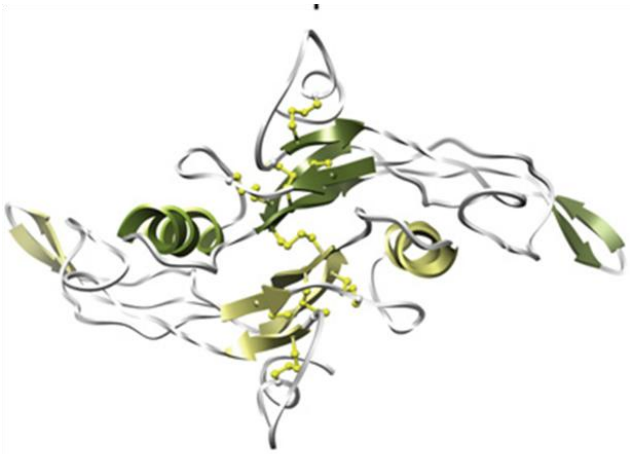

**Figure 3-1: TGFβ-1**. TGFβ-1 and other members of the TGFβ superfamily of signaling proteins share a similar homodimeric structure where the central α-helix of one monomer abuts against the concave surface of β-strands on the other monomer and interchain disulfide bonds stabilize the overall structure. (Adapted from Hinck, *et al.*[264])

First, acting on non-metastasized primary tumors, TGFβ plays an anti-tumorigenic role, suppressing cell proliferation and promoting apoptosis to limit tumor growth and working to prevent some tumor-associated inflammation[266]. In *in vivo* models of breast, skin and other cancers, knockdown of TGFβ receptors or expression of dysfunctional receptors leads to epithelial hyperplasia and the increased development of primary tumors while overexpression of TGFβ suppressed epithelial proliferation and

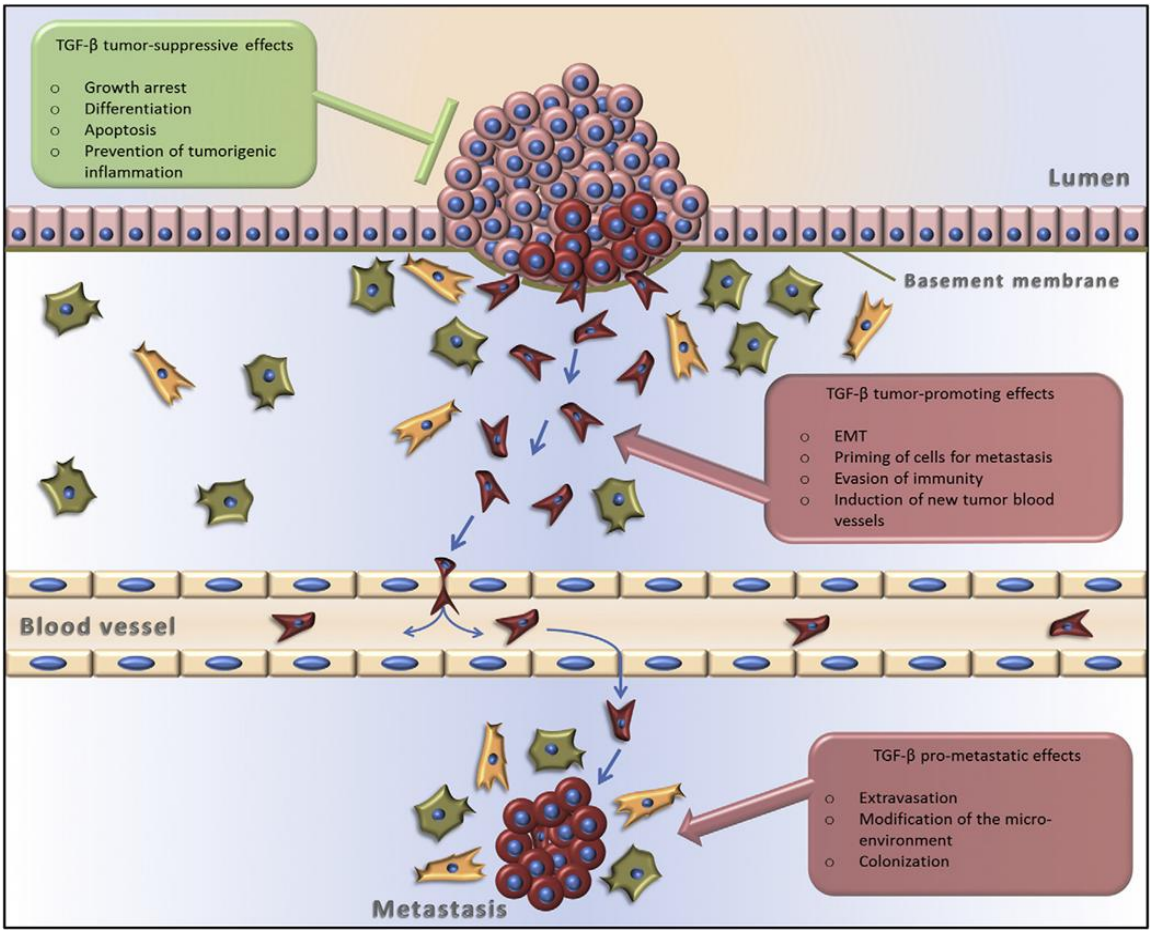


**Figure 3-2: Dual role of TGFβ in cancer**. TGFβ inhibits the growth and progression of hyperproliferating, but more benign tumor cells (round pink). However, in a second role, it promotes EMT of more transformed and advanced carcinoma cells (round red to red triangular), through multiple effects, priming them for metastasis. TGFβ also influences both stromal cells (yellow triangular) and immune cells (green) to facilitate this role and promotes extravastation and establishment of metastatic colonization. Adapted from Heldin, *et al*.[265]

reduced early tumor growth[267–270]. However, induced expression of TGFβ1 at later disease stages led to a higher rate of malignant and invasive tumors and, especially when combined with other common oncogenic mutations, led to increased circulating tumor cells, accelerated disease progression, and widely disseminated disease to metastatic sites[265,267,271,272].

Mounting research suggests that this second, pro-metastatic role of TGFβ is related to its induction of EMT in cancer cells. TGFβ binding and subsequent

phosphorylation of its serine/threonine kinase receptors activates the Smad family of transcription factors that initiate EMT, downregulating a number of epithelial genes and upregulating mesenchymal genes [263]. This response is mediated by a number of key EMT transcription factor intermediaries including Twist, Snail, Zeb1, Zeb2 and others. These factors regulate genes to promote a number of key EMT phenotypic changes like loss of cell polarity, disruption of cell-cell junctions, and initiation of a more migratory, mesenchymal phenotype [233]. TGFβ also promotes important EMT-related processes outside of this Smad signaling cascade. For example, via Ras activation TGFβ binding also activates the MAP kinase pathway, a pathway important to matrix mechanotransduction and motility[273]. TGFβ may also exert important effects on non-epithelial components of the tumor stroma, particularly related to its tumor suppressive role, as stromal cell-specific TGFβ receptor knockouts promote enhanced epithelial tumor growth due to stromal cell hyperplasia and subsequent production of hepatocyte growth factor, amongst other effects[109,274].

The EMT changes induced by TGFβ exposure promote tumor matrix invasion and metastasis through several mechanisms. TGFβ induces loss of polarity proteins like Par, Crumbs, and Scribble and tight junction disassembly[233]. These changes accompany RhoA degradation and cortical actin depolymerization, leading to disaggregation of tumor cells to permit invasion. Perhaps most notably, E-cadherin expression and binding is dramatically decreased during EMT, promoting a similar disaggregation, with EMT transcription factors Snail and Zeb acting directly to decrease E-cadherin transcription and Twist acting indirectly to alter its cytoplasmic location[275]. As reviewed in chapter 1, loss of E-cadherin binding frees β-catenin to accumulate in the cell and enter the nucleus

to assert transcriptional effects via the Tcf/Lef family of transcription factors, not only promoting increased cell proliferation, but also modulating genes related to migration and invasion[122,276].

EMT also may induce other changes that help promote ECM invasion of tumor cells. The switch from E-cadherin to N-cadherin expression may promote affinity to other mesenchymal cells in the matrix like fibroblasts or vascular endothelial cells[277]. N-cadherin binding also has downstream signaling effects, increasing cell migration and stabilizing the FGF receptor, which leads to enhanced FGF activity and the promotion of cell motility and MMP secretion[278,279]. Cell motility also is increased with EMT via other mechanisms, with breast cells showing increased single cell motility and directional movement towards blood vessels with TGFβ exposure, mediated by Smad4 and Rho GTPases. Finally, matrix invasion is promoted by Snail and Zeb action increasing tumor cell MMP secretion, permitting matrix degradation on the leading invasion edge[280].

The resulting matrix invasion by tumor cells in 3D is often mediated by invadopodia, specialized longer lasting podosomes that are actin- and integrin-rich and express and secrete important MMPs to induce invasion, prominently MT1-MMP[281,282]. It is likely that EMT is important for invadopodia formation and function at least in part because similar pro-tumorogenic growth factors induce both EMT and invadopodia formation. Also, EMT modulates expression of certain invadopodia-related proteins. These include $\beta_1$ and $\alpha_v\beta_3$ integrins that are vital to invadopodia binding and other EMT-related downstream protein signalers like N-cadherin that also may be important for invadopodia function[277,283,284].

Finally, TGFβ exposure and EMT alter aspects of the tumor-ECM relationship beyond matrix invasion. Through direct effects on cancer cells, indirect action on ECM fibroblasts, or conversion of epithelial cells to myofibroblasts, TGFβ induces significantly increased secretion of collagen I, fibronectin, and other matrix molecules that may act to promote malignant phenotypes, support integrin binding on invadopodia, and facilitate directional migration[66,233,265]. EMT events also modulate laminin secretion and remodeling, promoting its secretion as part of this hypersecretory phenotype[285] or downregulating particular laminin subunits that help constitute the basement membrane to facilitate invasion[233]. Disruption of organized epithelial polarity with EMT may be associated with significant spatial reorganization of laminin and collagen IV that surround epithelial structures with basement-membrane like phenotypic organization[175]. Similar collagen IV remodeling resulting in focal areas of basement membrane thickness or gaps is a hallmark of malignant and invasive tumors *in vivo* that have undergone EMT[21,60].

In the $KRas^{G12D}/p53^{R172H\Delta G}$ lung adenocarcinoma mouse model, TGFβ has proven to play a central role in EMT and malignant progression. In epithelial structures formed in 3D MG culture by the EMT-prone 344SQ line, TGFβ initiates EMT, inducing structures to become larger, lose apical-basal polarity, and form matrix-invasive outgrowths, coincident with alteration in expression of several EMT-related genes [232]. In this model and others, this response is mediated by the miR-200 family, with TGFβ activating the Akt2 serine/threonine kinase to downregulate all five members of the miR-200 family, leading to the accumulation of Zeb1 and Zeb2 that are otherwise held at low levels by miR-200 inhibition [286,287]. Zeb2 also binds to miR-200 promoters to repress

their expression, completing a double-negative feedback loop whose balance can be demonstrably perturbed by TGFβ exposure[237] (Fig. 3-3). 344SQ transfects that constitutively express miR200 (344SQ.429 cells) do not undergo these EMT-related changes and are incapable of causing metastatic disease owing to their miR200-maintained epithelial state, imperturbable by pro-metastatic cues like TGFβ[232]. In addition, protein expression of lines in the $KRas^{G12D}/p53^{R172H\Delta G}$ model with different EMT susceptibilities revealed that not only do these lines display differential expression of integrins and other proteins important for matrix invasion, but also altered expression of cell-secreted ECM molecules and the proteases involved in their remodeling, suggesting a possible matrix remodeling response in our lung adenocarcinoma model with TGFβ[238].

Because of its central role in promoting tumor metastasis, TGFβ is a target of research interest in investigations of new cancer therapeutics. Fc:TGFβ receptor fusion proteins, TGFβ antibodies, and small molecule inhibitors of TGFβ receptors have all

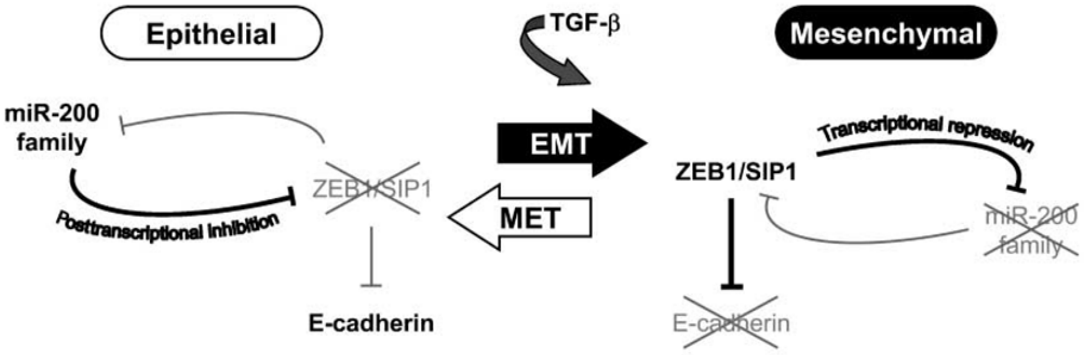


**Figure 3-3: Double-negative feedback loop between miR-200 and Zeb1 mediates EMT response to TGFβ**. High levels of miR-200 maintain a stable epithelial state in cells by inhibiting ZEB-1 which increases the expression of epithelial genes like E-cadherin and many others. TGFβ increases Zeb-1 levels which also represses miR-200 transcription to further increase Zeb1 levels. High Zeb1 eventually initiates an EMT response, inhibiting epithelial genes and promoting mesenchymal genes. This double-negative feedback system enables cells to undergo EMT or MET to switch between phenotypic states in response to external signals. Modified from Bracken, *et al.*[237]

demonstrated efficacy in diminishing or blocking metastasis *in vivo* and some are being investigated in clinical trials[288]. A better understanding of the role of TGFβ in EMT, matrix invasion and metastasis may help lead to the development of more selective or effective TGFβ-related cancer therapeutics. In this chapter, the effects of TGFβ on the $KRas^{G12D}/p53^{R172H\Delta G}$ cultured in the PEG system will be explored to illuminate potential matrix-related influences on this response and matrix invasion. First, EMT-related morphologic and epigenetic changes resulting from TGFβ exposure will be explored in 344SQ cultured in matrices that promote epithelial morphogenesis. Remodeling of cell-secreted ECM coincident with these changes and the influence of matrix parameters on this secretion will be explored. Finally, matrix invasion of TGFβ-treated 344SQ in the PEG system will be studied, both in PEG-PQ hydrogels with altered matrix parameters and in hydrogels featuring an alternative protease-cleavable sequence (PEG-MSM).

## 3.2 Materials and Methods

### 3.2.1 Cell Culture

344SQ derived from $KRas^{G12D}/p53^{R172H\Delta G}$ mice as described previously in Gibbons, *et al*. and Zheng, *et al*. [232,235]. All cells and cell-laden hydrogels were cultured in a humidified atmosphere at 37˚C and 5% $CO_2$ in RPMI 1640 (Mediatech) with 10% fetal bovine serum (Atlanta Biologicals), 10 μg/ml gentamicin and 0.25 μg/ml amphotericin B (Invitrogen).

### 3.2.2 Synthesis and Purification of PEG-RGDS, PEG-PQ-PEG and PEG-MSM-PEG

PEG-RGDS, PEG-c(RGDfK) and PEG-PQ-PEG ("PEG-PQ") were synthesized as described in Section 2.2.2 with conjugation confirmed with GPC. An alternative hydrogel backbone to PEG-PQ, PEG-MSM-PEG ("PEG-MSM") was synthesized, incorporating the peptide VPMSMRGG ("MSM") to enable enhanced degradation by MMP-1 and MMP-2 relative to PQ [227]. PEG-MSM was conjugated using an alternative NHS reactant, acrylate PEG-succinimidyl valerate (PEG-SVA, Laysan; Fig. 3-4). For conjugation, the MSM peptide was first dissolved in a HEPBS buffer (20 mM N-(2-Hydroxyethyl)piperazine-N'(4-butanesulfonic acid), 100 mM NaCl, 2 mM $CaCl_2$, 2 mM $MgCl_2$, pH 8.5) and the PEG-SVA powder added to this solution at a 2.1:1 PEG-SVA:MSM molar ratio and vortexed to dissolve. pH was maintained ~8 as the reaction proceeded overnight at 4˚C on a vortexer. The resulting solution was dialyzed against milliQ water in a 3500 MWCO regenerated cellulose membrane to remove unreacted peptide and then lyophilized. Conjugation efficiency was confirmed with GPC as in Section 2.2.2.

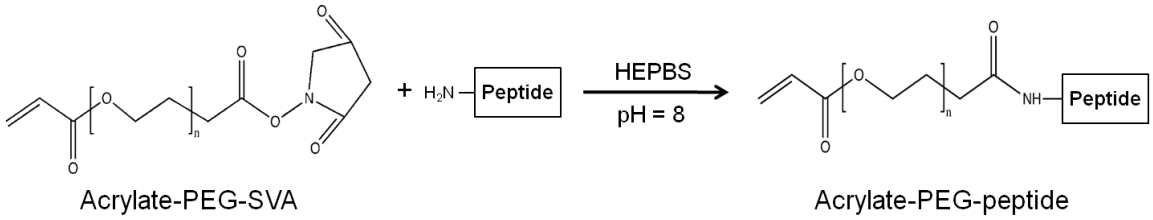


**Figure 3-4: Conjugation reaction with PEG-SVA.** With reaction with PEG-SVA, bioactive species are covalently tethered to acrylate-PEG for hydrogel incorporation with NHS chemistry similar to that used in PEG-SCM reactions. A notable difference is use of an aqueous HEPBS-based reaction buffer.

### 3.2.3 Cell Encapsulation in Hydrogels

Cell-laden hydrogels were prepared sterilely as in Section 2.2.3 using the same prepolymer solution constituents (HBS-TEOA buffer, eosin Y photoinitiator, etc.) and hydrogel disc fabrication methods (light exposure parameters, acrylated coverglass, etc.). Cells were encapsulated at 1500 cell/µl (1.5 M cell/ml) unless otherwise noted. PEG-RGDS and PEG-PQ concentrations were used at 3.5 mM and 5% (w/v) unless otherwise noted. For invasion studies, PEG-PQ and PEG-MSM were used at lower concentrations as noted and exposed to white light for 45 s to ensure complete polymerization.

### 3.2.4 Immunohistochemistry

Hydrogel-encapsulated cells were stained with similar methods for fixation, Triton-X permeabilization, blocking, and antibody incubation and rinsing as in Section 2.2.6. Primary antibodies used for polarity, apoptosis, and proliferation staining were the same as in 2.2.6. For cell-secreted ECM staining, rabbit anti-collagen IV (Abcam, Cambridge, MA), chicken anti-laminin (Abcam) and rabbit anti-fibronectin (Abcam) were used. Secondary antibodies were either an Alexafluor 488 or 555 tagged donkey anti-rabbit, -mouse or –chicken antibody (Invitrogen). As in Section 2.2.6, samples were counterstained with a DAPI solution and Alexafluor 647 phalloidin (Invitrogen) and imaged using a Zeiss 5Live confocal microscope.

### 3.2.5 Morphologic Response to TGFβ

To observe responses to TGFβ, hydrogel-encapsulated 344SQ cells were cultured for 12 days to allow the formation of lumenized spheres, and then 5 ng/ml TGFβ1 (Calbiochem/EMD Millipore, Billerica, MA) was added to culture media. TGFβ-

supplemented media was changed every 2 days. In some samples the TGFβ inhibitor SB431542 hydrate (Sigma) was added to media at 5 μM 4 hours prior to TGFβ exposure and with subsequent changes of TGFβ-supplemented media to block TGFβ response. Sphere morphological response was evaluated using samples encapsulated in 5% PEG-PQ / 7 mM PEG-RGDS hydrogels by imaging samples on an Axiovert 135 inverted fluorescent microscope (Zeiss).

Zymography was performed to analyze for changes in MMP expression following TGFβ exposure using a 10% gelatin precast Ready Gel (BioRad, Hercules, CA) per manufacturer's protocol. Media samples were diluted 1:1 with loading buffer (for 1x concentrations of 62.5 mM Tris-HCl, pH 6.8, 25% glycerol, 4% SDS, 0.01% Bromophenol Blue), and the gel was run at 100 V for 2 hours. Following a 30-minute incubation in a renaturing buffer (2.5% (v/v) Triton X-100 in MilliQ H2O), the gel was incubated overnight in developing buffer (50 mM Tris-HCl, 0.2 M NaCl, 5 mM $CaCl_2$, 0.02% (w/v) Brij 35, pH 7.5) at 37˚C, stained for 1 h at RT with Coomassie blue (Sigma), and destained for 30 minutes with a destain solution (40% (v/v) methanol and 10% acetic acid (v/v) in DI $H_2O$) before imaging on a LAS4000 Imager (Fujifilm, Tokyo, Japan).

TGFβ-treated samples were also stained for polarity markers and imaged with confocal microscopy to monitor loss of polar organization. 344SQ in 5% PEG-PQ samples with different PEG-RGDS concentrations (1 mM, 3.5 mM and 7 mM) with and without TGFβ exposure were also stained and imaged to analyze changes in cell number and sphere size. Using ImageJ, cell number was quantified as the number of nuclei per sphere at maximum sphere cross-section using a threshholded DAPI channel and sphere size was quantified as sphere diameter at maximum sphere cross-section using the

Phalloidin channel. These factors were also analyzed for TGFβ-exposed samples treated with TGFβ inhibitor.

### 3.2.6 Quantitative RT-PCR Analysis

RNA from TGFβ-exposed samples and unexposed controls was analyzed with RT-PCR for changes in expression of miR200 and EMT markers. 344SQ cells were encapsulated at 3000 cells/μl in hydrogels with matrix formulations with changing or fixed matrix stiffness and PEG-RGD concentration (5%, 10% or 15% PEG-PQ + 3.5 mM PEG-RGDS or 5% PEG-PQ + 1 mM, 3.5 mM or 7 mM PEG-RGDS, n = 6 per formulation) and cultured for 10 days, after which half of the samples were treated for 4 days with TGFβ1 with daily supplemented media changes (5 ng/ml). Hydrogels were then digested with proteinase K (15 mg/ml, Calbiochem) for 2 min at room temperature, and placed on ice prior to total RNA extraction with Trizol (Invitrogen) per manufacturer's protocol. Q-PCR was performed on a 7500 Fast Real-Time PCR System (Applied Biosystems, Carlsbad, CA). The analysis of the miR-200 family levels (miR-200a, -200b, -200c) and the mRNA for CDH1, CDH2, VIM, CRB3 and ZEB1 were performed using TaqMan MiR assays (Applied Biosystems) and the data expressed relative to same-sample controls for miR-16 or L32, respectively.

### 3.2.7 Quantifying Cell-secreted ECM and Remodeling with TGFβ

To analyze changes in cell-secreted ECM, 344SQ in 5% PEG-PQ and 3.5 MM PEG-RGDS with or without TGFβ treatment were stained for collagen IV or laminin with DAPI/phalloidin counterstain. Differences in collagen IV spatial organization were first quantified using images taken at maximum sphere cross-section using the Radial

Profile plug-in for ImageJ (NIH) that analyzes staining signal intensity in a series of concentric radial regions of interest from the center to periphery of a user-defined area around a sphere. Radial profile values were normalized to intrasphere minimum background, and to describe radial organization, values from the outer 10% of radial sections were compared with the inner 90% of radial sections. Quantification was also done using z-stack projections of sphere collagen IV signal made with the max-project function in ImageJ. To evaluate ECM coverage around spheres, ROIs of sphere area were made using the projection of phalloidin channel, and the percent area of positive staining signal of a threshholded collagen IV projection over this area was analyzed. Differences in collagen IV organization were also analyzed using these methods in spheres in 5% PEG-PQ matrices with 1 mM or 7 mM PEG-RGDS with and without TGFβ treatment.

### 3.2.8 Evaluating Matrix Invasion

344SQ cells were encapsulated in 2% PEG-PQ hydrogels with 7 mM PEG-RGDS, cultured for 12 days and then treated with 5 ng/ml TGFβ for 4 days to assess invasive response. Samples were fixed, stained for DAPI and phalloidin and imaged on confocal. Images taken at maximum sphere cross-sections were measured for sphere size (sphere diameter) and extent of lumenization (by E-score method, Fig. 2-3). Further, given the mixed populations observed, several phenotypic metrics of invasion were measured blinded to group per examples in Fig. 3-5. Spheres were scored for: scalloped edges, positive if sphere edges puckered outward around sphere periphery; degree of single-cell invasion, positive if extensions of single cells were observed migrating off of sphere peripheries, commonly evident by a fine peri-spheroid haze in the phalloidin

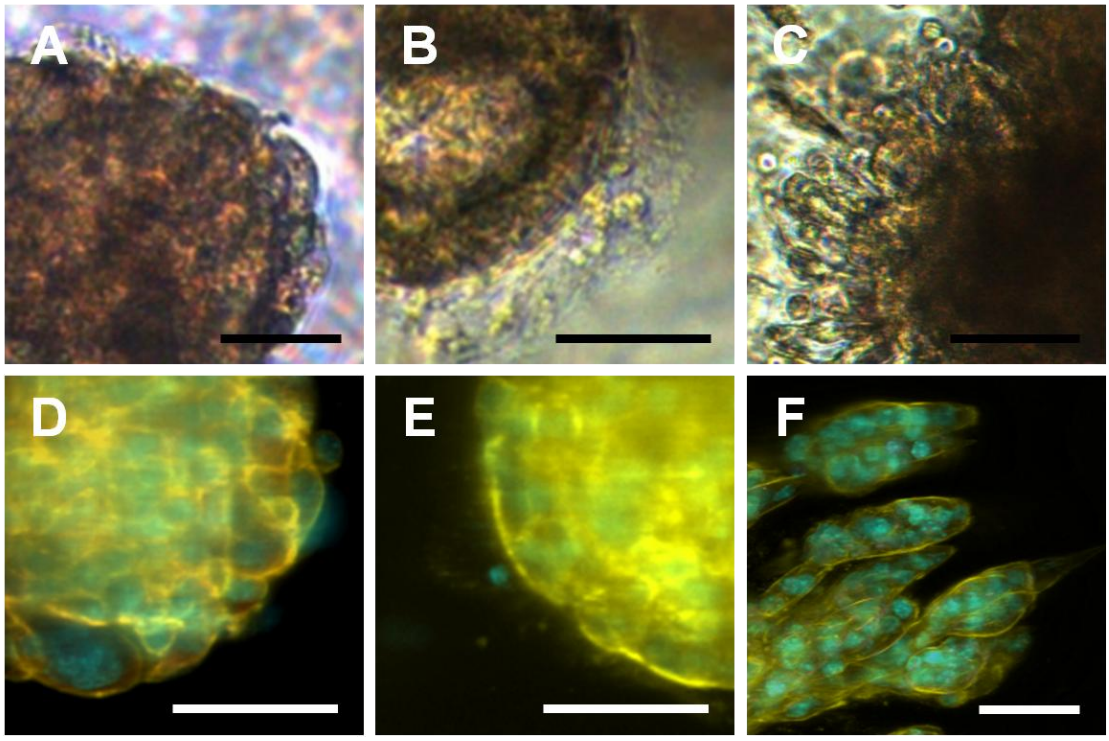


**Figure 3-5: Invasion Metrics.** For analysis of invasive phenotype, confocal images of DAPI/phallodin stained images were scored for phenotypic characteristics seen in representative images: scalloped or ruffled edges (*A, D*), fine, single-cell invasion (*B, E*) and/or multicellular invasive pseudopod formation (*C, F*). Scale bar = 50 μm.

channel; and multicellular pseudopod formation, positive if two or more cells formed an invasive matrix ingrowth greater than one-cell width off of the main sphere bulk. Values were quantified as the number of spheres positive for the invasion metric over total spheres measured and expressed as means per hydrogel sample. Furthermore, the number of distinct multicellular pseudopods were measured per sphere (scored as zero for spheres not featuring the characteristic) and expressed as a mean pseudopod number per sphere for a given hydrogel condition.

Some 2% PEG-PQ hydrogel samples were made with 15 mM linear PEG-RGDS or 7 mM cyclic PEG-RGDS, cultured for 12 days, and exposed to TGFβ. These spheres were imaged on an Axiovert 135 inverted fluorescent microscope (Zeiss) to note differences in invasive phenotype before and after treatment. Cells were also

encapsulated in 2% PEG-MSM and 3% PEG-MSM matrices with 7 mM PEG-RGDS and cultured in a similar fashion to assess differences in matrix invasion using these metrics.

## 3.3 Results and Discussion

### 3.3.1 TGFβ Induces EMT-related Morphologic Changes

Consistent with 344SQ's metastatic behavior *in vivo*, TGFβ has been shown to initiate EMT in well-organized structures of 344SQ cultured in MG through downregulation of miR-200 family members, inducing hyperproliferation, lumen filling and matrix invasion [232]. Probing for similar changes in spheres encapsulated in a PEG-based matrix, lumenized spheres were allowed to form in matrices composed of 5% PEG-PQ with 7 mM PEG-RGDS and then exposed to soluble TGFβ (Fig. 3-6). After 1 day of exposure (Fig. 3-6*B*), spheres began to lose organization and lumen clarity with epithelial organization continuing to diminish through 4 days of exposure (Fig. 3-6*C*) at which point lumens were completely filled. After 4 days of exposure, 0% of spheres were lumenized. Staining for polarity markers showed that polar organization was lost with unlocalized expression of β-catenin and ZO-1 throughout TGFβ-exposed spheres (Fig. 3-

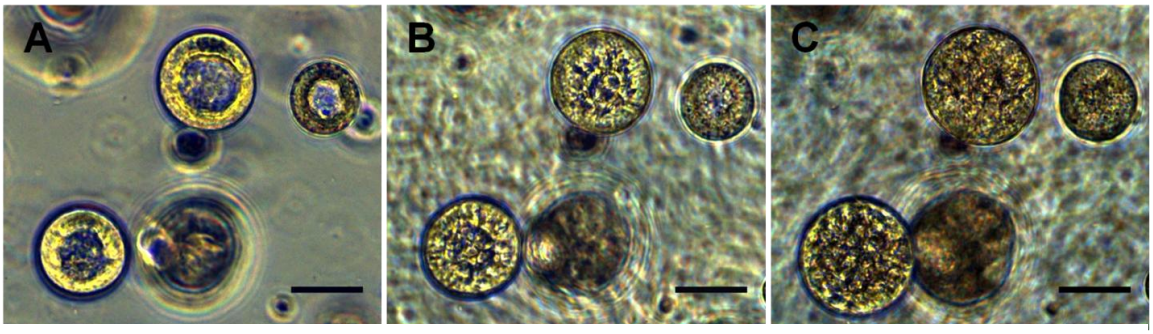


**Figure 3-6: PEG-encapsulated structures show EMT-related morphologic changes with exposure to TGFβ**. Brightfield images of lumenized spheres encapsulated in a 5% PEG-PQ, 7 mM PEG-RGDS hydrogel at 12 days in culture prior to 5 ng/ml TGFβ exposure (*A*) show breakdown of lumen organization after 1 day of treatment (*B*) and complete lumen filling and loss of organization after 4 days (*C*). Scale bar = 50 μm.

7*A*). Meanwhile, staining for Ki-67 and caspase-3 showed that these polarity changes were not accompanied by any organized patterns of proliferation or apoptosis activity as both stains showed random and unlocalized activity (Fig. 3-7*B*). However, per zymography results, TGFβ response was not accompanied by a large increase in MMP expression (Fig. 3-7*C*).

Loss of lumenization and abrogation of organized epithelial polarity with TGFβ were completely blocked with treatment with the TGFβ inhibitor SB431542 (Fig. 3-8*A*). Examination of sphere size and nuclei number with analysis of confocal images showed sphere sizes and the number of nuclei per sphere increased with TGFβ treatment consistent with enhanced proliferation and loss of tight cell-cell association seen in with EMT. These changes were prevented by exposure of the TGFβ inhibitor with TGFβ

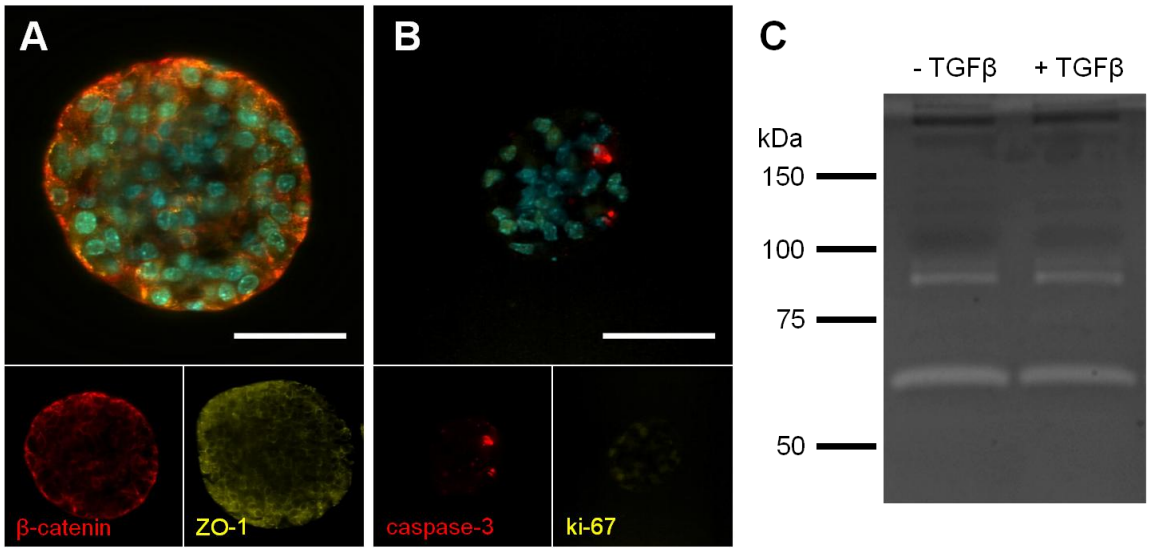


**Figure 3-7: Characterization of post-TGFβ phenotype of 344SQ in PEG**. *A*, representative image of a sphere in a 5% PEG-PQ, 7 mM PEG-RGDS hydrogel following 5 days of TGFβ stained for polarity markers β-catenin (red) and ZO-1 (yellow) shows loss of localization of polarity markers. Similar loss of polarity was seen following TGFβ regardless of matrix formulation. *B*, staining for cleaved caspase-3 (red) and ki-67 (yellow) shows that cells exhibit randomly organized apoptotic and proliferative activity following TGFβ. DAPI (cyan), scale bars = 50 μm. *C*, gelatin zymogram using media samples from PEG-encapsulated 344SQ cells before and after 5 days of TGFβ shows that the levels of MMP-2 and MMP-9 secreted, as indicated by clear bands at 62 kDa and 92 kDa, respectively, remained largely unchanged with treatment.

treatment (Fig. 3-8*B*). The influence of matrix adhesive ligand concentration on the TGFβ response was also examined in matrices with different PEG-RGDS concentration (Fig 3-8*C-D*). Prior to TGFβ treatment, matrices with a low, 1 mM PEG-RGDS concentration yielded larger spheres with greater number of nuclei than matrices with higher concentrations. This data is consistent with differences in epithelial polarity and sphere development previously observed (Section 2.3.5). Following TGFβ treatment

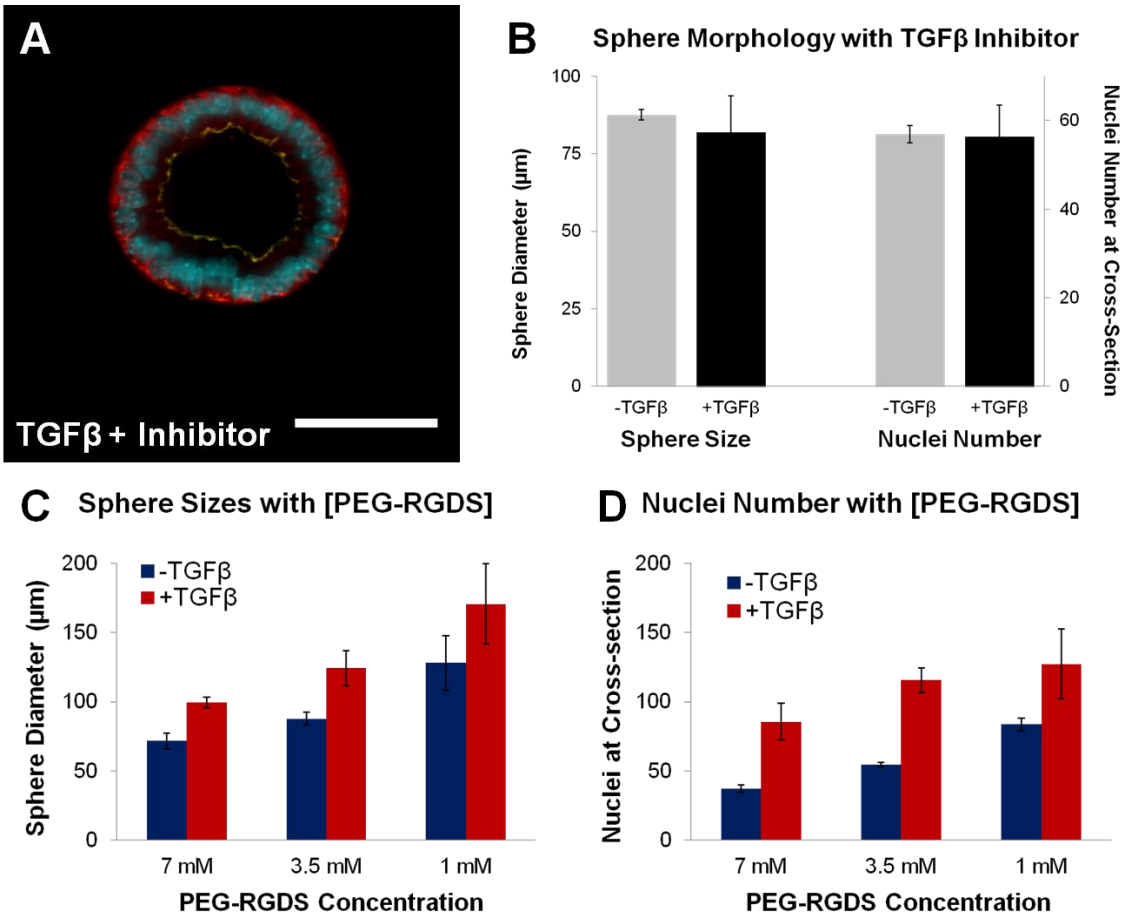


**Figure 3-8: TGFβ phenotype with TGFβ-inhibitor and altered [PEG-RGDS].** *A*, TGFβ-exposed 344SQ spheres remain lumenized with polar organization in the presence of the TGFβ-inhibitor SB431542 with (B) no changes in sphere size and nuclei number (*B*). β-catenin (red), ZO-1 (yellow) and DAPI (cyan), scale bar = 50 μm. *C-D*, both sphere size and nuclei number increase from –TGFβ baseline regardless of PEG-RGDS concentration indicating an EMT response (for both size and nuclei number, all same-concentration +/- TGFβ pairs, $p < 0.05$ except in the 1 mM group). Altering PEG-RGDS concentration led to differences in the metrics as both are increased in low PEG-RGSD matrices prior to TGFβ, and a greater post-TGFβ change from baseline is seen in the higher PEG-RGDS group (1 mM vs. 7 mM, -TGFβ, $p < 0.05$, amongst other significant differences).

spheres grew larger, and lumen filling and hyperproliferation contributed to an increase in nuclei number per sphere regardless of matrix formulation. The difference between pre- and post-TGFβ morphology was least profound in matrices with low concentrations of PEG-RGDS with spheres in the 1 mM group exhibiting lower percent increases in size and cell number than higher groups (for example, >120% increase in nuclei number for 7 mM group vs. ~50% for 1 mM).

This data shows a clear response to TGFβ with lumen filling, polarity marker de-localization and cellular hyperproliferation indicating loss of epithelial phenotype consistent with morphologic changes observed with 344SQ in MG and in other cancer models. While secretory MMP levels did not noticeably increase with TGFβ, dramatic increases in sphere sizes suggest enhanced localized gel degradation and matrix remodeling. EMT-related morphologic changes were observed regardless of matrix composition, but these changes were less substantial in matrices with 1 mM PEG-RGDS. This observation suggests that the degree of EMT response is influenced by matrix parameters or that matrices with low PEG-RGDS induced formation of a more mesenchymal phenotypic baseline even in the absence of TGFβ despite the pro-epithelial influence of culture in three-dimensions.

### 3.3.2 TGFβ Induces EMT Epigenetic Changes

To examine EMT-related microRNAs that may relate to this TGFβ response, quantitative RT-PCR was performed to measure the changes in miR-200 levels and EMT markers following TGFβ treatment of spheres in matrices with different formulations (fixed PEG-RGDS and varied PEG-PQ or fixed PEG-PQ and varied PEG-RGDS). Regardless of matrix composition, levels of the most well-studied miR-200 family

member, miR-200b, were elevated prior to TGFβ and fell after exposure, coincident with the morphologic changes observed (Fig. 3-9*A*-*B*). This pattern is similar to that seen in MG-encapsulated spheres and is consistent with the proposed double-negative feedback loop model between miR-200 and TGFβ-influenced ZEB1 (Fig. 3-3)[232,237] . Levels of miR-200a and miR-200c followed a similar pattern of decreased expression (Fig. 3-9*C*-

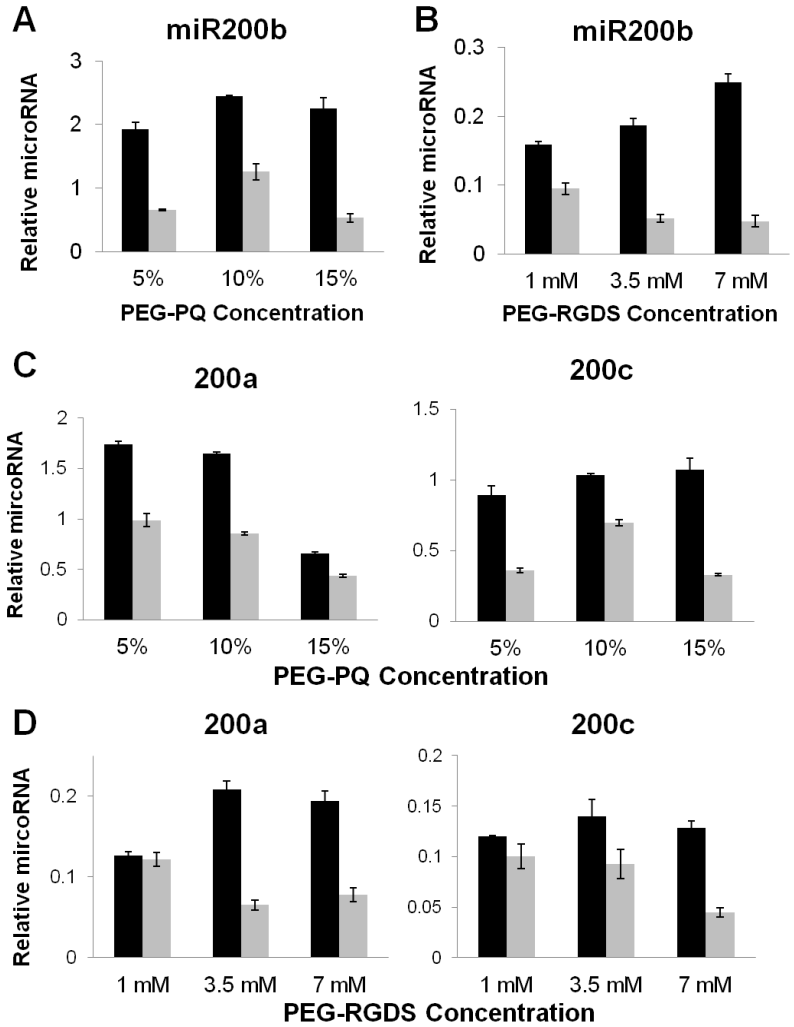


**Figure 3-9: PEG-encapsulated structures show epigenetic changes with TGFβ**. *A-B,* q-PCR data for miR-200b before (black bars) and after (gray bars) TGFβ in matrices with 3.5 mM PEG-RGDS and varied stiffness (*A*) and matrices with fixed 5% PEG-PQ stiffness and varied PEG-RGDS concentration (*B*) show a decrease in miR-200b. (For every formulation, before vs. after, $p < 0.01$). *C-D,* q-PCR data for miR-200a and miR-200c before (black bars) and after (gray bars) TGFβ treatment in these show a similar pattern of decreased expression as miR-200b indicating widespread epigenetic changes as these miR200 family members are found on different chromosomal loci. miR-200 expressed relative to miR16 levels.

*D*), indicating widespread epigenetic changes following TGFβ as miR-200b and miR-200c are found at two different chromosomal loci.

q-PCR also was used to probe for changes in expression of marker genes that are regulated by EMT-related transcription factors and help drive the EMT response. The epithelial markers analyzed include the seminal marker E-cadherin (*CDH1*) as well as the tight junction associated polarity marker Crumbs protein homolog 3 (*CRB3*). Mesenchymal markers include N-cadherin (*CDH2*), the mesenchymal intermediate filament vimentin (*VIM*), and Zeb1 itself. In all matrices following TGFβ treatment, fold-change expression of epithelial marker genes decreased and expression of mesenchymal marker genes generally increased indicating an extensive EMT response (Fig. 3-10 and Fig. 3-11). Notably, changes in EMT marker gene expression were less profound in the 1 mM PEG-RGDS group as Zeb levels were comparable before and after TGFβ treatment and vimentin levels actually showed a slight decrease with treatment (Fig. 3-11). This data is consistent with morphologic data of polarity stains and sphere parameters data showing blunted EMT response in this matrix formulation relative to others with less epithelial phenotype present even in the absence of TGFβ.

Overall, we observed a repression of miR-200 levels following TGFβ exposure and concomitant shift in EMT marker gene expression in the PEG system. To begin with, this finding is significant as it demonstrates an ability to harvest and collect RNA from a three-dimensional synthetic system, a non-trivial challenge to overcome when transitioning from natural to synthetic matrices. Furthermore, these epigenetic and gene expression changes demonstrate that the PEG-encapsulated cells engage physiological regulators of EMT, and that PEG is a useful 3D platform with which to study

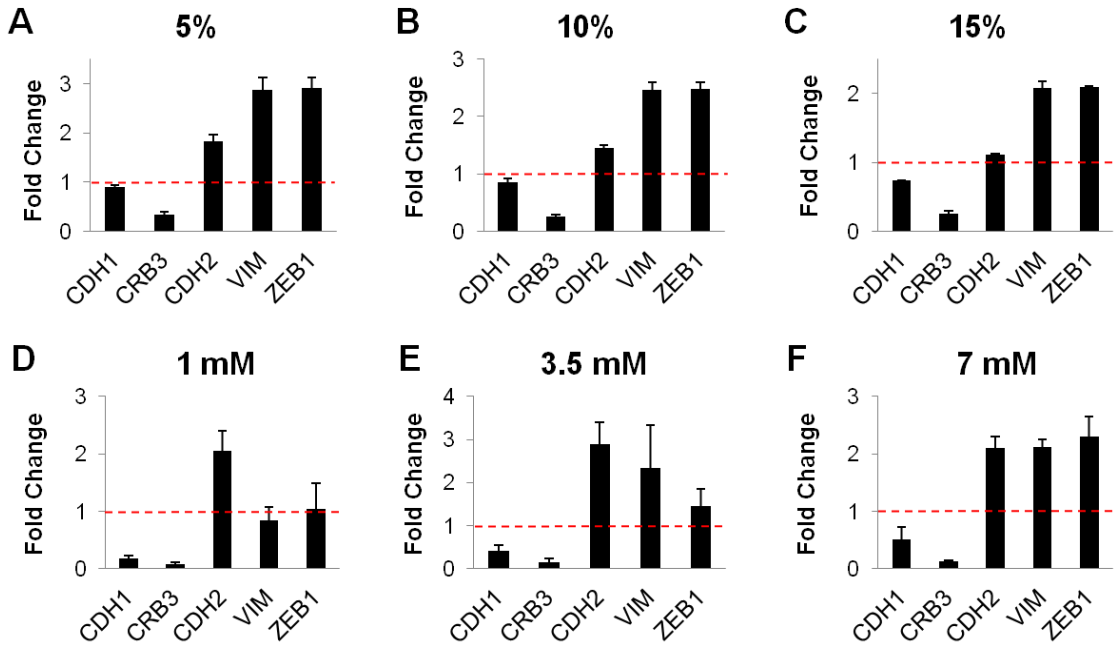


**Figure 3-10: PEG-encapsulated structures show changes in expression of EMT-associated genes with exposure to TGFβ**. Fold change in mRNA of EMT-related genes with TGFβ treatment in matrices with 3.5 mM PEG-RGDS and varied stiffness (*A-C*) and matrices with fixed 5% PEG-PQ concentration and varied PEG-RGDS concentration (*D-F*) show decreased expression of epithelial genes (*CDH1* and *CRB3*) and increased expression of mesenchymal genes (*CHD2*, *VIM*, *ZEB1*) in all matrix formulations following exposure consistent with EMT-related genetic changes seen in 344SQ in MG cultures. Fold change mRNA relative to *L32* mRNA.

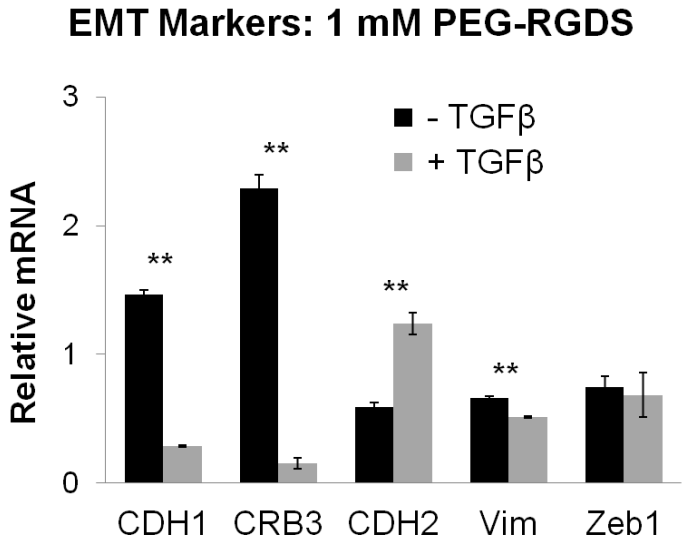


**Figure 3-11: Spheres in 1 mM PEG-RGDS matrices show tempered EMT gene expression response**. mRNA levels from 344SQ in 5% PEG-PQ with 1 mM PEG-RGDS show significantly decreased expression of epithelial genes *CDH1* and *CRB3* and significantly increased expression of the mesenchymal gene *CDH2*, but expression of *Zeb1* is unchanged and expression of *VIM* actually falls, suggesting an incomplete or tempered EMT response (**p < 0.01, -TGFβ vs. +TGFβ). Other matrix formulations showed uniformly expected responses. Levels relative to *L32* mRNA.

transcriptional events in response to extracellular signals. Together with morphologic observations and staining data, this data also indicates that PEG-encapsulated 344SQ undergo a dramatic EMT response and one that can be modified by altering certain matrix parameters.

### 3.3.3 TGFβ Induces Remodeling of Cell-secreted ECM

Following EMT, cells remodel their ECM environment, hypersecreting some ECM components like fibronectin and laminin to ligate integrins and assist in migration and degrading others like basement membrane-associated collagen IV to enable invasion [66,265]. To probe for similar ECM remodeling in 344SQ, spheres cultured in PEG matrices were stained for collagen IV, laminin, and fibronectin before and after TGFβ exposure and analyzed for changes in amount and organization. Staining 344SQ cultured in 5% PEG-PQ / 3.5 mM PEG-RGDS matrices at day 12 in culture (Fig. 3-12) revealed that collagen IV was organized in a strong, contiguous band around sphere peripheries prior to TGFβ exposure with the pattern suggestive of a contiguous basement membrane around epithelial glands (Fig. 3-12*A*). Following 4 days of TGFβ treatment, collagen IV organization changed dramatically (Fig. 3-12*B*). While spheres still stain positively for its presence, its tightly organized peripheral location was lost with no uniform band present around spheres and secretion evident between cells (Fig. 3-12*B*). These changes in collagen IV organization were abrogated with concomitant use of the TGFβ inhibitor SB431542 with TGFβ treatment (Fig. 3-12*C*).

Collagen IV spatial organization was first quantified using a radial profile method where signal intensity is measured in concentric radial regions of interest from the sphere center to periphery in images taken at maximum sphere cross-sections. In comparing

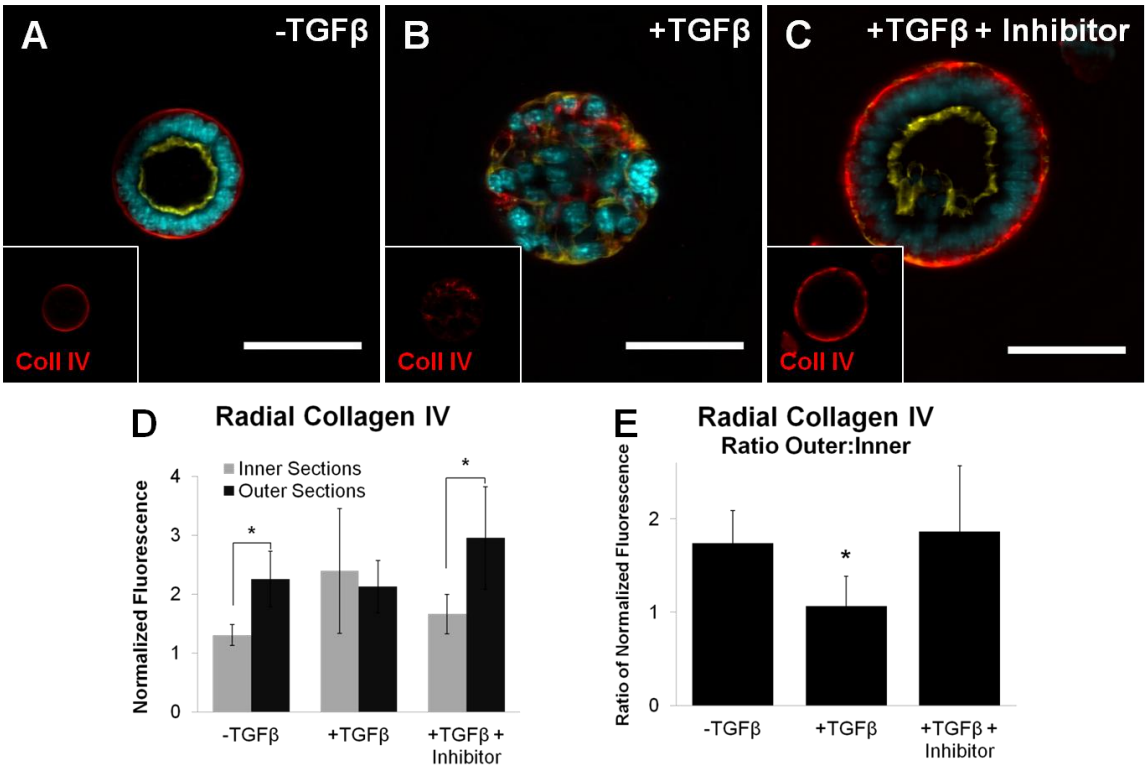


**Figure 3-12: Collagen IV radial organization altered with TGFβ exposure**. *A-B*, 344SQ cultured in 5% PEG-PQ / 3.5 mM PEG-RGDS hydrogels show (*A*) well-organized and intact band of collagen IV deposition around sphere periphery prior to TGFβ exposure that is (*B*) lost after 4 days of TGFβ as collagen IV features fractured expression throughout sphere interior. *C*, these changes are prevented with concomitant use of TGFβ inhibitor. DAPI (cyan), phalloidin (yellow), scale bar = 50 μm. *D-E*, quantifying radial profiles shows (*D*) significantly greater collagen IV intensity in outer radial sections in spheres not exposed to TGFβ or with TGFβ + inhibitor with comparable spatial location in TGFβ-treated spheres and (*E*) ratios of radial spatial signal showing no spatial preference (* $p < 0.05$ in outer vs. inner sections or +TGFβ alone vs. other groups).

means of outer and inner 10% of these radial sections, collagen IV location shows a significant preference for sphere periphery in the absence of TGFβ or with both TGFβ and its inhibitor (Fig. 3-12*D-E*). TGFβ-treated spheres showed no spatial collagen IV preference with comparable staining in both inner and outer radial sections.

Investigators studying other cancer spheroid models have used a different method to characterize ECM remodeling, analyzing projections of sphere z-stacks to examine the extent of 3D sphere coverage[175]. Analyzing spheres using a similar method in our system, prior to TGFβ exposure collagen IV projected evenly over the entire sphere

surface with comprehensive coverage (Fig. 3-13*A*). Following exposure it exhibited spotty and uneven coverage in sphere projections suggesting significant remodeling with EMT (Fig. 3-13*B*). These changes were prevented with the TGFβ-inhibitor SB431542. Quantifying mean fluorescence over sphere projection, there was no difference between groups in overall collagen IV signal intensity (Fig. 3-13*C*). However, in quantifying positive collagen IV pixels over total sphere projection area, total collagen IV coverage is significantly decreased in TGFβ groups relative to no TGFβ and TGFβ inhibitor groups (Fig. 3-13*D*). This data along with the radial profile data suggests that TGFβ-exposed spheres exhibit areas of focal collagen IV degradation and remodeling with uneven

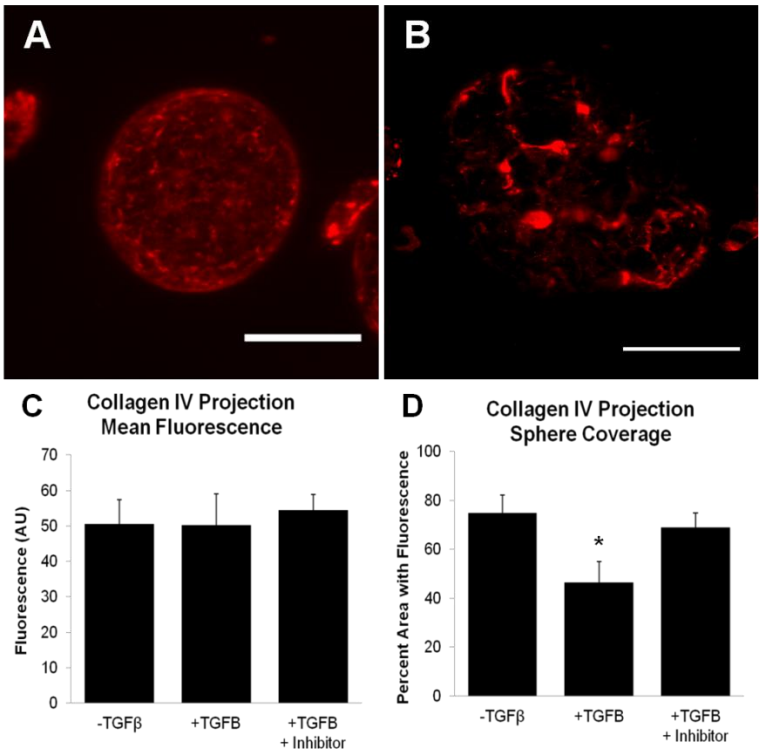


**Figure 3-13: Collagen IV sphere coverage altered with TGFβ**. *A-B*, z-stack projections collagen IV (red) through entire depth of 344SQ spheres cultured in 5% PEG-PQ / 3.5 mM PEG-RGDS hydrogels show (*A*) even deposition around spheres prior to exposure that is (*B*) remodeled after 4 days of TGFβ leaving intense, spotty deposition in some areas with poor coverage in others. Scale bar = 50 μm. *C-D*, quantifying projections, overall fluorescent intensity (*C*) shows no difference between groups, but percent of projected area positive for collagen IV (*D*) shows uniform deposition in untreated or TGFβ-inhibitor groups around most of sphere surface areas with significantly less coverage in TGFβ-exposed spheres suggesting significant collagen IV remodeling (*$p < 0.01$).

collagen IV deposition irrespective of changes in overall secretion.

344SQ cells in PEG-based matrices were also examined for cell-secreted fibronectin and laminin to probe for similar TGFβ-induced remodeling. Both fibronectin and laminin were deposited around spheres after 12 days in culture, but expression was not as focal and finely organized as collagen IV, showing more diffuse and variable deposition around and away from spheres (Fig. 3-14*A and C*). Following TGFβ exposure there was no notable change in this organization with diffuse peri-sphere deposition persisting for both fibronectin and laminin (Fig.3-14*B and D*). However, particularly for fibronectin, staining intensity was greatly enhanced, suggesting enhanced secretion following TGFβ exposure and EMT, consistent with other literature observations[237,289].

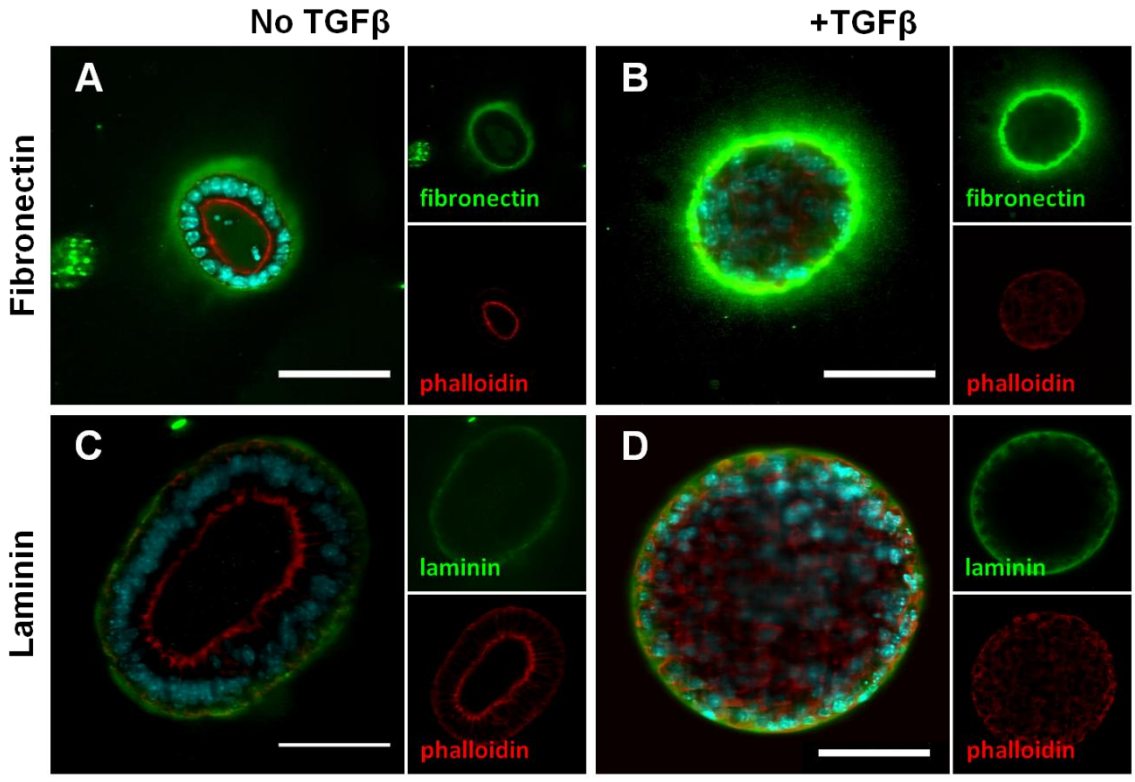


**Figure 3-14: Fibronectin and laminin secretion in 344SQ**. Staining for fibronectin (*A-B*) and pan-laminin (*C-D*) shows diffuse peri-spheroid deposition in spheres before (*A and C*) and after (*B and D*) TGFβ. There were no apparent differences in organization with TGFβ, however enhanced fluorescent intensity suggests enhanced secretion with EMT. DAPI (cyan), scale bar = 50 μm.

Finally, differences in ECM remodeling were analyzed in matrices with different PEG-RGDS concentrations to examine if previously observed differences in epithelial morphogenesis and EMT response are reflected in cell-secreted ECM. 344SQ cells cultured for 12 days in matrices with 5% PEG-PQ and 1 mM or 7 mM PEG-RGDS were stained for collagen IV and analyzed using both radial profile and projection methods (Fig. 3-15). Prior to TGFβ exposure, spheres in high PEG-RGDS matrices exhibited similarly well-organized and uniform bands of collagen IV staining around sphere peripheries (Fig. 3-15*A*), while spheres in low PEG-RGDS matrices showed spotty

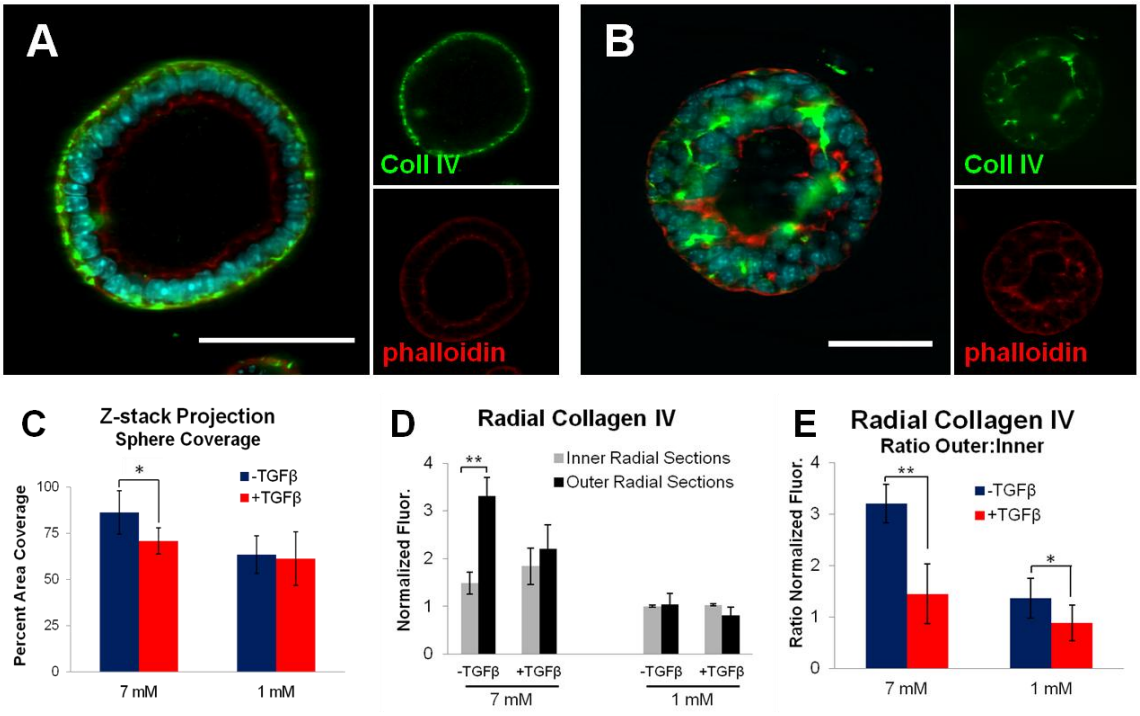


**Figure 3-15: Adhesive ligand concentration influences collagen IV deposition and remodeling**. *A-B*, 344SQ in 5% PEG-PQ matrices with 7 mM (*A*) or 1 mM (*B*) PEG-RGDS show differences in collagen IV deposition prior to TGFβ with 1 mM PEG-RGDS spheres lacking well-organized peri-spheroid radial deposition. Scale bar = 50 µm. *C*, quantification of sphere coverage shows previously observed remodeling with TGFβ in the 7 mM group, but no difference with TGFβ exposure in the 1 mM group. *D*, radial profile analysis shows significant differences in 7 mM spheres between staining intensity in outer vs. inner radial sections prior to TGFβ that is lost with treatment, but no difference in spatial organization in the 1 mM group before or after treatment. *E*, normalization of outer to inner radial intensity shows significant difference with 7 mM PEG-RGDS and a slight difference in localization with TGFβ in the 1 mM group (**$p < 0.01$, *$p < 0.05$).

collagen IV coverage with positive staining present throughout interior sphere areas (Fig. 3-15*B*). Quantifying these differences before and after TGFβ exposure in z-stack projections demonstrates comparably low levels of collagen IV sphere coverage in the 1 mM group regardless of TGFβ treatment (Fig. 3-15*C*). Meanwhile, sphere coverage is high prior to TGFβ in the 7 mM group, falling upon exposure to levels comparable to the 1 mM group. Similar observations are found when quantifying collagen IV radial profiles at sphere cross-sections, where 7 mM spheres show strong outer spatial localization prior to treatment and equivalent localization after exposure, whereas spheres in 1 mM matrices show comparable staining between inner and outer radial sections (Fig. 3-15*D*). Examining the ratios of outer to inner section staining intensity showed a difference spatiality in 1 mM matrices before and after TGFβ exposure, but that difference is far less profound that observed in 7 mM matrices (Fig. 3-15*E*).

The use of the synthetic PEG system enabled the above characterization of cell-secreted ECM by $KRas^{G12D}/p53^{R172H\Delta G}$ model for the first time as previous attempts were hampered by confounding MG constituents composed of ECM from its naturally-derived matrix source. Overall this data demonstrates an effort by 344SQ to remodel its own cell-secreted ECM in response to TGFβ. Following exposure, cells focally degraded previously well-organized, peripherally localized collagen IV leaving collagen deposition localized with no readily recognizable pattern throughout the TGFβ-treated sphere. This observation is consistent with observations in other spheroid cancer models and with collagen IV staining patterns in basement membranes of histological sections of *in vivo* tumors[21,60]. Investigators postulate that loss of collagen IV organization in basement

membranes is a necessary or supportive prelude to invasion and metastasis, and EMT-associated protein secretion changes in 344SQ may function similarly.

344SQ also showed increased deposition of other ECM molecules like fibronectin and laminin, consistent with ECM secretory behaviors following EMT[66,265]. While other studies have reported changes in laminin organization with EMT, this was not observed with 344SQ to a degree that enabled spatial quantification. There may be less of a change in laminin organization with EMT in our lung adenocarcinoma model or enhanced staining signal may mask subtle changes in organization. Finally, we observed that adhesive matrix parameters influenced 344SQ-secreted matrix and its EMT remodeling. Matrices with low PEG-RGDS concentration induced cells to secrete far less organized collagen IV with a spatial profile similar to that of TGFβ-exposed spheres. As reflected in this whole-population analysis of hundreds of spheres, this difference was true for lumenized as well as non-lumenized spheres in the 1 mM matrix, though as discussed in chapter 2, epithelial organization and E-scores were far lower in this group relative to matrices with higher PEG-RGDS (Sect. 2.3.5). **This data suggests that the outside-in matrix influences on cellular epithelial morphogenesis and genetics also lead to inside-out responses in how the cells themselves remodel their surrounding matrix environment.**

### 3.3.4 Matrix Invasion in PEG-encapsulated 344SQ

In the MG system one of the important responses to TGFβ is invasion into surrounding matrix by multicellular extensions radiating out of spheres in a phenotype that potentially mimics the ECM-invasive response of metastasizing primary tumors following EMT[232]. We sought to develop a PEG-based matrix formulation permissive to

studying this invasive phenotype. Pilot studies suggested that PEG-PQ hydrogels at the extreme low end of stiffness promoted invasion of TGFβ-exposed 344SQ. Spheres in these matrices showed dramatic size enlargement, and the relative intra-gel locations of spheres changed, culminating in complete gel degradation by cells if left for several days under TGFβ treatment.

To examine this enhanced degradative response further, 344SQ was encapsulated in very soft 2% PEG-PQ matrices with 7 mM PEG-RGDS. Cell viability remained high in these hydrogels and cultured 344SQ developed into multicellular spheres, though significantly larger than in previously studied matrices (>150 μm diameter). Subjectively, overall sphere lumenization percentage was poor, consistent with previous observations of decreasing lumenization with decreasing gel stiffness (Sect. 2.3.4). Some spheres did exhibit central cell clearing consistent with lumen formation. However, in some of these lumenized spheres and in others that did not exhibit lumenization, sphere borders were irregular with peripheral cells in some spheres sending fine cellular projections into the surrounding matrix (Fig. 3-16*A*). Prior to TGFβ, many structures did not exhibit this fine matrix invasion and overall structure shapes remained spherical (Fig. 3-16*B*). Following 4 days of TGFβ treatment, spheres not only grew larger and lost all degree of lumenization, but also readily formed multicellular matrix-invasive outgrowths with similar morphology to that observed in the MG system (Fig. 3-16*C-D*). Fine, single-cell matrix invasion was observed both in structures exhibiting these multicellular pseudopods and in those that did not. Spheres in these 2% PEG-PQ hydrogels were stained for DAPI and phalloidin and imaged with a confocal microscope to better visualize this invasive phenotype and quantify measures of invasion in this mixed

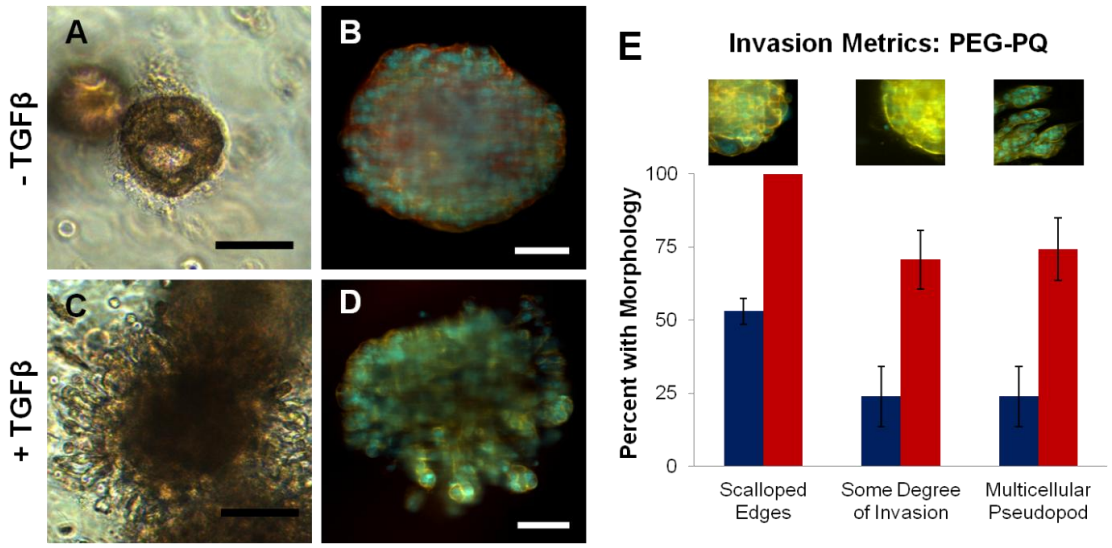


**Figure 3-16: Matrix invasion in very soft PEG-PQ matrices**. *A-B*, 344SQ spheres in 2% PEG-PQ matrices show poor epithelial organization with some structures exhibiting fine, single-cell matrix invasion even in the absence of TGFβ (*A*). Most structures are large with no lumen and ruffled sphere borders (*B*, polarity stains). *C-D*, after 4 days of TGFβ many structures exhibit substantial matrix invasion with the formation of multicellular invasive pseudopods. *E*, quantification of invasion metrics shows widespread poor structure formation before TGFβ with ruffled borders and some degree of both fine invasion and multicellular pseudopod invasion, both increasing substantially and featured in most structures after treatment. DAPI (cyan), β-catenin (red), phalloidin (yellow), scale bars = 50 μm.

population (Fig. 3-16*E*). Many structures prior to TGFβ exposure exhibited irregular borders with ruffled or scalloped edges, with upwards of 20% exhibiting some degree of matrix invasion. After TGFβ, however, no spheres showed regular borders with ~75% exhibiting some degree of invasion, commonly multiple, multicellular invasive pseduopods.

This matrix formulation was readily able to recapitulate the invasive phenotype observed in TGFβ-treated MG structures, but lacked a high degree of organized, polarized epithelial structure formation prior to exposure, exhibiting poor lumenization and in some cases showing matrix invasion despite lack of an EMT trigger. Given previous observations of higher PEG-RGDS concentrations and the cyclic formulation of PEG-RGDS promoting epithelialization (Sect. 2.3.6), an effort was made to deploy these

adhesive parameters in soft 2% PEG-PQ matrices to normalize pre-TGFβ structures (Fig. 3-17). Incorporation of high concentrations of PEG-RGDS (15 mM, Fig. 3-17*A*) or a 7 mM concentration of PEG-c(RGDfK) (Fig. 3-17*C*) induced the widespread formation of lumenized spheres in these soft hydrogels, rescuing the organized epithelial phenotype. In both cases TGFβ exposure induced many EMT-related morphogenic changes including loss of lumenization and polarity, increased sphere sizes, and irregular, scalloped sphere borders (Fig. 3-17*B and D*). However, spheres did not form the multicellular invasive pseudopods observed in TGFβ-exposed spheres in 2% PEG-PQ hydrogels with lower PEG-RGDS concentrations or MG. It seems that rescuing

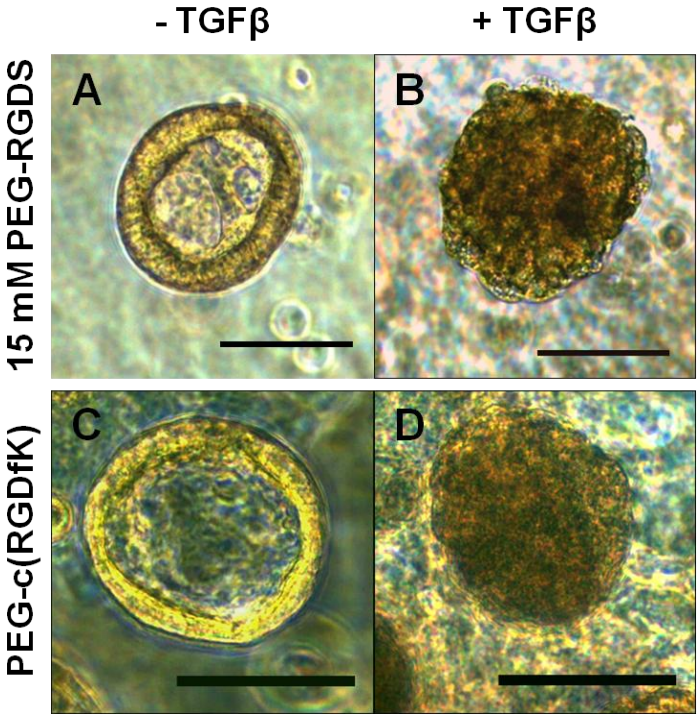


**Figure 3-17: Pre-TGFβ epithelial organization rescued with alteration of matrix adhesive properties**. 344SQ at day 12 in culture in 2% PEG-PQ hydrogels with 15 mM linear PEG-RGDS (*A-B*) or 7 mM PEG-c(RGDfK) (*C-D*) exhibit normalization of epithelial structure prior to TGFβ (*A, C*) with the presence of well-organized lumenized spheres and no degree of pre-EMT matrix invasion. Following TGFβ treatment *(B, D*) spheres exhibit an EMT response similar to that observed in stiffer hydrogels featuring sphere enlargement, lumen filling, and ruffled borders, but limited matrix invasion. Scale bars = 100 μm.

epithelial morphogenesis in these soft matrices with these approaches also restored the post-TGFβ phenotype observed in stiffer matrices.

Finally, in an effort to capture broader MMP susceptibility and in the event that invadopodia require faster kinetics in matrix degradation for proper formation, an alternative protease sequence to PQ was used in the PEG matrix backbone. The MSM sequence was recently characterized for vascular tissue engineering applications in a similar PEG system as the one used here[227]. It features a greater than two-fold increased kinetic reaction parameter ($k_{cat}$) for MMP-2 and captures substantial MMP-1 reactivity that PQ lacks (MMP-1 $k_{cat} \approx 7.9$ vs. 0.65 $s^{-1}$). These altered reactivities enabled more rapid hydrogel degradation in the presence of MMP-1 and MMP-2 and substantially greater fibroblast and endothelial cell migration and matrix invasion[227].

The MSM peptide was synthesized, pegylated, and polymerized with 7 mM PEG-RGDS and encapsulated 344SQ to probe for invasion, first at the 2% concentration that previously supported multicellular invasion in PEG-PQ hydrogels (Fig. 3-18). Prior to TGFβ, structures generally were large and did not widely lumenize consistent with observations previously made in soft matrices, but sphere morphology was also more normalized than in 2% PEG-PQ (Fig. 3-18*A and C*). Upon quantification of invasive metrics prior to TGFβ, it was observed that comparatively fewer structures in 2% PEG-MSM exhibited irregular edges, structures rarely showed fine, single-cell matrix invasion, and no structures featured multicellular invasive pseudopods (Fig. 3-18*E and G*). While no structures formed epithelial spheres with high organization (E-score = 5), a higher percentage of pre-TGFβ spheres did form structures with some degree of lumen (E-score ≥3) in PEG-MSM than PEG-PQ (26.1±3.6% vs.10.4 ± 5.5%, $p<0.05$).

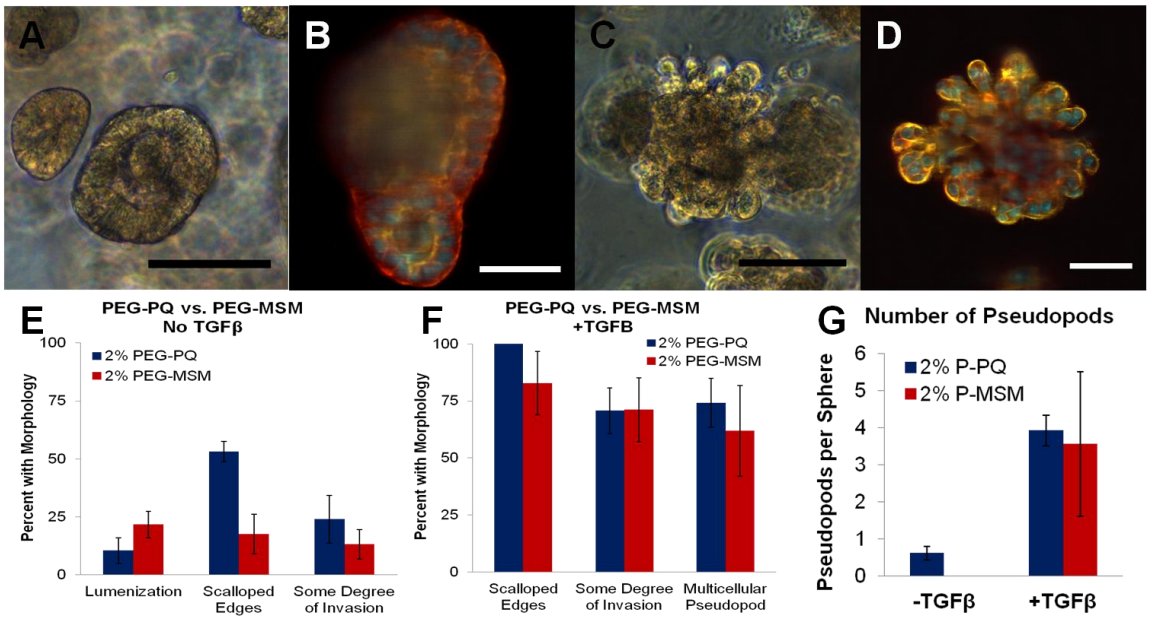


**Figure 3-18: PEG-MSM matrices permit substantial matrix invasion with TGFβ**. *A-B*, 344SQ spheres in 2% PEG-MSM matrices show better organization than spheres in 2% PEG-PQ with some central clearing, crisp borders and no invasion in the absence of TGFβ. Structures are large, but generally show some degree of polar organization (*B*, polarity stains). *C-D*, structures exhibit significant matrix invasion with multicellular invasive pseudopods after 4 days of TGFβ. *E*, quantification of invasion metrics before TGFβ shows improved lumenization and a lower percentage of spheres with scalloped edges or single-cell invasive phenotypes than in 2% PEG-PQ. *F-G*, quantification of metrics after TGFβ shows comparable degrees of invasion with treatment in between matrices, with a notable similarity in both the percentage of spheres with multicellular pseudopods and their average number per sphere. *A and C*, scale bars = 100 μm, *B and D*, scale bar = 50 μm; DAPI (cyan), β-catenin (red), phalloidin (yellow).

More regular pre-TGFβ structures may have formed in PEG-MSM due to slight differences in component acrylation or conjugation efficiency or there may have been differences in the structure of constituent amino acids that led to minor differences in hydrogel polymerization. These differences may have resulted in a more structurally supportive gel in PEG-MSM vs. PEG-PQ despite the same low 2% concentration. Following TGFβ treatment, however, spheres formed similar multicellular invasive pseudopods in PEG-MSM as in PEG-PQ (Fig. 3-18 *B and D*). TGFβ-treated spheres exhibited a similar degree of positivity for the invasive metrics including a similar percentage of spheres with multicellular invasive pseudopods (Fig. 3-18*F-G*). TGFβ-

treated PEG-MSM samples also showed a similar number of multicellular invasion pseudopods per sphere (Fig. 3-19). This comparable degree of post-TGFβ invasion despite greater normalization of sphere structure without substantial invasion before treatment suggests that the greater degradation of the MSM sequence left the matrix more susceptible to EMT-induced cell-mediated matrix invasion.

While the MSM sequence enabled a highly invasive post-TGFβ phenotype in these 2% PEG-MSM matrices, epithelial structure was still abnormal likely due to low matrix stiffness with poor overall lumenization rate and relatively disorganized lumenized structure compared to structures in stiffer matrices. In an effort to normalize epithelial structure but maintain the greater protease susceptibility that MSM affords, 344SQ were cultured in slightly stiffer 3% PEG-MSM matrices (Fig. 3-19). In these matrices pre-TGFβ spheres lumenized at a much higher rate (41.7 ± 3.6% vs. 26.1 ± 3.6% in 2% PEG-MSM, Fig. 3-19*A and C*). Some of these structures exhibited the highly organized lumenized phenotype (7.8 ± 6.8% with E-score = 5 in 3% PEG-MSM). Further, structures showed well-organized sphere edges and nearly no single-cell invasion pre-TGFβ. After 4 days of TGFβ exposure, however, structures exhibited a phenotype similar to that observed in stiffer PEG-PQ gels, with filled lumens, loss of polar organization, and some degree of display of invasive metrics (Fig. 3-19 *B and C*), but few structures exhibited the multicellular invasive pseudopods reflective of substantial matrix invasion (Fig. 3-19*D*). Thus, it seems that the presence of a more readily degradable sequence in the hydrogel backbone was an insufficient factor alone to permit a substantial grossly matrix-invasive post-TGFβ phenotype in matrices structurally capable of supporting widespread pre-TGFβ epithelial morphogenesis.

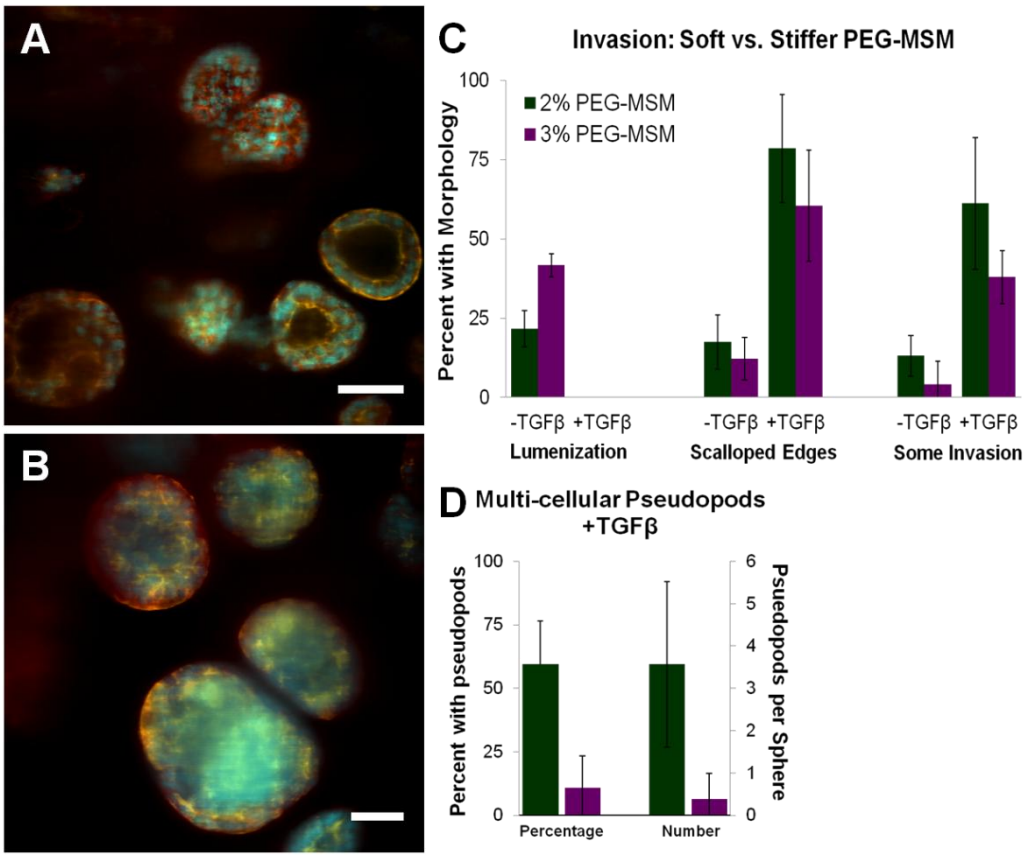


**Figure 3-19: Higher PEG-MSM concentration abrogates post-TGFβ invasive phenotype**. *A-B*, 344SQ spheres in 3% PEG-MSM matrices show improved lumenization in the absence of TGFβ (*A*), but generally show a similar post-TGFβ phenotype as in higher concentration PEG-PQ matrices (*B*). DAPI (cyan), β-catenin (red), phalloidin (yellow), scale bars = 50 μm. *C-D*, quantification of invasion metrics shows improved pre-TGFβ epithelial morphogenesis with some phenotypic changes after TGFβ in 3% PEG-MSM matrices (*C*), but little formation of multicellular invasive pseudopods (*D*).

Overall, the PEG system with PEG-PQ and PEG-RDGS bioactive components recapitulated a matrix-invasive response to TGFβ treatment, but did so at lower polymer concentrations where structural or other properties are not conducive to normal, non-matrix invasive sphere development in the absence of TGFβ. This result is first interesting as it describes a 3D matrix environment that is insufficient for normal 344SQ epithelial morphogenesis, even despite provision of relatively ample adhesive ligand (7 mM PEG-RGDS). Interestingly, the mechanics of these soft hydrogels are more similar to MG than other stiffer PEG hydrogels that facilitated substantial epithelial

morphogenesis. This suggests that while the excess bioactivity or contaminating growth factors in MG are not absolutely required for epithelial morphogenesis, they may be important in structurally weaker 3D environments.

More structurally stable gels were formed with use of a PEG-MSM backbone at the same low concentration that permitted normalized sphere structure with some degree of lumenization while maintaining a post-TGFβ phenotype characterized by the formation of multicellular invasive pseudopods. However, population-wide epithelial morphogenesis pre-TGFβ was still deficient relative to stiffer PEG formulations or MG. The use of higher concentrations or a more adhesive formulation of PEG-RGDS and an increase in the concentration of either backbone component were able to rescue pre-TGFβ epithelial phenotypes. However, these changes also abrogated post-TGFβ multicellular invasive pseudopod formation and matrix invasion, despite, in the case of PEG-MSM, the presence of a more readily degradable protease-sensitive sequence.

Future work may seek to modify and supplement the base PEG system to recapitulate matrix invasive phenotype. First, attempts could be made to normalize epithelial morphogenesis in the very soft matrices that permit post-TGFβ invasion. The inclusion of additional adhesive ligands, like those derived from laminin, the major MG constituent, may help normalize structures in these soft hydrogels. In a different approach, PEG-RGDS ligands could be modified with additional specific non-cell interactive cleavable sequences and incorporated at high concentrations to first normalize epithelial morphogenesis. Subsequently, the associated protease could be added to cleave this sequence to drop adhesive ligand levels to those that permit widespread pseudopod invasion.

Another possibility is that the reductionist PEG system used here is lacking matrix ligands that are necessary for full and proper invadopodia function. Modifications to the system can be targeted at adhesive components to facilitate greater interactivity with integrin ligands on leading edge of invadopodia or capture binding to other cell receptors. One prospect that may be worth exploring is incorporation of HA-derived sequences or others that can bind CD44, a cell surface molecule upregulated with EMT and important in cancer matrix migration[134,263,290,291]. Another idea is modification to facilitate greater interactivity with the important cell-membrane bound MMP, MT1-MMP, that typically promotes invadopodia matrix invasion through direct matrix cleavage or to a greater extent, more focalized MMP-2 activation.

## 3.4 Conclusion

TGFβ plays an important role in multiple aspects of tumorigenesis and is a critical inducer of EMT in many cancer models and the $KRas^{G12D}/p53^{R172H\Delta G}$ lung adenocarcinoma model. In PEG-based matrices, TGFβ initiated an EMT response in encapsulated 344SQ with changes in morphologic characteristics, polarity markers, and epigenetics and gene expression. EMT-related ECM remodeling was also characterized for the first time in 344SQ with notable changes in collagen IV spatial organization. Both this remodeling and the TGFβ-induced morphologic response were tuned by altering matrix adhesive ligand concentration, demonstrating matrix influences on EMT. Future work may seek to characterize any temporal relationship between ECM secretion and epithelial morphogenesis to ascertain if properly organized cell-secreted ECM promotes morphogenesis via subsequent integrin binding or is rather the result of secretion by organized spheres, and conversely, if disorganization is a prelude or result of

loss of epithelial morphogenesis with EMT. Such data may also work to explain the relationship between poor epithelial morphogenesis and poorly organized cell-secreted ECM in matrices with low adhesive ligand concentration and its less profound EMT response.

Finally, matrix invasion was also investigated in the PEG system with the formation of TGFβ-induced multicellular invasive pseudopod tuned by altering matrix parameters and protease susceptibility. This invasive phenotype closely mimicked that seen in TGFβ-treated MG-encapsulated 344SQ. Future work may seek to normalize pre-TGFβ epithelial morphogenesis in advance of this invasive phenotype using the above approaches. In further investigation of EMT and metastasis, additional matrix factors can also be introduced into the PEG system to probe for promotion or inhibition of invasion or invadopodia function, like ECM peptides or proteins that more specifically interact with specialized invadopodia integrins or cell-cell ligands like Jagged-2 whose binding has been shown to promote metastasis on tumor invasive edges[239].

# 4. 344SQ in PEG-cadherin Matrices

## 4.1 Introduction

### 4.1.1 Cadherins in Cancer

Cadherins are membrane-spanning glycoproteins that help mediate cell-cell adhesion to organize tissue architecture[292] (Fig. 4-1). The cadherin extracellular portion consists of five homologous repeat domains bridged by calcium that bind to other cadherin ectodomains on neighboring cells. An intracellular portion binds to a complex consisting of several proteins including p120-catenin, α-catenin and β-catenin, which in turn link to the actin cytoskeleton and help mediate intracellular signaling events[293]. Classically, cadherins bind more readily to like cadherin types to organize tissues; cells in epithelial tissues predominantly express E-cadherin to promote epithelial cell-cell adhesion while mesenchymal cells express a variety of other cadherins, notably N-cadherin.

The significance of cadherins in cancer pathogenesis has been outlined in part in Chapters 1 and 3. E-cadherin levels or function are altered in a number of epithelial

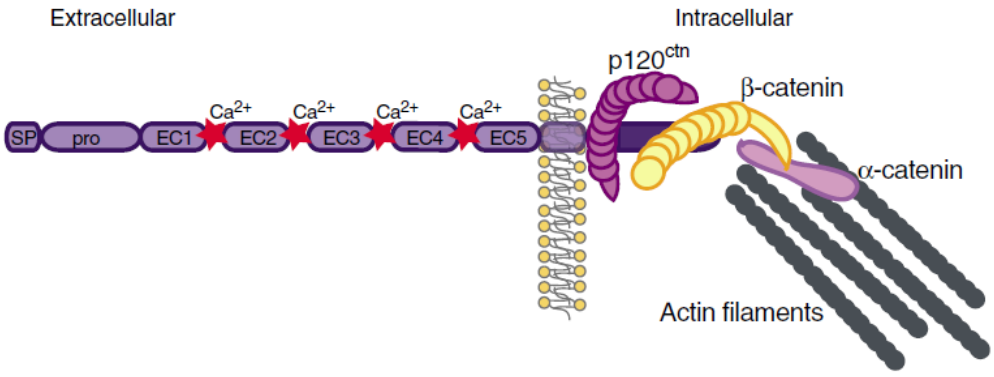


**Fig. 4-1: Cadherin Structure.** Cadherin subtypes share similar structural features consisting of five, calcium-dependent extracellular domains that mediate homophilic binding and an intercellular portion that interacts with a catenin protein complex (p120-, β- and α-catenin) as well as cytoskeletal components. From Wheelock, *et al.*[293]

cancers including lung cancer[125,127,128] and may serve as an independent prognostic factor for metastasis and survival[127,133,134]. Part of this relationship is thought to be related to β-catenin action upon release from unbound E-cadherin complexes with free β-catenin working with Tcf/Lef transcription factors to promote cell proliferation and upregulate other genes important for tumor progression[122,140,142,143,294] (See Fig. 1-5). E-cadherin's role in cancer is also related to cell disaggregation resulting from EMT that in turn facilitates tumor cell invasion and metastasis. A key EMT transcription factor, Twist, has been shown to decrease E-cadherin levels and binding, leading to loss of polarity and increased motility and invasion with resulting disaggregation[295].

The loss of E-cadherin binding likely works in concert with other pro-tumorigenic changes due to the gain of N-cadherin binding that results from the "cadherin switch" almost universally observed in EMT models[293]. In breast and melanoma models, increased N-cadherin binding enhances signaling through the ERK and MAPK pathways to increase cancer cell motility, matrix invasion and metastasis, in part aided by enhanced MMP-9 secretion[135,296,297]. Some of this effect is likely due to membrane localized N-cadherin stabilizing the FGF receptor, augmenting normally subdued pro-invasion mediated normal FGF signaling[135,279]. N-cadherin may play a role apart from those related to cell aggregation or matrix invasion, as homophilic adhesion of N-cadherin in a prostate model also showed increased levels of anti-apoptotic members of the BCL-2 family of apoptosis mediators, enhancing cancer cell survival[298]. Finally, in an interesting mechanism connecting different cell-cell contact networks, more aggressive growth phenotypes in a melanoma model resulting from Notch-1 binding were found to be regulated in part by an upregulation in N-cadherin expression[299]. This mechanism may

be of particular relevance to our lung adenocarcinoma model as Jagged-Notch signaling was found to mediate behavior of a particularly invasive subset of $KRas^{G12D}$ / $p53^{R172H\Delta G}$ cells[239].

Because of their role in adhesion between phenotypically similar adjacent cells, it is unsurprising that cadherins can also be seen as key players in the establishment of cell polarity, a critical phenotypic characteristic relevant to tumor progression. On a basic level, cadherins are a major component of adherens junctions, desmosomes, and other cellular junctions that are critical for organized polarity in multicellular structures [300]. In more complex polarity-related functions, E-cadherin, working with its associated bound cytoskeletal elements, ensures the proper targeting of vesicles containing apical and basolateral polarity proteins in the cell membrane[300–302]. For example, E-cadherin binding has been shown to promote targeting of the cell surface protein aquaporin-3, important to basolateral membrane function[303]. Also of increasing research interest is the relationship between cadherin binding and the localization and function of a group of polarity-determining factor complexes, among them the Scrib/Dlg/Lgl (Scribble/Discs large/Lethal giant larvae) complex[292].

### 4.1.2 Scribble: Polarity, Tumor Progression, and Relationship to Cadherin

Initially characterized in a developmental context in *Drosophila*, scribble helps regulate epithelial polarity in the Scrib/Dlg/Lgl complex by promoting lateral membrane identity and forming antagonizing signaling relationships with other complexes to define apical surfaces (Fig. 4-2). Scribble may also be important for normal tight junction formation in epithelial barriers independent of lateral polarity-defining effects[304]. Scribble's polarity-related role is of obvious importance to cancer as loss of its function

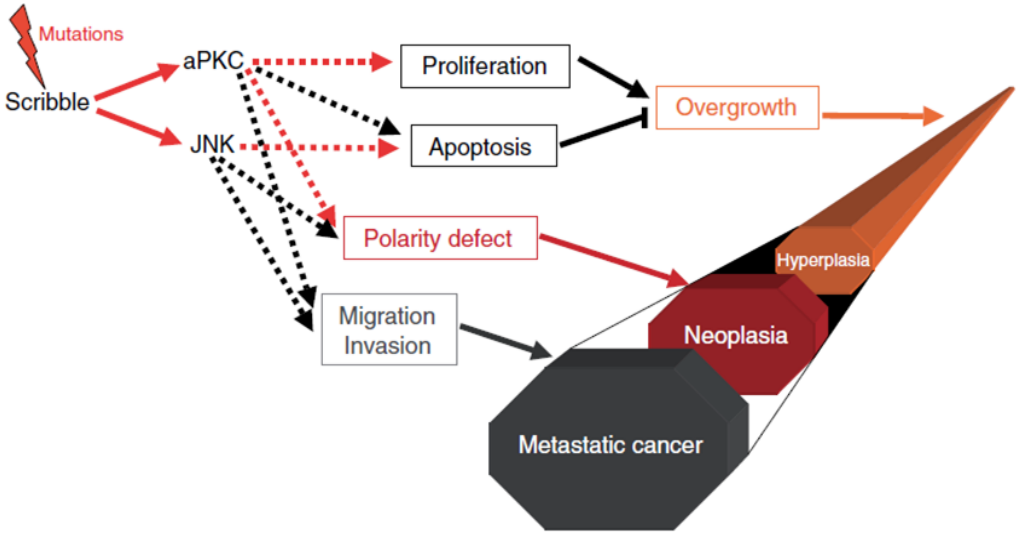


**Fig. 4-2: Multifaceted role of scribble.** Scribble interacts with other polarity complexes and signaling pathways associated with atypical protein kinase C (aPKC) and c-Jun N-terminal kinase (JNK) to regulate growth (proliferation/apoptosis) and migration in addition to polarity. Modified from Etienne-Manneville[305].

through knockdown or mislocation disrupts cell polarity and alters 3D morphogenesis. But scribble also has additional roles related to proliferation and tissue overgrowth that have led to its general designation as a tumor suppressor protein[305–307]. Scribble interacts with signaling pathways related to atypical protein kinase C (aPKC) and c-Jun N-terminal kinase (JNK) to regulate proliferation and apoptosis in roles completely apart from polarity mediation[305]. Through these mechanisms, scribble knockdown induces hyperproliferation and dysplasia[308].

It is through these roles that scribble functions with more direct and active phenotypic importance in cancer progression. In a mammary model with oncogenic Ras, the additional loss of scribble promoted matrix invasion through regulation of MAPK signaling[309]. In separate experiments with the MCF10A breast cancer model, scribble was actually not found to be essential for normal spheroid polarity, but was important for directional cell migration[310]. Upon induction in wound and chemotaxis experiments,

scribble knockdowns showed impaired single-cell migrational polarity and defects in leading-edge lamellipodia. In a report from a different group, the combination of knockdown of scribble with a second protumorigenic signal (Erb activation or pro-inflammatory cytokine exposure) or the combined loss of two different polarity complex proteins promoted invasion of the MCF10A model in a MG-based matrix[311].

Scribble and E-cadherin, thus, share an indirect relationship as they both influence cell polarity and cancer progression. But scribble also may have a more specific relationship to E-cadherin binding and signaling. In MDCK cells, scribble is recruited and restricted to lateral membranes at cell-cell junctions in a manner that is dependent on the proper binding of E-cadherin, evidenced by both E-cadherin knockdown and re-expression assays[312]. Furthermore, a knockdown of scribble disrupts adhesion between cells in a manner found to be mediated by disruption of E-cadherin binding[313]. The resulting migratory, mesenchymal phenotype of scribble knockdown was mimicked with a separate knockdown of E-cadherin, and adhesion in scribble knockouts could be partially rescued with forced expression of an E-cadherin-α-catenin fusion protein. The co-localization of scribble with E-cadherin at adherens junctions has been found to be controlled by a specialized phosphorylation state; the phosphor-form is co-expressed with E-cadherin-catenin complexes and the unphosphorylated form located more generally at other lateral membrane sites[314].

Either through interaction with E-cadherin or through the other tumor suppression roles outlined above, scribble mutations have been shown to drive tumor induction, overgrowth, and invasion in both *in vitro* models and *in vivo*, typically working in concert with another pro-oncogenic signal like activated Ras or mutant c-myc[308,315–317].

Furthermore, expression of scribble has been shown to be dysregulated in human cancers including breast, prostate, and many others[308,312,316,318]. Relatively little work has been done characterizing scribble's importance in lung cancer, though one study has shown that scribble is essential for normal epithelial cell-cell contacts in the developing mouse lung[319]; scribble mutants show malformed airways with abnormal acinar lumenization and morphogenesis, suggesting its particular importance in lung epithelial cell polarity.

### 4.1.3 Scribble in the KRas$^{G12D}$ / p53$^{R172H\Delta G}$ Lung Adenocarcinoma Model

Some initial work has been done studying the role of scribble in epithelial morphogenesis and invasion of the KRas$^{G12D}$ / p53$^{R172H\Delta G}$ model. The behavior of the non-invasive and metastasis-incompetent KRas$^{G12D}$/p53$^{R172H\Delta G}$ line 393P with a knockdown of scribble has been studied (393P.scrib)[311]. 393P.scrib was found to be more migratory in a transwell assay and more invasive in MG compared to parental controls (Fig. 4-3). Further, when injected into the tail vein of non-transgenic mice, 393P.scrib readily colonized and grew metastatic tumors in host lungs while parental controls did not.

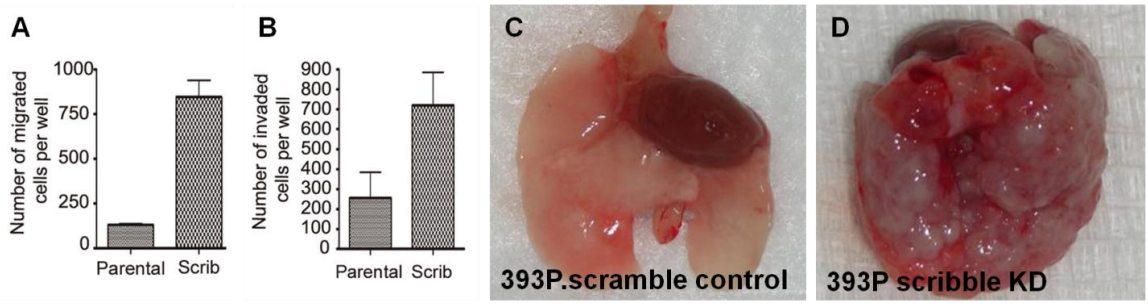


**Fig. 4-3: Scribble regulates metastatic potential of 393P.** *A-B*, 393P scribble knockdowns show enhanced *in vitro* (*A*) transwell migration and (*B*) invasion in a MG assay compared to parental 393P cells. *C-D*, following tail vein injection into non-transgenic mice, 393P control cells did not colonize or show metastatic growth in lungs (*C*) while the scribble knockdowns effectively colonized, forming large, bilateral tumor masses with overwhelming disease burden. Modified from Chatterjee, *et al.*[311]

Meanwhile, in unpublished data, scribble knockdown of the EMT-prone, representative metastatic line 344SQ (344SQ.scrib) induces formation of large, multicellular structures in 3D MG culture, but spheres showed no organized polarity or lumenization (Fig. 4-4). Depending on the batch of MG used, 344SQ.scrib colonies also sometimes show a minor degree of transient matrix invasion. miR-200 levels remain very low during scribble sphere morphogenesis even in the absence of TGFβ, suggesting a link between polarity and epigenetic control of EMT. Additional experiments have been done in MG matrices crosslinked with collagen to yield enhanced matrix stiffness and additional collagen-mediated bioactivity. In these matrices, 344SQ.scrib is remarkably more matrix-invasive with invasion blocked with antibodies against integrin

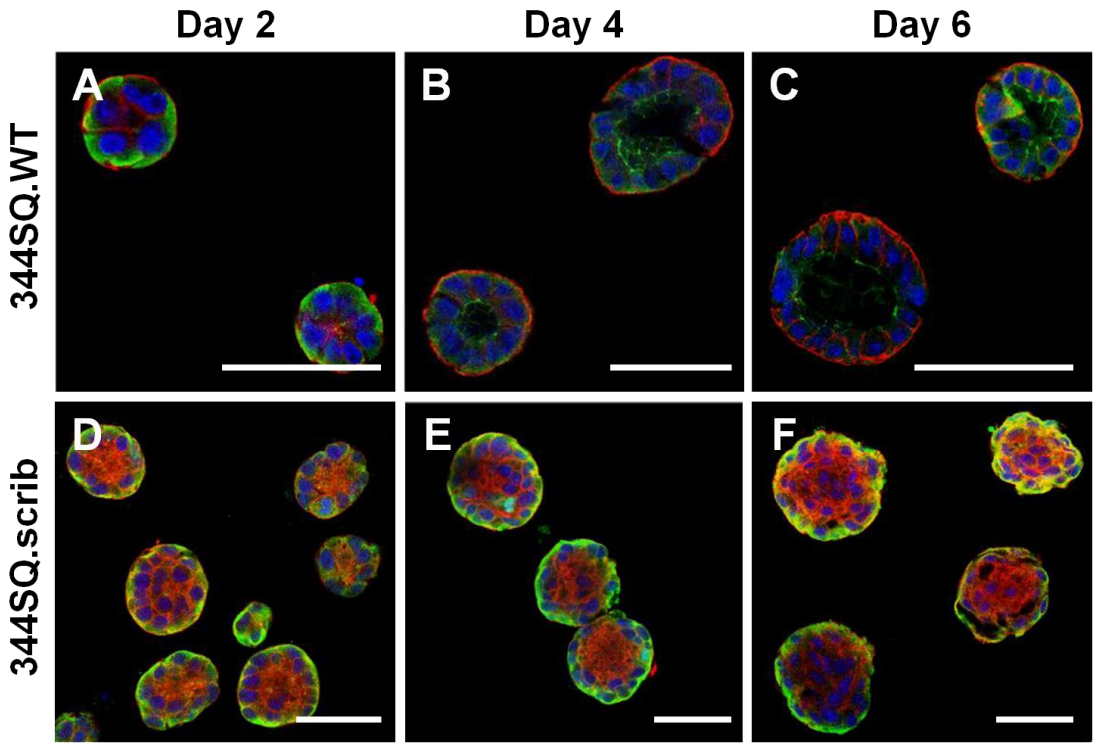


**Fig. 4-4: 344SQ.scrib shows no polar organization in MG.** While 344SQ.WT forms readily lumenizing spheres with segregation of epithelial polarity markers over six days in 3D MG culture (*A-C*), 344SQ scribble knockdowns demonstrate sphere growth, but no lumenal clearing or polar organization (*D-F*). 344SQ.scrib spheres also show some degree of irregular borders. ZO-1, apical (green); α6-integrin, basolateral (red), TORPRO3, nuclei (blue). Images courtesy of Don Gibbons.

$\beta_1$ (Fig. 4-5). This observation suggests that matrix contextual cues can regulate pro-malignant scribble effects.

Finally, 344SQ.scrib cells also exhibit an interesting behavior when in co-culture with wild-type 344SQ (344SQ.WT). When 344SQ.scrib cells are in direct contact with 344SQ.WT, the morphology of the resulting hybrid structure is completely epithelial-normalized, with structures forming lumenized spheres with epithelial polarity (Fig. 4-6). 344SQ.scrib is distinguished from 344SQ.WT in co-culture by co-expression of green fluorescent protein (GFP) in the vector with scribble-targeting RNAi, leaving a portion of hybrid spheres with positive GFP fluorescence (Fig. 4-6*B*). Persistent GFP signal indicates that knockdown of scribble is maintained despite the apparent ability of these hybrid spheres to polarize. In MG co-culture, lumenization in 344SQ.scrib-containing spheres is only observed when 344SQ.scrib and 344SQ.WT come together to form structures; spheres composed only of 344SQ.scrib cells still show no organization despite 344SQ.WT cells cultured in the same MG sample, indicating that this phenomenon is likely mediated by cell-cell contacts and not paracrine signaling.

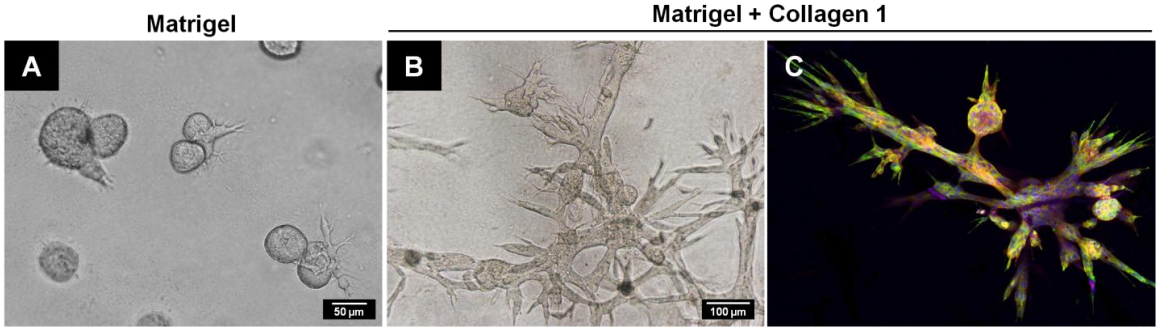


**Fig. 4-5: 344SQ.scrib morphology and metastatic phenotype regulated by matrix.** *A*, 344SQ.scrib in 3D MG form disorganized spheres with some limited and variable cellular invasion into the matrix. *B-C*, in MG matrices crosslinked with collagen-1, the alteration of matrix mechanics and/or biochemistry with collagen incorporation induces the formation of highly invasive structures (*C*, polarity stains: ZO-1 (green), α6-integrin (red), TORPRO3 (nuclei, blue)). Images courtesy of Don Gibbons.

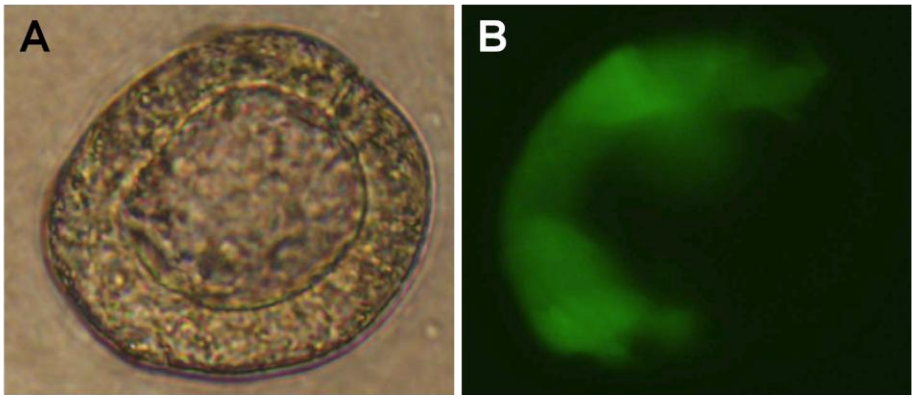


**Fig. 4-6: Epithelial normalization occurs in spheres with 344SQ.scrib and 344SQ.WT in contact.** Representative image of a lumenized sphere in a MG co-culture of 344SQ.scrib and 344SQ.WT (*A*) that is partially composed of 344SQ.scrib cells with maintenance of scribble knockdown in these cells apparent by GFP expression (*B*). 344SQ.WT cells in contact with 344SQ.scrib in hybrid sphere do not express GFP. Images courtesy of Don Gibbons.

This result suggests an intriguing link between scribble regulation of polarity and epithelial cell-cell contacts. Some data has demonstrated the effects of normal epithelial cells on contacting adjacent cells with scribble mutations, but study has largely been restricted to experiments in *Drosophila* showing a cell competition effect[320,321]. When surrounded by normal cells, these scribble mutants undergo apoptosis and are apically extruded from epithelial cell layers with effects mediated by MAPK activation and the JAK/STAT signaling pathway. In this system, the tissue overgrowth that would potentially result from aberrant proliferation in scribble mutants may be compensated for by increased cell death[307]. Beyond these reports, however, little data exists in mammalian models regarding the interaction of cells with deficient or mutant scribble and normal epithelium or in tumor spheroid metastasis models with mixed cell populations like those in the above 344SQ.scrib-WT hybrids.

The results from other tumor models showing the co-localization and functional relationship between E-cadherin and scribble, as well as other data demonstrating the significance of cadherin binding in polarity and tumor progression, provide an intriguing

possibility that the cadherin complexes may play a role in this cell-cell contact-mediated scribble regulation. Examination of this possibility or further study of other processes mediating 344SQ.scrib epithelial normalization is difficult in the MG co-culture experiments because the requisite contact between 344SQ.WT and 344SQ.is a relatively rare event in whole-population co-cultures. The PEG hydrogel system presents an opportunity to circumvent this problem. Potentially important cell-cell signals can be pegylated and covalently incorporated in the matrix and presented for signaling to encapsulated 344.scrib cells as a proxy for binding by neighboring cells.

In this chapter, E-cadherin and N-cadherin proteins will be pegylated and incorporated into PEG-PQ-based hydrogels to probe for effects on the $KRas^{G12D}/p53^{R172H\Delta G}$ model lines. First, PEG-E- and -N-cadherin will be incorporated in matrices with encapsulated 344SQ.WT to probe for an influence on epithelial morphogenesis and the loss of polarity with EMT. The influence of PEG-cadherins on 344SQ.WT sphere formation in matrices lacking other adhesive components will also be studied. Then, the PEG-cadherin factors will be analyzed for potential pro-epithelialization effects on the 344SQ.scrib line. PEG-E- and -N-cadherin will demonstrate different influences on 344SQ.scrib polarity and lumenization, and a possible role for intrasphere apoptosis and differential patterns of cell-expressed cadherin in this effect will be explored.

## 4.2 Materials and Methods

### 4.2.1 Cell Culture

344SQ was derived from $KRas^{G12D}/p53^{R172H\Delta G}$ mice as described previously in Gibbons, *et al*. and Zheng, *et al*[232,235]. 344SQ.scribble ("344SQ.scrib") cells were

derived from 344SQ parental cells and contain a vector with expression for GFP and short-hairpin RNAi sequence against scribble. The scribble RNAi sequence and the transfection and cell selection methods were as previously described[311,322]. All cells and cell-laden hydrogels were cultured in a humidified atmosphere at 37˚C and 5% $CO_2$ in RPMI 1640 (Mediatech) with 10% fetal bovine serum (Atlanta Biologicals), 10 μg/ml gentamicin and 0.25 μg/ml amphotericin B (Invitrogen).

### 4.2.2 Synthesis and Purification of PEG-RGDS and PEG-PQ-PEG

PEG-RGDS and PEG-PQ-PEG ("PEG-PQ") were synthesized and conjugation verified as described in Section 2.2.2.

### 4.2.3 Synthesis of PEG-N- and -E-cadherin

To synthesize PEG-cadherin conjugates, recombinant E-cadherin/Fc chimera and recombinant N-cadherin/Fc chimera (both carrier-free, R&D systems) were dissolved at 100 μg/ml using filter-sterilized HEPBS buffer (20 mM N-(2-Hydroxyethyl)piperazine-N'(4-butanesulfonic acid), 100 mM NaCl, 2 mM $CaCl_2$, 2 mM $MgCl_2$, pH 8.5) and kept on ice. Dissolved cadherin proteins were transferred to γ-irradiated 10,000 MWCO dialysis cassettes (Thermo Scientific, Waltham, MA) and dialyzed sterilely overnight against filter-sterilized cold HEPBS buffer at 4˚C with two buffer changes to remove the Tris buffer in which proteins were initially lyophilized. Separately, acryloyl-PEG-succinimidyl valerate (acryl-PEG-SVA, 3.4 kDa, Laysan Bio) was dissolved in HEPBS buffer and immediately sterilized with filtration (0.2 μm PES). For conjugation following cadherin dialysis, the acryl-PEG-SVA solution was added to the separate PEG-cadherin solutions at 20:1 molar ratio of PEG-SVA:protein and immediately vortexed

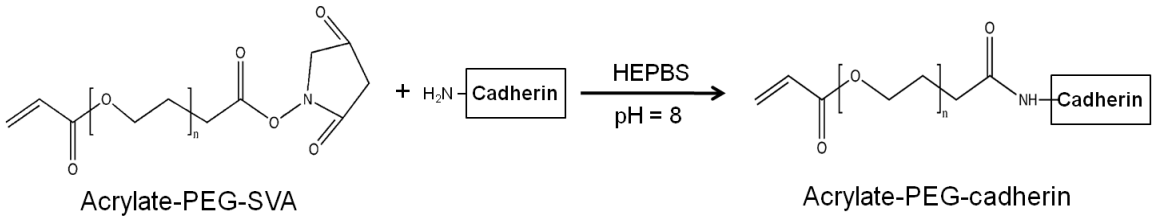


**Fig. 4-7: Cadherin conjugation.** E- and -N-cadherin are reacted with PEG-SVA via NHS chemistry with protein primary amines to leave pegylated proteins with one or more acrylate-PEG chains covalently attached. Aqueous HEPBS-based reaction buffer permits maintenance of protein structure.

(Fig. 4-7). The mixed solutions were left to react on a vortexer at 4 °C with pH checked after 30 minutes and 3 hours to verify pH~8. Following complete overnight reaction, aliquots of undiluted PEG-cadherin conjugates were stored at -80°C in sterile, low-bind tubes (Eppendorf, Hamburg, Germany).

### 4.2.4 Western Blot Determination of PEG-cadherin Conjugation Efficiency

To determine efficiency of the protein conjugation reaction, a Western blot was performed on the protein and PEG-protein conjugates. Protein samples were mixed with loading buffer (For 1x concentration of 50 mM Tris-HCl pH 6.8, 100 mM DTT, 1% SDS, 0.005% Bromophenol blue, 10% glycerol), loaded at 250 ng protein per lane, and run at 100V for 2 h on a 4-15% of 15% pre-cast Tris-HCL PA gel (ReadyGel, Biorad). Bands were then transferred to a nitrocellulose membrane at 80 V for 2 hours. The blot was incubated overnight at 4°C in a 5% milk solution for blocking. Following rinsing the next day, it was incubated for 1 hour with a 1:2000 dilution of goat anti-E-cadherin or 1:400 sheep anti-N-cadherin antibody (R and D) in 0.1% BSA in PBST (PBS + 0.1% Tween-20, Sigma) , rinsed twice for 5 minutes with PBST, and then incubated with the secondary antibodies HRP-conjugated rabbit anti-sheep or anti-goat (Santa Cruz Bio) at 1:2500 dilutions. Following development by the ECL chemiluminescent Western blot

analysis system (GE healthcare, Chalfont St. Giles, UK), chemiluminescent images of the blot were taken on an LAS 4000 (Fujifilm) for band visualization.

### 4.2.5 Cell Encapsulation in Hydrogels

PEG-PQ-based cell-laden hydrogels were prepared sterilely and polymerized using the same specifications as in Section 2.2.3 except cells were removed from culture plates prior to polymer resuspension using the non-enzymatic cell dissociation solution Versene (Invitrogen) in place of trypsin in an effort to maintain intact cadherin expression on cells. Flasks were first rinsed with -Ca / -Mg, Hank's balanced salt solution (Invitrogen) and then incubated in 4 ml Versene with periodic flask agitation. In samples with matrix-tethered cadherin, PEG-E- or -N-cadherin were added to the prepolymer mixture at 50 μg/ml unless otherwise noted (Fig. 4-8).

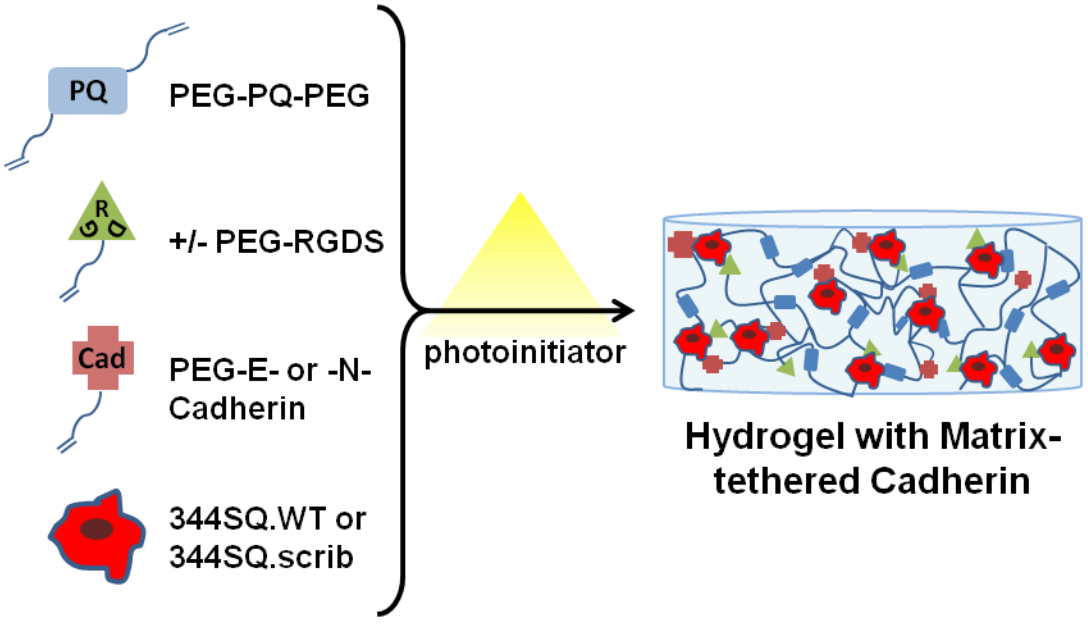


**Fig. 4-8: PEG-Cadherin Hydrogels.** Hydrogels were fabricated by mixing PEG-PQ backbone components with or without PEG-RGDS, pegylated cadherins, and 344SQ WT or scribble knockdown cells and exposing to white light in the presence of Eosin Y photoinitiator to leave cells encapsulated in hydrogels interacting with matrix-presented cadherins.

### 4.2.6 Immunohistochemistry

In the following experiments, hydrogel-encapsulated cells were evaluated with the same methods for fixation, Triton-X permeabilization, blocking, and antibody incubation as in Section 2.2.6. Primary antibodies used for polarity, apoptosis, and proliferation staining were also the same as in 2.2.6. For differences in cellular expression of E-cadherin, mouse anti-E-Cadherin (BD) targeting the intracellular domain was used. Secondary antibodies and DAPI and phalloidin counterstains were used as in Section 2.2.6. Samples were imaged using a Zeiss 5Live confocal microscope.

### 4.2.7 Probing Effects of PEG-cadherin on 344SQ.WT Morphogenesis

To observe morphologic response of 344SQ.WT to matrix-tethered cadherins in otherwise non-cell-adhesive PEG matrices, 344SQ.WT was first encapsulated in a 5% PEG-PQ hydrogels with no PEG-RGDS. PEG-E- and -N-cadherin were incorporated at 50 μg/ml in experimental groups compared to PEG-PQ only controls. Samples were imaged on a Zeiss Axio Observer A1m inverted fluorescent microscope to evaluate difference in sphere formation. The resulting brightfield images were used to measure structure size (structure diameter) using ImageJ and expressed as means per hydrogel sample.

To evaluate if differences in sphere formation were due to differences in viability, samples were stained with 2 μM calcein-AM and 10 μm ethidium homodimer at day 4 in culture (Live/Dead viability/cytotoxicity kit, Invitrogen) and imaged on a Zeiss Axio Observer A1m inverted fluorescent microscope. Because of difficulty discriminating individual cells that are closely approximated in these multicellular structures, images

were quantified as percent green fluorescent structures over total structures measured as a reflective measure of cell viability.

The influence of PEG-cadherin on improved morphogenesis of 344SQ.WT encapsulated in hydrogels with PEG-RGDS capable of supporting some degree of morphogenesis was then examined. 344SQ.WT was encapsulated in 3% PEG-PQ hydrogels with 4 mM PEG-RGDS, cultured for 14 days, and then fixed and stained for polarity markers per Section 4.2.6. Differences in morphogenesis and structure lumenization (n = 100-150 spheres per group) were evaluated using the E-score method (Section 2.2.7, Fig. 2-3).

To evaluate for potential influence of matrix-tethered cadherin on EMT response, additional samples were cultured for 12 days and exposed to TGFβ for 4 days. A lower, but more physiological concentration of TGFβ was used (0.5 ng/ml) to expose subtler matrix-derived influences. Samples were stained for polarity markers, imaged, and analyzed for lumenization by E-score method. For both TGFβ-exposed and unexposed samples Q-PCR was also run as above for differences in expression of miR-200 and EMT marker RNA.

### 4.2.8 344SQ.scrib in PEG Matrix Co-culture and in Matrices with PEG-cadherin

To compare 344SQ.scrib culture in the 3D PEG system to previous observations in the MG system, cells were first encapsulated in 10% PEG-PQ / 3.5 mM PEG-RGDS matrices, cultured for 12 days and imaged on an Axiovert 135 inverted fluorescent microscope (Zeiss). Hydrogel samples were also made to contain a co-culture of 344SQ.scrib and 344SQ.WT by centrifuging the two cell populations together and resuspending in the same polymer solution at 1.5 M cell/ml/cell type. Samples were

cultured for 12 days and imaged as above, distinguishing 344SQ.scrib by presence of the GFP signal.

To probe for pro-organizational effects of matrix-tethered cadherin on 344SQ.scrib morphology, 344SQ.scrib were encapsulated in 5% PEG-PQ / 3.5 mM PEG-RGDS matrices with PEG-E- or -N-cadherin at 50 μg/ml. Samples were cultured for 12 days, stained for expression of polarity markers, and imaged. Confocal images were evaluated using the E-score method (Section 2.2.7, Fig. 2-3) for degree of sphere epithelialization (n = 100-200 spheres per group). Sphere sizes were evaluated by measuring sphere diameters at maximum cross-section in the phalloidin channel and expressed as per hydrogel means. Q-PCR was performed as above to probe for differences in miR-200 expression and expression of EMT marker RNA. Changes in sphere development that may lead to observed differences in morphogenesis were assessed by staining for proliferation and apoptosis using antibodies against ki-67 and caspase-3 as in Section 4.2.6.

### 4.2.9 Effects of Matrix-tethered Cadherin on 344SQ.scrib Cellular Cadherin Expression

344SQ.scrib samples cultured for 12 days in 5% PEG-PQ / 3.5 mM PEG-RGDS matrices with or without PEG-E- or -N-cadherin were stained for expression and localization of E-cadherin. Samples were stained and imaged as in Section 4.2.6. Overall intensity of stain per sphere at maximum sphere cross-section was analyzed using phalloidin channel-derived sphere area ROIs in ImageJ. Radial organization was analyzed using the Radial Profile plug-in as in Section 3.2.7; the intensities of inner and

outer 10% of radial sections were compared between groups to describe spatial differences in expression.

### 4.2.10 Statistical Analysis

For size, E-score properties, staining localization, and all other comparisons between PEG-E-cadherin, PEG-N-cadherin and PEG-RGDS-only controls, statistical significance was determined using a one-way ANOVA with Tukey's HSD post-hoc.

## 4.3 Results and Discussion

### 4.3.1 Western Blot Confirms PEG-cadherin Conjugations

PEG-PQ and PEG-RGDS matrix constituents were synthesized as in Section 2.2.2, and PEG-E-cadherin and PEG-N-cadherin were synthesized via reaction with PEG-SVA as in Section 4.2.3 using a 20:1 PEG-SVA:PEG-Cadherin molar ratio. This relatively low molar ratio was used to ensure maximal bioactivity of pegylated products without PEG chains substantially interfering with binding. Western blotting was used to confirm conjugation with lanes for unpegylated cadherins and PEG-cadherin conjugates (Fig. 4-9). Both E- and N-cadherin have expected bands at ~120 kDa representing the ~88 kDa proteins linked to an IgG Fc fragment for stabilization, and double bands on the blot indicative of small post-translational cleavage and modification. The PEG-E- and -N-cadherin lanes on the blot show lack of resolution between the double bands and a higher molecular weight smear indicating the presence of one or more protein-bound PEG molecules that cause molecular size increases. Conjugation at higher PEG-SVA ratios showed a more significant molecular weight shift indicating more substantial PEG

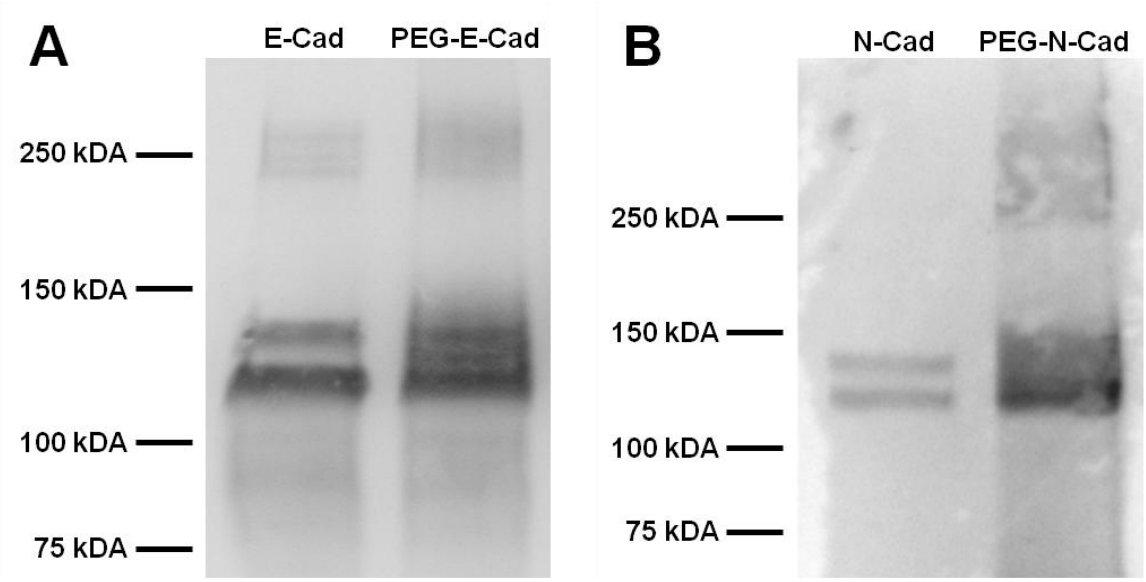


**Fig. 4-9: Western blots confirm PEG-cadherin conjugation.** Chemiluminescent image of Western blot for E-cadherin (*A*) and N-cadherin (*B*) and their associated pegylated species shows bands at ~120 kDa associated with cadherins in protein lanes with upstream smears in PEG-proteins lanes indicating attachment of PEG chains that increase species size.

conjugation (not shown), but these conjugation products were not used in experiments to facilitate maximum bioactivity.

### 4.3.2 Matrix-tethered Cadherin Influences Sphere Development in Matrices without PEG-RGDS

Some previous work using suspension culture suggests that 344SQ does not exhibit anchorage-dependent cell viability (unpublished observations). Experiments in previous chapters using specific adhesion afforded by PEG-RGDS incorporation on the non-cell adhesive PEG-PQ background has demonstrated the influence of adhesive ligand on 344SQ morphogenesis and EMT, but encapsulation in a completely non-cell-adhesive PEG system has yet to be explored. 344SQ.WT cells were encapsulated in hydrogels with backbone polymer constituents only (5% PEG-PQ, Fig. 4-10*A*). Over several days in culture cells formed a heterogeneous population, with most structures remaining rounded single cells or rounded clumps of a few cells and only a few structures

demonstrating demonstrable sphere growth. The overall population exhibited abnormal development, with no structures displaying lumenization. Polarity staining revealed many isolated cells and some small spheres composed of a few cells, but no degree of epithelial organization (Fig. 4-10*D*).

To probe for a normalization of 344SQ.WT sphere development afforded by binding of cells to matrix-tethered cadherins, both PEG-E- and -N-cadherin were added to pre-polymer mixtures with 5% PEG-PQ and no PEG-RGDS. In both PEG-E- and -N-cadherin matrices, cells proliferated to form spheres of considerable size, and while single-cell structures were still present after several days in culture, they constituted a noticeably decreased fraction in the population (Fig. 4-10*B*-*C*). While structure morphology was more typical of spheroids seen previously in cell-adhesive PEG matrices, structures did not lumenize in the absence of PEG-RGDS. There were no readily obvious differences between the two PEG-cadherin-constituent matrices. Staining for polarity markers revealed larger structures composed of more cells, with the nuclear arrangement in a few sphere suggesting organization, but limited organization and segregation of polarity markers were found in samples (Fig. 4-10*E*-*F*).

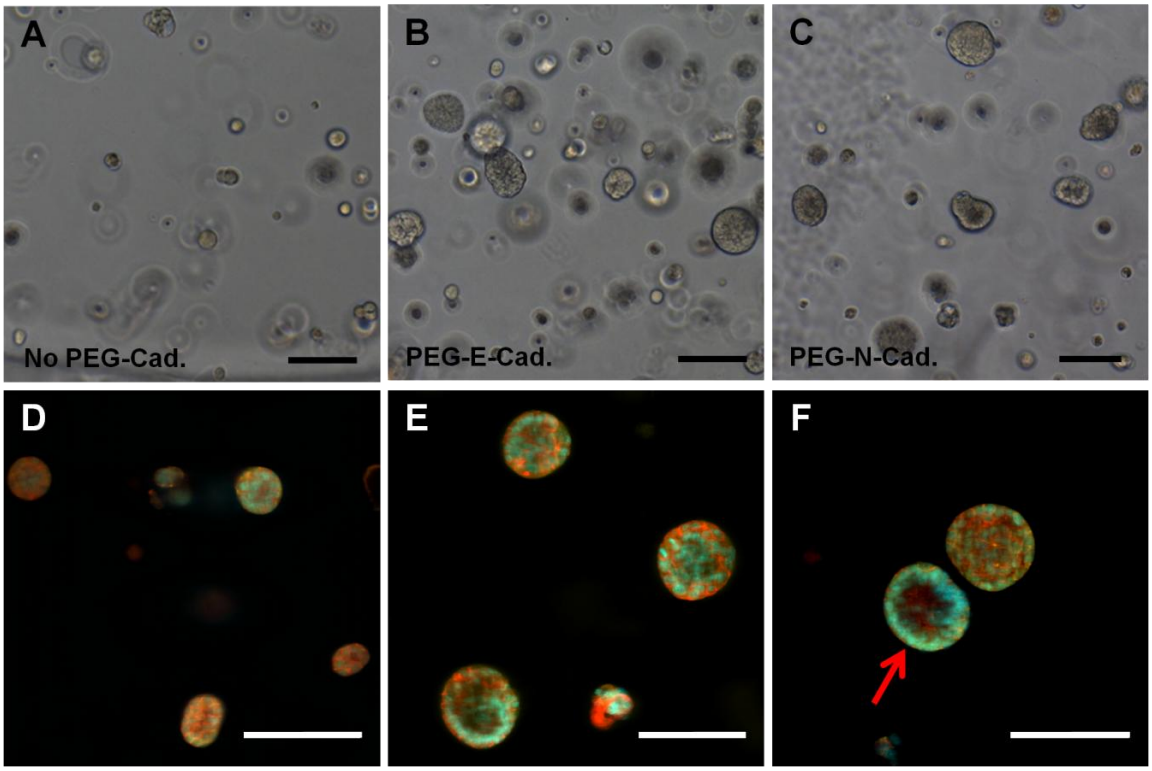


**Fig. 4-10: PEG-cadherin influences 344SQ.WT sphere morphology in PEG-RGDS-free matrices.** Brightfield images (*A*-*C*) and polarity staining (*D*-*F*) show that 344SQ.WT in matrices composed only of PEG-PQ (*A*, *D*) form small, disorganized structures, many with single or a few cells. Structures in matrices with PEG-E-cadherin (*B*, *E*) or PEG-N-cadherin (*C*, *F*) are larger with cell numbers more typical of spheres in matrices with PEG-RGDS. Though spheres do not feature normal epithelial morphogenesis or polar organization, a few show evidence of radial nuclear arrangement (example, arrow). β-catenin (red), ZO-1, (yellow), DAPI (blue). Scale bar = 100 μm.

To quantify some of these observed differences, structure sizes were measured from brightfield images. Mean per-hydrogel sphere diameters revealed significantly decreased structure sizes in PEG-cadherin-free matrices with comparable structure sizes measured in PEG-E- and -N-cadherin hydrogels (Fig. 4-11*A*). To better graphically represent differences in sphere populations, size measurements from all structures pooled across hydrogel samples were arranged in histograms (Fig. 4-11*B*-*D*). PEG-RGDS-free matrices without any PEG-cadherin showed a population skewed toward the lower end of size ranges as expected, with over 90% of structures having diameters under 40 μm and

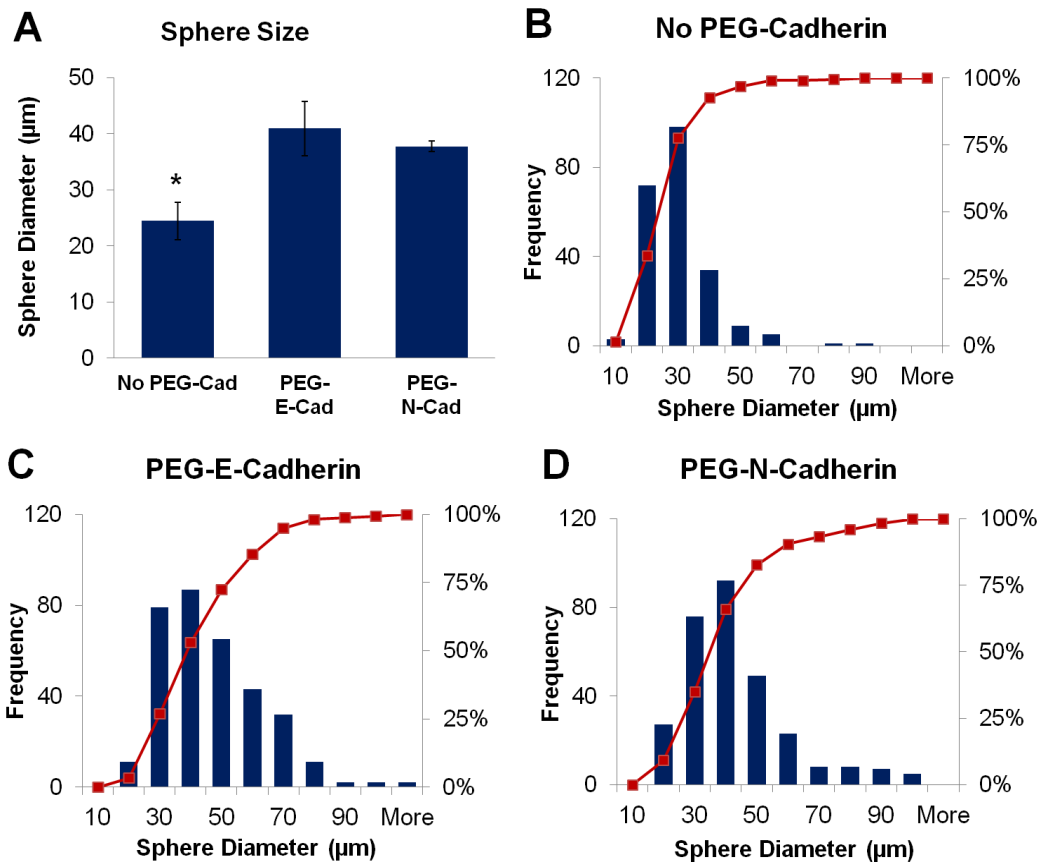


**Fig. 4-11: Sphere size differences are induced by PEG-cadherin incorporation in matrices without PEG-RGDS**. *A*, mean sphere diameter per hydrogel shows significantly decreased structure sizes in matrices without PEG-cadherin compared to PEG-E- and PEG-N-cadherin matrices (*$p < 0.05$). *B-D*, histograms of pooled size data show that in PEG-cadherin-free matrices (*B*) many structures approximate the size of single-cells with nearly no spheres forming above 70 µm. While small spheres were still widespread in PEG-cadherin matrices (*C-D*), many spheres were larger, with a sizable minority growing to 80-100 µm, a size more typical of matrices with PEG-RGDS.

nearly no structures over 70 µm. Meanwhile, matrices with PEG-cadherin showed a less skewed population with some spheres reaching sizes upwards of 80 - 100 µm in diameter.

Finally, to examine if these differences were due to differences in cell viability, spheres in these matrices were stained for calcein AM and ethidium homodimer. Viability staining showed few scattered dead cells present in all matrices and expected high viability in multicellular spheres in PEG-cadherin matrices (Fig. 4-12*A-B*). In PEG-PQ only matrices, the small, rounded single-cell structures generally stained brightly for calcein AM, suggesting that cells of this observed morphology were viable, but just did

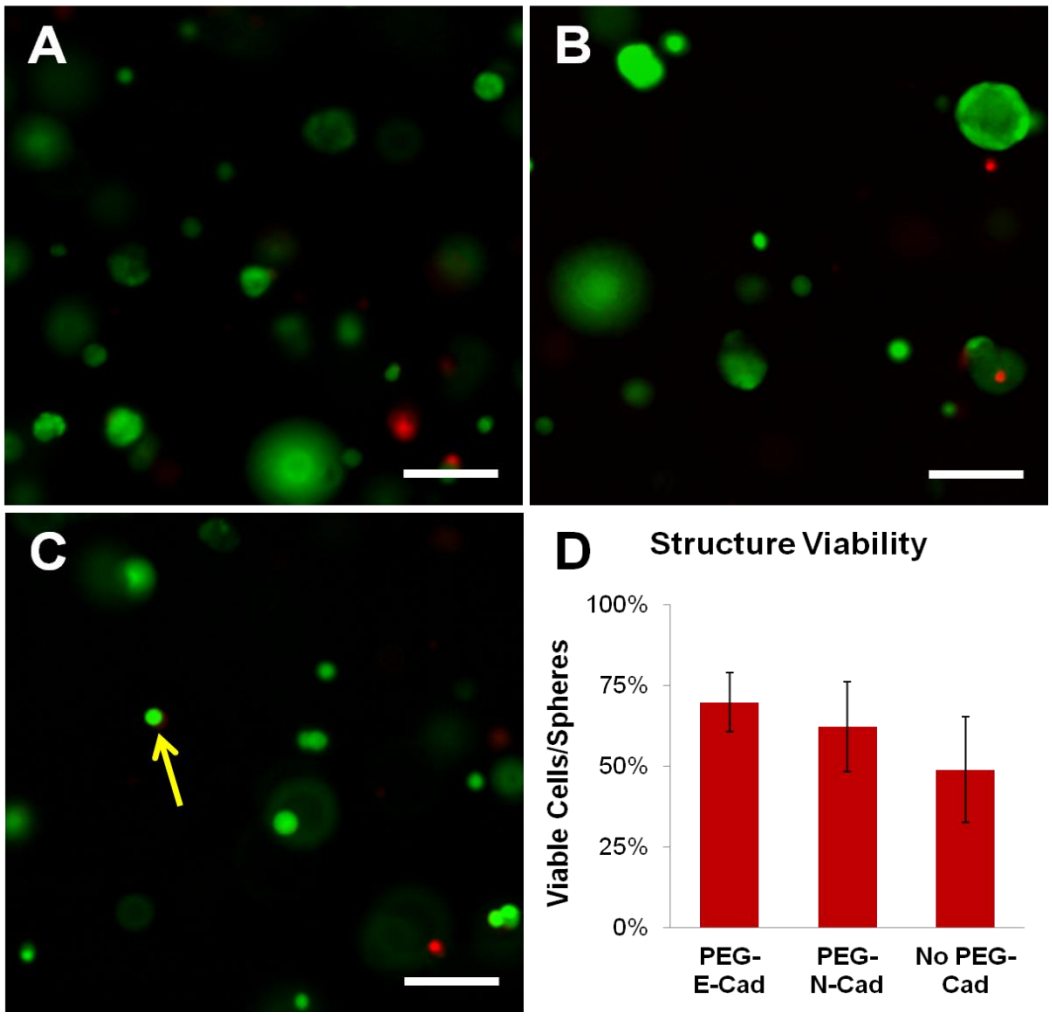


**Fig. 4-12: Live/dead staining shows morphology differences are not viability related.** *A-C*, calcein AM (green) / ethidium homodimer (red) staining of PEG-RGDS-free matrices with PEG-E-cadherin (*A*), PEG-N-cadherin (*B*) or no PEG-cadherin (*C*) reveals high viability in all matrices. The small, single-cell structures predominantly found in PEG-PQ-only controls were generally viable (*C*, example arrow). *D*, quantification of percent viable structures per hydrogel sample shows no significant difference in structure viability. Scale bar = 100 μm.

not proliferate normally to form larger spheres (Fig. 4-12*C*). While a quantification of true cell viability is complicated by difficulty distinguishing closely approximated cells in multicellular spheroids, the fraction of viable structures over the total measured was evaluated between gels. While there was some variation between samples using this metric, there was no statistically significant difference in viability among gels with and without PEG-cadherin (to significance level of $\alpha = 0.05$, Fig. 4-12*D*).

In this experiment, the 344SQ cell line was studied for the first time in PEG-based matrices that lack integrin-engaging adhesive ligands to probe for an initial biologic effect of matrix-tethered cadherins. In all matrices, including PEG-PQ-only controls, cell viability was maintained, but interesting differences in sphere development were found. 344SQ's apparent degree of substrate anchorage-independence upon loss of ECM binding is similarly shared with other cancer models, particularly those that are more malignant[323,324]. While loss of cell-adhesive surroundings typically induces cell death in non-transformed cells, these malignant lines resist this apoptotic signaling, a resistance that is likely important for the survival of metastasizing cells that must disengage from the matrix to disseminate.

The data does indicate, however, that normal 344SQ spheroid growth and epithelial morphogenesis in 3D culture requires at least some degree of adhesion to the matrix. Abnormal 344SQ sphere morphogenesis in matrices without adhesive ligand also makes sense in the context of other work in the field that has demonstrated the critical role of ligation of different key integrins in epithelial morphogenesis[174–176,179], and in the context of previous work in our lung adenocarcinoma model demonstrating significant differences in integrin expression between different phenotypic states[238]. This result further underscores previous data in the PEG system showing the influence of adhesive ligand concentration on morphogenesis (Section 2.3.5) and suggests that proper initiation of the 344SQ MET program in 3D culture likely depends on ligation of sphere-peripheral cells to properly orient 3D polarity.

The incorporation of PEG-cadherin had some effect normalizing sphere growth in PEG-RGDS matrices. Initially, this demonstrates a biologic effect of the pegylated

cadherins, with incorporation appearing to afford some degree of binding to cells to exert noticeable morphogenesis effects. There were, however, no readily observable differences between E- or N-cadherin groups in this experiment. This is a somewhat surprising result given the expectation of a high degree of E-cadherin expression and membrane localization in the epithelial state of 344SQ in 3D culture in the absence of TGFβ. It is likely that while 344SQ indeed preferentially expresses either cadherin depending on its EMT state[232,238], there can be some degree of expression of multiple cadherin types regardless of EMT state, a typical finding in many cell types, usually observed as a different cadherin co-expressed with E-cadherin[293]. The small degree of N-cadherin expression in the epithelial state appears may have been sufficient for the degree of normalization of sphere growth in hydrogels with PEG-N-cadherin. Alternatively, while homophilic binding between like cadherin types is stronger, cadherins are capable of some degree of weak heterophilic binding[325,326], a degree that may have been sufficient to facilitate some normalizing interaction despite matrix presentation of an unmatched cadherin type.

Finally, while there were significant differences between PEG-RGDS-free hydrogels with and without PEG-cadherins incorporated, epithelial morphogenesis in PEG-cadherin matrices was still abnormal, with many structures remaining small or comprised of single-cells, no structures showing complete lumenization, and spheres showing very little polar organization at all. This result suggests that while binding of encapsulated cells to matrix cadherins was able to at least partially restore normal growth patterns, proper morphogenesis may require stronger matrix adhesion or ligation of particular RGD-binding integrins. This observation again highlights the importance of

matrix adhesive properties to 344SQ morphogenesis suggested by previous data, and the importance of integrin ligation seen in other cancer models.

### 4.3.3 Matrix-tethered Cadherin Influences 344SQ.WT Epithelial Morphogenesis in Soft Matrices

We next sought to determine if the presence of PEG-cadherin in matrices that facilitate some degree of epithelial morphogenesis (with PEG-RGDS) in any way influences 344SQ.WT sphere development or EMT. Pilot studies using stiffer 5% and 10% PEG-PQ matrices with PEG-RGDS revealed little difference between matrices with and without PEG-cadherin and little difference between PEG-cadherin types. However, we also sought to test if matrix-tethered cadherins exerted a subtler influence that would be revealed in low-stiffness matrices that do not otherwise favor widespread epithelial morphogenesis. 344SQ.WT cells were encapsulated in 3% PEG-PQ matrices with 4 mM PEG-RGDS with or without PEG-N- or -E-cadherin, cultured for 14 days, stained for polarity markers, and analyzed for differences in degree of epithelial morphogenesis (Fig. 4-13*A*-*C*). As expected based on previous data, given the low matrix stiffness and moderate PEG-RGDS concentrations, sphere populations as a whole were not well organized regardless of group. Spheres were large, many did not lumenize, and of those that did show central clearing and lumenization, organization was relatively poor with few structures showing nuclei arranged in a single peripheral ring. In subjective observations, however, spheres in the PEG-N-cadherin matrices were generally larger with noticeably fewer structures showing intrasphere nuclear clearing.

Upon quantification of sphere organization using the E-score method, most structures did not show a well-organized lumenized phenotype (Only ~20% with E-score

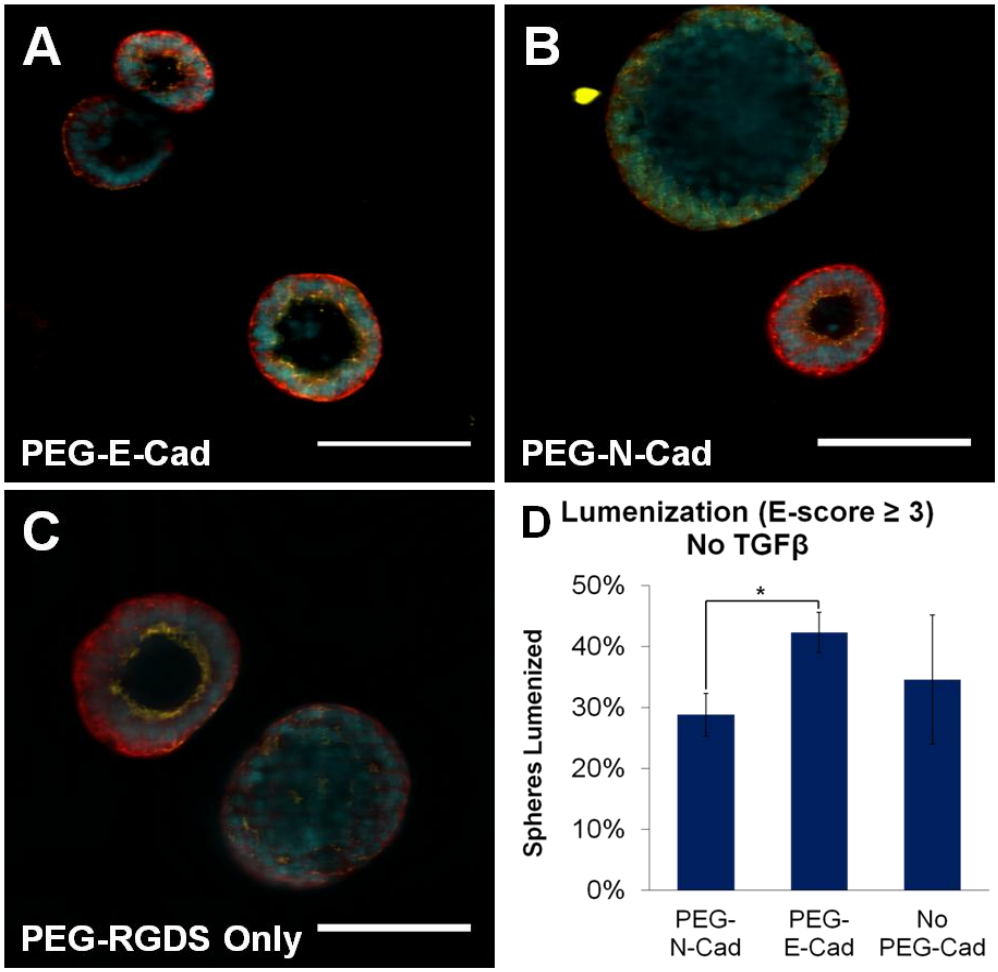


**Fig. 4-13: PEG-cadherin influences epithelial morphogenesis of 344SQ.WT in soft PEG-PQ matrices.** *A-C*, images of 344SQ.WT in 3% PEG-PQ / 4 mM PEG-RGDS matrices with PEG-E-cadherin (*A*), PEG-N-cadherin (*B*) or no PEG-cadherin (*C*) show structures forming with some degree of epithelial polarity and lumenization in all matrices, though less organized and larger structures in PEG-N-cadherin matrices. β-catenin (red), ZO-1, (yellow), DAPI (blue). Scale bar = 100 μm. *D*, comparison of the percentage of spheres per hydrogel showing some degree of lumen formation (E-score ≥ 3) revealed significantly greater lumenization in PEG-E-cadherin matrices compared to PEG-N-cadherin matrices (*$p<0.05$).

= 4 or 5). However, of structures with some degree of lumen (E-score ≥ 3), PEG-E-cadherin matrices showed a significantly higher degree of lumenization compared to PEG-N-cadherin matrices, suggesting a cadherin-specific effect on epithelial organization (Fig. 4-13*D*). Matrices without any PEG-cadherin showed more inter-sample variability, but mean lumenization percentage was closer to that of PEG-E-cadherin matrices and higher than that observed in PEG-N-cadherin matrices.

Given the relationship between cadherins and cancer EMT and invasion, we next asked if matrix-tethered cadherin modulated the EMT effect seen in 344SQ with exposure to TGFβ. Initial studies in these soft matrices with the concentration of TGFβ previously used showed a potent EMT response with rapid and complete loss of lumen and polar organization regardless of group. Because this concentration is super-physiologic, and in the event that subtler cadherin-related effects are revealed at less potent concentrations, a lower concentration of TGFβ (0.5 ng/ml) was administered to 344SQ.WT encapsulated in 3% PEG-PQ hydrogels with PEG-cadherin. Treatment with this lower concentration initiated EMT in encapsulated cells, with spheres in all groups showing intrasphere nuclear proliferation and a loss of at least some degree of polar organization (Fig. 4-14*A*-*C*). After exposure, no structures showed remnant lumens featuring substantial cell clearing (no spheres with E-score = 4 or 5). However, the EMT response was less complete than previously observed after 4 days of exposure as some structures remained at least partially lumenized (example in PEG-E-cadherin image, Fig. 4-14*A*) and other structures showed some degree of persistent polar localization despite lumen filling (Fig 4-14*B*-*C*).

Quantifying these changes, lumenization decreased in all groups, but was substantially more persistent in PEG-E-cadherin and PEG-RGDS-only hydrogels (Fig. 4-14*D*). In PEG-N-cadherin hydrogels, the percentage of lumenized structures dropped dramatically with fewer than 10% of structures remaining lumenized. In comparing structures that show at least some degree of polar organization with or without a lumen present (E-score $\geq 2$), there was a dramatic decrease in the percentage of these organized structures in the PEG-N-cadherin group as spheres more readily lost polar organization

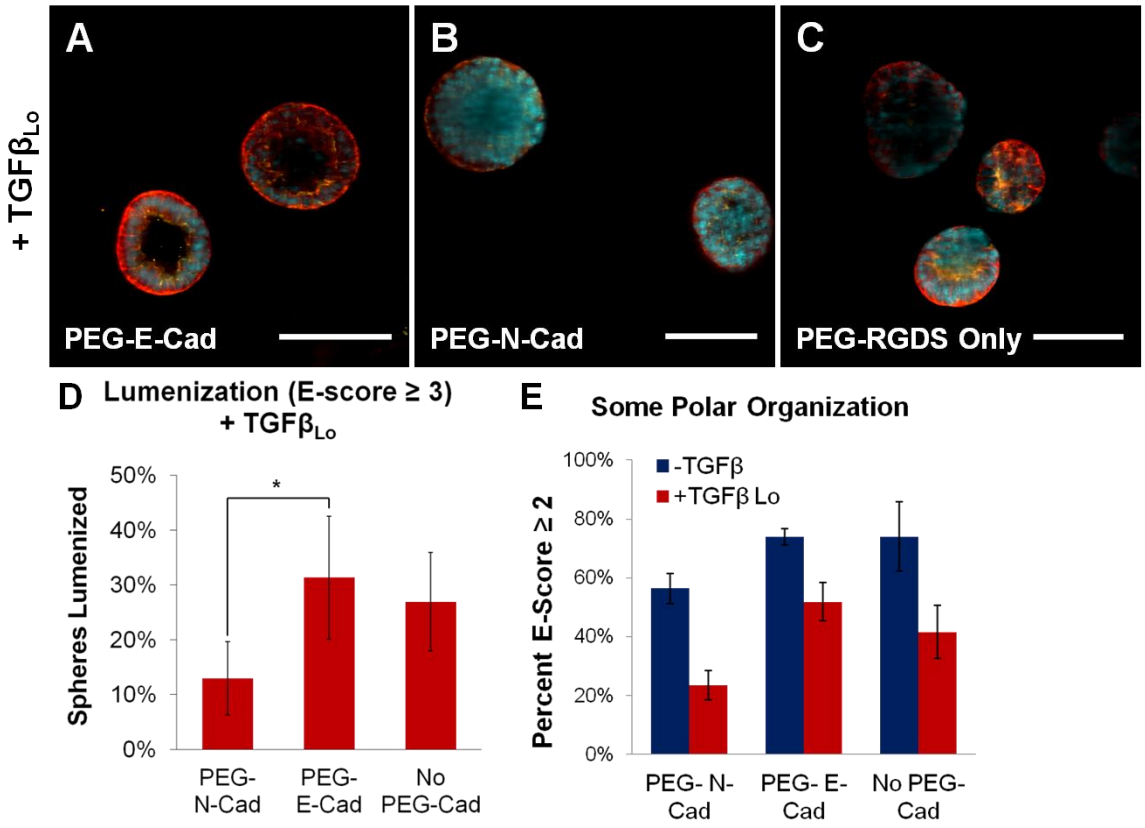


**Fig. 4-14: PEG-cadherin influences degree of loss of epithelial phenotype induced by TGFβ$_{Lo}$.** *A-C*, images of 344SQ.WT in 3% PEG-PQ / 4 mM PEG-RGDS matrices with PEG-E-cadherin (*A*), PEG-N-cadherin (*B*) or no PEG-cadherin (*C*) after 4 days of 0.5 ng/ml TGFβ exposure show a partial EMT response in all groups, but more persistent lumenization and epithelial organization in spheres in PEG-E-cadherin gels compared to spheres in PEG-N-cadherin gels. *D*, quantifying the percentage of structures with some degree of remnant lumen (E-score = 3) reveals a more dramatic decrease in the lumenized population in PEG-N-cadherin gels (*$p < 0.05$). *E*, comparing spheres with at least some degree of polar organization (E-score ≥ 2) reveals a more dramatic decrease in this sub-population upon TGFβ$_{Lo}$ treatment in PEG-N-cadherin gels compared to PEG-E-cadherin gels and PEG-RGDS-only controls. β-catenin (red), ZO-1, (yellow), DAPI (blue). Scale bar = 100 μm.

with exposure to TGFβ$_{Lo}$ (Fig. 4-14*E*). Spheres also lost some polar organization in PEG-E-cadherin and PEG-RGDS-only groups as well, but to a lesser degree, with upwards of 50% of spheres in PEG-E-cadherin gels still showing some organization of polarity markers after TGFβ exposure.

This experiment demonstrated a small effect of matrix-tethered cadherins on 344SQ.WT epithelial morphogenesis. Matrices with PEG-E-cadherin induced significantly greater lumenization in encapsulated spheres than in structures with PEG-N-

cadherin, and greater resistance to loss of lumenization and polar organization with EMT. This is consistent with literature reports demonstrating the link between E-cadherin and epithelial polarity and the role of N-cadherin in EMT-related phenotypic behaviors. However, as the PEG-RGDS-only control gels induced a similar degree of lumenization as the PEG-E-cadherin gels both before and after $TGF\beta_{Lo}$ exposure, this pro-epithelialization effect may be limited.

Alternatively, the external presentation of N-cadherin may have a more important role in limiting 344SQ epithelial morphogenesis and promoting polar disorganization than E-cadherin has in inducing the inverse. Not only did spheres in PEG-N-cadherin matrices less readily form lumenized spheres, but they were also more responsive in loss of lumenization and polarity with a milder TGFβ-initiated EMT. This observation suggests that engagement of N-cadherin induced cells to be less responsive to 3D matrix cues promoting epithelialization and more responsive to TGFβ-related cues promoting EMT.

It is worth noting that matrix-tethered cadherins had little effect on 344SQ.WT in more structurally stable matrices with higher PEG-PQ concentrations or in the face of more a potent EMT trigger at a higher TGFβ concentration. Cadherin-related influences were revealed only in a matrix with a low concentration of PEG-PQ that otherwise does not favor substantial epithelial organization and at a lower TGFβ concentration that initiates a slower or less complete EMT. These observations suggest that matrix cues related to 3D culture or stiffness and adhesive ligand concentration may be far more important to 344SQ MET and EMT than the engagement of cadherins, a result not

completely unsurprising given the potent effects previously observed in our cancer model and others when these factors are specifically altered.

The data showing that PEG-E-cadherin exerted limited if any pro-epithelialization effects over PEG-RGDS-only matrices is interesting given the previous data demonstrating a substantial effect on cultured cells in matrices without PEG-RGDS (Section 4.3.2). **This disparity suggests that once 344SQ cells are embedded in a 3D, cell-adhesive environment, a pro-epithelial program is potently initiated with any enhancement of this potent morphologic switch difficult to promote in any observable way.** It is possible that any further enhancement via matrix E-cadherin presentation of the MET effects already afforded by 3D culture are unseen as they are redundant in the face of changes already occurring (*i.e.* cells already presenting sufficient E-cadherin-related signaling to one another). Alternatively, any additional degree of epithelialization beyond that afforded by structural matrix cues may be limited by the genetic or epigenetic programming of the cells; the 344SQ line is significantly transformed, highly plastic, and EMT-prone, and these intrinsic influences may impose a maximal epithelial phenotypic limit irrespective additional matrix cues.

### 4.3.4 Matrix-tethered Cadherin Influences 344SQ.scrib Epithelial Organization

Loss of the scribble polarity complex protein induces a loss of polarity and pro-tumorigenic changes in multiple cell types and cancer models[305,308]. In the $KRas^{G12D}/p53^{R172H\Delta G}$ model, scribble knockdown induced metastatic changes in the otherwise non-metastatic 393P line[311]. Knockdown in 344SQ leads to structures without polarity that do not lumenize despite 3D MG culture, and are more invasive with enhanced metastatic phenotypes in the face of certain matrix cues. Because of the

emerging relationship between scribble and cadherin proteins and given observations of lumenized hybrid structures when 344SQ.scrib is cultured in contact with 344SQ.WT, we sought to test the influence of cadherins on 344SQ.scrib with incorporation of PEG-cadherin into matrices.

Initial experiments on 344SQ.scrib cells encapsulated in PEG-based hydrogels without PEG-cadherin showed general agreement to observations noted in MG experiments. In PEG-PQ hydrogels with PEG-RGDS alone (10% PEG-PQ / 3.5 mM PEG-RGDS), 344SQ.scrib formed large spheres with no lumenization evident by brightfield microscopy and no overt indication of polar organization (Fig. 4-15*A*). Co-culture of 344SQ.scrib with 344SQ.WT was then attempted in the PEG system to mimic results showing lumenization when cells are in contact. Predictably, however, the vast

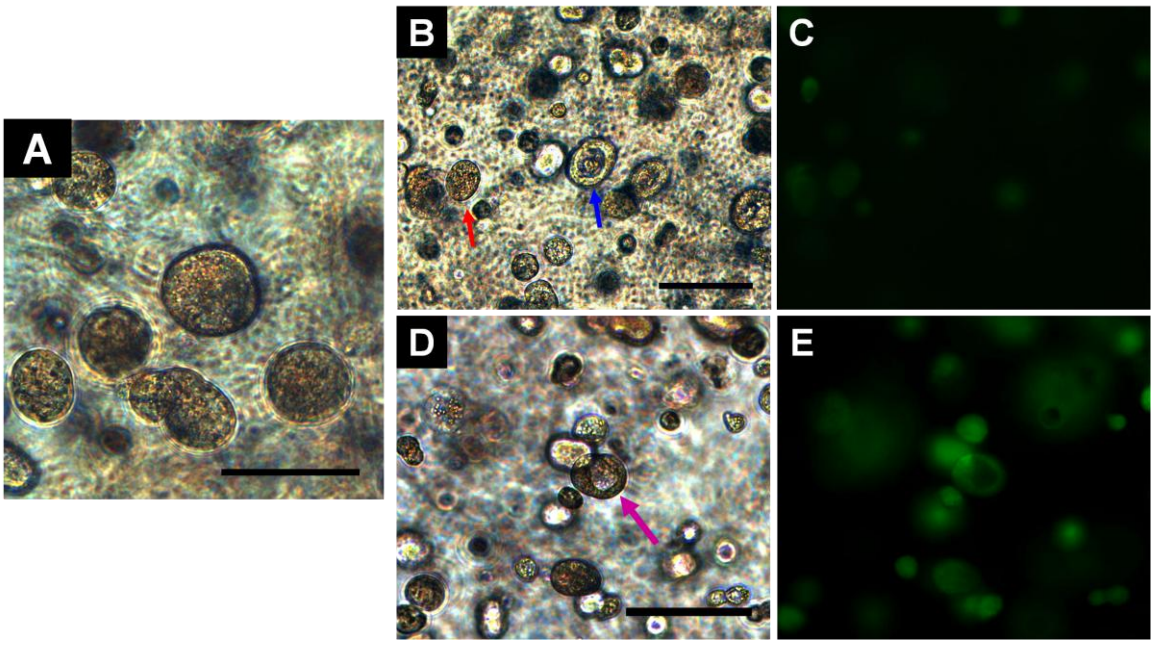


**Fig. 4-15: 344SQ.scrib in PEG-based hydrogels.** *A*, 344SQ.scrib in culture alone in a 10% PEG-PQ / 3.5 mM PEG-RGDS matrix forms large, multicellular spheres with no lumenization consistent with the polarity-inhibiting effects of scribble loss. *B-C*, co-culture of 344SQ.scrib and 344SQ.WT shows structures composed of 344SQ.WT forming lumens (*B*, blue arrow) that are distinguished from 344SQ.scrib structures (red arrow) by GFP expression in scribble knockdowns (*C*). *D-E*, a rare structure (*D*, purple arrow) in the co-culture shows both clear lumen formation as well as GFP expression (*E*), suggesting possible normalization of epithelialization despite scribble knockdown due to WT cell-cell contact. Scale bar = 100 μm.

majority of spheres were composed of either cell type alone, and 344SQ.scrib - 344SQ.WT contact events were rare (Fig. 4-15*B*-*C*). Spheres with scribble knockdowns as evident by GFP co-expression revealed no lumenization, and the only readily evident lumenized structures were composed of 344SQ.WT (indicated by lack of GFP). A very rare sub-population of spheres (~2 structures per hydrogel sample) featured both unambiguous luminal clearing and GFP expression by at least some sphere-constituent cells, suggesting the formation of polar, lumenized structures despite scribble knockdown of constituent cells (Fig. 4-15*D*-*E*). A possible explanation for this rare phenotype is a normalization of 344SQ.scrib epithelialization upon 344SQ.WT contact, as previously observed in the MG system.

344SQ.scrib cells were then encapsulated in matrices with PEG-cadherin to examine if these cell-cell contact-related findings are cadherin-mediated and if they can be more readily induced in a larger sub-population of structures than in rare co-culture events to enable more complete study. After 14 days in culture in 5% PEG-PQ matrices with or without PEG-cadherin, 344SQ.scrib in all matrices formed multicellular spheres with sphere populations showing a mixed epithelial phenotypic picture influenced by matrix-tethered cadherins. Primarily observed in matrices with PEG-E-cadherin, a small subpopulation of 344SQ.scrib formed spheres with a nuclei-cleared intrasphere lumen, clearly defined by the segregation of polarity markers (Fig. 4-16*A*). A minor, but substantial, sub-population of spheres formed structures with a unique pseudo-epithelial morphology featuring nuclei on sphere peripheries arranged with organized radial directionality (Fig. 4-16*B*). An area just interior to this peripheral layer was free of nuclei and showed expression of apical polarity markers typically indicative of a luminal edge.

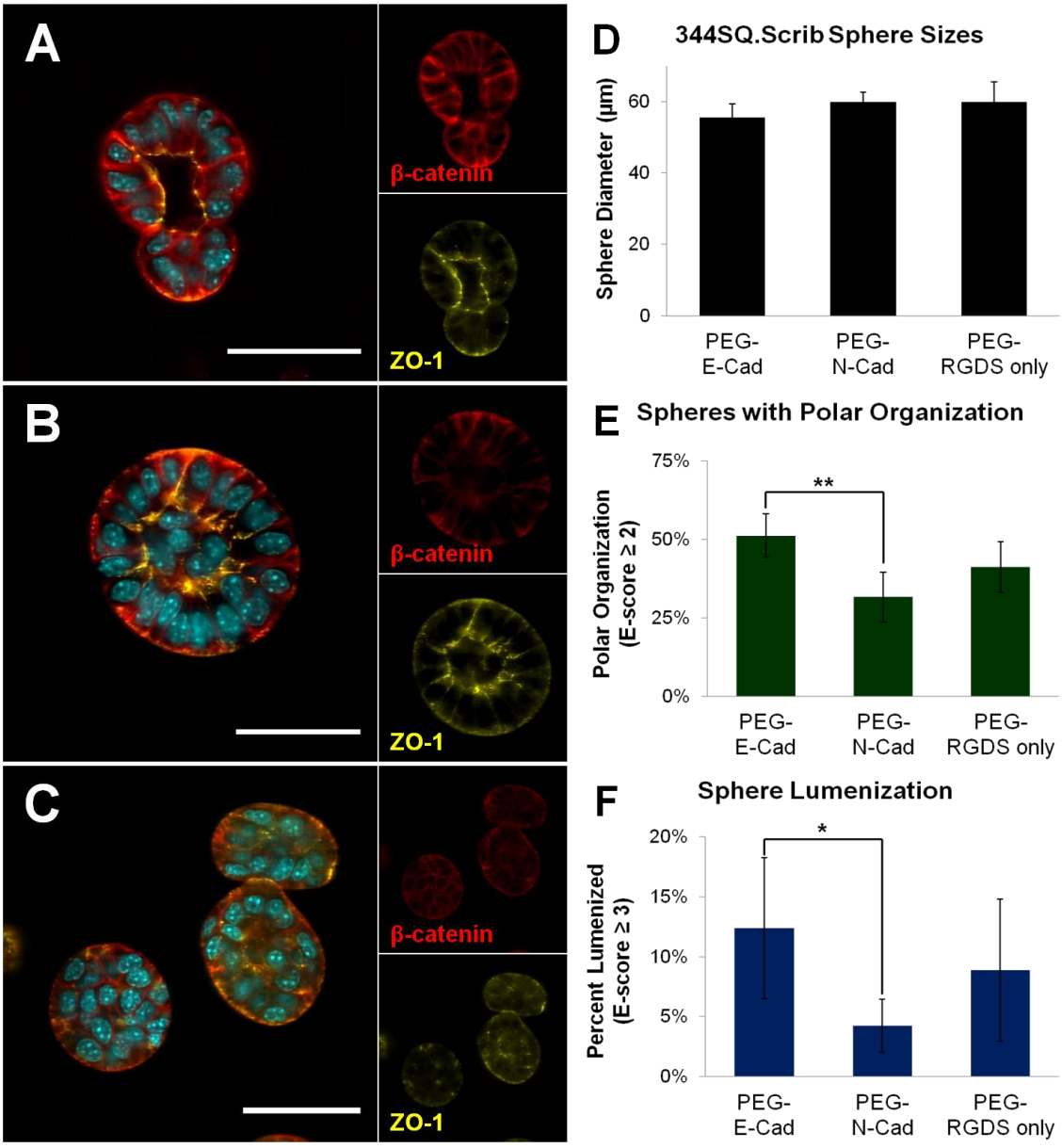


**Fig. 4-16: 344SQ.scrib shows a minor degree of epithelial morphogenesis with phenotypic sub-populations influenced by matrix-tethered cadherin**. *A-C*, representative images of phenotypic sub-populations of 344SQ.scrib revealed in PEG matrices include (*A*) a relatively rare lumenized phenotype, (*B*) a pseudo-epithelial phenotype featuring strong radial organization of peripheral nuclei and high polar organization but no actual lumen, and (*C*) a substantial proportion of spheres with no polar organization. Representative images taken from matrices with PEG-E-cadherin (*A*), no PEG-cadherin (*B*) and PEG-N-cadherin (*C*). *D-F*, in quantification of sub-population proportions, while sphere sizes showed no difference between groups (*D*), the PEG-E-cadherin group showed a significantly greater proportion of spheres with some degree of polar organization typical of the psuedo-epithelial phenotype (*E*) and a significantly greater proportion of spheres featuring a cleared lumen (*F*) than the PEG-N-cadherin group. *p<0.05, **p<0.01. β-catenin (red), ZO-1, (yellow), DAPI (blue). Scale bar = 50 μm.

But these structures lacked formation of an actual lumen as cells were present all throughout sphere volumes with nuclei generally clustered together at central sphere cores. This interesting phenotype was prominent in PEG-E-cadherin matrices, but also evident in PEG-RGDS-only controls. Finally, many structures in all matrix formulations exhibited no organized phenotype as would be expected with knockdown of such an important polarity complex protein as scribble (Fig. 4-16*C*).

To quantify the subjective differences observed in these mixed populations, polarity marker-stained spheres were imaged on a confocal microscope and analyzed using the E-score method. Sphere sizes showed a trending, but non-significant difference between groups with smaller spheres forming in the PEG-E-cadherin matrices relative to PEG-N-cadherin matrices and PEG-RGDS-only controls (Fig. 4-16*D*). The radially organized, pseudo-epithelial morphology (Fig. 4-16*B*) was scored as a phenotype showing epithelial organization but no lumenization (E-score = 2). Upwards of half of the spheres in PEG-E-cadherin groups exhibited this phenotype or greater epithelial lumenization, a significantly greater proportion than in spheres in the PEG-N-cadherin group (~25%, Fig. 4-16*E*). PEG-RGDS-only matrices showed a lower proportion of spheres with some degree of polar organization than in matrices with PEG-E-cadherin, but this difference was not significantly different from either PEG-cadherin group.

Specifically evaluating sphere lumenization (E-score $\geq$ 3) revealed no spheres in any matrix formed lumenized spheres with high organization and completely cleared lumen (E-score = 5) with most exhibiting an abnormal lumenized morphology with limited central clearing and nuclei poorly organized around small cleared lumenized spaces. A minor population of spheres in PEG-E-cadherin matrices exhibited this

lumenized phenotype, significantly greater than the proportion of spheres in PEG-N-cadherin matrices (12.4 ± 5.9% vs. 4.2 ± 2.2%, Fig. 4-16*F*). However, lumenization in PEG-cadherin matrices was not significantly different than that in PEG-RGDS-only controls. Control matrices showed more variability in 344SQ.scrib lumenized populations, but overall also featured a minor population of poorly lumenized spheres revealed by examination of stained confocal images that were otherwise not readily apparent in brightfield images of these matrices.

Pro-organizational changes observed in 344SQ.scrib in PEG-cadherin matrices were further explored by staining for markers of proliferation/apoptosis and for cellular expression of E-cadherin. Staining at day 7 in culture demonstrated many spheres across all groups with little or no proliferative or apoptotic activity as revealed by ki-67 and caspase-3 staining, respectively. This staining pattern was observed in some spheres despite formation of a radially organized, pseudo-epithelial phenotype (Fig. 4-17*A*). Overall, about 74% of spheres adopted this staining pattern. This observation suggests that the significant polar organization in these structures was potentially due to shifting orientation and rearrangement of cells at the sphere periphery and sphere core without major apoptotic events. Some spheres, however, did show spotty caspase activity in the nuclei-free areas just interior to the organized peripheral cell layers, suggesting a more mixed picture (Fig. 4-17*B*). Those showing apoptotic activity represented about 26% of the total sphere population across groups. The process of partial normalization of 344SQ.scrib sphere polarity may therefore encompass substantial cellular rearrangement with some degree of cell clearing by apoptosis, but far short of the mass central apoptosis that leads to complete lumenization in 344SQ.WT (Sect. 2.3.4-5).

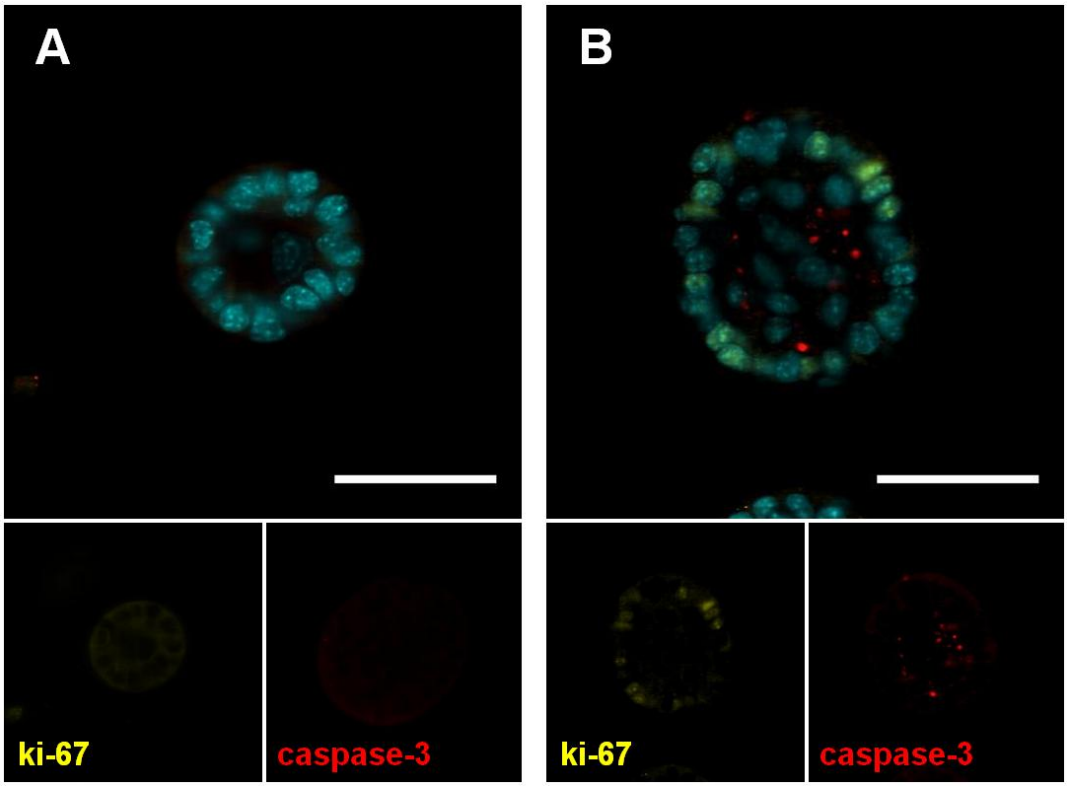


**Fig. 4-17: PEG-encapsulated 344SQ.scrib shows mixed patterns of apoptosis / proliferation.** Many 344SQ.scrib spheres in PEG-E-cadherin, PEG-N-cadherin and PEG-RGDS-only matrices demonstrated random or little proliferation with no apoptotic activity (*A*), but a minor population of spheres showed some caspase activity in the anuclear space interior to radially organized peripheral nuclei (*B*) suggesting that mixed organizational and apoptotic changes may form this unique phenotype. Both example images taken from PEG-E-cadherin gel, but staining phenotypes present to some degree in all groups. Ki-67 (proliferation, yellow), caspase-3 (apoptosis, red), DAPI (blue). Scale bar = 50 μm.

Some literature evidence suggests a link between E-cadherin and polarity proteins such as scribble with proper scribble function mediated by homophilic E-cadherin binding[312,313]. Probing for E-cadherin expression and cellular localization revealed that 344SQ.scrib cells encapsulated in matrices with PEG-E-cadherin, PEG-N-cadherin or PEG-RGDS-only controls were positive for an E-cadherin antibody recognizing an intracellular portion of the molecule. E-cadherin expression by cells generally also showed a mixed phenotypic staining pattern. Many structures in PEG-E-cadherin matrices showed strong staining of E-cadherin localized to basal and lateral surfaces of peripheral cells, typical of staining for E-cadherin as a lateral polarity marker observed in

other reports[303,313] (Fig. 4-18*A*). Spheres in matrices with PEG-N-cadherin exhibited strong overall E-cadherin staining, but it was more diffusively localized with positive staining throughout spheres and in between membranes (Fig. 4-18*B*). In matrices without PEG-E- or -N-cadherin, spheres displayed a more mixed staining pattern with some spheres showing sphere-exterior membrane-localized staining like in PEG-E-cadherin matrices, particularly if sphere nuclear arrangement suggested that the given sphere had adopted the pseudo-epithelial morphology (Fig. 4-18*C*).

To quantify differences between matrices, images were analyzed for overall E-cadherin expression in ImageJ and, using the Radial Profile plugin, degree of spatial organization, with stronger signal intensity in peripheral sphere sections suggesting the basolateral, membrane-localized phenotype. Overall E-cadherin staining intensity as measured by phalloidin-defined sphere-area ROIs was significantly higher in spheres in PEG-N-cadherin matrices than in spheres in PEG-E-cadherin matrices or PEG-RGDS-only controls (Fig. 4-18*D*). However, E-cadherin expression is most biologically relevant if localized to the membrane and available for binding. Therefore localized expression was analyzed by comparing staining intensity in outer radial sphere sections to inner radial sphere sections (Fig. 4-18*E*). Spheres in PEG-N-cadherin matrices showed a non-significant spatial expression imbalance showing stronger inner-sphere expression. Meanwhile, while both PEG-E-cadherin matrices and PEG-RGDS-only controls showed preferential outer sphere staining, the only significant difference between radial sections was found in PEG-E-cadherin matrices. Normalizing outer radial intensity to inner-sphere intensity to facilitate comparisons between groups, a significantly decreased

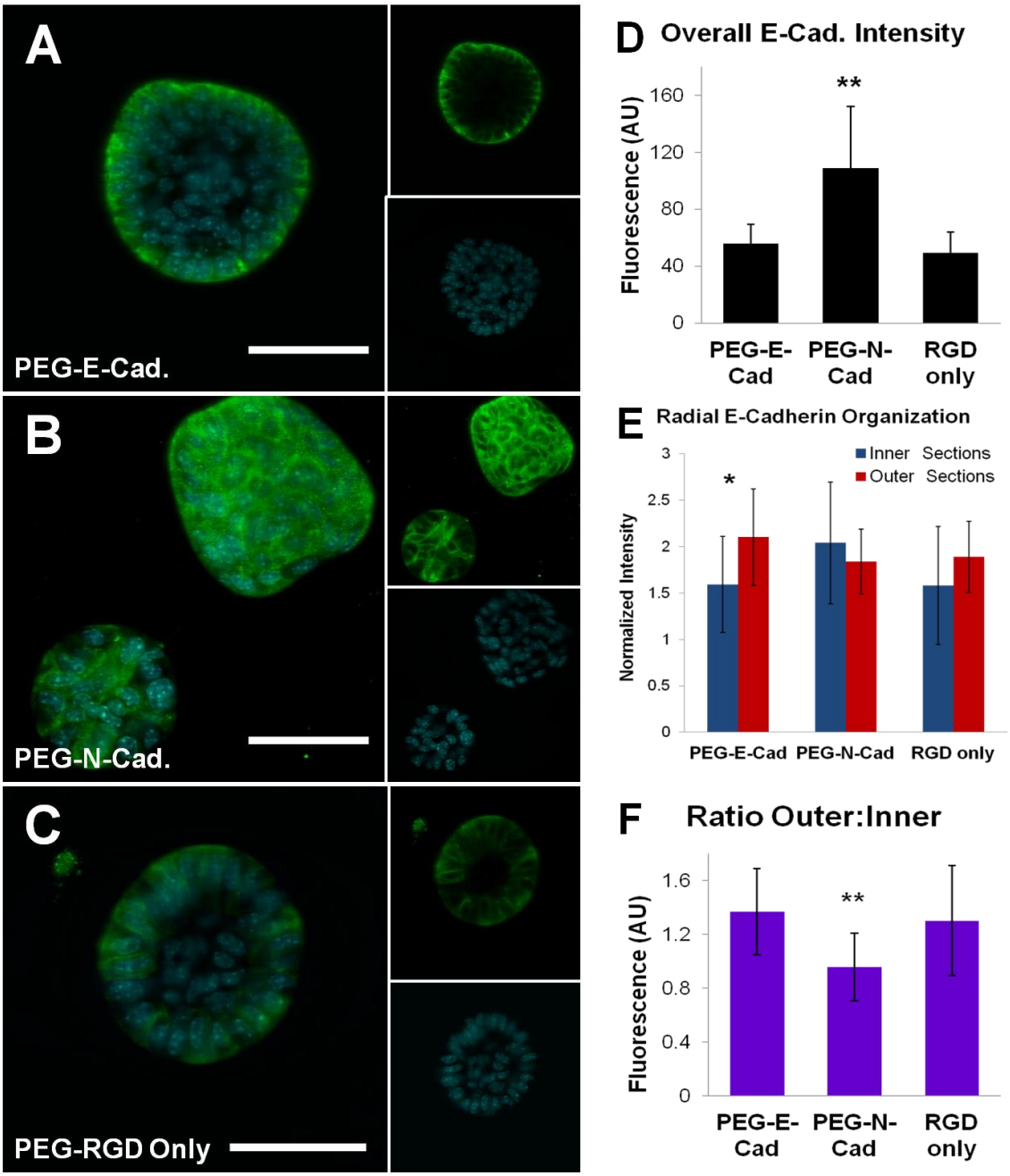


**Fig. 4-18: PEG-cadherin influences 344SQ.scrib cellular cadherin expression and localization.** *A-C*, representative images of staining for an intracellular portion of E-cadherin (green) in 344SQ.scrib show a (*A*) basolateral staining pattern in PEG-E-cadherin matrices with suggestion of membrane localization, (*B*) less organized expression in PEG-N-cadherin matrices despite ample expression, and (*C*) a mixed phenotype in PEG-RGDS-only controls with some spheres showing membrane localization. DAPI (blue), scale bar = 50 μm. *D-E*, quantifying differences, measurements of overall sphere intensity shows a high degree of E-cadherin expression by cells in PEG-N-cadherin matrices (*D*), but per radial profile analysis demonstrated statistically significant spatial preference for expression in outer, basolateral radial sphere sections vs. inner only in spheres in PEG-E-cadherin matrices (*E*). *F*, normalizing outer to inner radial section intensity, a statistically significant spatial pattern preference was found in both PEG-E-cadherin and PEG-RGDS-only matrices compared to PEG-N-cadherin matrices. *$p < 0.05$, **$p < 0.01$.

preference for basal membrane E-cadherin localization was found in spheres in PEG-N-cadherin matrices compared to the other groups (Fig. 4-18*F*).

Taken together, results from these studies indicate that matrix-tethered cadherin can influence the loss of epithelial polarity observed in 344SQ with knockdown of scribble polarity proteins. More comprehensive study of 344SQ.scrib in PEG-based matrices revealed two previously unobserved morphologies: a rare lumenized morphology and a pseudo-polar phenotype with a relatively high degree of nuclear and polar organization but lacking a true lumen. Both of these more organized forms showed greater prevalence in matrices with PEG-E-cadherin than those with PEG-N-cadherin. These phenotypes seemed to be controlled by a combination of apoptosis and non-apoptotic cellular rearrangement and were associated with enhanced membrane localization of cellular-expressed E-cadherin.

Like the experiments with 344SQ.WT, 344SQ.scrib's epithelial organization seemed to be more negatively influenced by the presence of N-cadherin in the matrix than positively promoted by the presence of E-cadherin because some of these pro-epithelial phenotypes were also observed in PEG-RGDS-only control matrices. Integrin binding to PEG-RGDS alone was sufficient to support some degree of this mixed epithelial-like population in encapsulated 344SQ.scrib. This is an interesting finding given work with 344SQ.scrib in MG where no organization at all is observed despite ample matrix integrin engagement. Indeed, epithelialization is so deficient in MG that some degree of matrix TGFβ-free invasion occurs in some cases.

This difference observed in the PEG system may result from more specific integrin binding, an avoidance of contaminating growth factors, a difference in matrix

mechanics or many other factors that differ among the culture platforms and may be worth further exploration in future experiments. An additional ligand effect on 344SQ.scrib not directly related to cell-cell contacts is a particular possibility given experiments in MG demonstrating extensive invasion in matrices crosslinked with collagen with this more invasive phenotype blocked with antibodies against integrin $\beta_1$ subunits (Fig. 4-5). It is possible that if ligation of $\beta_1$-related integrins facilitates invasion, integrins with other subunits, like $\beta_3$ for example, may promote the development of the more typical non-invasive 344SQ.scrib spheroids.

The more reductionist PEG system used here with only the RGD sequence present may preferentially bind the 344SQ.scrib integrins that support a more growth-normalized spheroid morphology. The hydrogel can be altered in future work with the addition of other peptide sequences that more avidly bind $\beta_1$-containing integrins to better characterize a potential ligand effect. Finally, an alternative mechanics-driven process is also possible given that the PEG matrices used with 344SQ.scrib are stiffer than the MG or MG-collagen matrices used in previous work with the cell line. Future work can test if there is a loss of these partially polarized phenotypes in softer PEG matrices with similar integrin-binding properties to explore if these morphologies result from organizational changes in spheres due to external matrix mechanical stresses unrelated to ligand concentration or identity.

There was also a slight, but non-significant enhancement of sphere characteristics suggestive of more organized epithelial morphologies in PEG-E-cadherin gels compared to PEG-RGDS-only controls. Given literature data linking E-cadherin to scribble function and the co-culture experiments showing restoration of 344SQ.scrib lumenization

in hybrid structures formed with 344SQ.WT (Fig. 4-6), an enhancement of epithelialization was expected in PEG-E-cadherin matrices over PEG-RGDS-only controls. Several reasons are possible for explaining why this was not more potently evident. While the literature does show a link between E-cadherin and scribble, much of that link has established the importance of proper E-cadherin binding in facilitating scribble location and function while fewer studies have documented E-cadherin's role and function in the face of scribble loss[312]. It is possible that a knockdown of scribble has too severe of polarity-related phenotypic consequences to be overcome by pro-organizational effects of additional E-cadherin binding.

Furthermore, staining for cell-expressed E-cadherin showed some degree of preferential membrane location in spheres in control matrices, demonstrating that 344SQ.scrib still expresses E-cadherin localized to cell membranes in 3D culture to facilitate cell-cell binding despite a scribble knockdown. It is possible that the limited difference in pro-organizational phenotypes seen between PEG-E-cadherin and PEG-RGDS-only groups may be because substantial homophilic binding between E-cadherin pairs on adjacent cells in 344SQ.scrib structures was already present without matrix-tethered cadherin. This binding may have supported a maximal pro-polar influence by E-cadherin in the face of scribble loss with little amplification of these effects upon additional matrix cadherin binding. It is also possible that even despite the use of relatively low PEG-SVA conjugation ratios, the pegylation of E-cadherin protein in PEG-E-cadherin species led to a sufficient enough loss of bioactivity that its additional matrix incorporation caused little effect on top of the baseline effects already present from binding between cells of fully functional, native cell-expressed E-cadherin. This

possibility, however, is less likely given the dramatic effects seen with PEG-cadherin incorporation in PEG-RGDS-free matrices in 344SQ.WT (Fig. 4-10); effects that were similarly observed in pilot studies with 344SQ.scrib in PEG-RGDS-free matrices.

A significant difference in organization was recorded, however, with 344SQ.scrib in matrices with PEG-N-cadherin, with a relative decrease in both lumenized and pseudo-epithelial organized phenotypes and in basolateral E-cadherin spatial location. Compared to E-cadherin, there is relatively little published information relating N-cadherin binding to scribble expression or function. Further, while the role N-cadherin has been studied in reference to polarity of neuronal cells or cancers of neuronal lineage [327–329], limited work has been done establishing a causal link between N-cadherin expression and polarity in epithelial cells of cancers beyond correlations observed in EMT (EMT induces both increased N-cadherin expression and loss of polarity). Instead, N-cadherin's effects on motility and matrix invasion have been more widely studied[135,279,296]. It is possible, if not likely, however, that N-cadherin binding directly influences both pro-malignant polarity and invasion changes, but invasion has been the focus of study as invasion-related observations that are more evident in naturally derived matrices may have masked subtler changes in polarity. The different invasive response observed in the PEG system may have made observable and facilitated study of subtler polarity differences.

Another potential explanation for the effects seen with PEG-N-cadherin that is discussed at length in the literature relates to findings that increased N-cadherin binding in cancer typically coincides with a loss of E-cadherin binding[292]. This possibility that increased N-cadherin binding influences polarity by altering E-cadherin binding and thereby acting through E-cadherin-related mechanisms is at least partially supported by

the data showing lack of E-cadherin membrane localization in spheres in PEG-N-cadherin matrices. Enhanced binding of N-cadherin of cells in PEG-N-cadherin matrices could shift the balance in the mixed cadherin expression phenotype, and the resulting decrease in E-cadherin binding between cells in spheres could mediate the effects on polar organization observed via the above E-cadherin-related mechanisms.

In any event, it seems that additional binding of E- or N-cadherin alone is not sufficient to restore 344SQ.scrib lumenization, suggesting a more complex mechanistic picture to explain the interesting findings of lumenization in hybrid 344SQ.WT:344SQ.scrib structures. It is possible that other cell-cell contacts mediate the complete normalization of 344SQ.scrib polarity. Jagged-notch signaling, for example, has been shown in the $KRas^{G12D}/p53^{R172H\Delta G}$ model to influence EMT and invasion[239]. It is also possible that the expression of different cadherin types or a different spatial or temporal pattern of N- and E-cadherin expression or concentrations that are not presented in the matrices tested may play the decisive role.

## 4.4 Conclusion

Cadherin cell-cell contacts play an important role in the establishment of proper epithelial polarity and in cancer progression and dissemination[292]. In this chapter, E- and -N-cadherin were presented via the PEG matrix to cells of the $KRas^{G12D}/p53^{R172H\Delta G}$ lung adenocarcinoma model to probe for effects on epithelial morphogenesis and EMT, and the potential influence of cell-cell contact-mediated normalization of cells with polarity defects. First, a dramatic effect of matrix-tethered cadherins was first found on 344SQ sphere morphogenesis in otherwise non-cell adhesive matrices. In matrices with PEG-RGDS, this effect on epithelial morphogenesis and related effects on resistance to TGFβ-

induced EMT were subtler, but incorporation of PEG-N-cadherin in particular negatively influenced epithelialization. Finally, in studies with the polarity-defective 344SQ.scrib line, PEG-based matrices promoted formation of partially polar-organized states, the degree to which was influenced by matrix-tethered cadherin, potentially mediated by differences in localization of cell-expressed E-cadherin.

Additional work could be done to fully characterize the role of cadherins in the $KRas^{G12D}/p53^{R172H\Delta G}$ model. As matrix incorporation of PEG-E- and -N-cadherin did have a subtle effect on aspects of both 344SQ.WT and 344SQ.scrib epithelial organization, additional studies may be done to establish a more causal link between its matrix incorporation and these effects; initial pilot experiments examining some of the more commonly studied downstream cadherin signaling targets (proliferation, β-catenin in Wnt pathway, BCL-2 pathway, etc.) were inconclusive. Furthermore, as studies with blocking antibodies proved difficult given so much bound cadherin present in hydrogels, $KRas^{G12D}/p53^{R172H\Delta G}$ lines with knockdowns of these cadherin components may be worth exploring to further probe for a possible causal link.

PEG-based hydrogels with or without PEG-cadherins could also be used in future studies to further examine other interesting findings with 344SQ.scrib unrelated to polarity normalization. For instance, the profoundly different invasive phenotype observed in scribble knockdowns in MG matrices with collagen incorporated could be further explored in the PEG system for specific causal biomechanical or biochemical relationships. Such work may have important implications for how cells with polarity loss in tumors interact with matrix cues that promote or inhibit cancer progression and metastasis. Finally, future studies may also work to characterize potential cell-cell

interactions in addition to E- and -N-cadherin that may mediate the behavior of 344SQ.WT:344SQ.scrib hybrid structures or special spatial or temporal relationships of those contacts that may mediate polar normalization despite scribble knockdown. Such work may have important implications for the mechanisms by which less transformed tumor cell subpopulations exert metastasis-tempering influence on more malignant neighboring subpopulations, an intriguing avenue for exploration and potential future therapeutic development.

# 5. Conclusions and Future Directions

## 5.1 Thesis Summary and Conclusions

Non-small cell lung cancer is the leading cause of cancer-related death largely due to a high incidence of metastatic disease for which few therapeutic options exist. Mounting research has defined a key role for the ECM in both cancer prevention and progression; normal ECM affords anti-neoplastic signaling from normal stromal cells and barrier basement membrane effects whereas a pathological ECM co-evolves with tumor progression that ultimately facilitates matrix invasion and metastasis. In addition to pro-tumorigenic signaling from TAFs, changes to tumor stroma include alterations in ECM protein concentration, composition, and architecture that produce important pathological changes in tumor ECM stiffness and growth factor signaling that promote tumor progression. In the hope that a better understanding of these changes and their pro-metastatic influence may reveal new therapeutic options, investigators have begun to study these extrinsic influences using cancer models cultured in *in vitro* matrix-mimetics. However, studies to probe for specific ECM influences have largely been restricted to naturally-derived matrix materials that afford ample cell engagement but limited experimental control.

Study of the $KRas^{G12D}$ / $p53^{R172H\Delta G}$ lung adenocarcinoma model in MG has demonstrated substantial contextual ECM control over metastatic behavior. Despite a similar genetic background, different lines in this model are subjected to varying degrees of EMT/MET, matrix invasion, and metastasis mediated by culture in a three-dimensional environment, exposure to TGFβ, epigenetic regulation by miR200, and differential expression of ECM-related proteins and the Jagged-Notch cell-cell contact

signaling system[232,238,239]. In this thesis, the study of the $KRas^{G12D}$ / $p53^{R172H\Delta G}$ model was translated into a synthetic PEG matrix to eliminate potential confounders in the MG system resulting from growth factor contamination and poor control over scaffold biomechanics and biochemistry. This PEG system featured biospecific cell adhesion and cell-mediated proteolytic degradation on an otherwise non-bioactive background, affording greater experimental control of matrix cues.

Epithelial morphogenesis of the EMT-prone 344SQ line was first studied in 3D culture in these modified PEG-based hydrogels. Bioactivity afforded by RGD-mediated cell adhesion and hydrogel backbone MMP-susceptibility was sufficient for 344SQ to form lumenized, polarized epithelial spheres in 3D PEG culture. Structure size, organization of epithelial polarity, and coordinated patterns of proliferation and apoptosis were altered by controlled modification of hydrogel stiffness and bioactivity, demonstrating key ECM influences on epithelial morphogenesis. Further, these morphogenic features were also found to be dependent on the spatial presentation of bioactive ECM ligands with cyclic formulations of RGDS affording significantly different morphogenic effects.

Potential EMT and matrix invasion responses to TGFβ in 344SQ cells cultured in the PEG system were next explored in this thesis. TGFβ plays a dual role in both inhibiting and promoting tumor growth and progression at different stages of tumorigenesis[265]. In 344SQ and other EMT models, it acts as a promoter of EMT-related transcription factors and inhibitor of pro-epithelial miR-200, initiating an EMT response and MG matrix invasion[232,237]. In PEG-encapsulated 344SQ, TGFβ was found to initiate a potent EMT response, inducing changes in sphere morphology, polarity, and expression

levels of both the epigenetic EMT-controller miR-200 and several EMT marker genes. For the first time, EMT-induced changes in cell-secreted ECM were also examined, and substantial organizational remodeling of basement membrane-marking collagen IV was found upon TGFβ exposure. Through these studies, a more important role for ECM adhesive ligand concentration in EMT was also revealed as 344SQ cells in low PEG-RGDS matrices showed a post-TGFβ phenotype with respect to genetic profile and ECM remodeling even in the absence of TGFβ exposure. Finally, the last key EMT-related response, matrix invasion, was studied in the PEG system. Experiments demonstrated that the degree and character of 344SQ matrix invasion can be tuned by altering matrix parameters and the protease susceptibility of the hydrogel backbone with structural hydrogel characteristics mediating an interplay between organized epithelial states and matrix-invasive phenotypes.

Finally, this thesis explored the potential effects on 344SQ morphogenesis and EMT mediated by cadherins, a family of cell-cell contacts that have been shown to play an important role in the establishment or breakdown of proper epithelial polarity and tumor dissemination[292,293]. The key EMT-related cadherins, E- and -N-cadherin, were pegylated and presented via the matrix to both wild-type 344SQ cells and those with a knockdown of scribble, an important member of an essential polarity-determining protein complex[307]. PEG-cadherin induced dramatic effects on 344SQ.WT sphere development in otherwise non-cell-adhesive PEG hydrogels and subtler effects on sphere polarity and TGFβ response in matrices with PEG-RGDS. In studies with 344SQ.scrib, matrix-tethered cadherins influenced the formation of spheres with partially normalized epithelial polarity with some degree of lumenization despite genetic limitations.

Significant differences in both 344SQ.WT and 344SQ.scrib epithelial organization were found between PEG-E-cadherin and PEG-N-cadherin matrices suggesting an identity-specific cadherin effect, potentially mediated by what staining for intracellular E-cadherin revealed to be dramatic differences in cell-expressed E-cadherin membrane localization.

In summary, this thesis has established the utility of the versatile PEG hydrogel matrix in which ECM influences on cancer progression can be studied with high experimental control. Experimental findings in this thesis have contributed to a greater understanding of the matrix biomechanical, biochemical, and cell-cell mediated relationships that influence lung cancer epithelial morphogenesis and EMT. These findings bring the field one step closer to an understanding of the important matrix-related cues mediating tumor progression and metastasis with the prospect that such knowledge might open new therapeutic avenues to treat advanced cancers.

## 5.2 Future Research Directions

This thesis represents the initial work moving the $KRas^{G12D}$ / $p53^{R172H\Delta G}$ model into the more experimentally controllable PEG hydrogel system. Amongst other related work outlined in previous chapters, potential future studies will seek to further characterize the 344SQ matrix invasion response and describe a more mechanistic role for cadherin signaling mediating 344SQ epithelial morphogenesis and EMT. Beyond these studies, future work may examine the role of additional matrix cues in lung cancer metastasis, including other cell-surface ligands like CD44 and cell-cell contact signaling systems like Jagged-Notch. In addition, future work may deploy the PEG system to

study the role of other stromal cell players in metastasis like tumor-associated fibroblasts and blood vessels.

### 5.2.1 CD44 in Lung Adenocarcinoma Progression and Matrix Invasion

CD44 is a single-chain transmembrane glycoprotein of considerable research interest as a marker and promoter of cancer progression[330]. In its primary role, CD44 is a primary receptor for HA, a large, linear non-sulfated glycosaminoglycan that is a major ECM constituent. HA binding to CD44 initiates most of its signaling activities and controls a large degree of non-integrin-mediated cell adhesion to the matrix[331]. In addition to significant glycosylation and other post-translational modifications, CD44 features a substantial number of variant domains whose flexible incorporation generates several variant splice isoforms that introduce cell- and tissue-specialized functionality. This structural variability in part affords CD44 the ability to bind several different ECM molecules including collagen, fibronectin, osteopontin, laminin, as well as major histocompatibility complexes[330]. Like many of these ECM components, CD44's principle binding partner, HA, is enriched in the ECM of multiple cancer types, including lung tumors[332]. CD44 itself is similarly upregulated in several tumor lines and in some cancers, with certain splice variants inducing a metastatic phenotype[107,330,333]. CD44 has also been studied as a key marker in cancer-initiating cells or cancer stem cells, the minor cell populations in tumors essential for tumor maintenance and progression, with CD44 contributing to the activation of certain stem cell regulatory genes and conferring apoptotic resistance[331].

Of particular relevance to the $KRas^{G12D}$ / $p53R^{172H\Delta G}$ lung adenocarcinoma model is literature indicating a role for CD44 in EMT and matrix invasion. CD44 shows greater

expression upon EMT in several cancer models[291,330,332] and potentially plays an important role in cell migration and matrix invasion following EMT. In studies of different tumor models, CD44-HA binding promoted Rac-mediated cytoskeletal reorganization and cell migration[334], tumor cells enhanced their own migration by generating HA fragments to interact with their upregulated CD44 receptors[68], and CD44 expression distinguished more invasive cell populations from otherwise similar non-invasive populations with anti-CD44 antibodies blocking matrix invasion[290]. And in a study of retinal epithelial cells, not only did CD44-HA binding promote cell motility, but it also activated TGFβ-related signaling to further promote EMT[335].

A functional role for CD44 in invasion has further been suggested by data showing that CD44 is highly localized to invadopodia in some cell types; CD44 directly associates with invadopodia actin cores and its adhesion to HA on invadopodia termini may help initiate recruitment of other integrins and complete invadopodia assembly[283]. Finally, CD44-HA binding has been shown to concentrate MMPs at the cell surface, in particular MMP-2 and MMP-9, with increased leading edge MT1-MMP activity[331]. CD44's role in EMT and invasion is likely of specific relevance to our lung adenocarcinoma model as protein expression analysis revealed significant upregulation in CD44 in metastatic $KRas^{G12D}$ / $p53^{R172H\Delta G}$ cells relative to their non-metastatic counterparts[336].

Pilot studies in PEG hydrogels have suggested a role for CD44 in 344SQ EMT. 344SQ.WT spheres cultured in a 5% PEG-PQ hydrogel with 7 mM PEG-RGDS show limited CD44 expression prior to TGFβ exposure that dramatically increases after 4 days of exposure with much more intense staining, preferentially localized to sphere

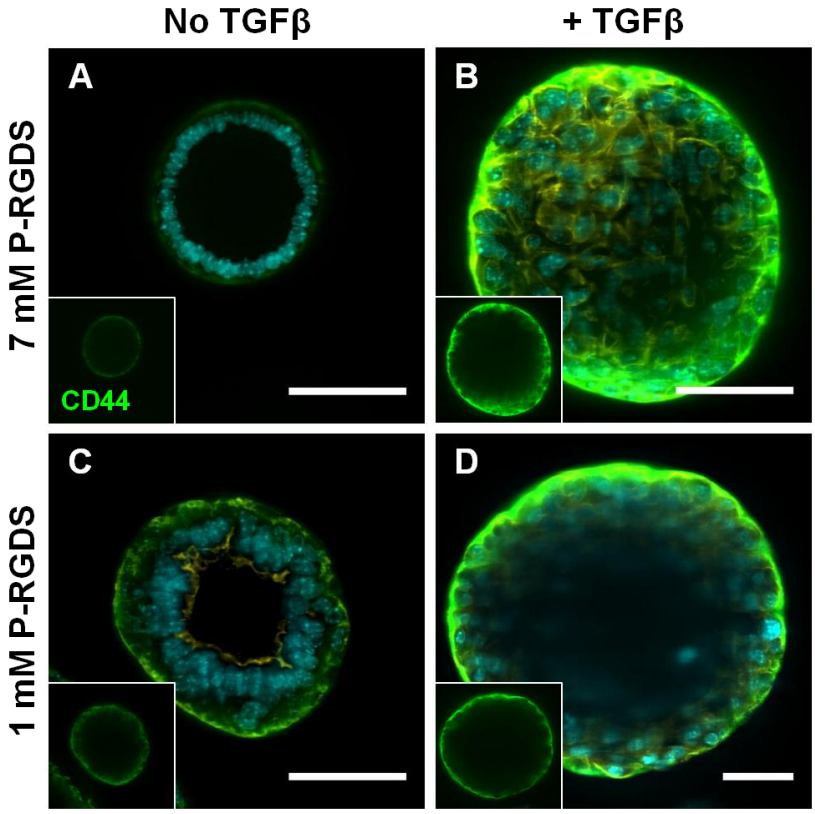


**Fig. 5-1: CD44 expression in PEG-encapsulated 344SQ is altered with TGFβ exposure and PEG-RGDS concentration**. *A-B*, 344SQ cells encapsulated in a 5% PEG-PQ hydrogel with 7 mM PEG-RGDS and stained for CD44 (multi-isoform; green) reveals limited expression prior to TGFβ exposure (*A*) and much greater intensity following EMT (*B*), with expression localized to structure periphery. *C-D*, spheres in 5% PEG-PQ / 1 mM PEG-RGDS matrices exhibit enhanced CD44 expression prior to TGFβ (*C*) compared to the 7 mM group that is similarly strong following TGFβ exposure (*D*). DAPI counterstain (cyan), scale bar = 50 μm.

peripheries. (Fig. 5-1*A-B*). Interestingly, in spheres in matrices with 1 mM PEG-RGDS, expression is somewhat elevated compared to 7 mM PEG-RGDS spheres even in the absence of TGFβ (Fig. 5-1*C*). This observation reinforces previous data that suggest a post-EMT phenotype in gels with little adhesive ligand (Chapter 3).

The substantial increase in CD44 staining intensity after TGFβ exposure (Fig. 5-1*B and D*) suggests a dramatic upregulation in this ECM binding ligand in 344SQ upon EMT. Along with literature reports describing CD44's role in invadopodia function and matrix invasion, this data suggests that CD44 may be of particular importance for 344SQ

invasion and establishment of the metastatic phenotype following EMT. However, the reductionist PEG system used in this thesis with RGD sequences alone to facilitate cell-matrix binding does not afford cleavage of CD44 ligands, leaving the dramatically increased expression of CD44 in 344SQ upon EMT unable to exert a biologic effect.

If the role of CD44 is of high importance in 344SQ matrix invasion, this difference may explain why an altered matrix invasion phenotype was found in the PEG system compared to MG, which likely features contaminating HA or other ECM constituents with CD44-binding domains. Future studies may seek to modify the PEG hydrogels to probe for this role of CD44. HA peptide derivatives that bind CD44 can be pegylated or whole HA molecules acrylated for incorporation into the matrix to enable CD44 bioactivity. Such work may unveil a more potent matrix invasion phenotype in PEG-cultured 344SQ cells and provide important information on an additional cell-matrix interaction that promotes lung adenocarcinoma metastasis.

### 5.2.2 Cell-cell Contacts in Mediating Lung Adenocarcinoma EMT

Paracrine and contact-mediated influences from adjacent cells are capable of both working to prevent cancer progression and providing pro-metastatic cues (Section 1.1.3). In this thesis, initial study for the role of cadherins in 344SQ behavior has been done in the PEG system, with focus primarily on the influence on polarity and the promotion of the epithelial state. However, cadherins also play an important role in cancer metastasis; in particular N-cadherin, which has been shown to influence cell motility and matrix invasion[135,296]. Future work may probe for a cadherin role in promoting a more metastatic phenotype in the $KRas^{G12D}$ / $p53^{R172H\Delta G}$ model with incorporation of PEG-cadherin into the low concentration-PEG matrices used previously to study TGFβ-

induced matrix invasion (Chapter 3). Exploration of potential modulation of invasion in soft PEG hydrogels with matrix-tethered N- or E-cadherin may further illuminate the relationship between cell-cell contacts and matrix invasion.

Beyond the cadherins, PEG hydrogels are well-suited for examination of the role of other cell-cell contact mechanisms, including the Jagged-Notch system. Notch cell-cell signaling is important to a variety of biologic processes including tissue development, cell fate decisions, stem cell expansion, and cancer pathogenesis[337]. In the $KRas^{G12D}$ / $p53^{R172H\Delta G}$ model, metastatic subpopulations express both Notch and Notch ligands, and the Notch ligand Jagged2 promotes EMT and metastasis by GATA transcription factor suppression of miR-200[239]. These findings were described using the MG system and relied on knockdowns to probe Jagged-Notch signaling, a somewhat less physiological representation of how increased Jagged presentation might actually signal neighboring cells to promote metastasis. In future work, the use of PEG hydrogels with matrix-tethered Jagged may allow for an exploration of this signaling in otherwise unmodified cancer cells that more accurately mimics the outside-in matrix signaling that might be important for EMT and invasion of metastasizing cell subpopulations of primary tumors.

### 5.2.3 PEG Hydrogels to Study Cancer Angiogenesis

Advanced tumor growth and metastasis is promoted in part by the angiogenesis of a structurally deficient, but rapidly forming and expansive tumor-associated blood vessel network[85,90]. Study of angiogenic signaling in the lung adenocarcinoma model has previously showed that VEGF Receptor-1 (Flt1) is a miR-200 target in $KRas^{G12D}$ / $p53^{R172H\Delta G}$ cell lines with anti-VEGF antibodies or Flt1 knockdowns decreasing growth

and metastasis of tumor cells[338]. A separate K-ras activated lung adenocarcinoma cell line (LKR-13) showed a high expression of VEGF that was significantly augmented in co-culture with stromal cells[339]. However, limited work has been done to study the interaction of model lung cancer cells with vessel cells *in vitro* or *in vivo*. The PEG system is well-suited to the study of vessel cells and has been successfully deployed in vascular tissue engineering applications[207,208]. Further, PEG hydrogels have been used in an *in vivo* mouse corneal angiogenesis assay to study host angiogenesis in the face of growth factor signaling from implanted hydrogels and anastomosis of this recruited host vasculature to implanted pre-formed vascular networks [208,210].

The differential VEGF-related signaling in $KRas^{G12D}$ / $p53^{R172H\Delta G}$ lines and the augmentation of angiogenic-related signaling found with co-culture of cancer-associated fibroblasts present intriguing areas for further study in the PEG system that is so well-characterized in modeling angiogenesis. To this end, pilot studies *in vitro* have deployed a dual-gel experimental set-up featuring 344SQ and vessel-forming cells in separate hydrogels in close approximation (Figure 5-2*A*). This set-up permits compartmentalized vessel formation in the angiogenic gel (human umbilical vein endothelial cells (HUVEC) and human brain pericytes (HBP)) in the face of potential paracrine signaling from the cancer-laden gel (344SQ), enabling examination of potential differences in the rate of vessel formation, vessel structural parameters, or vessel migration with cancer co-culture. It also affords potential pro-tumorigenic signaling from vessel cells to cancer cells. Initial studies have demonstrated a degree of HUVEC/HBP in-growth from the vessel gels into cancer-laden gels with some association between 344SQ spheres and the infiltrating vessel-like structures (Fig. 5-2*B*).

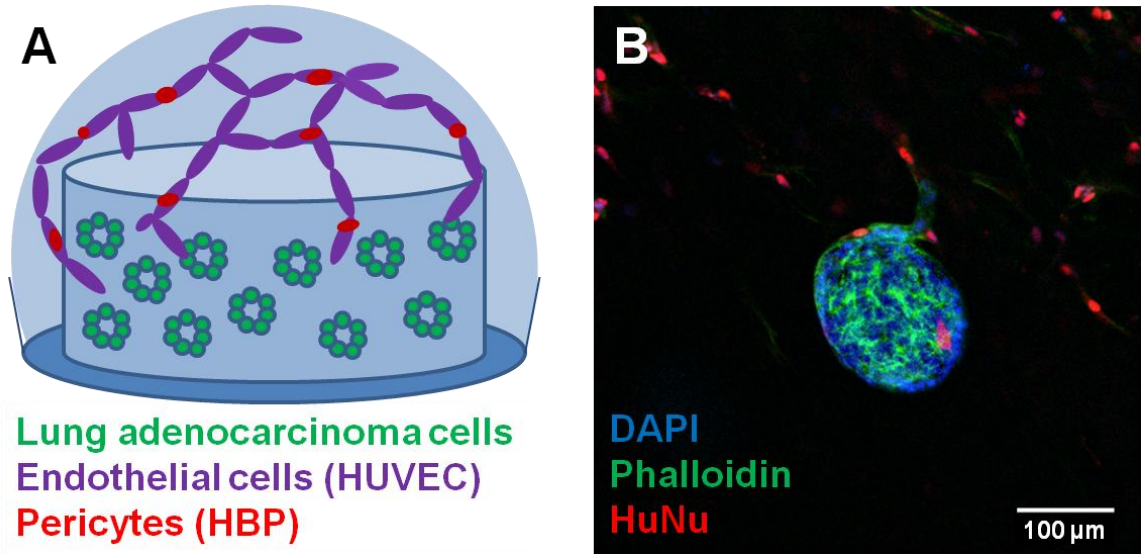


**Fig. 5-2: Modeling lung cancer angiogenesis in PEG hydrogels.** *A*, schematic of a "dual gel" featuring the vessel-forming cells (co-culture of HUVECs (purple) and HBP pericytes (red)) in a PEG-PQ hydrogel polymerized over a separate gel with encapsulated $KRas^{G12D}$ / $p53^{R172H\Delta G}$ cells (green) to enable visualization of potential differences in vessel formation, directional angiogenesis, or cancer cell behavior resulting from compartmentalized co-culture. *B*, image of a 344SQ sphere in the cancer gel component of a dual gel system formed near the border with the vessel gel. HUVEC and HBP cells (positive for human nuclear antigen (HuNu), red) form linear, organized vessel-like structures (top of image), some of which infiltrate into the cancer gel below and interact with the 344SQ sphere (HuNu negative, DAPI (blue) only). Phalloidin counterstain (green). Images courtesy of Laila Roudsari.

Future work in similar *in vitro* systems will explore differences in angiogenic and cancer cell behavior in the face of this co-culture signaling and elaborate potential angiogenesis-related mechanisms that help account for phenotypic differences in $KRas^{G12D}$ / $p53^{R172H\Delta G}$ lines of differing metastatic potential or miR-200 expression. In addition, tumor-associated fibroblasts can be incorporated into the co-culture alone to probe for non-angiogenesis-related influences on lung cancer cell phenotype or in combination with vessel cells to further elaborate their role in aiding metastasis via promotion of tumor angiogenesis. Finally, future work may introduce this system into the *in vivo* corneal angiogenesis assay to study the recruitment of host vessels by $KRas^{G12D}$ / $p53^{R172H\Delta G}$ cells in implanted hydrogels to facilitate improved *in vivo* study of potential

metastatic events. For example, potential intravasation of implanted cancer cells into recruited vessels in advance of spread throughout the host would represent a more cell-mediated and physiological model of metastasis than that afforded by tail vein injection of cancer cells or other methods used in previous study.

## 5.3 Overall Summary

In summary, this thesis deployed a tunable bioactive PEG hydrogel to study matrix influences on cancer cell behavior and progression. Findings herein have provided greater insight into stromal biomechanical, biochemical, and cell-cell factors that guide lung adenocarcinoma epithelial morphogenesis and EMT. These contributions advance an understanding of the extrinsic matrix influences that mediate invasion and dissemination of cancer and bring investigators one step closer to identifying new metastasis-targeting therapeutics to treat patients with advanced cancer.

# 6. References


1. Siegel, R., Ward, E., Brawley, O. & Jemal, A. Cancer Statistics , 2011: The Impact of Eliminating Socioeconomic and Racial Disparities on Premature Cancer Deaths. *CA Cancer J Clin* **61**, 212–36. (2011).

2. Ingber, D. E. Can cancer be reversed by engineering the tumor microenvironment? *Seminars in Cancer Biology* **18**, 356–64 (2008).

3. Cukierman, E. & Bassi, D. E. Physico-mechanical aspects of extracellular matrix influences on tumorigenic behaviors. *Seminars in Cancer Biology* **20**, 139–45 (2010).

4. Rosso, F., Giordano, A., Barbarisi, M. & Barbarisi, A. From cell-ECM interactions to tissue engineering. *Journal of Cellular Physiology* **199**, 174–80 (2004).

5. Van der Rest, M. & Garrone, R. Collagen family of proteins. *The FASEB Journal* **5**, 2814–2823 (1991).

6. Colognato, H. & Yurchenco, P. D. Form and Function : The Laminin Family of Heterotrimers. *Developmental Dynamics* **218**, 213–234 (2000).

7. Ruoslahti, E. Fibronectin and its receptors. *Annual Review of Biochemistry* **57**, 375–413 (1988).

8. Hardingham, T. & Fosang, A. Proteoglycans: many forms and many functions. *The FASEB Journal* **6**, 861–870 (1992).

9. Hynes, R. O. The extracellular matrix: not just pretty fibrils. *Science* **326**, 1216–9 (2009).

10. Jones, J. I., Gockerman, A., Busby, W. H., Camacho-Hubner, C. & Clemmons, D. R. Extracellular matrix contains insulin-like growth factor binding protein-5: potentiation of the effects of IGF-I. *The Journal of Cell Biology* **121**, 679–87 (1993).

11. Kanematsu, A. *et al*. Type I collagen can function as a reservoir of basic fibroblast growth factor. *Journal of Controlled Release* **99**, 281–92 (2004).

12. Yayon, a, Klagsbrun, M., Esko, J. D., Leder, P. & Ornitz, D. M. Cell surface, heparin-like molecules are required for binding of basic fibroblast growth factor to its high affinity receptor. *Cell* **64**, 841–8 (1991).

13. Rozario, T. & DeSimone, D. W. The extracellular matrix in development and morphogenesis: a dynamic view. *Developmental Biology* **341**, 126–40 (2010).

14. Ten Dijke, P. & Arthur, H. M. Extracellular control of TGFbeta signalling in vascular development and disease. *Nature Reviews. Molecular Cell Biology* **8**, 857–69 (2007).

15. Tran, K. T., Lamb, P. & Deng, J.-S. Matrikines and matricryptins: Implications for cutaneous cancers and skin repair. *Journal of Dermatological Science* **40**, 11–20 (2005).

16. Burgess, J. K. & Weckmann, M. Matrikines and the lungs. *Pharmacology & Therapeutics* **134**, 317–37 (2012).

17. Schenk, S. & Quaranta, V. Tales from the crypt[ic] sites of the extracellular matrix. *Trends in Cell Biology* **13**, 366–375 (2003).

18. Schenk, S. *et al.* Binding to EGF receptor of a laminin-5 EGF-like fragment liberated during MMP-dependent mammary gland involution. *The Journal of cell biology* **161**, 197–209 (2003).

19. Engel, J. EGF-like domains in extracellular matrix proteins: localized signals for growth and differentiation? *FEBS letters* **251**, 1–7 (1989).

20. Panayotou, G., End, P., Aumailley, M., Timpl, R. & Engel, J. Domains of laminin with growth-factor activity. *Cell* **56**, 93–101 (1989).

21. Rowe, R. G. & Weiss, S. J. Breaching the basement membrane: who, when and how? *Trends in Cell Biology* **18**, 560–74 (2008).

22. Provenzano, P. P., Inman, D. R., Eliceiri, K. W., Trier, S. M. & Keely, P. J. Contact guidance mediated three-dimensional cell migration is regulated by Rho/ROCK-dependent matrix reorganization. *Biophys J* **95**, 5374–84 (2008).

23. Provenzano, P. P. *et al.* Collagen reorganization at the tumor-stromal interface facilitates local invasion. *BMC Med* **4**, 38 (2006).

24. Ingber, D. E. Tensegrity-based mechanosensing from macro to micro. *Progress in Biophysics and Molecular Biology* **97**, 163–79 (2008).

25. Ghosh, K. *et al.* Cell adaptation to a physiologically relevant ECM mimic with different viscoelastic properties. *Biomaterials* **28**, 671–9 (2007).

26. Yeung, T. *et al.* Effects of substrate stiffness on cell morphology, cytoskeletal structure, and adhesion. *Cell Motility and the Cytoskeleton* **60**, 24–34 (2005).

27. Pelham, R. & Wang, Y. Cell locomotion and focal adhesions are regulated by substrate flexibility. *PNAS* **94**, 13661–13665 (1997).

28. Lo, C. M., Wang, H. B., Dembo, M. & Wang, Y. L. Cell movement is guided by the rigidity of the substrate. *Biophysical Journal* **79**, 144–52 (2000).

29. Engler, A. J. *et al.* Myotubes differentiate optimally on substrates with tissue-like stiffness: pathological implications for soft or stiff microenvironments. *The Journal of Cell Biology* **166**, 877–87 (2004).

30. Jacot, J. G., McCulloch, A. D. & Omens, J. H. Substrate stiffness affects the functional maturation of neonatal rat ventricular myocytes. *Biophysical Journal* **95**, 3479–87 (2008).

31. Khatiwala, C. B., Peyton, S. R., Metzke, M. & Putnam, A. J. The Regulation of Osteogenesis by ECM Rigidity in MC3T3-E1 Cells Requires MAPK Activation. *Journal of Cellular Physiology* **211**, 661–672 (2007).

32. Leipzig, N. D. & Shoichet, M. S. The effect of substrate stiffness on adult neural stem cell behavior. *Biomaterials* **30**, 6867–78 (2009).

33. Engler, A. J., Sen, S., Sweeney, H. L. & Discher, D. E. Matrix elasticity directs stem cell lineage specification. *Cell* **126**, 677–89 (2006).

34. Reilly, G. C. & Engler, A. J. Intrinsic extracellular matrix properties regulate stem cell differentiation. *Journal of Biomechanics* **43**, 55–62 (2010).

35. Chen, C. S. Geometric Control of Cell Life and Death. *Science* **276**, 1425–1428 (1997).

36. Chen, C. S., Alonso, J. L., Ostuni, E., Whitesides, G. M. & Ingber, D. E. Cell shape provides global control of focal adhesion assembly. *Biochemical and Biophysical Research Communications* **307**, 355–361 (2003).

37. Thomas, C. H., Collier, J. H., Sfeir, C. S. & Healy, K. E. Engineering gene expression and protein synthesis by modulation of nuclear shape. *PNAS* **99**, 1972–7 (2002).

38. McBeath, R., Pirone, D. M., Nelson, C. M., Bhadriraju, K. & Chen, C. S. Cell shape, cytoskeletal tension, and RhoA regulate stem cell lineage commitment. *Developmental Cell* **6**, 483–95 (2004).

39. Kilian, K. a, Bugarija, B., Lahn, B. T. & Mrksich, M. Geometric cues for directing the differentiation of mesenchymal stem cells. *PNAS* **107**, 4872–7 (2010).

40. Shen, Q. *et al.* Adult SVZ stem cells lie in a vascular niche: a quantitative analysis of niche cell-cell interactions. *Cell Stem Cell* **3**, 289–300 (2008).

41. Cawston, T. E. & Young, D. a Proteinases involved in matrix turnover during cartilage and bone breakdown. *Cell and Tissue Research* **339**, 221–35 (2010).

42. Page-McCaw, A., Ewald, A. J. & Werb, Z. Matrix metalloproteinases and the regulation of tissue remodelling. *Nature Reviews. Molecular Cell Biology* **8**, 221–33 (2007).

43. Levental, K. R. *et al.* Matrix crosslinking forces tumor progression by enhancing integrin signaling. *Cell* **139**, 891–906 (2009).

44. Lu, P., Takai, K., Weaver, V. M. & Werb, Z. Extracellular matrix degradation and remodeling in development and disease. *Cold Spring Harbor Perspectives in Biology* **3**, (2011).

45. Van Hinsbergh, V. W. M. & Koolwijk, P. Endothelial sprouting and angiogenesis: matrix metalloproteinases in the lead. *Cardiovascular Research* **78**, 203–12 (2008).

46. Sakai, T., Larsen, M. & Yamada, K. M. Fibronectin requirement in branching morphogenesis. *Nature* **423**, 876–881 (2003).

47. Fukuda, Y. *et al.* The role of interstitial collagens in cleft formation of mouse embryonic submandibular gland during initial branching. *Development* **103**, 259–67 (1988).

48. Wolfe, J. Risk for breast cancer development determined by mammographic parenchymal pattern. *Cancer* **37**, 2486–2492 (1976).

49. Frantz, C., Stewart, K. M. & Weaver, V. M. The extracellular matrix at a glance. *Journal of Cell Science* **123**, 4195–200 (2010).

50. Claridge, M. W. *et al.* Measurement of arterial stiffness in subjects with vascular disease: Are vessel wall changes more sensitive than increase in intima-media thickness? *Atherosclerosis* **205**, 477–80 (2009).

51. Langley, R. R. & Fidler, I. J. Tumor cell-organ microenvironment interactions in the pathogenesis of cancer metastasis. *Endocrine reviews* **28**, 297–321 (2007).

52. Maffini, M. V, Soto, A. M., Calabro, J. M., Ucci, A. a & Sonnenschein, C. The stroma as a crucial target in rat mammary gland carcinogenesis. *Journal of Cell Science* **117**, 1495–502 (2004).

53. Cunha, G. R., Hayward, S. W. & Wang, Y. Z. Role of stroma in carcinogenesis of the prostate. *Differentiation* **70**, 473–85 (2002).

54. Maffini, M. V, Calabro, J. M., Soto, A. M. & Sonnenschein, C. Stromal regulation of neoplastic development: age-dependent normalization of neoplastic mammary cells by mammary stroma. *The American Journal of Pathology* **167**, 1405–10 (2005).

55. Kuperwasser, C. *et al.* Reconstruction of functionally normal and malignant human breast tissues in mice. *PNAS* **101**, 4966–71 (2004).

56. Sakakura, T., Nishizuka, Y. & Dawe, C. Mesenchyme-dependent morphogenesis and epithelium-specific cytodifferentiation in mouse mammary gland. *Science* **194**, 1439–1441 (1976).

57. Banerjee, S. D., Cohn, R. H. & Bernfield, M. R. Basal lamina of embryonic salivary epithelia. Production by the epithelium and role in maintaining lobular morphology. *The Journal of Cell Biology* **73**, 445–63 (1977).

58. Nogawa, H., Morita, K. & Cardoso, W. V Bud formation precedes the appearance of differential cell proliferation during branching morphogenesis of mouse lung epithelium in vitro. *Developmental Dynamics* **213**, 228–35 (1998).

59. Bosman, F. T. The borderline: basement membranes and the transition from premalignant to malignant neoplasia. *Microscopy Research and Technique* **28**, 216–25 (1994).

60. Carter, R., Burman, J., Barr, L. & Gusterson, B. Immunohistochemical localization of basement membrane type IV collagen in invasive and metastatic squamous carcinomas of the head and neck. *The Journal of Pathology* **147**, 159–64 (1985).

61. Abrahamson, D. Recent studies on the structure and pathology of basement membranes. *The Journal of Pathology* **149**, 257–78 (1986).

62. Pitelka, D. R., Hamamoto, S. T. & Taggart, B. N. Basal lamina and tissue recognition in malignant mammary tumors. *Cancer Research* **40**, 1600–11 (1980).

63. Tarin, D. Ultrastructural features of neural induction in Xenopus laevis. *Journal of Anatomy* **111**, 1–28 (1972).

64. Bonkhoff, H., Wernert, N., Dhom, G. & Remberger, K. Distribution of basement membranes in primary and metastatic carcinomas of the prostate. *Hum Pathol* **23**, 934–9 (1992).

65. Parekh, A. & Weaver, A. M. Regulation of cancer invasiveness by the physical extracellular matrix environment. *Cell Adhesion & Migration* **3**, 288–92 (2009).

66. Wolf, K. & Friedl, P. Mapping proteolytic cancer cell-extracellular matrix interfaces. *Clinical & Experimental Metastasis* **26**, 289–98 (2009).

67. Carragher, N. O., Levkau, B., Ross, R. & Raines, E. W. Degraded collagen fragments promote rapid disassembly of smooth muscle focal adhesions that correlates with cleavage of pp125(FAK), paxillin, and talin. *The Journal of Cell Biology* **147**, 619–30 (1999).

68. Sugahara, K. N. *et al.* Tumor cells enhance their own CD44 cleavage and motility by generating hyaluronan fragments. *The Journal of Biological Chemistry* **281**, 5861–8 (2006).

69. Friedl, P., Maaser, K., Klein, C. & Niggemann, B. Migration of highly aggressive MV3 melanoma cells in 3-dimensional collagen lattices results in local matrix reorganization and shedding of alpha-2 and beta-1 integrins and CD44. *Cancer Research* **57**, 2061–2070 (1997).

70. Tlsty, T. D. & Coussens, L. M. Tumor stroma and regulation of cancer development. *Annual Review of Pathology* **1**, 119–50 (2006).

71. Boyd, N. F. *et al.* Mammographic densities and breast cancer risk. *Breast Disease* **10**, 113–26 (1998).

72. Alowami, S., Troup, S., Al-Haddad, S., Kirkpatrick, I. & Watson, P. H. Mammographic density is related to stroma and stromal proteoglycan expression. *Breast Cancer Research* **5**, R129–35 (2003).

73. Martin, L. J. & Boyd, N. F. Mammographic density. Potential mechanisms of breast cancer risk associated with mammographic density: hypotheses based on epidemiological evidence. *Breast Cancer Research* **10**, 201 (2008).

74. Egeblad, M., Rasch, M. G. & Weaver, V. M. Dynamic interplay between the collagen scaffold and tumor evolution. *Current Opinion in Cell Biology* **22**, 697–706 (2010).

75. Desmoulière, A., Guyot, C. & Gabbiani, G. The stroma reaction myofibroblast: a key player in the control of tumor cell behavior. *The International Journal of Developmental Biology* **48**, 509–17 (2004).

76. Imamura, T. *et al.* Quantitative analysis of collagen and collagen subtypes I, III, and V in human pancreatic cancer, tumor-associated chronic pancreatitis, and alcoholic chronic. *Pancreas* **11**, 357–64 (1995).

77. Kauppila, S., Stenback, F., Risteli, J., Jukkola, A. & Risteli, L. Aberrant type I and type III collagen gene expression in human breast cancer in vivo. *J Pathol* **186**, 262–268 (1998).

78. Ilan, N., Elkin, M. & Vlodavsky, I. Regulation, function and clinical significance of heparanase in cancer metastasis and angiogenesis. *The International Journal of Biochemistry & Cell Biology* **38**, 2018–39 (2006).

79. Barker, H. E., Cox, T. R. & Erler, J. T. The rationale for targeting the LOX family in cancer. *Nature Reviews. Cancer* **12**, 540–52 (2012).

80. Erler, J. *et al.* Hypoxia-induced lysyl oxidase is a critical mediator of bone marrow cell recruitment to form the premetastatic niche. *Cancer Cell* **15**, 35–44 (2009).

81. Nadiarnykh, O., LaComb, R. B., Brewer, M. a & Campagnola, P. J. Alterations of the extracellular matrix in ovarian cancer studied by Second Harmonic Generation imaging microscopy. *BMC Cancer* **10**, 94 (2010).

82. Ambekar, R., Lau, T.-Y., Walsh, M., Bhargava, R. & Toussaint, K. C. Quantifying collagen structure in breast biopsies using second-harmonic generation imaging. *Biomedical Optics Express* **3**, 2021–35 (2012).

83. Provenzano, P. P. *et al.* Collagen density promotes mammary tumor initiation and progression. *BMC Med* **6**, 11 (2008).

84. Cil, T. *et al.* Mammographic density and the risk of breast cancer recurrence after breast-conserving surgery. *Cancer* **115**, 5780–7 (2009).

85. Hagendoorn, J. *et al.* Onset of abnormal blood and lymphatic vessel function and interstitial hypertension in early stages of carcinogenesis. *Cancer Research* **66**, 3360–4 (2006).

86. Hofmann, M. *et al.* Long-term lowering of tumour interstitial fluid pressure reduces Ki-67 expression. *Journal of Biomechanics* **40**, 2324–9 (2007).

87. Nathan, S. S. *et al.* Tumor interstitial fluid pressure may regulate angiogenic factors in osteosarcoma. *Journal of Orthopaedic Research* **26**, 1520–5 (2008).

88. Padera, T. P. *et al.* Lymphatic metastasis in the absence of functional intratumor lymphatics. *Science* **296**, 1883–6 (2002).

89. Shi, Z.-D., Ji, X.-Y., Qazi, H. & Tarbell, J. M. Interstitial flow promotes vascular fibroblast, myofibroblast, and smooth muscle cell motility in 3-D collagen I via upregulation of MMP-1. *American Journal of Physiology. Heart and Circulatory Physiology* **297**, H1225–34 (2009).

90. Shieh, A. C. Biomechanical forces shape the tumor microenvironment. *Annals of Biomedical Engineering* **39**, 1379–89 (2011).

91. Fleury, M. E., Boardman, K. C. & Swartz, M. a Autologous morphogen gradients by subtle interstitial flow and matrix interactions. *Biophysical Journal* **91**, 113–21 (2006).

92. Shields, J. D. *et al.* Autologous chemotaxis as a mechanism of tumor cell homing to lymphatics via interstitial flow and autocrine CCR7 signaling. *Cancer Cell* **11**, 526–38 (2007).

93. Helmlinger, G. & Netti, P. Solid stress inhibits the growth of multicellular tumor spheroids. *Nature Biotechnology* **15**, 778–83 (1997).

94. Wipff, P.-J. & Hinz, B. Myofibroblasts work best under stress. *Journal of Bodywork and Movement Therapies* **13**, 121–7 (2009).

95. Yu, H., Mouw, J. K. & Weaver, V. M. Forcing form and function: biomechanical regulation of tumor evolution. *Trends in Cell Biology* **21**, 47–56 (2011).

96. Butcher, D. T., Alliston, T. & Weaver, V. M. A tense situation: forcing tumour progression. *Nature Reviews. Cancer* **9**, 108–22 (2009).

97. Emerman, T., Burwen, J. & Pitelka, D. Substrate properties influencing ultrastructural differentiation of mammary epithelial cells in culture. *Tissue and Cell* **11**, 109–119 (1979).

98. Egeblad, M., Nakasone, E. S. & Werb, Z. Tumors as organs: complex tissues that interface with the entire organism. *Developmental Cell* **18**, 884–901 (2010).

99. Paszek, M. J. *et al.* Tensional homeostasis and the malignant phenotype. *Cancer Cell* **8**, 241–54 (2005).

100. Wipff, P., Rifkin, D., Meister, J. & Hinz, B. Myofibroblast contraction activates latent TGF-1 from the extracellular matrix. *J Cell Bio* **179**, 1311–1323 (2007).

101. Beacham, D. a & Cukierman, E. Stromagenesis: the changing face of fibroblastic microenvironments during tumor progression. *Seminars in Cancer Biology* **15**, 329–41 (2005).

102. Barsky, S. & Karlin, N. Myoepithelial cells: autocrine and paracrine suppressors of breast cancer progression. *Journal of Mammary Gland Biology and Neoplasia* **10**, 249–60 (2005).

103. Sadlonova, A. *et al.* Breast fibroblasts modulate epithelial cell proliferation in three-dimensional in vitro co-culture. *Breast Cancer Research* **7**, R46–59 (2005).

104. Krause, S., Maffini, M. V, Soto, A. M. & Sonnenschein, C. The microenvironment determines the breast cancer cells' phenotype: organization of MCF7 cells in 3D cultures. *BMC Cancer* **10**, 263 (2010).

105. Allinen, M. *et al.* Molecular characterization of the tumor microenvironment in breast cancer. *Cancer Cell* **6**, 17–32 (2004).

106. Cheng, N. *et al.* Loss of TGF-beta type II receptor in fibroblasts promotes mammary carcinoma growth and invasion through upregulation of TGF-alpha-, MSP- and HGF-mediated signaling networks. *Oncogene* **24**, 5053–68 (2005).

107. Kunz-Schughart, L. & Knuechel, R. Tumor-associated fibroblasts (Part I): active stromal participants in tumor development and progression? *Histol Histopathol* **17**, 599–621 (2002).

108. Orimo, A. *et al.* Stromal fibroblasts present in invasive human breast carcinomas promote tumor growth and angiogenesis through elevated SDF-1/CXCL12 secretion. *Cell* **121**, 335–48 (2005).

109. Bhowmick, N. A., Neilson, E. G. & Moses, H. L. Stromal fibroblasts in cancer initiation and progression. *Nature* **432**, 332–7 (2004).

110. Huber, M. a *et al.* Fibroblast activation protein: differential expression and serine protease activity in reactive stromal fibroblasts of melanocytic skin tumors. *The Journal of Investigative Dermatology* **120**, 182–8 (2003).

111. Chiquet-Ehrismann, R. & Chiquet, M. Tenascins: regulation and putative functions during pathological stress. *The Journal of Pathology* **200**, 488–99 (2003).

112. Kunz-Schughart, L. & Knuechel, R. Tumor-associated fibroblasts (part II): Functional impact on tumor tissue. *Histol Histopathol* **17**, 623–637 (2002).

113. Hlatky, L., Tsionou, C., Hahnfeldt, P. & Coleman, C. Mammary fibroblasts may influence breast tumor angiogenesis via hypoxia-induced vascular endothelial growth factor up-regulation and protein expression. *Cancer Research* **54**, 6083–6086 (1994).

114. Hsu, M.-Y., Meier, F. & Herlyn, M. Melanoma development and progression: a conspiracy between tumor and host. *Differentiation* **70**, 522–36 (2002).

115. Knudson, W., Biswas, C. & Toole, B. P. Interactions between human tumor cells and fibroblasts stimulate hyaluronate synthesis. *PNAS* **81**, 6767–71 (1984).

116. Noël, A., Munaut, C., Nusgens, B., Lapiere, C. & Foidart, J. Different mechanisms of extracellular matrix remodeling by fibroblasts in response to human mammary neoplastic cells. *Invasion & Metastasis* **13**, 72–81 (1993).

117. Gudjonsson, T. *et al.* Normal and tumor-derived myoepithelial cells differ in their ability to interact with luminal breast epithelial cells for polarity and basement membrane deposition. *Journal of Cell Science* **115**, 39–50 (2002).

118. Man, Y. *et al.* Cell clusters overlying focally disrupted mammary myoepithelial cell layers and adjacent cells within the same duct display different immunohistochemical and genetic features: implications for tumor progression and invasion. *Breast Cancer Research* **5**, R231–41 (2003).

119. Man, Y.-G. *et al.* A subset of in situ breast tumor cell clusters lacks expression of proliferation and progression related markers but shows signs of stromal and vascular invasion. *Cancer Detection and Prevention* **29**, 323–31 (2005).

120. Kaplan, R. N. *et al.* VEGFR1-positive haematopoietic bone marrow progenitors initiate the pre-metastatic niche. *Nature* **438**, 820–7 (2005).

121. Kaplan, R. N., Rafii, S. & Lyden, D. Preparing the "soil": the premetastatic niche. *Cancer Research* **66**, 11089–93 (2006).

122. Wijnhoven, B. P., Dinjens, W. N. & Pignatelli, M. E-cadherin-catenin cell-cell adhesion complex and human cancer. *The British Journal of Surgery* **87**, 992–1005 (2000).

123. Frixen, U. H. *et al.* E-cadherin-mediated cell-cell adhesion prevents invasiveness of human carcinoma cells. *The Journal of Cell Biology* **113**, 173–85 (1991).

124. Watabe, M., Nagafuchi, A., Tsukita, S. & Takeichi, M. Induction of polarized cell-cell association and retardation of growth by activation of the E-cadherin-catenin adhesion system in a dispersed carcinoma line. *The Journal of Cell Biology* **127**, 247–256 (1994).

125. Perl, A., Wilgenbus, P., Dahl, U., Semb, H. & Christofori, G. A causal role for E-cadherin in the transition from adenoma to carcinoma. *Nature* **392**, 190–3 (1998).

126. Zheng, Z. *et al.* Downregulation and abnormal expression of E-cadherin and beta-catenin in nasopharyngeal carcinoma: close association with advanced disease stage and lymph node metastasis. *Human Pathology* **30**, 458–66 (1999).

127. Richmond, P. J. M., Karayiannakis, A. J., Nagafuchi, A., Kaisary, A. V & Pignatelli, M. Aberrant E-Cadherin and α-Catenin Expression in Prostate Cancer : Correlation with Patient Survival. *Cancer Research* **57**, 3189–3193 (1997).

128. Sulzer, M., Leers, M., Van Noord, J., Bollen, E. & Theunissen, P. Reduced E-cadherin expression is associated with increased lymph node metastasis and unfavorable prognosis in non-small cell lung cancer. *American Journal of Respiratory and Critical Care Medicine* **157**, 1319–1323 (1998).

129. Birchmeier, W. & Behrens, J. Cadherin expression in carcinomas: role in the formation of cell junctions and the prevention of invasiveness. *Biochimica et Biophysica Acta* **1198**, 11–26 (1994).

130. Richmond, P. J. M., Karayiannakis, A. J., Nagafuchi, A., Kaisary, A. V & Pignatelli, M. Aberrant E-Cadherin and α -Catenin Expression in Prostate Cancer : Correlation with Patient Survival. *Cancer Research* **57**, 3189–3193 (1997).

131. Shimazui, T. *et al.* Decreased expression of alpha-catenin is associated with poor prognosis of patients with localized renal cell carcinoma. *International Journal of Cancer* **74**, 523–8 (1997).

132. Franchi, A., Gallo, O., Boddi, V. & Santucci, M. Prediction of occult neck metastases in laryngeal carcinoma: role of proliferating cell nuclear antigen, MIB-1, and E-cadherin immunohistochemical determination. *Clinical Cancer Research* **2**, 1801–8 (1996).

133. Ropponen, K. M., Eskelinen, M. J., Lipponen, P. K., Alhava, E. M. & Kosma, V. M. Reduced expression of alpha catenin is associated with poor prognosis in colorectal carcinoma. *Journal of Clinical Pathology* **52**, 10–6 (1999).

134. Bànkfalvi, A. *et al.* Immunophenotypic and prognostic analysis of E-cadherin and beta-catenin expression during breast carcinogenesis and tumour progression: a comparative study with CD44. *Histopathology* **34**, 25–34 (1999).

135. Hazan, R. B., Phillips, G. R., Qiao, R. F., Norton, L. & Aaronson, S. a Exogenous expression of N-cadherin in breast cancer cells induces cell migration, invasion, and metastasis. *The Journal of Cell Biology* **148**, 779–90 (2000).

136. Behrens, J. *et al.* Functional Interaction of an Axin Homolog, Conductin, with beta-catenin, APC, and GSK3beta. *Science* **280**, 596–599 (1998).

137. Willert, K., Shibamoto, S. & Nusse, R. Wnt-induced dephosphorylation of Axin releases β -catenin from the Axin complex. *Genes Dev* **13**, 1768–1773 (1999).

138. McVicar, D. W. & Trinchieri, G. CSF-1R, DAP12 and beta-catenin: a ménage à trois. *Nature Immunology* **10**, 681–3 (2009).

139. Aoki, M., Hecht, A., Kruse, U., Kemler, R. & Vogt, P. K. Nuclear endpoint of Wnt signaling: neoplastic transformation induced by transactivating lymphoid-enhancing factor 1. *PNAS* **96**, 139–44 (1999).

140. Behrens, J. *et al.* Functional interaction of B-catenin with the transcription factor LEF-1. *Nature* **382**, 638–42 (1996).

141. Fagotto, F., Funayama, N., Gluck, U. & Gumbiner, B. M. Binding to cadherins antagonizes the signaling activity of beta-catenin during axis formation in Xenopus. *The Journal of Cell Biology* **132**, 1105–14 (1996).

142. Gottardi, C. J., Wong, E. & Gumbiner, B. M. E-Cadherin Suppresses Cellular Transformation by Inhibiting beta-Catenin Signaling in an Adhesion-independent Manner. *J Cell Bio* **153**, 1049–1059 (2001).

143. Stockinger, A., Eger, A., Wolf, J., Beug, H. & Foisner, R. E-cadherin regulates cell growth by modulating proliferation-dependent beta-catenin transcriptional activity. *J Cell Biol* **154**, 1185–1196 (2001).

144. St Croix, B. *et al.* E-Cadherin-dependent growth suppression is mediated by the cyclin-dependent kinase inhibitor p27(KIP1). *The Journal of Cell Biology* **142**, 557–71 (1998).

145. Perrais, M., Chen, X., Perez-moreno, M. & Gumbiner, B. M. E-Cadherin Homophilic Ligation Inhibits Cell Growth and Epidermal Growth Factor Receptor Signaling Independently of Other Cell Interactions. *Molecular Biology of the Cell* **18**, 2013–2025 (2013).

146. Hutmacher, D. W. *et al.* Can tissue engineering concepts advance tumor biology research? *Trends in Biotechnology* **28**, 125–133 (2010).

147. Evenou, F., Fujii, T. & Sakai, Y. Spontaneous formation of highly functional three-dimensional multilayer from human hepatoma Hep G2 cells cultured on an oxygen-permeable polydimethylsiloxane. *Tissue Engineering Part C* **16**, (2010).

148. Ghosh, S. *et al.* Three-dimensional culture of melanoma cells profoundly affects gene expression profile: a high density oligonucleotide array study. *Journal of Cellular Physiology* **204**, 522–31 (2005).

149. Kenny, P. a *et al.* The morphologies of breast cancer cell lines in three-dimensional assays correlate with their profiles of gene expression. *Molecular Oncology* **1**, 84–96 (2007).

150. Yamada, K. M. & Cukierman, E. Modeling tissue morphogenesis and cancer in 3D. *Cell* **130**, 601–10 (2007).

151. Harunaga, J. S. & Yamada, K. M. Cell-matrix adhesions in 3D. *Matrix Biology* **30**, 363–368 (2011).

152. Cukierman, E., Pankov, R., Stevens, D. R. & Yamada, K. M. Taking cell-matrix adhesions to the third dimension. *Science* **294**, 1708–12 (2001).

153. Mccaffrey, L. M. & Macara, I. G. Epithelial organization , cell polarity and tumorigenesis. *Trends in Cell Biology* **21**, 727–735 (2011).

154. Griffith, L. G. & Swartz, M. A. Capturing complex 3D tissue physiology in vitro. *Nature Reviews Molecular Cell Biology* **7**, 211–224 (2006).

155. Partanen, J. I., Nieminen, A. I., Mäkelä, T. P. & Klefstrom, J. Suppression of oncogenic properties of c-Myc by LKB1-controlled epithelial organization. *PNAS* **104**, 14694–9 (2007).

156. Hehlgans, S., Lange, I., Eke, I. & Cordes, N. 3D cell cultures of human head and neck squamous cell carcinoma cells are radiosensitized by the focal adhesion kinase inhibitor TAE226. *Radiotherapy and Oncology* **92**, 371–8 (2009).

157. Feder-Mengus, C., Ghosh, S., Reschner, A., Martin, I. & Spagnoli, G. C. New dimensions in tumor immunology: what does 3D culture reveal? *Trends in Molecular Medicine* **14**, 333–40 (2008).

158. Ohmori, T., Yang, J. L., Price, J. O. & Arteaga, C. L. Blockade of tumor cell transforming growth factor-betas enhances cell cycle progression and sensitizes human breast carcinoma cells to cytotoxic chemotherapy. *Experimental Cell Research* **245**, 350–9 (1998).

159. Kim, J. Bin Three-dimensional tissue culture models in cancer biology. *Seminars in Cancer Biology* **15**, 365–77 (2005).

160. Twardowski, T., Fertala, A., Oregel, J. & San Antonio, J. Type I collagen and collagen mimetics as angiogenesis promoting superpolymers. *Curr Pharm Des* **13**, 3608 (2007).

161. Lee, K. & Mooney, D. Hydrogels for tissue engineering. *Chem Rev* **101**, 1869–79 (2001).

162. Wallace, D. G. & Rosenblatt, J. Collagen gel systems for sustained delivery and tissue engineering. *Advanced Drug Delivery Reviews* **55**, 1631–1649 (2003).

163. Li, M. L. *et al.* Influence of a reconstituted basement membrane and its components on casein gene expression and secretion in mouse mammary epithelial cells. *PNAS* **84**, 136–40 (1987).

164. Barcellos-Hoff, M. H., Aggeler, J., Ram, T. G. & Bissell, M. J. Functional differentiation and alveolar morphogenesis of primary mammary cultures on reconstituted basement membrane. *Development* **105**, 223–35 (1989).

165. Foster, C. S., Smith, C. a, Dinsdale, E. a, Monaghan, P. & Neville, a M. Human mammary gland morphogenesis in vitro: the growth and differentiation of normal breast epithelium in collagen gel cultures defined by electron microscopy, monoclonal antibodies, and autoradiography. *Developmental Biology* **96**, 197–216 (1983).

166. Yang, J. *et al.* Sustained growth and three-dimensional organization of primary mammary tumor epithelial cells embedded in collagen gels. *PNAS* **76**, 3401–5 (1979).

167. Ojakian, G. K., Nelson, W. J. & Beck, K. a Mechanisms for de novo biogenesis of an apical membrane compartment in groups of simple epithelial cells surrounded by extracellular matrix. *Journal of Cell Science* **110 ( Pt 2**, 2781–94 (1997).

168. Petersen, O. W., Rønnov-Jessen, L., Howlett, a R. & Bissell, M. J. Interaction with basement membrane serves to rapidly distinguish growth and differentiation pattern of normal and malignant human breast epithelial cells. *PNAS* **89**, 9064–8 (1992).

169. Blatchford, D. R. *et al.* Influence of microenvironment on mammary epithelial cell survival in primary culture. *Journal of Cellular Physiology* **181**, 304–11 (1999).

170. Coucouvanis, E. & Martin, G. R. Signals for death and survival: a two-step mechanism for cavitation in the vertebrate embryo. *Cell* **83**, 279–87 (1995).

171. Li, G. N., Livi, L. L., Gourd, C. M., Deweerd, E. S. & Hoffman-Kim, D. Genomic and morphological changes of neuroblastoma cells in response to three-dimensional matrices. *Tissue Engineering* **13**, 1035–47 (2007).

172. Stadler, E. & Dziadek, M. Extracellular matrix penetration by epithelial cells is influenced by quantitative changes in basement membrane components and growth factors. *Exp Cell Res* **229**, 360–9 (1996).

173. Kramer, R. H., Bensch, K. G., Wong, J. & Cells, T. Invasion of Reconstituted Basement Membrane Matrix by Metastatic Human Tumor Cells. *Cancer Research* **46**, 1980–1989 (1989).

174. Weaver, V. M. *et al.* Reversion of the malignant phenotype of human breast cells in three-dimensional culture and in vivo by integrin blocking antibodies. *The Journal of Cell Biology* **137**, 231–45 (1997).

175. Yu, W. *et al.* Beta1-integrin orients epithelial polarity via Rac1 and laminin. *Molecular Biology of the Cell* **16**, 433–45 (2005).

176. Weaver, V. M. *et al.* Beta4 Integrin-Dependent Formation of Polarized Three-Dimensional Architecture Confers Resistance To Apoptosis in Normal and Malignant Mammary Epithelium. *Cancer cell* **2**, 205–16 (2002).

177. Roskelley, C. D., Desprez, P. Y. & Bissell, M. J. Extracellular matrix-dependent tissue-specific gene expression in mammary epithelial cells requires both physical and biochemical signal transduction. *PNAS* **91**, 12378–82 (1994).

178. O'Brien, L. E. *et al.* Rac1 orientates epithelial apical polarity through effects on basolateral laminin assembly. *Nature Cell Biology* **3**, 831–8 (2001).

179. Rebustini, I. T. *et al.* Laminin alpha5 is necessary for submandibular gland epithelial morphogenesis and influences FGFR expression through beta1 integrin signaling. *Developmental Biology* **308**, 15–29 (2007).

180. Montesano, R., Matsumoto, K., Nakamura, T. & Orci, L. Identification of a fibroblast-derived epithelial morphogen as hepatocyte growth factor. *Cell* **67**, 901–8 (1991).

181. Wang, F. *et al.* Reciprocal interactions between B1-integrin and epidermal growth factor receptor in three-dimensional basement membrane breast cultures: a different perspective in. *PNAS* **95**, 14821–14826 (1998).

182. Howlett, A. R., Petersen, O. W., Steeg, P. & Bissell, M. J. A Novel Function for the nm23-H1 Gene: Overexpression in Human Breast Carcinoma Cells Leads to the Formation of Basement Membrane and Growth Arrest. *J Natl Cancer Inst* **86**, 1838–1844 (2010).

183. Muthuswamy, S., Li, D., Lelievre, S., Bissell, M. & Brugge, J. ErbB2, but not ErbB1, reinitiates proliferation and induces luminal repopulation in epithelial acini. *Nature Cell Biology* **3**, 785–92 (2001).

184. Provenzano, P. P., Inman, D. R., Eliceiri, K. W. & Keely, P. J. Matrix density-induced mechanoregulation of breast cell phenotype, signaling and gene expression through a FAK-ERK linkage. *Oncogene* **28**, 4326–43 (2009).

185. Hughes, C. S., Postovit, L. M. & Lajoie, G. A. Matrigel: a complex protein mixture required for optimal growth of cell culture. *Proteomics* **10**, 1886–90 (2010).

186. Vukicevic, S. *et al.* Identification of multiple active growth factors in basement membrane Matrigel suggests caution in interpretation of cellular activity related to extracellular matrix components. *Exp Cell Res* **202**, 1–8 (1992).

187. Lutolf, M. P. & Hubbell, J. A. Synthetic biomaterials as instructive extracellular microenvironments for morphogenesis in tissue engineering. *Nat Biotechnol* **23**, 47–55 (2005).

188. Gribova, V., Crouzier, T. & Picart, C. A material's point of view on recent developments of polymeric biomaterials: control of mechanical and biochemical properties. *J Mater Chem* **21**, 14354–66 (2011).

189. Nemir, S. & West, J. L. Synthetic materials in the study of cell response to substrate rigidity. *Ann Biomed Eng* **38**, 2–20 (2010).

190. Hakkinen, K., Harunaga, B., Doyle, A. D., Ph, D. & Yamada, K. M. Direct Comparisons of the Morphology, Migration, Cell Adhesions, and Actin Cytoskeleton of Fibroblasts in Four Different Three-Dimensional Extracellular Matrices. *Tissue Engineering Part A* **17**, 713–24 (2011).

191. Ananthanarayanan, B., Kim, Y. & Kumar, S. Elucidating the mechanobiology of malignant brain tumors using a brain matrix-mimetic hyaluronic acid hydrogel platform. *Biomaterials* **32**, 7913–23 (2011).

192. Miroshnikova, Y. *et al.* Engineering strategies to recapitulate epithelial morphogenesis within synthetic three-dimensional extracellular matrix with tunable mechanical properties. *Phys Biol* **8**, 026013 (2011).

193. Drury, J. L. & Mooney, D. J. Hydrogels for tissue engineering: scaffold design variables and applications. *Biomaterials* **24**, 4337–4351 (2003).

194. Levy-Mishali, M., Zoldan, J. & Levenberg, S. Effect of scaffold stiffness on myoblast differentiation. *Tissue Engineering Part A* **15**, 935 (2009).

195. Patel, Z. & Mikos, A. Angiogenesis with biomaterial-based drug-and cell-delivery systems. *Journal of Biomaterials Science, Polymer Edn* **15**, 701–726 (2004).

196. Fischbach, C. *et al.* Engineering tumors with 3D scaffolds. *Nature Methods* **4**, 6–11 (2007).

197. Sahoo, S. K., Panda, A. K. & Labhasetwar, V. Characterization of porous PLGA/PLA microparticles as a scaffold for three dimensional growth of breast cancer cells. *Biomacromolecules* **6**, 1132–9 (2005).

198. Chen, C., Chen, K. & Yang, S.-T. Effects of three-dimensional culturing on osteosarcoma cells grown in a fibrous matrix: analyses of cell morphology, cell cycle, and apoptosis. *Biotechnology Progress* **19**, 1574–82 (2003).

199. Ma, L. *et al.* Towards personalized medicine with a three-dimensional micro-scale perfusion-based two-chamber tissue model system. *Biomaterials* **33**, 4353–61 (2012).

200. Blanco, T. M., Mantalaris, A., Bismarck, A. & Panoskaltsis, N. The development of a three-dimensional scaffold for ex vivo biomimicry of human acute myeloid leukaemia. *Biomaterials* **31**, 2243–51 (2010).

201. Tilghman, R. W. *et al.* Matrix rigidity regulates cancer cell growth and cellular phenotype. *PloS One* **5**, e12905 (2010).

202. Ulrich, T. A., De Juan Pardo, E. M. & Kumar, S. The mechanical rigidity of the extracellular matrix regulates the structure, motility, and proliferation of glioma cells. *Cancer Res* **69**, 4167–74 (2009).

203. Alexander, N. R. *et al.* Extracellular matrix rigidity promotes invadopodia activity. *Curr Biol* **18**, 1295–9 (2008).

204. Weigel, T., Schinkel, G. & Lendlein, A. Design and preparation of polymeric scaffolds for tissue engineering. *Expert Review of Medical Devices* **3**, 835–51 (2006).

205. Xi, T. *et al.* Cytotoxicity and altered c-myc gene expression by medical polyacrylamide hydrogel. *Journal of Biomedical Materials Research Part A* **78**, 283–90 (2006).

206. Franco, C. L., Price, J. & West, J. L. Development and optimization of a dual-photoinitiator, emulsion-based technique for rapid generation of cell-laden hydrogel microspheres. *Acta Biomater* **7**, 3267–76 (2011).

207. Moon, J. J. *et al.* Biomimetic hydrogels with pro-angiogenic properties. *Biomaterials* **31**, 3840–7 (2010).

208. Saik, J. E., Gould, D. J., Keswani, A. H., Dickinson, M. E. & West, J. L. Biomimetic hydrogels with immobilized ephrinA1 for therapeutic angiogenesis. *Biomacromolecules* **12**, 2715–22 (2011).

209. Nguyen, K. T. & West, J. L. Photopolymerizable hydrogels for tissue engineering applications. *Biomaterials* **23**, 4307–14 (2002).

210. Saik, J. E., Gould, D. J., Watkins, E. M., Dickinson, M. E. & West, J. L. Covalently immobilized platelet-derived growth factor-BB promotes angiogenesis in biomimetic poly(ethylene glycol) hydrogels. *Acta Biomaterialia* **7**, 133–43 (2011).

211. Weber, L., Lopez, C. & Anseth, K. Effects of PEG hydrogel crosslinking density on protein diffusion and encapsulated islet survival and function. *J Biomed Mater Res A* **90**, 720–9 (2009).

212. Gombotz, W., Wang, G., Horbett, T. & Hoffman, A. Protein adsorption to poly(ethylene oxide) surfaces. *J Biomed Mater Res* **25**, 1547 (1991).

213. Ostuni, E., Chapman, R. G., Holmlin, R. E., Takayama, S. & Whitesides, G. M. A Survey of Structure−Property Relationships of Surfaces that Resist the Adsorption of Protein. *Langmuir* **17**, 5605–5620 (2001).

214. Slaughter, B. V, Khurshid, S. S., Fisher, O. Z., Khademhosseini, A. & Peppas, N. a Hydrogels in regenerative medicine. *Advanced Materials* **21**, 3307–29 (2009).

215. Roberts, M. J., Bentley, M. D. & Harris, J. M. Chemistry for peptide and protein PEGylation. *Advanced Drug Delivery Reviews* **54**, 459–476 (2012).

216. Hern, D. & Hubbell, J. Incorporation of adhesion peptides into nonadhesive hydrogels useful for tissue resurfacing. *Journal of Biomedical Materials Research* **39**, 266–76 (1998).

217. DeLong, S. a, Gobin, A. S. & West, J. L. Covalent immobilization of RGDS on hydrogel surfaces to direct cell alignment and migration. *Journal of Controlled Release* **109**, 139–48 (2005).

218. Gobin, A. & West, J. Val-ala-pro-gly, an elastin-derived non-integrin ligand: Smooth muscle cell adhesion and specificity. *Journal of Biomedical Materials Research Part A* **67**, 255–9 (2003).

219. Gunn, J. W., Turner, S. D. & Mann, B. K. Adhesive and mechanical properties of hydrogels influence neurite extension. *Journal of Biomedical Materials Research. Part A* **72**, 91–7 (2005).

220. Veronese, F. M. Peptide and protein PEGylation: a review of problems and solutions. *Biomaterials* **22**, 405–17 (2001).

221. Leslie-Barbick, J. E., Moon, J. J. & West, J. L. Covalently-immobilized vascular endothelial growth factor promotes endothelial cell tubulogenesis in poly(ethylene glycol) diacrylate hydrogels. *Journal of Biomaterials Science. Polymer Edition* **20**, 1763–79 (2009).

222. Mann, B. K., Schmedlen, R. H. & West, J. L. Tethered-TGF-beta increases extracellular matrix production of vascular smooth muscle cells. *Biomaterials* **22**, 439–44 (2001).

223. Liu, H.-W., Chen, C.-H., Tsai, C.-L., Lin, I.-H. & Hsiue, G.-H. Heterobifunctional poly(ethylene glycol)-tethered bone morphogenetic protein-2-stimulated bone marrow mesenchymal stromal cell differentiation and osteogenesis. *Tissue Engineering* **13**, 1113–24 (2007).

224. Kuhl, P. & Griffith-Cima, L. Tethered epidermal growth factor as a paradigm for growth factor–induced stimulation from the solid phase. *Nature Medicine* **2**, 1022–7 (1996).

225. West, J. L. & Hubbell, J. A. Polymeric biomaterials with degradation sites for proteases involved in cell migration. *Macromolecules* **32**, 241–44 (1999).

226. Gobin, A. S. & West, J. L. Cell migration through defined, synthetic extracellular matrix analogues. *FASEB J* **16**, 751–3 (2002).

227. Patterson, J. & Hubbell, J. a Enhanced proteolytic degradation of molecularly engineered PEG hydrogels in response to MMP-1 and MMP-2. *Biomaterials* **31**, 7836–45 (2010).

228. Nemir, S., Hayenga, H. N. & West, J. L. PEGDA hydrogels with patterned elasticity: Novel tools for the study of cell response to substrate rigidity. *Biotechnol Bioeng* **105**, 636–44 (2010).

229. Hahn, M. S. *et al.* Photolithographic patterning of polyethylene glycol hydrogels. *Biomaterials* **27**, 2519–24 (2006).

230. Hoffmann, J. C. & West, J. L. Three-dimensional photolithographic patterning of multiple bioactive ligands in poly(ethylene glycol) hydrogels. *Soft Matter* **6**, 5056–63 (2010).

231. Leslie-Barbick, J., Shen, C., Chen, C. & West, J. Micron-Scale Spatially Patterned, Covalently Immobilized Vascular Endothelial Growth Factor on Hydrogels Accelerates Endothelial Tubulogenesis and Increases Cellular Angiogenic Responses. *Tissue Engineering Part A* **17**, 221–229 (2011).

232. Gibbons, D. L. *et al.* Contextual extracellular cues promote tumor cell EMT and metastasis by regulating miR-200 family expression. *Genes Dev* **23**, 2140–51 (2009).

233. Thiery, J. P., Acloque, H., Huang, R. Y. J. & Nieto, M. A. Epithelial-mesenchymal transitions in development and disease. *Cell* **139**, 871–90 (2009).

234. Polyak, K. & Weinberg, R. a Transitions between epithelial and mesenchymal states: acquisition of malignant and stem cell traits. *Nature Reviews. Cancer* **9**, 265–73 (2009).

235. Zheng, S., El-Naggar, a K., Kim, E. S., Kurie, J. M. & Lozano, G. A genetic mouse model for metastatic lung cancer with gender differences in survival. *Oncogene* **26**, 6896–904 (2007).

236. Gibbons, D. L. *et al.* Expression signatures of metastatic capacity in a genetic mouse model of lung adenocarcinoma. *PloS One* **4**, e5401 (2009).

237. Bracken, C. P. *et al.* A double-negative feedback loop between ZEB1-SIP1 and the microRNA-200 family regulates epithelial-mesenchymal transition. *Cancer Research* **68**, 7846–54 (2008).

238. Schliekelman, M. J. *et al.* Targets of the tumor suppressor miR-200 in regulation of the epithelial-mesenchymal transition in cancer. *Cancer Res* **71**, 7670–82 (2011).

239. Yang, Y. *et al.* The Notch ligand Jagged2 promotes lung adenocarcinoma metastasis through a miR-200–dependent pathway in mice. *J Clin Invest* **121**, 1373–85 (2011).

240. Wang, H., Dembo, M. & Wang, Y. Substrate flexibility regulates growth and apoptosis of normal but not transformed cells. *Am J Phsyiol Cell Physiol* **279**, 1345–1350 (2000).

241. Parekh, A. *et al.* Sensing and modulation of invadopodia across a wide range of rigidities. *Biophys J* **100**, 573–82 (2011).

242. Xu, X. *et al.* Recreating the tumor microenvironment in a bilayer, hyaluronic acid hydrogel construct for the growth of prostate cancer spheroids. *Biomaterials* **33**, 9049–9060 (2012).

243. Ulrich, T. a, Jain, A., Tanner, K., MacKay, J. L. & Kumar, S. Probing cellular mechanobiology in three-dimensional culture with collagen-agarose matrices. *Biomaterials* **31**, 1875–84 (2010).

244. Liang, Y. *et al.* A cell-instructive hydrogel to regulate malignancy of 3D tumor spheroids with matrix rigidity. *Biomaterials* **32**, 9308–15 (2011).

245. Lutolf, M. *et al.* Synthetic matrix metalloproteinase-sensitive hydrogels for the conduction of tissue regeneration: Engineering cell-invasion characteristics. *PNAS* **100**, 5413–8 (2003).

246. Yamada, K. M. Adhesive recognition sequences. *J Biol Chem* **266**, 12809–12812 (1991).

247. Hahn, M., McHale, M., Wang, E., Schmedlen, R. & West, J. Physiologic pulsatile flow bioreactor conditioning of poly(ethylene glycol)-based tissue engineered vascular grafts. *Ann Biomed Eng* **35**, 190–200 (2007).

248. Hurst, R. E., Kyker, K. D., Bonner, R. B., Bowditch, R. D. & Hemstreet III, G. P. Matrix-dependent plasticity of the malignant phenotype of bladder cancer cells. *Anticancer Res* **23**, 3119–28 (2003).

249. Alcaraz, J. *et al.* Laminin and biomimetic extracellular elasticity enhance functional differentiation in mammary epithelia. *EMBO J* **27**, 2829–38 (2008).

250. Kostic, A., Lynch, C. D. & Sheetz, M. P. Differential matrix rigidity response in breast cancer cell lines correlates with the tissue tropism. *PloS One* **4**, e6361 (2009).

251. Lam, W. A. *et al.* Extracellular matrix rigidity modulates neuroblastoma cell differentiation and N-myc expression. *Mol Cancer* **9**, 35 (2010).

252. Baker, E. L., Srivastava, J., Yu, D., Bonnecaze, R. T. & Zaman, M. H. Cancer cell migration: integrated roles of matrix mechanics and transforming potential. *PLoS One* **6**, e20355 (2011).

253. Indra, I. & Beningo, K. A. An in vitro correlation of metastatic capacity, substrate rigidity and ECM composition. *J Cell Biochem* **112**, 3151–8 (2011).

254. Tseng, Q. *et al.* A new micropatterning method of soft substrates reveals that different tumorigenic signals can promote or reduce cell contraction levels. *Lab Chip* **11**, 2231–40 (2011).

255. Kumagai, H., Tajima, M., Ueno, Y., Giga-Hama, Y. & Ohba, M. Effect of cyclic RGD peptide on cell adhesion and tumor metastasis. *Biochemical and Biophysical Research Communications* **177**, 74–82 (1991).

256. Aumailley, M. *et al.* Arg-Gly-Asp constrained within cyclic pentapoptides: Strong and selective inhibitors of cell adhesion to vitronectin and laminin fragment P1. *FEBS Letters* **29**, 50–54 (1991).

257. Xiao, Y. & Truskey, G. a Effect of receptor-ligand affinity on the strength of endothelial cell adhesion. *Biophysical Journal* **71**, 2869–84 (1996).

258. Hersel, U., Dahmen, C. & Kessler, H. RGD modified polymers: biomaterials for stimulated cell adhesion and beyond. *Biomaterials* **24**, 4385–4415 (2003).

259. Temming, K., Schiffelers, R. M., Molema, G. & Kok, R. J. RGD-based strategies for selective delivery of therapeutics and imaging agents to the tumour vasculature. *Drug Resistance Updates* **8**, 381–402 (2005).

260. Liu, S. Radiolabeled Multimeric Cyclic RGD Peptides as Integrin AlphavBeta3 Targeted Radiotracers for Tumor Imaging. *Molecular Pharmaceutics* **3**, 472–487 (2006).

261. Mousa, S. Anti-integrin as novel drug-discovery targets : potential therapeutic and diagnostic implications. *Current Opinion in Chemical Biology* **6**, 534–541 (2002).

262. Lee, S. H., Moon, J. J. & West, J. L. Three-dimensional micropatterning of bioactive hydrogels via two-photon laser scanning photolithography for guided 3D cell migration. *Biomaterials* **29**, 2962–8 (2008).

263. Massagué, J. TGFbeta in Cancer. *Cell* **134**, 215–30 (2008).

264. Hinck, A. P. Structural studies of the TGF-βs and their receptors - insights into evolution of the TGF-β superfamily. *FEBS letters* **586**, 1860–70 (2012).

265. Heldin, C.-H., Vanlandewijck, M. & Moustakas, A. Regulation of EMT by TGFβ in cancer. *FEBS Letters* **586**, 1959–70 (2012).

266. Bierie, B. & Moses, H. Tumour microenvironment: TGFbeta: the molecular Jekyll and Hyde of cancer. *Nat Rev Cancer* **6**, 506–20 (2006).

267. Cui, W. *et al.* TGFbeta1 inhibits the formation of benign skin tumors, but enhances progression to invasive spindle carcinomas in transgenic mice. *Cell* **86**, 531–42 (1996).

268. Amendt, C., Schirmacher, P., Weber, H. & Blessing, M. Expression of a dominant negative type II TGF-beta receptor in mouse skin results in an increase in carcinoma incidence and an acceleration of carcinoma development. *Oncogene* **17**, 25–34 (1998).

269. Siegel, P. M., Shu, W., Cardiff, R. D., Muller, W. J. & Massague, J. Transforming growth factor beta signaling impairs Neu-induced mammary tumorigenesis while promoting pulmonary metastasis. *PNAS* **100**, 8430–5 (2003).

270. Lu, S.-L. *et al.* Loss of transforming growth factor-beta type II receptor promotes metastatic head-and-neck squamous cell carcinoma. *Genes & Development* **20**, 1331–42 (2006).

271. Weeks, B., He, W., Olson, K. & Wang, X. Inducible expression of transforming growth factor beta1 in papillomas causes rapid metastasis. *Cancer Research* **61**, 7435–7443 (2001).

272. Muraoka-Cook, R. S. *et al.* Conditional overexpression of active transforming growth factor beta1 in vivo accelerates metastases of transgenic mammary tumors. *Cancer Research* **64**, 9002–11 (2004).

273. Kang, J., Liu, C. & Derynck, R. New regulatory mechanisms of TGF-beta receptor function. *Trends Cell Biol* **19**, 385–94 (2009).

274. Bhowmick, N. a *et al.* TGF-beta signaling in fibroblasts modulates the oncogenic potential of adjacent epithelia. *Science* **303**, 848–51 (2004).

275. Yang, J. & Weinberg, R. Epithelial-mesenchymal transition: at the crossroads of development and tumor metastasis. *Dev Cell* **15**, 818–29 (2008).

276. Arce, L., Yokoyama, N. & Waterman, M. Diversity of LEF/TCF action in development and disease. *Oncogene* **25**, 7492–504 (2006).

277. Yilmaz, M. & Christofori, G. EMT, the cytoskeleton, and cancer cell invasion. *Cancer Metastasis Reviews* **28**, 15–33 (2009).

278. Nieman, M., Prudoff, R., Johnson, K. & Wheelock, M. N-cadherin promotes motility in human breast cancer cells regardless of their E-cadherin expression. *The Journal of Cell Biology* **147**, 631–643 (1999).

279. Suyama, K., Shapiro, I., Guttman, M. & Hazan, R. A signaling pathway leading to metastasis is controlled by N-cadherin and the FGF receptor. *Cancer Cell* **2**, 301–14 (2002).

280. Giampieri, S. *et al.* Localised and reversible TGFβ signalling switches breast cancer cells from cohesive to single cell motility. *Nat Cell Biol* **11**, 1287–1296 (2009).

281. Linder, S. The matrix corroded: podosomes and invadopodia in extracellular matrix degradation. *Trends Cell Biol* **17**, 107–17 (2007).

282. Artym, V. V, Zhang, Y., Seillier-Moiseiwitsch, F., Yamada, K. M. & Mueller, S. C. Dynamic interactions of cortactin and membrane type 1 matrix metalloproteinase at invadopodia: defining the stages of invadopodia formation and function. *Cancer Research* **66**, 3034–43 (2006).

283. Destaing, O., Block, M., Planus, E. & Albiges-Rizo, C. Invadosome regulation by adhesion signaling. *Curr Opin Cell Biol* **23**, 597–606 (2001).

284. Deryugina, E. *et al.* MT1-MMP initiates activation of pro-MMP-2 and integrin alphavbeta3 promotes maturation of MMP-2 in breast carcinoma cells. *Exp Cell Res* **263**, 209–23 (2001).

285. Wilkins-Port, C. E. & Higgins, P. J. Regulation of extracellular matrix remodeling following transforming growth factor-beta1/epidermal growth factor-stimulated epithelial-mesenchymal transition in human premalignant keratinocytes. *Cells, tissues, organs* **185**, 116–22 (2007).

286. Burk, U. *et al.* A reciprocal repression between ZEB1 and members of the miR-200 family promotes EMT and invasion in cancer cells. *EMBO Reports* **9**, 582–9 (2008).

287. Korpal, M., Lee, E. S., Hu, G. & Kang, Y. The miR-200 family inhibits epithelial-mesenchymal transition and cancer cell migration by direct targeting of E-cadherin transcriptional repressors ZEB1 and ZEB2. *The Journal of Biological Chemistry* **283**, 14910–4 (2008).

288. Hawinkels, L. & Ten Dijke, P. Exploring anti-TGF-β therapies in cancer and fibrosis. *Growth Factors* **29**, 140–52 (2011).

289. Chen, X.-F. *et al.* Transforming growth factor-β1 induces epithelial-to-mesenchymal transition in human lung cancer cells via PI3K/Akt and MEK/Erk1/2 signaling pathways. *Molecular Biology Reports* **39**, 3549–56 (2011).

290. Uchino, M. *et al.* Nuclear beta-catenin and CD44 upregulation characterize invasive cell populations in non-aggressive MCF-7 breast cancer cells. *BMC Cancer* **10**, 414 (2010).

291. Cho, S. *et al.* CD44 enhances the epithelial-mesenchymal transition in association with colon cancer invasion. *Int J Oncol* **41**, 211–8 (2012).

292. Jeanes, a, Gottardi, C. J. & Yap, a S. Cadherins and cancer: how does cadherin dysfunction promote tumor progression? *Oncogene* **27**, 6920–9 (2008).

293. Wheelock, M. J., Shintani, Y., Maeda, M., Fukumoto, Y. & Johnson, K. R. Cadherin switching. *Journal of Cell Science* **121**, 727–35 (2008).

294. Orsulic, S., Huber, O., Aberle, H., Arnold, S. & Kemler, R. E-cadherin binding prevents beta-catenin nuclear localization and beta-catenin/LEF-1-mediated transactivation. *Journal of Cell Science* **112 ( Pt 8**, 1237–45 (1999).

295. Onder, T. T. *et al.* Loss of E-cadherin promotes metastasis via multiple downstream transcriptional pathways. *Cancer Research* **68**, 3645–54 (2008).

296. Hulit, J. *et al.* N-cadherin signaling potentiates mammary tumor metastasis via enhanced extracellular signal-regulated kinase activation. *Cancer Research* **67**, 3106–16 (2007).

297. Maeda, M., Johnson, K. R. & Wheelock, M. J. Cadherin switching: essential for behavioral but not morphological changes during an epithelium-to-mesenchyme transition. *Journal of Cell Science* **118**, 873–87 (2005).

298. Tran, N. L., Adams, D. G., Vaillancourt, R. R. & Heimark, R. L. Signal transduction from N-cadherin increases Bcl-2. Regulation of the phosphatidylinositol 3-kinase/Akt pathway by homophilic adhesion and actin cytoskeletal organization. *The Journal of Biological Chemistry* **277**, 32905–14 (2002).

299. Liu, Z.-J. *et al.* Notch1 signaling promotes primary melanoma progression by activating mitogen-activated protein kinase/phosphatidylinositol 3-kinase-Akt pathways and up-regulating N-cadherin expression. *Cancer Research* **66**, 4182–90 (2006).

300. Wheelock, M. J. & Johnson, K. R. Cadherins as modulators of cellular phenotype. *Annual Review of Cell and Developmental Biology* **19**, 207–35 (2003).

301. McNeill, H., Ozawa, M., Kemler, R. & Nelson, W. J. Novel function of the cell adhesion molecule uvomorulin as an inducer of cell surface polarity. *Cell* **62**, 309–16 (1990).

302. Vega-Salas, D., Salas, P., Gundersen, D. & Rodriguez-Boulan, E. Formation of the apical pole of epithelial (Madin-Darby canine kidney) cells: polarity of an apical protein is independent of tight junctions while segregation of a basolateral marker requires cell-cell interactions. *The Journal of Cell Biology* **104**, 905–916 (1987).

303. Nejsum, L. N. & Nelson, W. J. A molecular mechanism directly linking E-cadherin adhesion to initiation of epithelial cell surface polarity. *The Journal of Cell Biology* **178**, 323–35 (2007).

304. Ivanov, A. I. *et al.* Tumor suppressor scribble regulates assembly of tight junctions in the intestinal epithelium. *The American Journal of Pathology* **176**, 134–45 (2010).

305. Etienne-Manneville, S. Scribble at the crossroads. *Journal of Biology* **8**, 104 (2009).

306. Bilder, D. Epithelial polarity and proliferation control: links from the Drosophila neoplastic tumor suppressors. *Genes & Development* **18**, 1909–25 (2004).

307. Humbert, P., Russell, S. & Richardson, H. Dlg, Scribble and Lgl in cell polarity, cell proliferation and cancer. *BioEssays* **25**, 542–53 (2003).

308. Zhan, L. *et al.* Deregulation of scribble promotes mammary tumorigenesis and reveals a role for cell polarity in carcinoma. *Cell* **135**, 865–78 (2008).

309. Dow, L. E. *et al.* Loss of human Scribble cooperates with H-Ras to promote cell invasion through deregulation of MAPK signalling. *Oncogene* **27**, 5988–6001 (2008).

310. Dow, L. E. *et al.* The tumour-suppressor Scribble dictates cell polarity during directed epithelial migration: regulation of Rho GTPase recruitment to the leading edge. *Oncogene* **26**, 2272–82 (2007).

311. Chatterjee, S. *et al.* Dysregulation of cell polarity proteins synergize with oncogenes or the microenvironment to induce invasive behavior in epithelial cells. *PloS one* **7**, e34343 (2012).

312. Navarro, C. *et al.* Junctional recruitment of mammalian Scribble relies on E-cadherin engagement. *Oncogene* **24**, 4330–9 (2005).

313. Qin, Y., Capaldo, C., Gumbiner, B. M. & Macara, I. G. The mammalian Scribble polarity protein regulates epithelial cell adhesion and migration through E-cadherin. *The Journal of Cell Biology* **171**, 1061–71 (2005).

314. Yoshihara, K. *et al.* Phosphorylation state regulates the localization of Scribble at adherens junctions and its association with E-cadherin-catenin complexes. *Experimental Cell Research* **317**, 413–22 (2011).

315. Leong, G. R., Goulding, K. R., Amin, N., Richardson, H. E. & Brumby, A. M. Scribble mutants promote aPKC and JNK-dependent epithelial neoplasia independently of Crumbs. *BMC Biology* **7**, 62 (2009).

316. Pearson, H. B. *et al.* SCRIB expression is deregulated in human prostate cancer , and its deficiency in mice promotes prostate neoplasia. *Journal of Clinical Investigation* **121**, 4257–4267 (2011).

317. Wu, M., Pastor-Pareja, J. C. & Xu, T. Interaction between Ras(V12) and scribbled clones induces tumour growth and invasion. *Nature* **463**, 545–8 (2010).

318. Gardiol, D., Zacchi, A., Petrera, F., Stanta, G. & Banks, L. Human discs large and scrib are localized at the same regions in colon mucosa and changes in their expression patterns are correlated with loss of tissue architecture during malignant progression. *International Journal of Cancer.* **119**, 1285–90 (2006).

319. Yates, L. L. *et al.* Scribble is required for normal epithelial Cell-Cell contacts and lumen morphogenesis in the mammalian lung. *Developmental Biology* **373**, 267–80 (2012).

320. Norman, M. *et al.* Loss of Scribble causes cell competition in mammalian cells. *Journal of Cell Science* **125**, 59–66 (2012).

321. Schroeder, M. C., Chen, C.-L., Gajewski, K. & Halder, G. A non-cell-autonomous tumor suppressor role for Stat in eliminating oncogenic scribble cells. *Oncogene* 1–9 (2012).doi:10.1038/onc.2012.476

322. Aranda, V. *et al.* Par6-aPKC uncouples ErbB2 induced disruption of polarized epithelial organization from proliferation control. *Nature Cell Biology* **8**, 1235–45 (2006).

323. Taddei, M. L., Giannoni, E., Fiaschi, T. & Chiarugi, P. Anoikis: an emerging hallmark in health and diseases. *The Journal of Pathology* **226**, 380–93 (2012).

324. Buchheit, C. L., Rayavarapu, R. R. & Schafer, Z. T. The regulation of cancer cell death and metabolism by extracellular matrix attachment. *Seminars in Cell & Developmental biology* **23**, 402–11 (2012).

325. Prakasam, a K., Maruthamuthu, V. & Leckband, D. E. Similarities between heterophilic and homophilic cadherin adhesion. *PNAS* **103**, 15434–9 (2006).

326. Katsamba, P. *et al.* Linking molecular affinity and cellular specificity in cadherin-mediated adhesion. *PNAS* **106**, 11594–9 (2009).

327. Hong, E. & Brewster, R. N-cadherin is required for the polarized cell behaviors that drive neurulation in the zebrafish. *Development* **133**, 3895–905 (2006).

328. Gärtner, A., Fornasiero, E. & Dotti, C. N-cadherin: A new player in neuronal polarity. *Cell Cycle* 2223–2224 (2012).

329. Camand, E., Peglion, F., Osmani, N., Sanson, M. & Etienne-Manneville, S. N-cadherin expression level modulates integrin-mediated polarity and strongly impacts on the speed and directionality of glial cell migration. *Journal of Cell Science* **125**, 844–57 (2012).

330. Naor, D., Wallach-Dayan, S. B., Zahalka, M. a & Sionov, R. V. Involvement of CD44, a molecule with a thousand faces, in cancer dissemination. *Seminars in Cancer Biology* **18**, 260–7 (2008).

331. Zöller, M. CD44: can a cancer-initiating cell profit from an abundantly expressed molecule? *Nature Reviews. Cancer* **11**, 254–67 (2011).

332. Chow, G., Tauler, J. & Mulshine, J. L. Cytokines and growth factors stimulate hyaluronan production: role of hyaluronan in epithelial to mesenchymal-like transition in non-small cell lung cancer. *Journal of Biomedicine & Biotechnology* **2010**, 485468 (2010).

333. Günthert, U. *et al.* A new variant of glycoprotein CD44 confers metastatic potential to rat carcinoma cells. *Cell* **65**, 13–24 (1991).

334. Thomas, L., Byers, H. R., Vink, J. & Stamenkovic, I. CD44H regulates tumor cell migration on hyaluronate-coated substrate. *The Journal of Cell Biology* **118**, 971–7 (1992).

335. Takahashi, E. *et al.* Tumor necrosis factor-alpha regulates transforming growth factor-beta-dependent epithelial-mesenchymal transition by promoting hyaluronan-CD44-moesin interaction. *The Journal of Biological Chemistry* **285**, 4060–73 (2010).

336. Schliekelman, M. J. *et al.* Targets of the tumor suppressor miR-200 in regulation of the epithelial-mesenchymal transition in cancer. *Cancer Res* **71**, 7670–82 (2011).

337. Louvi, A. & Artavanis-Tsakonas, S. Notch and disease: a growing field. *Seminars in Cell & Developmental Biology* **23**, 473–80 (2012).

338. Roybal, J. D. *et al.* miR-200 Inhibits lung adenocarcinoma cell invasion and metastasis by targeting Flt1/VEGFR1. *Molecular Cancer Research* **9**, 25–35 (2011).

339. Zhong, L. *et al.* Identification of secreted proteins that mediate cell-cell interactions in an in vitro model of the lung cancer microenvironment. *Cancer Research* **68**, 7237–45 (2008).